Soumyajit Mukherjee *Editor*

Petroleum Geosciences: Indian Contexts

Springer Geology

More information about this series at http://www.springer.com/series/10172

Soumyajit Mukherjee
Editor

Petroleum Geosciences: Indian Contexts

Springer

Editor
Soumyajit Mukherjee
Department of Earth Sciences
Indian Institute of Technology Bombay
Powai, Mumbai, Maharashtra
India
e-mail: soumyajitm@gmail.com

Contents

Plate-Tectonic Evolution of the Deep Ocean Basins Adjoining the Western Continental Margin of India—A Proposed Model for the Early Opening Scenario

G.C. Bhattacharya and V. Yatheesh

Abstract The available plate-tectonic evolution models suggest that the deep ocean basins adjoining the western continental margin of India have evolved largely due to break-up and dispersal of India, Seychelles and Madagascar continental blocks since Late Cretaceous. Mainly owing to the availability of large number of well identified magnetic anomaly picks, the evolution of the region from chron C28ny (∼62.5 Ma) and younger times is better constrained than the preceding period of its early evolution. Using constraints of several recently mapped regional scale tectonic features, a plausible model for that early evolution is proposed in this paper. Around 88.0 Ma the involved continental blocks were in their immediate pre-drift configuration where a wide continental rift zone existed between India and Madagascar. Seafloor spreading in the Mascarene Basin commenced shortly before 83.0 Ma. A ternary rift system off Saurashtra peninsula of western India, formed shortly before 68.5 Ma, reached seafloor spreading stage in the Laxmi and Gop basins around 67.6 and 64.7 Ma respectively. Around 62.5 Ma the ancestor of the Carlsberg Ridge spreading center developed between the Seychelles Plateau and the Laxmi Ridge while spreading in the northern Mascarene Basin ceased and spreading in the Laxmi and Gop basins continued at very slow rate. Between 60.9 and 57.9 Ma the spreading in the southern Mascarene Basin also ceased and the spreading center jumped north between the Laccadive Plateau and the northern boundary of the Mascarene Basin. The divergence regimes of the Gop, Laxmi and Laccadive basins ceased between 57.6 and 56.4 Ma, and the Laccadive Plateau and the Laxmi Ridge got welded to the Indian plate.

G.C. Bhattacharya (✉) · V. Yatheesh
CSIR-National Institute of Oceanography, Dona Paula 403004, Goa, India
e-mail: bhattacharya.gc@gmail.com

V. Yatheesh
e-mail: yatheesh@nio.org

1 Introduction

The broad plate-tectonic evolutionary model for the Indian Ocean region first emerged through three pioneering studies (McKenzie and Sclater 1971; Norton and Sclater 1979; Besse and Courtillot 1988) published during 1970s and 1980s. According to those studies, the western region (Fig. 1) of the Indian Ocean [hereafter referred as the Western Indian Ocean (WIO)] evolved by rifting and drifting of the major Gondwanaland fragments of Africa (AFR), Madagascar (MAD), Seychelles (SEY) and India (IND) from each other. Those studies also proposed that the eastern part of WIO, which is the area of focus of the present paper (i.e. the deep ocean basins (WCMI-ADOB) that lie between the Laxmi Ridge and the western conti-nental margin of India–Pakistan subcontinent) evolved in two stages mainly by rifting and drifting of MAD, SEY and IND continental blocks. In the first stage a conjoined IND–SEY block drifted from Madagascar since ∼chron C34n, which formed the Mascarene Basin. In the second stage, IND drifted from SEY since chron C28ny creating the conjugate Arabian and Eastern Somali basins. These broad models however did not accommodate vast oceanic areas adjacent to the continental margins apparently due to paucity of appropriate geophysical data from those regions. With the availability of newer and denser coverage of geophysical transects and advanced tools for plate-tectonic reconstructions, those initial models for the Indian Ocean region as a whole continues to improve through large number of subsequent studies (e.g. Naini 1980; Schlich 1982; Naini and Talwani 1982; Royer and Schlich 1988; Bhattacharya et al. 1992; Chaubey et al. 1993, 1995, 1998; Dyment 1998; Krishna et al. 2012; Gibbons et al. 2013 and references therein; references cited in Yatheesh et al. 2013a; Jacob et al. 2014; see Misra and Mukherjee 2015) in different parts of the Indian Ocean area. However, till date, the nature and genesis of the crust underlying the WCMI-ADOB region remained vague. Naini and Talwani (1982) and Kolla and Coumes (1990) opined that the WCMI-ADOB areas are underlain by thinned continental crust, while Biswas and Singh (1988) opined that the underlying crust is oceanic. However, for many years subsequent researchers did not consider the possibility of oceanic crust underlying the WCMI-ADOB areas, and instead based their models with the assumption of an underlying thinned con-tinental crust. The idea of oceanic crust underlying the WCMI-ADOB areas gained strength with an apparent breakthrough few years later, when Bhattacharya et al. (1994a) reported the presence of short sequence of two-limbed seafloor spreading type magnetic anomalies in the Laxmi Basin sector of the WCMI-ADOB. Subsequently, Malod et al. (1997) reported the presence of two-limbed seafloor spreading type magnetic anomalies in the Gop Basin sector of WCMI-ADOB. In the subsequent years several publications (Reeves and Leven 2001; Chatterjee et al. 2006, 2013; Bastia et al. 2010; Calvès et al. 2011; Gibbons et al. 2013; Torsvik et al. 2013) presented models for the evolution of the WIO region with the consideration that the WCMI-ADOB region represents extinct oceanic spreading regime. A recent study of Misra et al. (2015) treated various geophysical data over a large part of the WCMI-ADOB region. Their interpretations (Figs. 5 and 9 of Misra et al. 2015) of
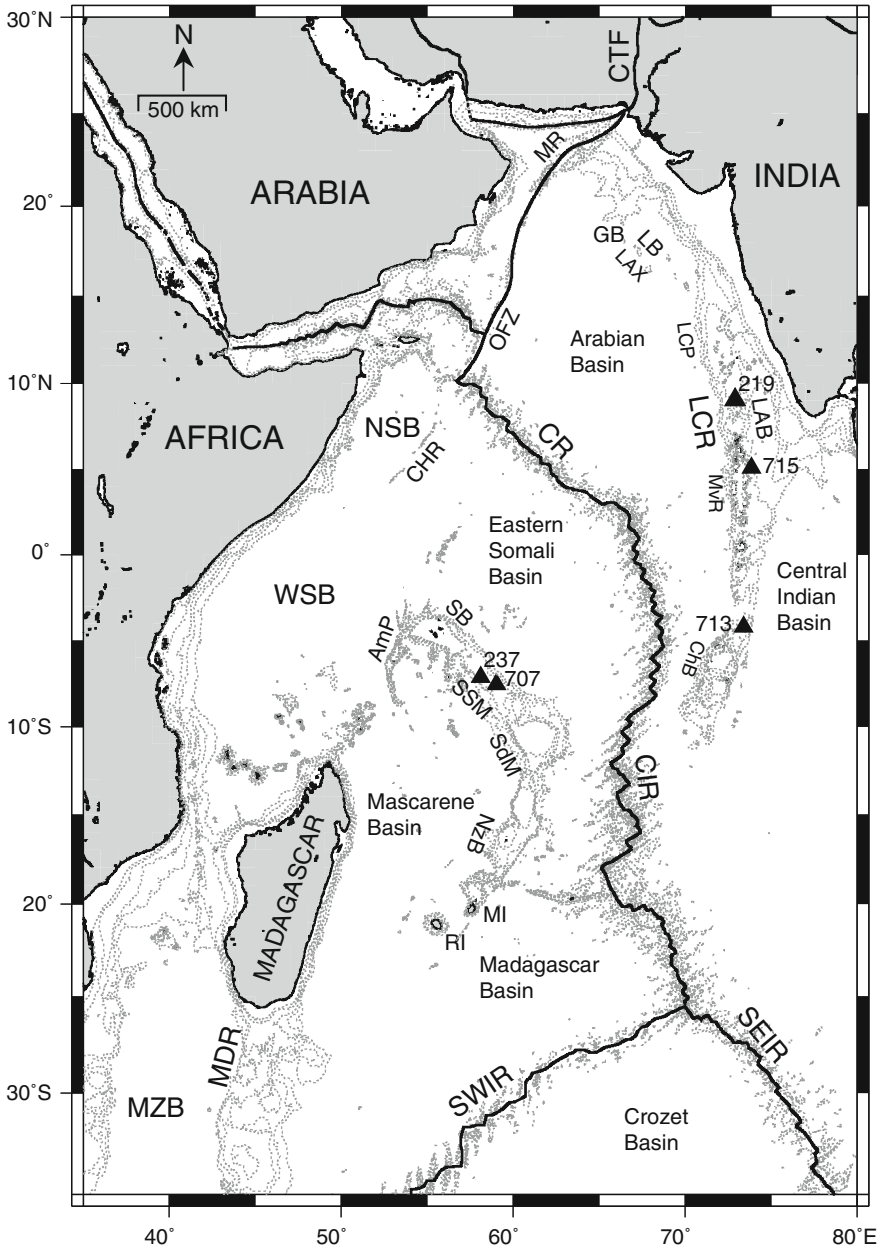
Fig. 1 Generalized map of a part of the Western Indian Ocean area depicting various major tectonic elements referred in the text. *Thin dotted lines* are selected (200, 1000, 2000, 2500 and 3000 m) isobaths from GEBCO digital data set (IOC-IHO-BODC 2003). Abbreviations used are as in Table 1

Table 1 List of selected abbreviations used to refer various tectonic elements and domains in this study

Abbreviations	Tectonic elements and domains	Abbreviations	Tectonic elements and domains
Indian side		*Seychelles side*	
BH	Bombay High	AmP	Amirante Plateau
CG	Cambay rift graben	MI	Mauritius Island
ChB	Chagos Bank	NzB	Nazareth Bank
CKE	Chain Kairali Escarpment	RI	Réunion Island
CTF	Chaman Transform fault	SB	Seychelles Bank
DFB	Deccan Flood Basalt	SMP	Seychelles-Mascarene Plateau Complex
ESC	Extinct Spreading Centre	SdM	Saya de Malha Bank
GB	Gop Basin	SEY	Seychelles Plateau
IND	Indian continental block	SSM	Seychelles—Saya de Malha saddle
IPS	Indian Peninsular shield	ESB	Eastern Somali Basin
KG	Kutch rift graben	*Madagascar side*	
LAB	Laccadive Basin	AnE	Angavo Escarpment
LAX	Laxmi Ridge continental sliver	MAD	Madagascar continental block
LB	Laxmi Basin	MDB	Madagascar Basin
LCP	Laccadive Plateau	MDR	Madagascar Ridge
LCR	Laccadive-Chagos Ridge	MhnFZ	Mahanoro Fracture Zone
MvR	Maldive Ridge	MSB	Mascarene Basin
NG	Narmada rift graben	MauFZ	Mauritius Fracture Zone
NPB	Northern Indian Protocontinental block	Rg	Ranotsara Gap
P	Panikkar Seamount	*African side*	
PB	Padua Bank	AFR	African continental block
Pg	Palghat Gap	MZB	Mozambique Basin
PTR	Palitana Ridge	NSB	Northern Somali Basin
R	Raman Seamount	WSB	Western Somali Basin
Sau	Saurashtra Peninsula	*Deep oceanic regions*	
SPB	Southern Indian Protocontinental block	CR	Carlsberg Ridge
		CIR	Central Indian Ridge
		CHR	Chain Ridge
SVP	Saurashtra volcanic Platform	MR	Murray Ridge
W	Wadia Guyot	OFZ	Owen Fracture Zone
WgE	Western Ghat Escarpment	SEIR	Southeast Indian Ridge
		SWIR	Southwest Indian Ridge

high quality deep penetration seismic reflection data of recent vintage apparently supported the oceanic nature of the Laxmi Basin. However, despite those advancements, the geodynamic evolution of the WIO region particularly for the period prior to chron C28ny ($\sim$62.5 Ma[1]) has not yet been well constrained. In this paper, we propose a plausible plate-tectonic evolutionary model of the WCMI-ADOB region, for its early opening period, i.e. from the time of initiation of the India-Madagascar break-up ($\sim$88.0 Ma; Late Cretaceous) to chron C25no ($\sim$56.4 Ma; Late Paleocene). Before proceeding to present our proposed model, in the following section, we will discuss the constraints and implications of the relevant tectonic elements and geological events, which in our opinion should be considered for constructing models for early plate-tectonic evolution of the WCMI-ADOB region. It may be mentioned here that some of these aspects have not been holistically considered in any such model for the region so far.

2 Relevant Tectonic Elements and Geological Events

Since the evolution of the WCMI-ADOB region began with separation of India and Madagascar; therefore our description will include the relevant features from the Indian side as well from the Madagascar counterpart. However, the emphasis will be for the features from the land and offshore areas of the eastern part of Madagascar and its conjugate western part of India.

2.1 Features on the Western Part of the Indian Peninsular Shield and Adjacent Continental Margin

The geological formation of the southernmost region of the western part of Indian peninsular shield (IPS), approximately south of Kasaragod (Fig. 2), is the Southern Granulite Terrain (SGT), which is a Neoproterozoic mobile belt, made mainly of granulite facies rocks (age range of 700–500 Ma). North of this area, approximately between Kasaragod and north of Goa, is the western part of Dharwar Craton, where linear belts of Late Archaean schistose rocks (age range of 2800–2600 Ma) overlie a basement of Archaean gneisses (age of >3000 Ma) with an unconformity (Sharma 2009). Further north the deeper geology lie hidden under Deccan Flood Basalts (DFB), the commonly known Deccan Traps, of Late Cretaceous to Early Paleocene age (Radhakrishna and Vasudev 1977; Subrahmanya 2001; Chenet et al. 2007). Probably much of the terrain onto which the DFB were erupted consisted of the Dharwar Craton (Jerram and Widdowson 2005). The Saurashtra Peninsula, a region almost in the northwestern limit of DFB province, represents a cratonic horst-like

---

[1]Ma: millions of years before present.

uplift, which appear to be bordered in the north, east and south by continental rift grabens or their offshore extensions. Here again the deeper geology lie hidden under DFB. However, from some deep drill wells at Lodhika and Dhanduka it was inferred that DFB in the Saurashtra region overlie Creatceous/Jurassic sediments, volcanic tuffs and possibly another sedimentary layer, which overlie a Precambrian crystalline basement. The central western part of the Saurashtra Peninsula also contains several volcanic plugs (Singh et al. 1997; Rao and Tewari 2005).

The crystalline terrain of the southern region of IPS is dissected by several shear zones, the most prominent of which are the Achankovil Shear Zone, the Palghat-Cauvery Shear Zone, Bhavani Shear Zone and the Moyar Shear Zone (Kroner and Brown 2005). These shear zones are important in the context of India-Madagascar
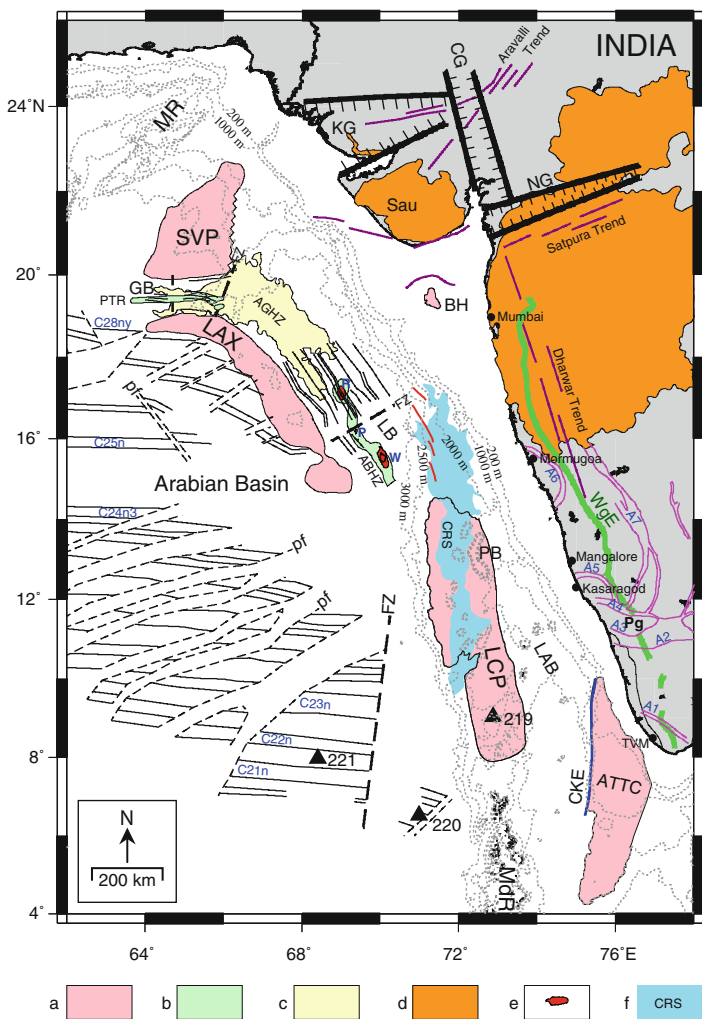
◄ **Fig. 2** Generalized map of the western continental margin of India and the adjoining land and deep ocean basin areas for depicting the locations of various onshore and offshore tectonic elements referred in the text. The continuous *black lines* in the offshore areas represent the mapped seafloor spreading type magnetic lineations. *Dashed lines* orthogonal to magnetic lineations represent fracture zones (labeled FZ). In the Arabian Basin area the *thin dashed lines* (labeled pf) oblique to the magnetic lineations are the inferred pseudo-faults related to propagating ridges. Hachured *thick black lines* represent postulated boundaries of rift graben basins onland. *Pink lines* over southwestern India represent the inferred shear zones. *A1* Achankovil Shear Zone; *A2* Palghat-Cauvery Shear Zone; *A3* Bhavani Shear Zone; *A4* Moyar Shear Zone; *A5* Coorg Shear Zone; *A6* Kumta Shear Zone; *A7* Chitradurga Shear Zone. *Thick green line* (labeled WgE) along the western edge of Indian mainland represents Western Ghat Escarpment (digitized from satellite imagery available at http://commons.wikimedia.org/wiki/File:South_India_satellite.jpg). The *red lines* located north of the Laccadive Plateau represent the segments of the Ratnagiri Fracture Zone postulated by Misra et al. (2015). ATTC: Alleppey-Trivandrum Terrace Complex; *ABHZ* Axial basement high zone coinciding with the inferred extinct spreading axis of the Laxmi Basin. Solid annotated black triangles are DSDP/ODP drill hole sites annotated with site numbers. Explanation of items of the legend—(a) Continental slivers; (b) Extent of ABHZ in Laxmi Basin and PTR in Gop Basin; (c) anomalous gravity high zone (AGHZ); (d) extents of Deccan Flood Basalts; (e) Seamounts in the Laxmi Basin. *R* Raman seamount; *P* Panikkar seamount; *W* Wadia Guyot; (f) Cannanore Rift System. Tectonic elements were compiled from several sources (Biswas 1982; Bhattacharya et al. 1994a, b; Chaubey et al. 2002a; Srinivas 2004; Yatheesh 2007; Calvès et al. 2011; Yatheesh et al. 2013b; DGH 2014; Ishwar-Kumar et al. 2013 and Ratheesh-Kumar et al. 2014). Other abbreviations used are as in Table 1 and the other details are as in Fig. 1

pre-drift juxtaposition, as they are often considered as conjugate of several comparable shear zones in the Madagascar and therefore used as constraints by researchers (e.g. Crawford 1978; Katz and Premoli 1979; Windley et al. 1994; Menon and Santosh 1995; Yoshida et al. 1999). However, opinions differ amongst researchers about the exact conjugate correspondence of these onshore shear zones. The recently identified Kumta Suture (Ishwar-Kumar et al. 2013) and Mercara (Coorg) Suture (Santosh et al. 2014) in western India and their continuation to eastern Madagascar as the Betsimisarka-Kumta-Coorg Suture (Ishwar-Kumar et al. 2013), appears to have provided valuable constraint to establish more reliable conjugate correspondence of other shear zones of India and Madagascar as well as best fit reconstruction of India and Madagascar. The three major Precambrian tectonic trends, which predominate this western part of IPS are; the NNW-SSE Dharwar trend, the NE-SW Aravalli trend and the ENE-WSW Satpura trend (Fig. 2). These three major tectonic trends were the zones of deformed and weakened crust along which later Phanerozoic rifting was facilitated. The three intra-continental rift basins which formed by rifting along these trends are the; Kutch, Cambay and Narmada rift basins. The geological history of these intra-continental rift basins indicates that they were formed sequentially from north to south around the Saurashtra horst by reactivation of primordial faults. The Kutch rift basin opened up first during Jurassic—Early Cretaceous along the Aravalli trend and was aborted in Late Cretaceous. The Cambay rift basin opened in the Early Cretaceous along the Dharwar trend and was aborted in Late Cretaceous. The Narmada rift basin opened in the Late Cretaceous time along the Satpura trend and was aborted in Late Cretaceous—early Paleocene time (Biswas 1982, 1987, 1988;

Gombos et al. 1995). This Narmada rift basin has been considered as an important aulacogen in our reconstruction model. The Narmada rift basin zone is considered to be a prominent, ancient line of weakness which developed along a Proterozoic protocontinental suture between two protocontinents of the Indian shield; a northern, Aravalli protocontinent and a southern, Dharwar protocontinent (Naqvi 2005; Sharma 2009). One major geomorphic feature of the western part of Indian peninsular shield, which we have considered in our model, is the Western Ghats Escarpment (or, Sahyadri Escarpment). This great escarpment is manifest as a coast parallel precipitous terrain separating the coastal lowlands and the eastward sloping central highlands of the peninsular India. The westward (seaward) facing Western Ghats Escarpment, which is clearly discernible in the satellite imagery, is a continental scale ($\sim$1500 km long) lineament, with only a prominent breach in its continuity at one place, known as the Palghat Gap. Considering the earlier mentioned description of the western part of IPS, the geological formations and age vary along the length of the Western Ghats Escarpment, although morphologically the feature is continuous. This escarpment is believed to represent the easterly, possibly uplifted, rift shoulder related to India—Madagascar rifting episode that was much older than the time of DFB event. The present day location and morphology of this escarpment possibly are the outcome of various processes, such as, denudation, scarp retreat and marine regression (Radhakrishna 2001; Subrahmanya 2001; Gunnell and Harbor 2008).

The shelf break in the western continental margin of India (Fig. 2) occurs at an average depth of about 200 m (Naini 1980). Towards north this shelf is relatively wider, being more than 300 km in the areas off Mumbai, whereas towards south this width gradually narrows down to about 50 km off Trivandrum. In contrast to this, the continental slope is narrow in the north but widens towards south (Biswas 1989). The paleo-shelf edge is situated (Raju et al. 1981; Rao and Srivastava 1981) much landwards of the present day shelf edge. A system of nearly coast parallel narrow horst and graben structures characterizes the basement trends of the shelf area approximately up to the northern limit of the Bombay High. This horst—graben system also had the same trend as the NNW-SSE Dharwar trend and perhaps is related to the Dharwarian basement grain parallel rifting event that preceded separation of Madagascar from India (Biswas 1989; Gombos et al. 1995). A conspicuous positive basement feature off Saurashtra Peninsula is the Saurashtra Arch. This ENE–WSW trending arch is a broad structural high on a regional scale and extends from the shelf across the slope to deep sea areas. The continental shelf part of the arch is manifest as a simple anticline, but its deepwater part contains a horst and graben structure at the crestal region (Sriram et al. 2006). As evidenced by the continuation of the Narmada and Kutch rifts and Saurashtra Arch onto the continental shelf (Biswas 1982; Bhattacharya and Subrahmanyam 1986), it appears that, in the areas northwards of Mumbai the basement trends are nearly orthogonal to the coast.

A prominent and anomalous lateral bathymetric protrusion in the form of two contiguous terrace-like features, named 'Alleppey-Trivandrum Terrace Complex (ATTC)', exists in the mid-continental slope region off southwest coast of India. A conspicuous, nearly 500 km long, steep escarpment named 'Chain-Kairali Escarpment (CKE)', demarcates the westward limit of the ATTC. The crust of this region was inferred to be thinned continental type that was intermingled with extensive volcanic intrusive emplacements, perhaps related to Marion hotspot volcanism. This ATTC region and a bathymetric notch in the northern Madagascar Ridge was postulated as conjugate features related to India-Madagascar separation, where the 'Chain-Kairali Escarpment (CKE)' forms a sheared continental margin segment along which the continental margin off the nearly straight southeast coast of Madagascar glided past India (Yatheesh et al. 2006, 2013b).

2.2 Laxmi Ridge and Laccadive Plateau

The Laxmi Ridge, located in the deep (average water depth $\sim$2.8 km) offshore region of west coast of India (Figs. 1 and 2), is a prominent aseismic basement high feature. At seafloor the Laxmi Ridge is expressed as thin sediment covered basement high having a maximum relief of only $\sim$0.7 km. However, as its flanks are covered by thick sediments hence the actual relief of this basement high is $\sim$2.0 km. This ridge is expressed as NW–SE trending bathymetric high in its southern end, while its bathymetric expression is not discernible northwards beyond 18°30′N. Further, even though this ridge is a positive basement feature all along its extent and a positive seafloor feature in its southern end, it is associated with a characteristic broad negative free-air gravity anomaly ($\sim$50 mgal). However, based on associated characteristic gravity anomaly and adjacent magnetic anomalies (Fig. 3), it appears that around 65°30′E this ridge turns nearly E-W and extends westwards at least up to 63°40′E (Miles and Roest 1993). As will be discussed later (in Sect. 2.4.3), in our opinion this bight of the Laxmi Ridge provides important clue for the early evolution of the WCMI-ADOB region. The southward extent of the seafloor expression of the NW-SE trending most prominent southerly segment of the Laxmi Ridge appears to terminate abruptly against an oceanic crust containing east–west trending small segment of magnetic lineation, which is identifiable as anomaly C27n (Chaubey et al. 1998; Bhattacharya and Chaubey 2001). Based on seismic refraction studies, Naini and Talwani (1982) proposed a continental sliver genesis of the Laxmi Ridge. Todal and Eldholm (1998) opined that it is a marginal high complex, comprising both continental and oceanic crust, where inner part of the ridge is underlain by faulted continental blocks. From identified seafloor spreading magnetic anomalies, it was established that the Laxmi Ridge is that conjugate continental sliver, which was severed from the Seychelles when
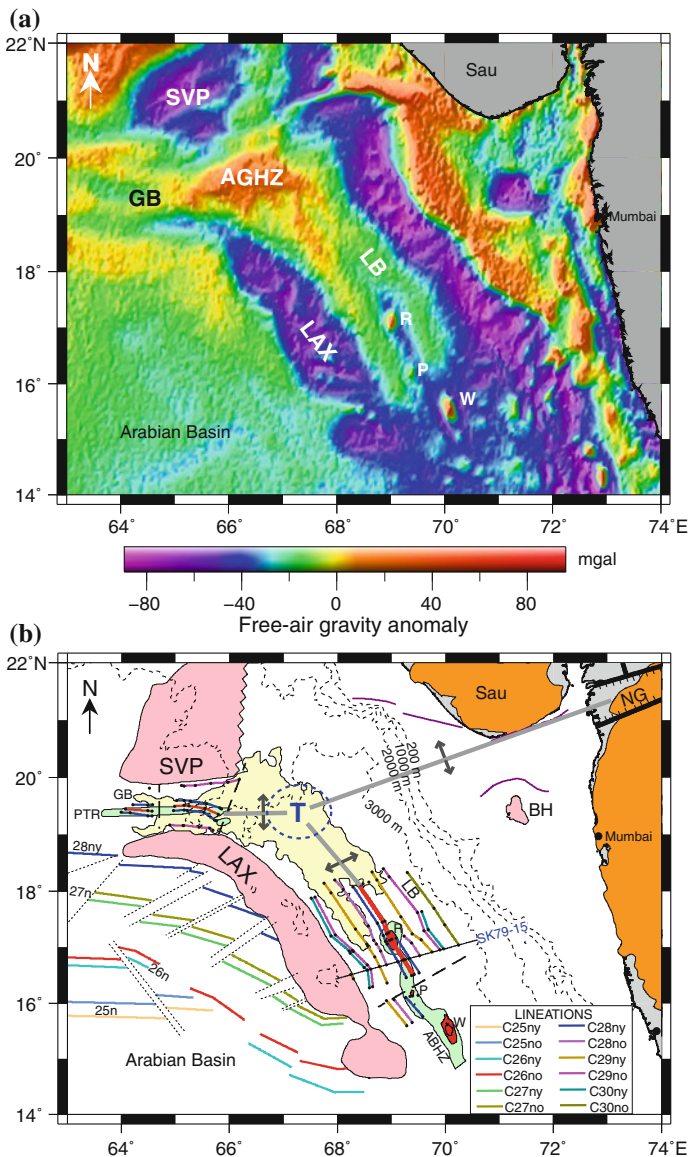
Fig. 3 Tectonic elements of the deep offshore regions adjoining northern part of the western continental margin of India. **a** Colour shaded-relief image of the satellite derived free-air gravity anomalies version 23.1 (Sandwell et al. 2014). **b** Major tectonic elements on a generalized map of the region. Location of profile SK79-15 used for magnetic anomaly modelling in this study is shown as *annotated line*. *Solid coloured lines* represent the mapped seafloor spreading type magnetic lineations inferred in the Laxmi Basin (after Bhattacharya et al. 1994a; Yatheesh 2007), in the Gop Basin (after Yatheesh et al. 2009), and in the Arabian Basin (after Chaubey et al. 2002a). *Thin dotted lines* are pseudofaults. *T* postulated Gop-Narmada-Laxmi (GNL) fossil triple junction off Saurashtra peninsula; *AGHZ* anomalous gravity high zone. Other abbreviations used are as in Table 1 and the other details are as in Figs. 1 and 2

spreading was initiated along the Carlsberg Ridge sometimes during the younger part of anomaly C28n. Collier et al. (2004) reported the presence of seaward dipping reflectors (SDRs) on the southwards regions of the Laxmi Ridge. It may be mentioned here that Misra et al. (2015) reported to have identified several geological/geophysical signatures over the Laxmi Ridge, which according to them suggest that the ridge is composed of oceanic crust formed at an abandoned oceanic spreading centre. They (ibid.) however candidly admitted that the debate on the crustal nature of the Laxmi Ridge would still remain owing to the non-uniqueness of geophysical analyses. In our opinion, although genesis of the Laxmi Ridge as an abandoned oceanic spreading centre could be a possibility, but that does not appear to have been firmly established in this study. In view of this we maintain what the researchers in general agree—that the Laxmi Ridge is a continental sliver.

The Laccadive-Chagos Ridge (LCR) is a prominent aseismic bathymetric high feature of the Western Indian Ocean (Fig. 1). The LCR is a slightly arcuate elongated feature, which extends for about 2500 km between 12°S and 14°N. This feature appears to be divided into three main segments by the presence of several relatively deep saddle-like features. These three main segments, from north to south have been referred by Bhattacharya and Chaubey (2001) as the Laccadive Plateau, the Maldives Ridge and the Chagos Bank. The genesis of the LCR still remains an enigma. The proposed views about its genesis are varied, such as, it is: a leaky transform fault, a hotspot trail, a composite structural elements of various origins etc. (references cited in Bhattacharya and Chaubey 2001). Out of these, the hotspot trail genesis appears to have broad acceptance, but as have been discussed later in this paragraph, we believe that at least the northern part of the LCR, i.e. the Laccadive Plateau (LCP) region is a continental sliver. The linearity of the LCR and the inferred age progression along its extent were considered as evidences for its hotspot trail genesis (Morgan 1972, 1981; Whitmarsh 1974; Duncan 1981). This age progression was inferred from the basement age determinations at the DSDP site 219 and ODP sites 713 and 715 (Fig. 1). Out of these three sites, the basement ages for sites 713 and 715 are radiometric ages of the basement basalts (Duncan and Hargraves 1990), and for site 219 it is an estimate from the bio-stratigraphic age (Whitmarsh et al. 1974) of the oldest sediment overlying the basement. Even though the radiometric ages for sites 713 and 715 were qualified as imprecise by a later researcher (Baksi 2005), still the ages of the three sites together do appear to suggest a pattern of increasing age of basement northward along the LCR. We, however believe that this observation of age progression on its own do not rule out the possibility that the Laccadive Plateau is a continental sliver. The reasons for believing so are two; firstly, the ODP sites 713 and 715 are not located over the Laccadive Plateau and volcanics were not sampled at DSDP site 219, which appears to lie at the southern fringe of the Laccadive Plateau. Secondly, mere existence of age progressive volcanics along parts of LCR do not indicate anything unequivocal about the nature of the country rocks, because volcanics along the trail of a hotspot are expected to show evidence of age progression, irrespective of

whether those volcanics are intrusives/extrusives over continents/continental slivers or are manifested as volcanic islands in the oceanic area. On the other hand, there are several observations, which strongly suggest that the Laccadive Plateau region may be a continental sliver. For example, based on estimation of crustal thickness from seismic refraction experiments, Naini and Talwani (1982) arrived at crustal thickness (∼15 km) of the Laccadive Plateau region, which is higher than normal oceanic crust. This prompted them to suggest a continental fragment nature of the Laccadive Plateau. Some insight about the geological configuration of the Laccadive Plateau perhaps can be obtained from the situation at Padua Bank—a shallow carbonate bank atop the northern part of the Laccadive Plateau (Fig. 2). It was reported (Murty et al. 1999; Kothari et al. 2001) that industry well drilled over the Padua Bank reached basalt layer underlying the tertiary sedimentary section. If this drilled basalt forms the basement then this is the only well to have sampled basaltic basement over the Laccadive Plateau or in its near vicinity. Unfortunately, no results of further studies of those basalts are available in public domain. Further, based on study of seismic reflection sections, presence of clearly identifiable rotated fault blocks have been observed by Murty et al. (1999) on either side of the Padua Bank. They (ibid.) considered those fault blocks are akin to typical stretched continental crust. It may be mentioned here that rotated fault blocks represent extensional tectonic event, but on their own they cannot be considered to represent only stretched continental crust, because rotated fault blocks were also reported (Salisbury and Keen 1993) from the regions of oceanic crust. In view of this we feel the presence of rotated fault blocks in the Padua Bank region can only be considered as a possible indicator of the continental nature of the Laccadive Plateau, not as an evidence to confirm that nature. Therefore, considering the drilled basalts and the basement characteristics we surmise that the Padua Bank and its vicinity represent an area of stretched crust, possibly of continental affinity, which is overlain by basaltic rocks. It has been reported (DGH 2014) that the Laccadive Plateau area has a complex basement structure, comprising of single normal faults, half grabens and grabens, which as a whole appear as a rift system. This rift system, named as 'Cannanore Rift System' (Fig. 2), extends along eastern part of the ridge in N-S direction from ∼17°N to 9.5°N. Yatheesh et al. (2006) have shown that in a close fit India—Madagascar juxtaposition in their immediate pre-drift scenario, there is space to accommodate the Laccadive Plateau region as a continental sliver in between India and Madagascar. Later, Yatheesh (2007) made a more detail examination of the Laccadive Plateau as a possible continental sliver in the perspective of plate-tectonic evolution of the Western Indian Ocean. It may be mentioned here that most of the plate-tectonic reconstruction models, which included the period of early evolution of the WCMI-ADOB region (e.g. Norton and Sclater 1979; Besse and Courtillot 1988; Reeves and Leven 2001), considered the hotspot trail genesis for the LCR. Therefore in those models the LCR appeared into the reconstructions of periods younger than ∼65 Ma, i.e. since the postulated time of peak of Réunion hotspot volcanism on Indian mainland. Whereas, some other

reconstructions of recent vintage (e.g. Torsvik et al. 2013; Calvès et al. 2011; Ganerød et al. 2011) appear to consider the Laccadive Plateau region as continental sliver. In view of above, in our present model we have assumed that the Laccadive Plateau part of the LCR is a continental sliver that was severed from the western Indian Peninsula by a regime of crustal divergence and was intruded by volcanics as the area passed over the Réunion hotspot.

2.3 Conjugate Arabian and Eastern Somali Basins

The Arabian and Eastern Somali basins are two large conjugate ocean basins, which formed by seafloor spreading across the still active Carlsberg Ridge (Fig. 1). The conjugate seafloor spreading magnetic anomalies of these basins were mapped way back in 1960s with limited magnetic traverses and later with some additional magnetic data McKenzie and Sclater (1971) identified them as anomalies sequence C28n–C23n. In the subsequent years, large amount of magnetic profiles were acquired by various agencies in this area and study of those magnetic profiles enabled to establish the tectonic framework of these basins. However, we will restrict our discussion only to those aspects which are relevant to our reconstruction model. Now we know that these conjugate Arabian and Eastern Somali basins were formed within the broad geographical bounds of the submarine Laxmi Ridge in the north and the Seychelles Plateau in the south. The Chain Ridge—Owen Fracture Zone system marks the western boundary of these basins and the northern portion of the LCR marks their easterly boundary. Recent seismic investigations (Collier et al. 2004, 2009) across the conjugate Seychelles—Laxmi Ridge continental margins appears to have firmly established the northerly and southerly bounds of these two basins. So far the oldest confidently identified magnetic anomalies in these two basins are the anomaly C27n lineations. However, the younger ends of anomaly C28n lineations are considered to be present in the Arabian Basin immediately south of the Laxmi Ridge (Miles and Roest 1993; Chaubey et al. 1998, 2002a). These two basins appear to have experienced long sustained spreading ridge propagation activities. The Spreading ridge propagation is one of the processes by which spreading ridges reconfigure their geometry and this process, also consistent with rigid plate hypothesis, is different from ridge jump. In case of ridge jump, the ridge segments relocate as a whole on one of the flanks. In ridge propagation a new spreading ridge segment with new trend gradually advances into the crust previously created by the adjacent retreating ridge segment and in due course replaces the ridge with old trend. Oblique offsets of magnetic lineations in the ocean basins are considered (Hey 1977; Hey et al. 1980) as the diagnostic feature of the propagating spreading ridges. Miles and Roest (1993) were the first to report the existence of ridge propagation in the northern sector of the Arabian Basin. Later, independent as well as collaborative studies by Indian and French research groups (Bhattacharya et al. 2001, 2003a, b; Chaubey et al. 1998, 2002a; Dyment 1998; Dyment et al. 2001; Royer et al. 2002) thoroughly established the ridge propagation

pattern that took place during the accretion of oceanic crust in these conjugate basins during their first ~ 16 myr[2] (i.e. chron C28ny–chron C21ny) of formation. According to these studies, there were three major stages of ridge propagation during that period with dominant propagation pattern characterizing each stage. The first stage of propagation commenced at about chron C28ny (~ 62.5 Ma) and continued at least till chron C27ny (~ 60.9 Ma). The propagation in this stage was along short segments and the direction of propagation was dominantly westward. The second stage of propagation, which started some time during chron C26r (~ 57.9–60.9 Ma) was characterized by a general eastward propagation, and the propagation of this stage continued in the same direction at least till chron C25n (~ 55.9 Ma). The third and last stage of propagation commenced some time during chron C24r (~ 53.3–55.9 Ma) and ended gradually around chron C21ny (~ 46.3 Ma). Propagation direction during this last stage was systematically towards west along all the spreading ridge segments. The crust generated during each of these propagation stages is delimited by unique tectonic boundaries, which are even decipherable from satellite gravity anomaly data (see Fig. 8 of Chaubey et al. 2002a). The ridge propagation system resulted in an asymmetric crustal accretion in these conjugate basins with gross additional crust in the Arabian Basin. Several processes, such as thermal triggering by Réunion hotspot, attempt by ridge segments to remain in proximity of the hotspot or its trailing thermal anomaly, and the processes of lengthening of short ridge segments formed along an initially curved margin, are suggested to have causal relationship with these ridge propagation events.

2.4 Laxmi and Gop Basins

The Laxmi and Gop basins are the two relatively narrow deep sea basins, which exist within the bounds of the Laxmi Ridge and the India-Pakistan continental margin. These two basins (Figs. 2 and 3) assume significance in our study, because we believe they contain valuable clues regarding the early opening history of the WCMI-ADOB region.

2.4.1 The Laxmi Basin

The Laxmi Basin is the ~ 250 km wide deep offshore region lying approximately between the NW-SE trending southern part of the Laxmi Ridge and the continental slope off western India. Bhattacharya et al. (1994a) were the first to recognize and designate the distinct entity of the Laxmi Basin. Towards south, this basin abuts the

---

[2]myr: millions of years.

northern extremity of the Laccadive Plateau, while towards north this basin appears to merge with the E-W trending Gop Basin.

Differences of opinions appear to exist regarding the nature of the crust underlying the Laxmi Basin. Some believe, the underlying crust is thinned and volcanics intruded continental crust (Naini and Talwani 1982; Kolla and Coumes 1990; Rao et al. 1992; Todal and Eldholm 1998; Krishna et al. 2006). On the other hand, Biswas and Singh (1988) favoured an oceanic nature, because they observed hyperbolic reflection pattern, which is typical for an oceanic crust, in the seismic reflection from basement in the region. Subsequently, Bhattacharya et al. (1994a) mapped the existence of well-correlatable NNW-SSE trending linear axi-symmetric magnetic anomalies in this basin (see Figs. 4 and 5 of Bhattacharya et al. 1994a), and inferred them to represent a two-limbed seafloor spreading anomaly sequence. Several subsequent studies (e.g. Talwani and Reif 1998; Bernard and Munschy 2000; Eagles and Wibisono 2013) favoured oceanic nature of the crust underlying the Laxmi Basin. However, Krishna et al. (2006) opined that the magnetic anomalies in the Laxmi Basin, that Bhattacharya et al. (1994a) interpreted as seafloor spreading magnetic anomalies, could best be explained as volcanic intrusives within the stretched continental crust. We agree that volcanic intrusives within the stretched continental crust can generate magnetic anomalies. However, we do not think any physical model can rationally explain the formation of several hundreds of kilometers long axi-symmetric linear magnetic anomalies within such stretched continental crust. The seaward dipping reflectors (SDRs) are considered as a veritable clue to demarcate continent ocean transition (Mutter et al. 1982). Of late, based on high quality 2D seismic reflection imaging, presence of such SDRs was reported (Corfield et al. 2010; Siawal et al. 2014) on both the easterly and westerly margins of the Laxmi Basin. Misra et al. (2015) have further distinguished the SDRs of the Laxmi Basin region as Outer SDRs and indicated (Fig. 2 and 5b of Misra et al. 2015) that the Laxmi Basin is flanked on both sides by Outer SDRs and normal oceanic crust exists basinwards beyond the termination of the Outer SDRs. In view of above we maintain that the Laxmi Basin is underlain by oceanic crust.

It cannot be denied, that dating of seafloor spreading type magnetic anomalies of the Laxmi Basin is very difficult due to their short extent. The problem gets further compounded as no characteristic signatures of those anomalies, which can aid their identification with respect to geomagnetic timescale, have been detected so far. Age constraints from drill hole samples or seismic stratigraphic data from the area are also not available so far. The preferred interpretation of Bhattacharya et al. (1994a) suggested a slow spreading (<10 mm/yr Half Spreading Rate) C33n-C28n-C33n sequence (corresponding ∼79.5 to ∼62.5 Ma) aged oceanic crust for the Laxmi Basin. Recently, Eagles and Wibisono (2013) opined that the smooth nature of the acoustic basement of the area as inferred from seismic reflection data, is not compatible with such a slow spreading model, and instead they (ibid.) proposed a C29n-C28n-C29n sequence (corresponding ∼64.7 to ∼62.5 Ma) to the Laxmi Basin magnetic lineations. In view of this wide variation in interpreted age bounds of the Laxmi Basin oceanic accretion, we carefully examined the interpretations of Bhattacharya et al. (1994a) vis-à-vis the interpretations of Eagles and Wibisono

(2013). We viewed their (ibid.) magnetic profile along with the large amount of magnetic profiles available with us, and observed that the magnetic profile (apparently a R.S.S. Shackleton cruise profile of 1975 vintage) used by them (ibid.) for modelling can not be considered to represent the two limbs of the Laxmi Basin anomalies sequence properly. This is because their (ibid.) profile is located near the northern limit of the Laxmi Basin, where the magnetic lineations start veering towards the Gop Basin. Further, the westerly part of their (ibid.) profile actually merges with the strike of an E-W trending magnetic anomaly high that lies over the Laxmi Ridge. In view of these we could not agree with the C29n-C28n-C29n age bound assigned by them (ibid.) for the Laxmi Basin. Nevertheless, we revisited the interpretation of Bhattacharya et al. (1994a) by taking cognizance of other inconsistency, such as smooth basement despite slow spreading rate, pointed out by Eagles and Wibisono (2013). Further, this revisit also became necessary as C33n-C28n-C33n age of Laxmi Basin oceanic accretion as assigned by Bhattacharya et al. (1994a) was quite at variance with the C31r-C25r-C31r or C29r-C25r-C29r interpretation of Yatheesh et al. (2009) for sequence of anomalies of the neighbouring Gop Basin. We re-modelled the same Laxmi Basin magnetic profile (SK 79-15) used by Bhattacharya et al. (1994a) to find out the possibility of other interpretation options. While doing this re-modelling we considered that the spreading pattern of the Laxmi Basin was similar to that assumed for the Gop Basin, i.e. a reasonable slow to intermediate Half Spreading Rate (HSR) for most of the period and a gradually decreasing very slow (<10 mm/yr) HSR during the waning phase commencing at chron C28ny. Our modelling (Fig. 4) under these two conditions yielded three possible interpretations of the Laxmi Basin anomalies sequence, i.e. either as C33n-C25r-C33n or C31n-C25r-C31n or C30n-C25r-C30n sequences. However, out of these three possible interpretations we favour the C30n-C25r-C30n sequence as it involves least variation of spreading rates for consecutive blocks and the HSR remains in the level of about 20 mm/yr for most of the time only to drop at a very low level (<5 mm/yr) during a waning phase (Fig. 5). This model also suggested a drop in the HSR after the time of peak[3] of DFB volcanism. We believe this reinterpretation also reconciles many other perceived inconsistencies about the situation in the Laxmi Basin. First of all, with this model, there will not be much difference in the ages of the Laxmi Basin and Gop Basin spreading regimes. Secondly, the conjoined Seychelles-Laxmi Ridge block will not be very far from western Indian land mass at the time of DFB event. Thirdly, this higher HSR will be compatible with the relatively smooth nature of the basement. In view of these, for the reconstruction models proposed in the present study, we used the constraints of this revised interpretation of the Laxmi Basin magnetic anomalies.

---

[3]The peak, i.e. the main phase of DFB volcanism (as will be discussed in a later section), which most likely was around 65–66 Ma.
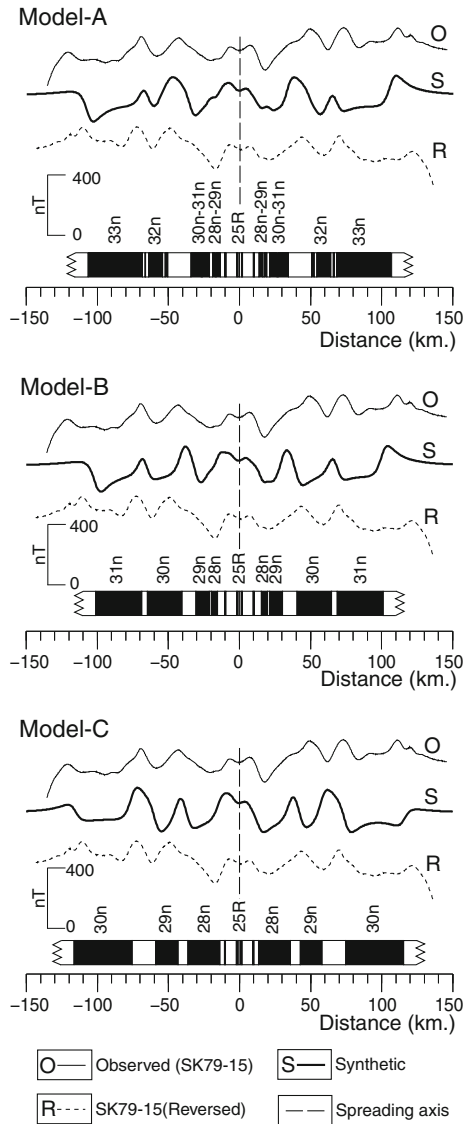
Fig. 4 Interpretative modelling of magnetic lineations of the Laxmi Basin. Three alternative models for interpretation. *Model-A* corresponds to anomaly sequence C33n-C25r-C33n; *Model-B* corresponds to anomaly sequence C31n-C25r-C31n and *Model-C* corresponds to anomaly sequence C30n-C25r-C30n. The simulated magnetic anomalies are shown along with observed anomalies (projected to an azimuth of 60°) along profile SK79-15 of Bhattacharya et al. (1994a). Simulated magnetic profiles were generated for a ridge formed near 15°S, 53°E and presently located near 17°N, 69°E as a N30°W striking body. Assumed magnetized layer (susceptibility 0.01 cgs units) is considered to be flat, 2.0 km thick, and its top lies at 5.5 km below the sea surface. Normally magnetized blocks are indicated with *black*. *Thin dashed line* represents the axis of the Laxmi Basin now extinct oceanic spreading center. *Model-C* is our preferred interpretation
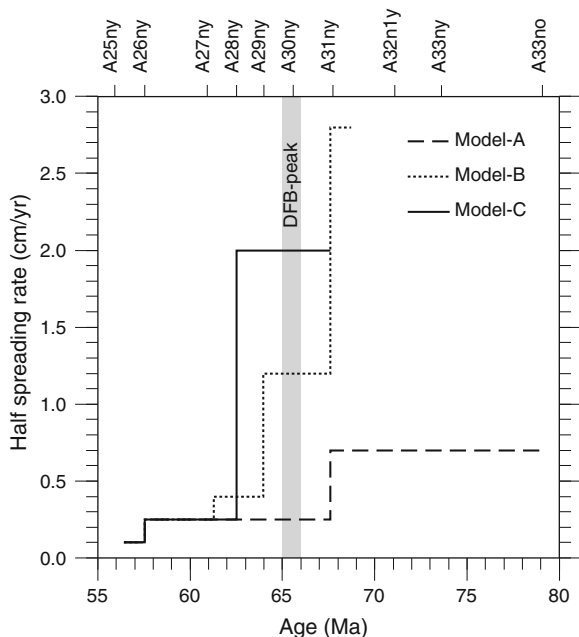
Fig. 5 Variation of half spreading rates yielded by three alternative models proposed (presented in Fig. 4) in the present study for interpretation of magnetic lineations of the Laxmi Basin. *Dashed line* corresponds to *Model-A* (i.e. anomaly sequence C33n-C25r-C33n), *dotted line* corresponds to *Model-B* (i.e. anomaly sequence C31n-C25r-C31n) and *continuous line* corresponds to *Model-C* (i.e. anomaly sequence C30n-C25r-C30n). *Grey shaded limit* (labeled DFB-peak) corresponds to the timing of the peak of Deccan Flood Basalt volcanism on the adjacent western Indian mainland

It may be mentioned here that, Bhattacharya et al.'s (1994a) interpretation of chron C33n (∼79.5 Ma; Late Cretaceous) opening of the Laxmi Basin implied two things. Firstly, it suggested that the opening of the Laxmi Basin was older than the peak of DFB volcanism. Secondly, it implied existence of Mesozoic basins on the flanks of the Laxmi Basin. We noted that a study (Roberts et al. 2010) of specially processed high quality seismic reflection data reported existence of Mesozoic basins underlying basalt (DFB?) layer on the continental margin off Mumbai (i.e. on the eastern flank of the Laxmi Basin). If this interpretation is correct, then it confirms our implied suggestions. The chron C30no (∼67.6 Ma) opening of the Laxmi Basin, as revised in the presented study, also conform to those implied suggestions.

The axial part of the Laxmi Basin is characterized by a narrow quasi-linear NNW-SSE trending basement high zone (Fig. 2), which at places is expressed (Bhattacharya et al. 1994b) as subtle subcrop and at few places the basement high zone is overlain by large seamounts. Rao et al. (1992) inferred this axial basement high zone as a ∼360 km long feature and named it as the Panikkar Ridge. Interestingly, the inferred extinct spreading centre of the Laxmi Basin (Bhattacharya et al. 1994a) was observed to approximately coincide with this basement high zone.

2.4.2 The Gop Basin

The Gop Basin (Figs. 2 and 3) is the ∼100 km wide deep offshore region located immediately north of the E–W trending northerly segment of the Laxmi Ridge (Yatheesh et al. 2009). The Gop Basin can be considered as a sub-basin of the larger Offshore Indus Basin (Miles et al. 1998; Bhattacharya and Chaubey 2001) i.e. the large deepwater area lying between the landward boundary of the Laxmi Ridge and the India–Pakistan continental shelf. Malod et al. (1997) were the first to recognize the Gop Basin (referred by them as Gop Rift) as a distinct entity in view of its basement fabric and conspicuous magnetic lineations. They (ibid.) inferred that the basement of the Gop Basin forms a sediment-filled E-W graben with a prominent central E–W trending basement high zone. They (ibid.) designated this basement high feature as 'Palitana Horst'; however following Yatheesh et al. (2009) hereafter we refer this feature as 'Palitana Ridge'.

Most researchers agree that the Gop Basin represents an oceanic crust formed by an extinct seafloor spreading regime. However, opinion varies regarding the location of the extinct spreading center (ESC) and thereby the identification of the conspicuous magnetic lineations (see Fig. 6a of Yatheesh et al. 2009) of the basin. Yatheesh et al. (2009) proposed that the Palitana Ridge represents the ESC of the Gop Basin and opined that magnetic anomalies across the Palitana Ridge ESC can be reasonably explained as the axi-symmetric magnetic anomalies sequence, either C31r-C25r-C31r or C29r–C25r-C29r. On the other hand, Minshull et al. (2008) and Collier et al. (2008) placed the ESC of the Gop Basin to a different basement high about ∼50 km north of the Palitana Ridge and thereby considered a different segment of the magnetic lineations as representing the axi-symmetric magnetic anomalies sequence of the Gop Basin. Collier et al. (2008) arrived at three different possible sequences to explain the axi-symmetric magnetic anomalies of the Gop Basin (corresponding to their ESC), such as, C29r–C28r-C29r, or C31r–C29r-C31r, or C32n.1r–C31r-C32n.1r. In contrast to this, Minshull et al. (2008) opined that the entire sequence of the same axi-symmetric magnetic anomalies segment can be due to basement relief on a single reversed polarity block (C29r or C31r) and the edge effects at the margins of such a block. Detail critique of these various interpretations is beyond the scope of this paper. However, we would like to mention that, we have thoroughly examined (Bhattacharya and Yatheesh under preparation) the location of the extinct spreading center proposed by Collier et al. (2008) and Minshull et al. (2008), in the backdrop of large magnetic database of the area available with us and the published seismic reflection data (Calvès et al. 2011; Gaedicke et al. 2002) of various vintage acquired by different organizations. From this examination, we came to the conclusion that, the magnetic anomaly, which Collier et al. (2008) and Minshull et al. (2008) considered as axial anomaly (corresponding to their ESC) actually coincides with the zone of SDRs identified (Calvès et al. 2011) at the southern edge of the Saurashtra Volcanic Platform (SVP), which as will be discussed later, represents a thinned continental crust region north of the Gop Basin. We are not aware that an extinct spreading center was found to be associated with SDRs anywhere in the world oceans. Further, we also observed that the basement

high, which was considered by Collier et al. (2008) and Minshull et al. (2008) as the ESC, actually is a NE-SW trending isolated basement high trend of limited extent and that trend also is not parallel to the distinct E-W trending magnetic lineations of the Gop Basin. In view of these shortcomings, we could not agree with Collier et al. (2008) and Minshull et al. (2008) location of ESC and their consequent identifications of magnetic anomalies sequence of the Gop Basin. Instead, we maintained the conclusion of Yatheesh et al. (2009) that the Palitana Ridge is the ESC of the Gop Basin. Further, out of the two possible identification of the anomalies sequence of Gop Basin proposed by Yatheesh et al. (2009), we adopted the C29r-C25r-C29r model as it provides a reasonable high Half Spreading Rate (HSR) of ∼30 mm/yr for most of the period and a gradually decreasing very slow (<10 mm/yr) HSR during its waning phase of Gop Basin spreading center since chron C28ny (∼62.5 Ma). Admittedly like the situation in the Laxmi Basin, the magnetic anomalies sequence in the Gop Basin also is very short, hence their unique identification is difficult. Therefore these identifications will remain tentative till some other constraints are available to confirm them.

Recent studies (Calvès et al. 2011; Carmichael et al. 2009; Corfield et al. 2010) of the Offshore Indus Basin area brought out the existence of a sediment covered prominent basement platform structure of large areal extent in the areas immediate north of the Gop Basin. The areal extent of the mapped portion (which is restricted within Pakistan EEZ) of this basement platform structure, was reported (Calvès et al. 2011) to be about 42,500 km^2. The structure appears to extend further eastward into Indian EEZ and thus may occupy much greater areal extent. This basement platform structure is inferred to be characterized by volcanic centres, sub-aerial lava flows, volcaniclastic clinoforms and marine volcaniclastic sediments. The extrusive volcanism is estimated to be at least 5 km thick in many parts of the platform. Apparently in view of the predominance of volcanic build up features, Corfield et al. (2010) referred this platform structure as Saurashtra Volcanic Platform (SVP). The northwestern boundary of the SVP is a pronounced linear NE–SW trend that separates the SVP from deep water, probably an oceanic crust strip of Offshore Indus Basin that parallels the Murray Ridge. The published seismic sections suggest that the northern boundary of the SVP is defined by a narrow, thick sediment filled, nearly E-W trending basin that abuts the Pakistan continental slope. Perhaps this E-W basin is a remnant of the fossil Kutch Rift. A prominent fault zone is inferred to exist towards the southeastern part of the SVP. This faulted area conforms to the NE-SW trending so-called Somnath Fracture Zone reported by Malod et al. (1997). The easterly boundary of the SVP is poorly constrained, apparently as the data were restricted within the EEZ of Pakistan. The crustal thicknesses of the SVP region was interpreted (Corfield et al. 2010) to be around 15 km. We observe that the basement grain of the SVP is largely NE-SW which is in clear contrast to the E-W trend of the magnetic lineations of the Gop Basin or its axial Palitana Ridge. Based on reflection seismic data, Carmichael et al. (2009) inferred presence of syn-rift sedimentary packages in the SVP region, which at places were intruded by seamount forming volcanics. Based on reflection seismic data, Calvès et al. (2011) also mapped the presence volcano-stratigraphic features of

Outer and Inner SDRs and the Outer High towards the southwestern boundary of the SVP. According to Planke et al. (2000) such volcano-stratigraphic features are associated with volcanic continental margins. Apparently aided by these identifications, Calvès et al. (2011) demarcated the continent ocean boundary coinciding with the landward edge of the Inner SDRs zone, where the SVP was inferred as an area of stretched continental crust. In view of these observations and inferences and presence of extinct spreading center in the Gop Basin, we infer that the SVP represents a conjugate continental sliver of the Laxmi Ridge in the Gop Basin sector and include the SVP element in our model accordingly.

2.4.3 Proposed Gop-Narmada-Laxmi Triple Junction

As mentioned earlier (Fig. 3), the inferred extinct spreading center of the Gop Basin region (i.e. the Palitana Ridge ESC) trends E-W and that of the Laxmi Basin region trends NW-SE. We believe these distinctly different directions of spreading between a plate pair (India and Laxmi Ridge) is inconsistent unless a third plate is involved in the scenario. We therefore look for those possible three plates, the three plate boundaries separating them and a triple junction connecting these plate boundaries. The spreading centres in the Gop and Laxmi basins obviously represent the two plate boundaries (or arms) of this triple junction. We feel that the Narmada Rift on the Indian peninsula in the east can be considered as the third plate boundary, or the third arm of the triple junction. The reasons for such a consideration are following. As mentioned earlier, three continental rift basins (Kutch Rift, Cambay Rift and Narmada Rift) exist in the western part of adjacent Indian mainland, but location and orientation wise, the Narmada Rift appears a more reasonable candidate for this third arm. The Narmada Rift is an ENE–WSW trending major basinal trend on the Indian mainland. This basin is considered to have developed within a rift graben that meets the western continental margin of India. The inferred Late Cretaceous initiation of the Narmada Rift also appear to be compatible with this three plate scenario, as the spreading/rifting in the Laxmi and Gop basins were also inferred to have commenced during the same period. In such a scenario, the extinct spreading centers of the Gop and Laxmi basins may represent the two ridge axes of an once-active ridge-rift-ridge ternary system of crustal divergence, where the Narmada Rift represented the third, rift arm. Such a proposition, have also been forwarded by Malod et al. (1997). If this assumption about the presence of a ternary system of crustal divergence is correct, then it requires the existence of two separate continental blocks of Indian peninsula across the Narmada Rift at that time. The geological scenario of Indian peninsula appears to support the existence of two such continental blocks. As discussed earlier, the Narmada Rift is considered to have developed along a prominent, ancient line of weakness, which was a Proterozoic proto-continental suture between the northern, Aravalli protocontinent and the southern, Dharwar protocontinent (Naqvi 2005; Sharma 2009). Therefore, when the Narmada Rift developed along that suture, it was causing divergence of the above mentioned two protocontinents. In view of

these we feel, for our model we can reasonably assume the existence of a northern Indian protocontinental block (NPB), which is equivalent to Aravalli protocontinent and a southern Indian protocontinental block (SPB), which is equivalent to Dharwar protocontinent. Further, according to Biswas (1982) the Surat Depression is the offshore extension of the Narmada rift graben trend. In view of such assumption, the genesis of Gop and Laxmi basins can be explained as results of crustal divergences between Greater Seychelles [Seychelles + Laxmi Ridge] and NPB and Greater Seychelles and SPB, respectively. It may be mentioned here that all earlier workers explained the early evolution of the WCMI-ADOB region in terms of a two-plate system. In contrast to those models, we considered the scenario as a three-plate system.

Since this three-plate system required a triple junction to connect the intervening ternary system of crustal divergence, so we postulate the existence of such a triple junction and for ease of further reference in this article we denote that postulated triple junction as Gop-Narmada-Laxmi (GNL) Triple junction. It can be seen (Fig. 3) that, between Saurashtra peninsula and the bight of the Laxmi Ridge, there exists an anomalous wide gravity high zone (AGHZ) centered around 19°30′N, 67° 00′E. Interestingly this AGHZ has similar orientational attitude as the Laxmi Ridge, including its bight. Based on the magnetic anomaly patterns over and around this AGHZ (Yatheesh 2007), it appears that the NW-SE trending Laxmi Basin extinct spreading center and E-W trending Gop Basin extinct spreading center abut this AGHZ. We are tempted to speculate that the central part of this AGHZ perhaps represent the present day location of that postulated fossil GNL triple junction. We further believe, the bight of the Laxmi Ridge also supports the postulation of a triple junction, because such a shape can be inherited by a margin close to a triple junction, where two initial plate boundaries met at an angle. Having postulated the triple junction and its axial framework, we now examine the possible time when the GNL triple junction might have come into existence and its probable genesis.

As has been discussed earlier (in Sect. 2.4.1), an oceanic spreading in the Laxmi Basin had started by the time of C30no (∼67.6 Ma), hence we believe the triple junction can not be younger than ∼67.6 Ma. To guess the minimum older age bound for formation of the triple junction, we considered that the triple junction might have developed as a result of domal uplift of the crust, which preceded the Réunion hotspot related DFB volcanism. According to Basu et al. (1993) the earliest manifestations of DFB volcanism are the alkaline volcanic and intrusive complexes in extensional areas north of the main DFB province, and those volcanics are dated ∼68.5 Ma. It is interesting to note that even a more recent study of Chenet et al. (2007) also identified an older pulse of DFB volcanism between 68 and 67 Ma. In consideration of these above, we believe that the triple junction off Saurashtra perhaps have developed around 68.5 Ma, i.e. contemporaneous with the earliest manifestation of DFB volcanism. We admit that this assumed time of the formation of the GNL triple junction is poorly constrained, but the existence of a ternary rift pattern off Saurashtra well before chron C30no (∼67.6 Ma) appear as a reasonable assumption. Further, although the ternary rift pattern appears to be very similar to situations which lead to splitting of continents in many parts of the world (Burke and

Dewey 1973), this could have also been the outcome of a thermally-induced extensional rifting or a mantle convection induced rifting. Therefore, instead of our assumption, that the genesis of this triple junction is due to crustal doming preceding DFB volcanism, there could be other reason for the genesis of this triple junction. However, due to spatial proximity of the triple junction with the DFB province it may not be unreasonable to assume a causal relationship amongst them as we have assumed. However we feel it puzzling, that neither the pre-existing horst-graben complex closer to west coast of India nor the Cambay rift system evolved into oceanic spreading, when that area came under the influence of Réunion hotspot. Instead the regions of Laxmi and Gop basins, which were further to the west, evolved into oceanic spreading. Possibly this suggests that the Gop–Laxmi basins area, before it came under the influence of Réunion hotspot, was already experiencing some tensional stress, due to development of some pre-Deccan thermal build-up or asthenospheric convection underneath. As a result of which a "ternary rift pattern" had already developed in that region, and that could get easily accentuated under the influence of Réunion hotspot, when it arrived in the adjacent region. If our interpretation of Gop and Laxmi basins magnetic anomalies are correct, then they point towards existence of such a pre-DFB event extension regime in these two areas.

2.5 Seamount Chain of the Laxmi Basin

Three prominent seamounts, namely Raman Seamount, Panikkar Seamount and Wadia Guyot, exist along the axial part of the Laxmi Basin (Figs. 2 and 3). Together, these three seamounts form a ∼N30°W trending linear seamount chain of about 250 km length. These seamounts are the first ones in the Arabian Sea whose detail bathymetry has been established through swath-bathymetric investigations (Bhattacharya et al. 1994b) and they were found to be considerably large in dimensions. The basal areas of these three seamounts range between 300–1200 km^2 and heights range from 1068 to 2240 m. These basal areas and heights are with reference to the surrounding seafloor. Therefore, considering the presence of 1–2 km thick sediment overburden on the surrounding areas (Naini 1980), the actual heights and basal areas of the seamounts, with respect to the basement, will be much greater. The morphology of these seamounts are characterized by relatively flat summit surface, secondary peaks, steep lower flanks with terraces at places, and an extensive pattern of dendritic gully like features. These gullies resemble a relict drainage pattern of sub-aerial erosional origin. Hence, we infer that during course of their growth, those seamounts became wholly/partially sub-aerial for some protracted period during which they experienced erosion, which resulted in the formation of dendritic drainage pattern. The seamounts subsequently subsided and during the course of subsidence, wave-base erosion caused formation of flat terraces/surfaces. Seismic reflection profiles available over Raman and Panikkar seamounts indicated (Srinivas 2004) that the top of those seamounts are covered with ∼500 ms (TWT) thick acoustically transparent sedimentary unit.

This thickness is comparable with the thickness of similar acoustically transparent sedimentary unit observed in seismic records at DSDP drill site 219 in the adjacent Laccadive Plateau. Most likely, these acoustically transparent sedimentary unit over the seamounts represent the carbonate reef build up structures, when the seamount was slowly subsiding from very shallow water depths. This reef build up stopped at some stage, probably when the subsidence rate outpaced the rate of reef growth.

As mentioned in Sect. 2.4.1, this seamount chain clearly overlies the narrow quasi-linear NNW-SSE trending basement high zone, which characterizes the axial part of the Laxmi Basin. When viewed in conjunction with the interpreted magnetic lineations of the Laxmi Basin, it appears that the extents of the seamounts are restricted within the basement younger than chron C28no ($\sim$63.6 Ma). From this we infer that the formation of seamounts has started some time during chron C28n, or in other words they are not older than $\sim$63.6 Ma (i.e. chron C28no). Bhattacharya et al. (1994b) attributed the genesis of the seamount chain to an anomalous volcanism resulting from the interaction of the Réunion hotspot with the extinct or waning Laxmi Basin spreading centre, when they were in close proximity. As will be shown later from the predicted location of Réunion hotspot, the Laxmi Basin spreading center was in close proximity of the hotspot during chron C28n. Thereby, inference of Bhattacharya et al. (1994b) about the genesis of the seamounts looks reasonable.

We believe the growth of the seamounts could not have stopped before cessation of spreading along the spreading centre, because in that case the continued spreading would have caused seamount edifices to be splitted into two halves. It may be mentioned here that the seamount complex of Guadalupe Island of eastern Pacific Ocean is also located above an extinct spreading center, but there it is inferred that the building up of Guadalupe seamount complex commenced probably several million years after the spreading center became extinct (Batiza 1977). Such a post spreading-abandonment genesis can also be argued for the Laxmi Basin seamounts. But, that option appears unlikely in the case of the Laxmi Basin seamounts, because the presence of a hotspot in the vicinity and thereby hotspot–spreading ridge interaction is apparent here, whereas there is no evidence of a hotspot activity in the vicinity of Guadalupe seamount complex. From these, we infer that volcanism along the Laxmi Basin seamounts also stopped simultaneously with the extinction of Laxmi Basin spreading center during chron C25r, when the seamount area moved far away from the area of influence of the Réunion hotspot.

The dendritic gullie pattern observed over the Laxmi Basin seamounts was inferred to have been caused by sub-aerial erosion. A sub-aerial erosional origin of these gullies necessitates emergence of the entire edifices above sea level and subsequent subsidence by about 3700 m (Bhattacharya et al. 1994b). A subsidence of this magnitude appears to be anomalously high as compared to the inferred (Whitmarsh et al. 1974) subsidence of only 2075 m of the nearby DSDP Site 219 over the Laccadive Plateau. Perhaps this difference in subsidence amounts is indicative of differing lithospheric domains of the Laccadive Plateau and the Laxmi Basin. The Laccadive Plateau region subsided less as this area corresponds to thicker continental lithosphere, whereas the seamounts subsided more as their loads

were emplaced over relatively thinner oceanic lithosphere of the Laxmi Basin. The sedimentary history of DSDP Site 219 over the nearby Laccadive Plateau in the south suggested that, after deposition of shallow water (water depths of less than 100 m) limestones, sandstones and siltstones of Late Paleocene age (ibid.) on a subsiding foundation, the site began to sink in Early Eocene (56.0–47.8 Ma) time. We presume that the Laccadive Plateau started subsiding only when the area was no more under the influence of Réunion hotspot, which had caused bulging of crust in that area. Further, as the location of DSDP Site 219 is much southwards of the Laxmi Basin seamounts, therefore we can also assume that the effect of Réunion hotspot on the Laxmi Basin seamounts area might have stopped before the time its influence stopped in the area of Site 219. In view of these, we infer that the seamounts started subsiding after their growth stopped some time during chron C25r ($\sim$57.6–56.4 Ma). Perusal of seismic reflection records across Raman Seamount does not indicate any deformation of the flanking sequence of Indus Fan sediments. This perhaps indicates that the subsidence of seamounts stopped before the Indus fan sediments were deposited in the Laxmi Basin area, probably around Middle to Late Oligocene time (i.e. $\sim$23.0–28.0 Ma). Subsidence of the Laxmi Basin seamounts could have even stopped earlier, but definitely not at a time younger to this period.

It may be mentioned here that so far no plate-tectonic evolutionary model of the Western Indian Ocean has taken cognizance of these Laxmi Basin seamounts. Therefore we attempted to weave into our model the broad sequence of events, which we think are inferable from the Laxmi Basin seamounts.

2.6 The Laccadive Basin

The Laccadive Basin (LAB) is a narrow triangular shaped basin lying (Fig. 2) between the Laccadive Plateau in the west and the continental slope of south-western India in the east. Towards north, this basin appears to extend up to $\sim$16°N, where the northern extremity of the Laccadive Plateau apparently converge with the adjacent continental slope off central part of western India. Towards south, this basin appears to open into the Central Indian Basin (Bhattacharya and Chaubey 2001). However, in consideration of a recent study (Yatheesh et al. 2013b) we consider that the southern extent of the Laccadive Basin, to a large extent, abuts the Chain–Kairali Escarpment (CKE). The water depth in this basin varies from $\sim$2000 m in the north to $\sim$2800 m in the south. The width of the basin gradually decreases from $\sim$215 km in the south to $\sim$70 km in the north. The basement of this depression is complicated by normal faulting and a series of basement tilted blocks. The total thickness of sediments varies broadly between 200 and 3200 m but at few places it reaches a maximum value of about 5500 m. The underlying basement widens and deepens towards south and is characterized by several basement high features (DGH 2014; Bhattacharya and Chaubey 2001 and references therein). As rightly pointed out by Gunnell (2001), the exact nature of

the crust underlying the LAB has not been established as yet. Based on observations of rotated fault blocks akin to half-grabens, which flank a central basement high, Chaubey et al. (2002b) suggested that the basin represents a failed rift and volcanism of the stretched continental regime. While studying the morphotectonic architecture of the adjacent submarine Alleppey Trivandrum Terrace Complex (ATTC), Yatheesh et al. (2013b) have demonstrated by gravity anomaly modelling, that the crust in the LAB region could either be a much thinned continental crust or an anomalously thick oceanic crust.

So far no seafloor spreading type magnetic lineations have been reported from any part of this basin. It could be that the seafloor spreading type magnetic anomalies actually existed in the Laccadive Basin, but they were obscured by overprinting of Réunion hotspot related volcanism, when that hotspot was close to the area between ∼60–55 Ma. In view of this ambiguous nature of the underlying crust and to explain its triangular shape, for the present study we consider that Laccadive Basin was formed as a result of a crustal divergence that separated Laccadive Plateau from southern Indian peninsula and the rift/spreading ridge that caused this divergence gradually progressed from south to north. Further, we also assumed that the LAB divergence system were active during the interval between stoppage of N-S trans-tensional movement along eastern Madagascar margin and initiation of margin oblique seafloor spreading between Laccadive Plateau and eastern Madagascar. We came to this conclusion because, as will be discussed later, the shear movement across CKE appears to have taken place between southern Laccadive Plateau and SE coast of Madagascar on one side and the ATTC region on the other side.

2.7 India–Madagascar–Seychelles Separation Related Volcanisms

Various researchers considered that the separations of India, Madagascar and Seychelles are causally and temporally related to two widespread and few localized volcanic emplacements evident on the land areas of these continental blocks. The older of these two widespread volcanic emplacements, considered to be related to separation of India and Madagascar, is Late Cretaceous in age and is represented by the ∼83.6–91.6 Ma aged Cretaceous volcanic rocks of Eastern Madagascar, the ∼85–91 Ma aged igneous rocks of southwestern India and the St. Mary Islands on the adjacent Indian offshore (Valsangkar et al. 1981; Storey et al. 1995; Torsvik et al. 2000; Pande et al. 2001; Melluso et al. 2009; Radhakrishna and Joseph 2012). These older set of igneous rocks are considered to have resulted, (i) either as direct magmatism of Marion hotspot, where thick lava piles at Volcan de l'Androy located in the southeastern Madagascar mark the focal point of the Marion hotspot activity, or (ii) from the rift related extensional processes initially induced by Marion hotspot (Torsvik et al. 2000). It may be worthwhile to note that on the Madagascar side such igneous rocks are considered to be present almost along the

entire stretch of straight eastern coast of Madagascar, whereas on the Indian side such older igneous rocks could only be found in the areas of southwestern India. An explanation (Kumar et al. 2001) for this enigmatic absence of those older igneous rocks on northern and central part of western India could be that those rocks, even if exists, presently underlie the younger DFB volcanics, which almost entirely covers those regions. We think a satisfactory explanation for such a conspicuous absence is required to be found, as it may provide better understanding of the process by which the initial wide rift zone between India and Madagascar developed.

The second of these two widespread volcanic emplacements, is represented by the extensive and mainly tholeiitic Deccan Trap Flood Basalts (commonly known as Deccan Traps but referred as DFB; see Misra et al. 2014), which encompass an area of about 500,000 km^2 of the western and central India. The published literatures suggest considerable difference of opinion regarding the age, duration and even about genesis of DFB volcanism. It was generally believed (Courtillot et al. 1988; Vandamme et al. 1991; Hooper 1999; Sen 2001) that bulk of DFB erupted around 65–66 Ma within a simple C30N-C29R-C29N magnetic polarity sequence and a large fraction of the activity to have taken place during the middle reversed chron C29R. On the contrary to this general belief, Pande (2002) based on a critical evaluation of the available absolute age data and paleomagnetic constraints, concluded that DFB volcanism continued over a prolonged period from ∼69 to ∼62 Ma with several episodes of eruptions punctuated by periods of quiescence and the most intense pulse occurred around ∼67 Ma (∼chron C30R). Further, according to him (ibid.) the duration of DFB volcanic activity, instead of a simple C30N-C29R-C29N magnetic polarity sequence, appears to have continued over a longer period encompassing several N-R-N magnetic polarity sequences. In a later publication, Courtillot and Renne (2003) maintained support to the theory of short duration (∼1.0 myr) of DFB volcanism and concurred with the results of Hofmann et al. (2000) that bulk of Deccan volcanics erupted close to 65.5 Ma. The more recent study of Chenet et al. (2007) identified two pulses of DFB volcanism. The smaller but significant earlier pulse of volcanism was between 68 and 67 Ma, and after a quiescence of about 2–3 Ma the major phase of volcanism occurred around 65 Ma.

The genesis of DFB is another subject of debate. Many researchers (e.g. Morgan 1981; Courtillot et al. 1986; Devey and Stephens 1991) believe this to have been caused by plume magmatism when the Indian Plate came over the Réunion hotspot. However, Sheth (2005) has contested the plume theory as far as the origin of the DFB is concerned and proposed a non-plume, plate-tectonic model involving continental break-up and related mantle convection and decompression melting. According to Bhattacharji et al. (1996), the onset of the main DFB eruptions during 67–64 Ma was with concurrent reactivation of the intra-plate Narmada Rift and N-S crustal extension. The peak of eruptive activities occurred at 65–66 Ma with propagation of dikes from a plume center located at the intersection of the present day Narmada and Cambay rifts. Some authors (Chatterjee and Rudra, 1996; Chatterjee et al. 2006) even suggested that DFB volcanics owes its origin to magma generated from melting of the lithosphere caused by a large bolidal ('Shiva bolide') impact in the areas near the present day 'Bombay High'. We do not have any

evidence to support or contradict this bolidal impact theory, but some behaviours of the seafloor spreading systems of the WCMI-ADOB region appears to suggest passage of the region over the Réunion hotspot. This aspect will be discussed in a later section. Mahoney et al. (2002) concluded that the Bibai volcanics from the Quetta–Zhob area of Pakistan, dated 73.4–72.0 Ma, represents the marine phase of Réunion hotspot activity in an area northwards of the main DFB province on the Indian subcontinent. Therefore, if the genesis of DFB is attributed to Réunion hotspot, then considering their (ibid.) conclusion, the Indian subcontinent region might have experienced the effect of Réunion hotspot much earlier than believed so far. Discussion about the merits/demerits of these inferences related to age, duration etc. of DFB is beyond the scope of the present article. We mentioned these aspects only to highlight that knowledge about the age, duration, main phase of DFB volcanic activity, genesis etc. of DFB, as it stands today, is not sacrosanct and it is still evolving. Some of these changes appear to have resulted due to evolution of geochronological dating techniques or geochemical analysis tools and methodologies. In view of this situation, we urge caution while anchoring interpretation of other geophysical data, particularly related to evolution of WCMI-ADOB region on the existing knowledge about the age, duration, genesis etc. of DFB.

The other localized volcanics considered to be related to India–Madagascar–Seychelles separation, are represented by the Late Cretaceous–Paleocene volcanic rocks from the islands and offshore areas of the continental fragment of the Seychelles Plateau and the Amboronala volcanics of the northeast coast of Madagascar. Some of these volcanic occurrences of Seychelles region are the ~69–73 Ma aged tholeiitic dykes of Praslin Island, the ~60–63 Ma aged alkaline rocks of the Silhouette and North Islands (Plummer and Belle 1995 and references therein) and the 63.7 ± 1.1 Ma aged tholeiitic basalts drilled at ODP site 707 (Duncan and Hargraves 1990). It was inferred (Devey and Stephens 1991) that the tholeiitic dykes of Praslin Island are geochemically very similar to the Bushe formation magmas of the DFB. Ganerød et al. (2011) have recently provided a revised dating between 63.0 and 63.5 Ma for the alkaline rocks of the Silhouette and North Islands. From the isotopic and trace element compositions of the Seychelles alkaline suite, Owen-Smith et al. (2013) concluded that these magmas were derived from the Réunion hotspot source, equivalent to that of the DFB, with an additional minor contribution from an enriched source, likely sub-continental mantle lithosphere. Thus it can be seen that the volcanics of the Seychelles Plateau area, which are believed to be related to DFB event have a wide range of age starting from 73 Ma (which is nearly the age of Bibai volcanics mentioned earlier) to 63.0 Ma, which is the age of the oldest magnetic anomaly identified north of Seychelles. It is agreeable that this age range is nearly same as of DFB, and on that basis Late Cretaceous–Palaeocene volcanic rocks of Seychelles Plateau region can surely be considered as coeval with DFB, but it is not clear to us, how confidently one could say that this Late Cretaceous–Palaeocene volcanics of Seychelles Plateau surely were derived from the Réunion hotspot source.

The southern part of Seychelles Plateau is considered to have been separated from the northeastern continental margin of Madagascar. According to Plummer (1995)

the ∼91.0 Ma dated (Randrianaloso et al. 1981 cited in Plummer 1995) volcanics present at the Amboronala on the northeast coast of Madagascar relates to the short phase of transform rifting and pull-apart basin formation that separated Seychelles Plateau from Madagascar. However, volcanics are yet to be recognized in Seychelles Plateau related to the rift between Seychelles Plateau and Madagascar, which is predicted to have occurred at around 96–84 Ma (Plummer 1995).

2.8 Constraints from Madagascar

Madagascar is the largest island (Fig. 6) of the Indian Ocean area. By now it stands well established that Madagascar, Seychelles Plateau and India were once a conjoined continental landmass in the Gondwanaland framework. In that conjoined framework, the straight edges of eastern and northeastern Madagascar are considered to have been facing the western India and southern Seychelles Plateau respectively. Even though researchers agree on the concept of this conjoined Madagascar-Seychelles-India continental landmass, opinions differ regarding their exact juxtaposition, in particular in their immediate pre-drift scenario. Probably lack of distinct and dependable 'piercing points', which could have constrained these juxtapositions, is one of the reasons for such varied inferences.

Considerable research has been carried out to examine the compatibility and congruity of the onshore geological and tectonic scenario of Madagascar and India. Although, such relationship do not appear to be straightforwardly discernible, still in broad sense the Precambrian geology of Madagascar and the south Indian shield area have geological affinity in many aspects. For example both India and Madagascar are characterized by Archean-greenstone terrains to the north and the Proterozoic granulite terrains to the south (Yoshida et al. 1999 and references therein). The Precambrian terrain of Madagascar, like the Precambrian terrain of the southern India, also contains several shear zones, the most prominent of which are the Ranotsara Shear Zone and Angavo Shear Zone. Based on lithological and geochronological similarity, two cratonic strips of eastern Madagascar are considered to be 'chipped-off-parts' of the westernmost boundary of the Western Dharwar Craton (WDC) of India. These cratonic strips are the Antongil and Masora cratonic blocks, which are located close to the northern and central part of eastern coast of Madagascar (Raval and Veeraswamy 2003 and references therein). The eastern Madagascar contains a remarkable continental scale topographic scarp, which according to Subrahmanya (2001) appear as a mirror image of the Western Ghat Escarpment of western Indian Peninsula. We found this feature interesting in the context of India—Madagascar juxtaposition and rifting and therefore included in our proposed model. Gunnell and Harbor (2008) denoted this feature as 'Angavo Escarpment' and made detail examination of its morphological similarities with the Western Ghats Escarpment of India. The Angavo Escarpment (AnE) is manifest as the steep eastern edge of the westward tilting central highlands of Madagascar (Fig. 6). This AnE is nearly 1000 km long lineament that is even perceptible in the
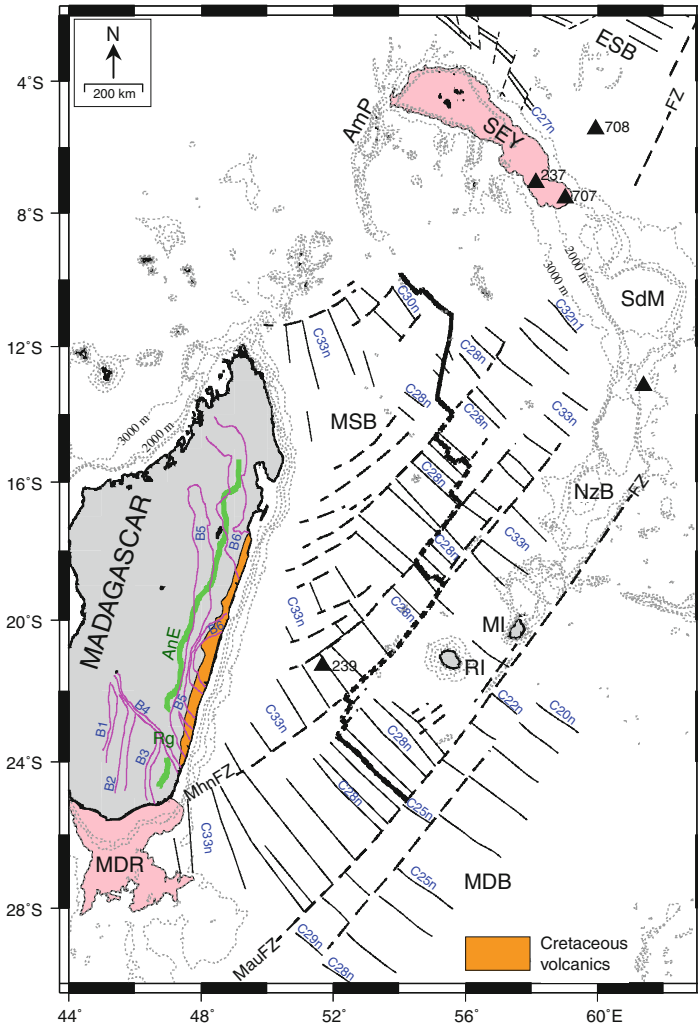
Fig. 6 Generalized map of the land and deep ocean basin areas adjoining the Seychelles–Mascarene Plateau Complex and Madagascar for depicting the locations of various onshore and offshore tectonic elements referred in the text. These tectonic elements were compiled from several publications (Eagles and Wibisono 2013; Ratheesh-Kumar et al. 2014; Matthews et al. 2011). *Thick green line* (labeled AnE) along the eastern edge of Madagascar mainland represents Angavo Escarpment (digitized from satellite imagery available at http://en.wikipedia.org/wiki/File: Madagascar_sat.png). *Pink lines* over land areas represent the inferred shear zones. *B1* Amphanihy Shear Zone; *B2* Betroka Shear Zone; *B3* Tranomaro Shear Zone; *B4* Ranotsara Shear Zone; *B5* Angavo Shear Zone; *B6* Betsimisaraka Shear Zone. Other abbreviations used are as in Table 1 and the other details are as in Figs. 1 and 2

satellite imagery. The westward tilt of the central highlands is highlighted by westward course of all major drainage systems over it. The AnE has a major topographic breach in its continuity, the Ranotsara Gap. This Ranotsara Gap (Rg) and the Palghat Gap (Pg) of India is considered to have common genesis in a cross-cut Precambrian shear zone (Palghat–Cauvery Shear Zone) structure that continued from India to Madagascar (Gunnell and Harbor 2008). The present day location and morphology of this escarpment possibly is also the outcome of various processes, such as, denudation, scarp retreat and marine regression. The eastern and north-eastern edges of Madagascar contain volcanic emplacements that are inferred to be related to separation of Madagascar from India and Seychelles and we have discussed those volcanic emplacements in the preceding section.

The continental shelf of Madagascar is generally narrow, averaging about 25 km in width. At some places, all along the northeast coast, no shelf is present. The straight east coast is bordered by the narrow shelf whose edge appears as a fault scarp (Pepper and Everhart 1963). Transform motion between India and Madagascar dating prior to the opening of the Mascarene Basin has been suggested as responsible for the linearity of the shelf, but its details are controversial. From the characteristics of gravity anomalies, a strip of extended continental crust appears to exist in the eastern continental margin of Madagascar further eastwards of the continental shelf (Eagles and Wibisono 2013). The landward terminations of fracture zone traces in satellite derived gravity anomalies map appears to suggest that such extended continental crust is predominant in the areas off the central part of eastern Madagascar.

2.9 Constraints from Seychelles

The Seychelles Bank is the northern end of a long arcuate complex [Seychelles–Mascarene Plateau complex (SMP)] of wide, partially isolated shallow banks and small islands, that is located (Figs. 1 and 6) in the areas between Madagascar Island and the Central Indian–Carlsberg ridge segments. Except the Seychelles Bank part, the genesis of other parts of SMP still remains ambiguous. Although situated in an oceanic environment, the continental character of the Seychelles Bank has been confirmed from the presence of Precambrian granitic rocks, of ~ 700 Ma age, as basement of many of the islands. The seismic refraction profiling also indicated a continental crustal thickness of ~ 33 km beneath the Seychelles Bank (Laughton et al. 1970; Khanna and Walton 1992 cited in Plummer and Belle 1995; Collier et al. 2009 and references therein). Being surrounded by oceanic crust, the Seychelles Bank thus qualified as a Precambrian continental fragment in the Western Indian Ocean. This oval shaped bank, of an area of about 80,000 km^2, has an almost flat top lying at an average water depth of 50 m. The edge of the bank is

well defined by steep slopes, which drops to depths exceeding 3000 m in all directions, except for the southwest and the southeast. The Seychelles Bank is connected by a 2000 m deep saddle to the Amirante Plateau in the southwest, whereas to the southeast it abuts a 1500 m deep saddle [Seychelles-Saya de Malha saddle (SSM)] that in turn connects with the other elements of the SMP (Bhattacharya and Chaubey 2001 and references therein). The crustal nature of complete SSM up to Saya de Malha Bank is not yet established. However, the seismic data (Plummer 1996) suggested the presence of tilted fault blocks akin to rifted continental crust near the location of DSDP site 237 and ODP-707. Further, the basalts drilled at ODP site 707 (dated at 63.7 ± 1.1 Ma) was inferred to have been extruded sub-aerially or in very shallow water during a period of transition between continental rifting and the initiation of the spreading center (Duncan and Hargraves 1990; Plummer 1995). In view of these, we have considered that the continental crust regime of the Seychelles Bank area extends at least up to the location of ODP site 707 and refer that extended continental crust regime as Seychelles Plateau. The remaining part of the SMP perhaps was formed as a result of passage of the region over the Réunion hotspot (Duncan 1981; Morgan 1981). Rifting between NE Madagascar and the Seychelles Plateau was probably in the form of a pull-apart basin that was initiated between 100 and 95 Ma from a releasing bend that joined the East African–Tethyan transform fault and the transform fault adjacent to eastern Madagascar. The Amirante Plateau (AmP) is a ∼400 km long arcuate conjoined ridge-trough system, which extends southwards from northwestern limit of the Seychelles Plateau. Genesis of the AmP still remains an enigma. Some researchers (Plummer and Belle 1995; Plummer 1996) opined that AmP developed due to complex geodynamics effected modification of a transform boundary that coincided with northernmost point of Madagascar and western most point of Seychelles. While Mukhopadhyay et al. (2012) suggested that AmP is the product of a short duration subduction event in the northern Mascarene Basin region, when the oceanic crust of the area experienced compression due to the combined effects of commencement of spreading of the Carlsberg Ridge and cessation of spreading in the Mascarene Basin.

2.10 Constraints from Mascarene Basin

The Mascarene Basin (Fig. 6) is bordered on the west by the steep and linear eastern margin of the Madagascar Precambrian massif and to the east by the arcuate Seychelles–Mascarene Plateau complex. The northerly extent of the Mascarene Basin is considered to be defined by a boundary joining the northern tip of the Madagascar Island, the Farquhar Group of Islands, the Amirante Plateau and the Seychelles Plateau, while the NE-SW trending Mauritius Fracture Zone is

considered to define its southerly boundary. The fact that Mascarene Basin represents an oceanic domain formed by an extinct seafloor spreading regime was recognized during the initial magnetic studies of the region (Schlich 1982 and references therein). However, apparently due to paucity of data and complexity of magnetic fabric, the identifications of anomalies and fracture zones at that time were restricted only to the southern part of the basin. Several subsequent studies (Dyment 1991; Sahabi, 1993; Bernard and Munschy 2000; Bissessur et al. 2009; Eagles and Wibisono 2013) aided with more magnetic transects, satellite derived gravity anomalies and other tectonic informations, improved the identifications of magnetic lineations and fracture zones and extended many of those identifications even to the northerly part of the basin. The present understanding is that the Mascarene Basin contains two-limbed magnetic anomalies sequence C34ny through C27ny and the spreading became extinct some time shortly after chron C27ny. Further, the extinction appeared to have progressed gradually from the north across the basin. The magnetic lineations trend approximately northwest-southeast and series of northeast-southwest trending fracture zones offset the magnetic lineations. The Mascarene Basin is considered to be divided into northern and southern parts. The geometrical relationship of the magnetic lineations with the adjacent Madagascar continental margin is different in these two parts. The southern Mascarene Basin is adjacent to the straight eastern edge of the Madagascar and the oldest magnetic lineations are oblique to this straight margin. The northern Mascarene Basin lies eastwards of the straight north-eastern edge of the Madagascar peninsula and the magnetic lineations in that area are margin parallel. The widths of the oceanic crusts accreted during same periods are also different in these two parts. The oceanic crust of the southern Mascarene Basin is relatively wider as compared to contemporary oceanic crust of northern Mascarene Basin. It has been earlier believed that the northern Mascarene Basin sector evolved due to ocean crust accretion between the Seychelles Plateau and the north-eastern edge of the Madagascar peninsula, whereas the southern Mascarene Basin evolved by ocean crust accretion between the continental margins off western India and the eastern Madagascar. The Mascarene Basin appears as the northwestern continuation of the Madagascar Basin. However these two basins, despite geographical contiguity, are considered as two separate entities due to following reasons. The Madagascar Basin does not represent an extinct spreading regime oceanic crust like Mascarene Basin. Rather, the spreading in the Madagascar Basin, which commenced around chron C30ny, was a separate spreading ridge segment; where the conjugate of oceanic crust accreted during C30ny-C20ny period formed part of the Central Indian Basin in the north and the oceanic crust of further younger accretion till present lies across the Central Indian Ridge (Schlich 1982). Since anomaly C34ny (83 Ma) is the oldest identified anomaly in the Mascarene Basin off Madagascar margin, hence it is believed that the seafloor spreading in the Mascarene Basin commenced sometime during Late Cretaceous (Norton and Sclater 1979; Besse and Courtillot 1988).

However, as this time falls under the Cretaceous long normal superchron, the precise age of the rift-drift transition could not be determined from the magnetic lineations.

3 Data and Adopted Methodology

The main continental blocks/slivers, which have been considered in our reconstruction models, are India (IND), Madagascar (MAD), Seychelles Plateau (SEY), Laxmi Ridge (LAX) and Laccadive Plateau (LCP). For reference to various features in this study, we have used the nomenclatures proposed by Bhattacharya and Chaubey (2001). The term India unless specified refers to Indian subcontinent that includes the geographical and political regions of India and Pakistan.

The continent-ocean boundary in the study area is poorly constrained; as a result, the extents of the continental blocks under consideration were defined by various researchers using different criteria. Following Norton and Sclater (1979), we used the 2000 m isobaths to define the boundaries of India and Madagascar continental blocks. We defined the extent of the Seychelles Plateau by the 2000 m isobath surrounding the Seychelles Bank and part of the SSM up to the location of ODP drill well 707. The basement high feature of the Laxmi Ridge is buried under sediment and its physiographic expression lies at depths greater than 2000 m. Therefore we approximated the outline of the Laxmi Ridge based on the extents of the characteristic gravity anomaly low as decipherable from image and contours of the satellite-derived free-air gravity anomalies and the mapped seafloor spreading magnetic lineations in the surrounding Arabian (Chaubey et al. 2002a), Gop (Yatheesh et al. 2009) and the Laxmi (Bhattacharya et al. 1994a; Yatheesh 2007) basins. In this study we considered the Laccadive Plateau as a continental sliver and used the surrounding 2000 m bathymetry contour to approximate its extent. However, its southern extent have been extended (by including few isolated 2000 m contour closures in such a way that the extent of Laccadive Plateau touches the Chain-Kairali Escarpment in the reconstruction of immediate pre-drift juxtaposition.

During the course of discussion in this article, as far as possible the event timings have been mentioned with reference to an integrated geologic time scale (Table 2). The directions, wherever mentioned are with respect to present day orientations of the concerned features, they will be somewhat different if viewed in the context of their paleo-position. All the plate-tectonic reconstructions presented in this paper were computed with the software package ROTPXY (Bhattacharya and Yatheesh 2013) and the Euler rotation parameters wherever estimated in this study were made using GPlates package (Boyden et al. 2011). Finite rotation parameters describing

Table 2 Integrated geologic time scale for the period under consideration in this study. The ages of stratigraphic boundaries are based on Walker et al. (2013) and the ages of seafloor spreading magnetic anomalies are based on the geomagnetic time scale of Cande and Kent (1995)

Era	Period	Epoch		Age (Ma)	Anomaly number and Age (Ma)
CENOZOIC	Paleogene	Eocene	Middle	47.8	
			Early		C24n (52.36-53.35)
				56.0	C25n (55.90-56.39)
		Paleocene	Late		C26n (57.55-57.91)
				59.2	
			Middle		C27n (60.92-61.28)
				61.6	C28n (62.50-63.63)
			Early		C29n (63.98-64.75)
				66.0	C30n (65.58-67.61)
MESOZOIC	Cretaceous	Late			C31n (67.74-68.74)
					C32n (71.07-73.00)
					C33n (73.62-79.08)
				100.0	C34n (83.00-118.0)
		Early			
				145.0	

relative motions between various plates/continental slivers used for making plate-tectonic reconstruction maps in the present study are given in Table 3.

All the reconstructions presented in this study (Figs. 7a–i) are in fixed African (now Somali) plate reference frame. Earlier, in absence of directly estimated Indian–African plate Euler rotation parameters, reconstructions of India with respect to African plate were achieved by following the Indian–Antarctic and then Antarctic–African plate rotation circuit. Euler rotation parameters estimations for Indian–African plate relative motion during chron C27ny–chron C21ny, are now available (Royer et al. 2002) directly from conjugate Arabian and Eastern Somali basins magnetic picks. Similarly, Eagles and Wibisono (2013) provided the Euler rotation parameters estimations for Indian–African plate relative motion during chron C34ny to ∼60.25 Ma (i.e. time of abandonment of Mascarene Basin

Table 3 Finite rotation parameters describing relative motions between various plates used for making plate-tectonic reconstruction maps in the present study. Angle is positive when the motion of the moving plate is counter clockwise with respect to the fixed plate when viewed from outside the earth. Ages are after Cande and Kent (1995). CST Cessation of spreading/rifting; INT Initiation of spreading/rifting

Chron	Age (Ma)	Finite rotation parameters			Reference
		Lat. (deg.)	Long. (deg.)	Angle (deg.)	
(a) *Seychelles block to Laxmi Ridge* ($_{LAX}$ROT$_{SEY}$)					
C25ny	55.904	19.41	29.02	30.111	Royer et al. (2002)
C26ny	57.554	19.61	25.62	30.729	Royer et al. (2002)
C27ny	60.920	18.83	24.86	35.411	Royer et al. (2002)
C28ny	62.499	23.57	−20.08	23.799	This study
Close-fit	62.800	20.75	−47.00	24.750	This study
(b) *Laxmi Ridge to Southern Indian Protocontinent* ($_{SPB}$ROT$_{LAX}$)					
CST	56.400	−8.95	78.79	0.000	This study
C26no	57.911	−8.95	78.79	−0.100	This study
C28ny	62.499	−8.95	78.79	−0.460	This study
C28no	63.634	−8.95	78.79	−1.000	This study
C29ny	63.976	−8.95	78.79	−1.740	This study
C29no	64.745	−8.95	78.79	−2.700	This study
C30ny	65.578	−8.95	78.79	−3.020	This study
C30no	67.610	−8.95	78.79	−4.200	This study
INT	68.500	−8.95	78.79	−7.500	This study
(c) *Saurashtra Volcanic Platform to Laxmi Ridge* ($_{SVP}$ROT$_{LAX}$)					
CST	56.400	20.68	56.77	0.000	This study
C28ny	62.499	20.68	56.77	−1.280	This study
C29no	64.745	20.42	60.79	−9.760	This study
INT	68.500	19.22	70.28	11.114	This study
(d) *Laccadive Plateau to Southern Indian Protocontinent* ($_{SPB}$ROT$_{LCP}$)					
CST	56.400	15.26	68.32	0.000	This study
C28ny	62.499	15.26	68.32	10.000	This study
C34ny	83.000	15.26	68.32	18.000	This study
INT	88.000	15.26	68.32	20.000	This study
(e) *Northern to Southern Indian Protocontinent* ($_{SPB}$ROT$_{NPB}$)					
CST	56.400	26.00	94.00	0.000	This study
INT	68.500	26.00	94.00	1.000	This study
(f) *Southern Indian Protocontinent at 60.25 Ma to Madagascar* ($_{MAD}$ROT$_{SPB}$)					
CST	60.250	−15.91	−163.75	0.000	Eagles and Wibisono (2013)
C27ny	60.920	−15.99	−163.66	0.570	Eagles and Wibisono (2013)
C28ny	62.499	−18.09	−160.76	2.060	Eagles and Wibisono (2013)
C28no	63.634	−17.26	−161.82	3.050	Eagles and Wibisono (2013)
C29no	64.745	−17.11	−162.41	5.060	Eagles and Wibisono (2013)

Table 3 (continued)

Chron	Age (Ma)	Finite rotation parameters			Reference
		Lat. (deg.)	Long. (deg.)	Angle (deg.)	
C30ny	65.578	−15.06	−158.30	6.940	Eagles and Wibisono (2013)
C30no	67.610	−16.73	−158.93	9.590	Eagles and Wibisono (2013)
C31no	68.737	−18.51	−160.06	10.270	Eagles and Wibisono (2013)
C32n1y	71.071	−20.29	−160.67	11.960	Eagles and Wibisono (2013)
C33ny	73.619	−22.42	−162.39	13.120	Eagles and Wibisono (2013)
C33no	79.075	−31.59	−171.23	13.580	Eagles and Wibisono (2013)
C34ny	83.000	−21.19	−152.99	18.000	This study
Close-fit	88.000	−21.19	−152.99	20.270	This study

spreading modified as per Cande and Kent 1995 timescale), directly from conjugate anomaly picks of the Mascarene Basin. Therefore we have carried out the required reconstructions in fixed African plate reference frame by using these two direct estimations of Indian–African plate relative motions. By following this route, we could also avoid the effect of deformation in the Central Indian Basin. We however adopted the Indian–African plate rotation parameters of Eagles and Wibisono (2013) for period younger to chron C34ny. We felt that the chron C34ny rotation parameters estimate of Eagles and Wibisono (2013) is not well-constrained as they had chron C34ny pick only in one flank of the Mascarene Basin. Therefore, we estimated the Indian–African plate rotation parameters for the chron C34ny and further close-fit by trial and error until we got an improved fit for the ATTC and the bathymetric notch of the northern Madagascar Ridge. For reconstructions of continental slivers (including Seychelles Plateau), we followed the following approach: (i) reconstructed sliver to India for close fit and considered that close fit sliver position as sliver's new position, (ii) reconstructed that sliver's new position to desired reconstruction time using appropriate sliver—India rotation parameters, (iii) considered those reconstructed sliver positions as fixed to Indian plate and achieved their further reconstruction with respect to African plate in the same way as was done for Indian plate.

4 Proposed Plate-Tectonic Evolution Model

We describe our views about the plate-tectonic evolution of the eastern part of the Western Indian Ocean for the period ∼88.0 to ∼56.4 Ma, through a sequence of plate-tectonic reconstruction maps made in fixed Africa reference frame (Figs. 7a–i). We consider this period to correspond to the early evolution of the western
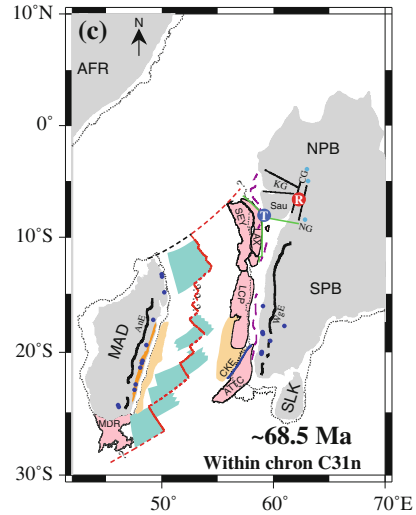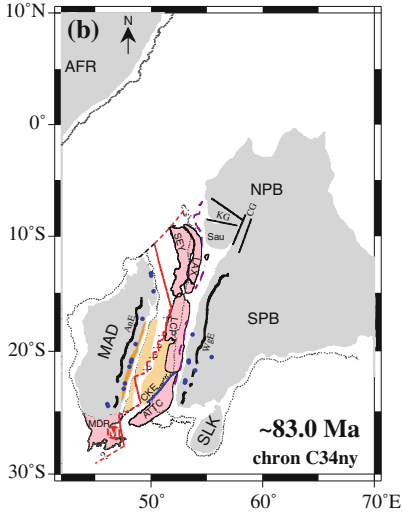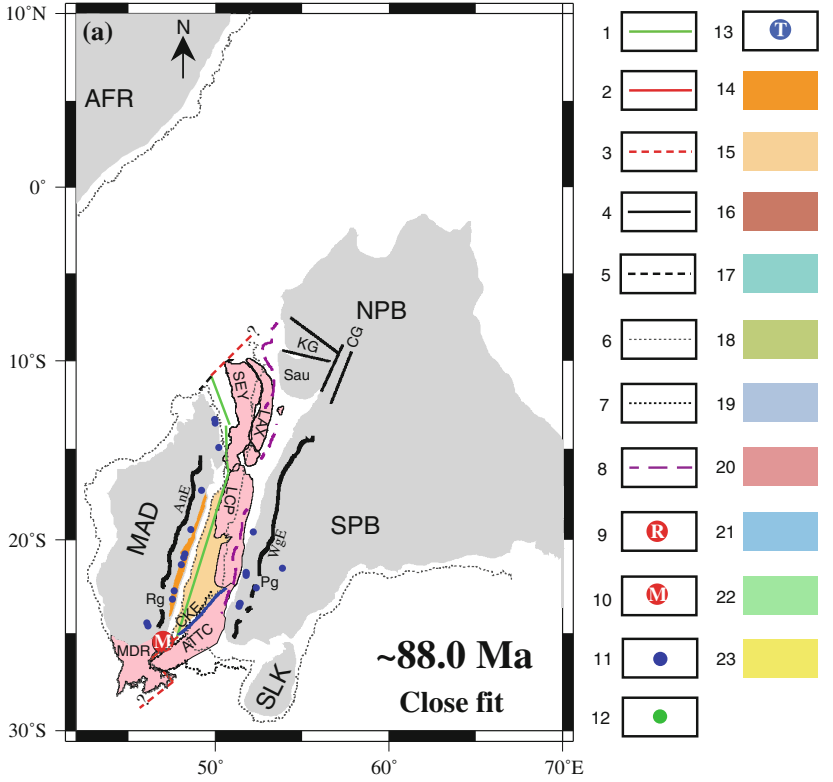
◀ **Fig. 7** Simplified plate-tectonic reconstruction maps (in fixed Africa reference frame) of the Western Indian Ocean region depicting evolution of the ocean basins and associated tectonic features discussed in this study. **a** Reconstruction for a close-fit juxtaposition of involved continental blocks at 88.0 Ma (Late Cretaceous). **b** Reconstruction for chron C34ny (~83.0 Ma, Late Cretaceous). **c** Reconstruction at 68.5 Ma (within chron C31n; Late Cretaceous). **d** Reconstruction for chron C30no (~67.6 Ma, Late Cretaceous). **e** Reconstruction for chron C29no (~64.7 Ma, Early Paleocene). **f** Reconstruction for chron C28ny (~62.5 Ma, Early Paleocene). **g** Reconstruction for chron C27ny (~60.9 Ma, Middle Paleocene). **h** Reconstruction for chron C26no (~57.9 Ma, Late Paleocene). **i** Reconstruction for chron C25no (~56.4 Ma, Late Paleocene). *NG* Narmada rift graben dividing the Indian continental areas into northern (NPB) and southern (SPB) proto-continental blocks: Explanation of items of the legend—*1* Rift axis; *2* Ridge axis; *3* Transform fault; *4* Extinct spreading centre; *5* Paleo Transform fault; *6* 2000 m isobath; *7* 2500 m isobath; *8* Paleo shelf edge; *9* Réunion hotspot location for the time of the presented reconstruction. Trailing open circles corresponds to the predicted Réunion hotspot locations for times of successive previous reconstructions; *10* Marion hotspot location for the time of the presented reconstruction; Rift stage crust; *11* Locations of 80.0–92.0 Ma volcanics; *12* Locations of 60.0–70.0 Ma volcanics; *13 T* postulated Gop-Narmada-Laxmi (GNL) fossil triple junction off Saurashtra peninsula (Sau); *14* Deccan Trap volcanics; *15* Ultra thinned continental crust; *16* Oceanic/rift stage crust of the Laccadive Basin; *17* Oceanic crust formed during 83.0–68.5 Ma; *18* Oceanic crust formed during 68.5–67.6 Ma; *19* Oceanic crust formed during 67.6–64.7 Ma; *20* Oceanic crust formed during 64.7–62.5 Ma; *21* Oceanic crust formed during 62.5–60.9 Ma; *22* Oceanic crust formed during 60.9–57.9 Ma; *23* Oceanic crust formed during 57.9–56.4 Ma. Other abbreviations used are as in Table 1. Note that the comprehensive legend of symbols, shades, designs given in Fig. 7a as well the abbreviations provided in this caption are common to the reconstruction maps 7a–i for denoting/labelling various features. Oceanic crust was shaded only at places where identified magnetic lineations are available. Other details are as in Figs. 1, 2, 3 and 6

continental margin of India and the adjacent deep offshore basins. The reconstructions presented are for 88.0 Ma (close-fit), 83.0 Ma (chron C34ny), ~68.5 Ma (within chron C31n), ~67.6 Ma (chron C30no), ~64.7 Ma (chron C29no), ~62.5 Ma (chron C28ny), ~60.9 Ma (chron C27ny), ~57.9 Ma (chron C26no) and ~56.4 Ma (chron C25no). Recently Gibbons et al. (2013) forwarded an updated model of East Gondwanaland breakup, wherein they have incorporated several of the constraints from the Cretaceous ocean basins around India, which were not considered in earlier reconstructions. However, our model somewhat differs from theirs (ibid.) in a way, because of our detail treatment of the constraints from the WCMI-ADOB region.

4.1 From Gondwanaland to India-Madagascar Break-up, the Evolution in Brief

It is generally believed that arrangement of continents, continental fragments and ocean basins as we see today in the Indian Ocean area is related to the fragmentation and dispersal of components of the Gondwanaland. The Gondwanaland was comprised of present-day South America, Africa, Arabia, Madagascar, Seychelles, India, Sri Lanka, Antarctica, Australia and New Zealand. The fragmentation of
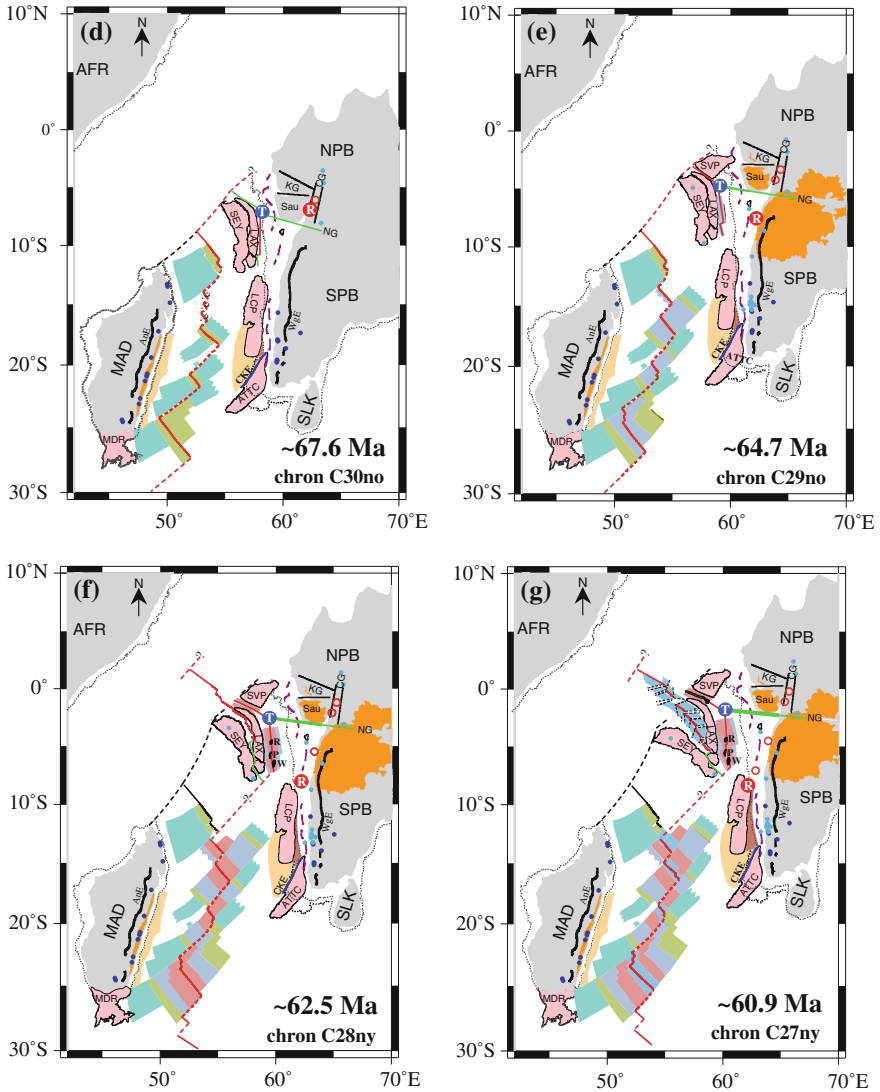
Fig. 7 (continued)

Gondwanaland seems to have resulted from its interaction with a series of hotspots or mantle plumes and the Karoo mega-plume effect is considered to be the cause (Lawver et al. 1998) of the first split of the Gondwanaland into two halves, the east Gondwanaland and the west Gondwanaland. This split was manifested with the commencement of seafloor spreading at ~150 Ma (chron M22, Late Jurassic) between those two halves along short E-W trending spreading segments offset by long N-S trending transform faults. This seafloor spreading ultimately resulted in

Fig. 7 (continued)

the formation of Mozambique, Western Somali and probably Northern Somali basins and thus marked the opening of the Indian Ocean. The rifting episode, which preceded this split, might have been initiated several million years before this time. Afte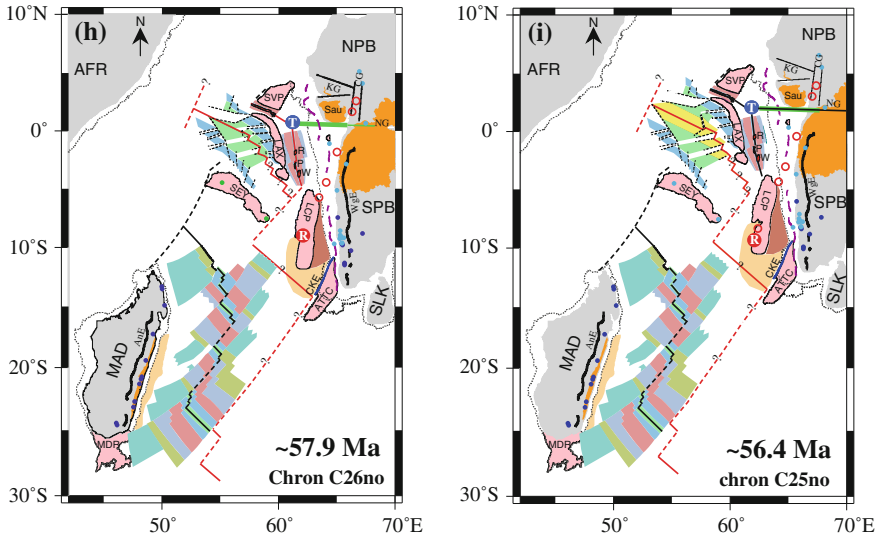r the first split, the east Gondwanaland moved south with respect to west Gondwanaland and both the Gondwanaland halves witnessed further splits in the subsequent period. The evolution of the Indian Ocean area is related to further break-up of east Gondwanaland, which consisted of Antarctica, Australia, New Zealand, Madagascar, Seychelles, India and Sri Lanka. Around 136 Ma (chron M11n, Early Cretaceous) a conjoined Madagascar-Seychelles-India-Sri Lanka continental block rifted and drifted away from conjoined Antarctica-Australia. Following separation of Madagascar-Seychelles-India-Sri Lanka block from Antarctica-Australia block, a uniform pattern of seafloor spreading continued for the subsequent ∼15 myr. However, after this period the spreading pattern between Africa-Arabia and Madagascar-Seychelles-India-Sri Lanka blocks experienced a change. In the changed scenario, shortly after the time of anomaly M0 (∼118 Ma, Early Cretaceous), spreading stopped in Western Somali and Northern Somali basins, while it continued in the Mozambique Basin. As a result of this spreading center reorganization, the conjoined Madagascar-Seychelles-India-Sri Lanka block got attached to African plate (Rabinowitz et al. 1983; Bhattacharya and Chaubey 2001 and references therein). The subsequent rifting and drifting of Madagascar-Seychelles-India-Sri Lanka block closely relates to the early evolution of the WCMI-ADOB region, the focus of the present paper and we discuss that part in detail in the following sections.

4.2 India-Seychelles-Madagascar Pre-break-up Close Fit Scenario (~88.0 Ma; Late Cretaceous)

Our model of early evolution of the WCMI-ADOB region begins with the presentation of a reconstruction (Fig. 7a) at about 88.0 Ma, which we infer was the time when all the continental blocks/slivers under consideration were juxtaposed in their immediate pre-drift close fit configuration. However, at that time Sri Lanka, which was attached to southeastern coast of India in Gondwanaland configuration, attained its present position with respect to India probably being separated from India by an aulacogen (Bhattacharya and Chaubey 2001 and references therein). Earlier, Yatheesh et al. (2006) ascribed this close fit time as 86.5 Ma, but we revise that time to 88.0 Ma in consideration of the average 88.0 Ma ages of the rift related volcanics emplaced on the eastern edge of the Madagascar.

At that time a wide continental rift zone of hitherto obscure origin existed between the larger continental blocks of India and Madagascar. This rift zone developed in a direction parallel to the pre-Cambrian Dharwarian basement grain and was flanked on the west by the eastern edge of Madagascar and on the east by the western edge of the Indian peninsula. In appreciation of suggestions of Gunnell and Harbor (2008) and Subrahmanya (2001) perhaps it can be assumed that the western shoulder of this major rift zone was expressed on the eastern Madagascar as the Angavo Escarpment and the conjugate eastern shoulder of the rift was in the western India as the Western Ghat Escarpment. The horst graben complex, which characterizes a major part of the present day continental shelf of western India perhaps was another contemporary feature related to that rifting parallel to Dharwarian basement grain. The thinning crust of the wide rift zone was the parental material from which the smaller continental blocks/slivers of Seychelles Plateau, Laxmi Ridge, Laccadive Plateau, etc., had developed. The Seychelles Plateau and Laxmi Ridge at that time was not separate entities, and we refer that conjoined continental sliver as Greater Seychelles. The major southerly part of the Laxmi Ridge area of the Greater Seychelles and the Laccadive Plateau were juxtaposed to western India perhaps with a Dharwarian basement grain parallel NNW-SSE trending zone of crustal weakness in between. The northwestern part of the Laxmi Ridge area of Greater Seychelles was adjacent to that part of the Saurashtra Arch, which forms its deep water part at present. Further, the area situated between this northwestern part of the Laxmi Ridge and the northwestern Indian peninsula perhaps contained the remnants of pre-existing older (of Jurassic age) Kutch rift and/or relatively younger (of Late Cretaceous age) Narmada rift.

With all those zones of weaknesses, initially between ~ 100 and ~ 88 Ma, the movement of crustal blocks across the major rifts between India and Madagascar were N-S translational, perhaps to accommodate the reorganized direction of relative plate motions across the incipient southeast Indian Ridge. During this period of translational motion, a major transform fault existed along the eastern edge of Madagascar, along which the Madagascar was gradually sliding with respect to continental slivers of Laccadive Plateau and southerly part of Greater Seychelles.

This transform fault adjacent to eastern Madagascar was connected to an East African–Tethyan transform fault system via a releasing bend passing between Seychelles continental block and the northeastern Madagascar (Plummer 1996; Plummer and Belle 1995). During the relative movement of these continental blocks across this transform boundary, a remarkably straight eastern continental edge developed between eastern Madagascar and opposing continental slivers while the releasing bend between Seychelles and the northeastern Madagascar evolved into a pull-apart basin. In the 88 Ma juxtaposition model, the southern extent of ATTC region fitted into the bathymetric notch of the northern Madagascar Ridge and the conjoined Seychelles Plateau-Laxmi Ridge and the Laccadive Plateau have been accommodated with nearly their present outlines. It may be mentioned here that we have been guided by this 88.0 Ma juxtaposition to iteratively arrive at the assumed southern limit of the Laccadive Plateau. We believe this 88.0 Ma reconstruction (Fig. 7a) clearly suggests that the southern limit of the continental sliver of the Laccadive Plateau can be considered to extend only up to the northern boundary of ATTC, which in turn is defined by the Chain-Kairali Escarpment. With these outlines, at places some overlaps could be seen onto the present day continental shelf areas, which we believe, do not pose serious challenge to our proposed juxtaposition model. This is because the extent of these continental slivers surely were much less in their original pre-thinning state and considering the much landward location of the seismically imaged paleo-shelf edge, a tighter fit also looks feasible. It is agreeable that these blocks would have fitted slightly better and closer within their un-stretched dimension but the overall scenario would have remained the same. It may be worthwhile to mention here that all existing plate-tectonic models suggest that, except the conjugate areas of Seychelles, the remaining part of western margin of India was conjugate to eastern margin of Madagascar. Whereas according to our proposed model the conjugate of eastern Madagascar was not the western margin of India, rather it was mostly the western margin of the continental sliver of the Laccadive Plateau.

4.3 Reconstruction at Chron C34ny (~83 Ma; Late Cretaceous)

The chron C34ny (~83.0 Ma) reconstruction (Fig. 7b) corresponds to 5.0 myr younger time than the previous reconstruction. Shortly before this time, a seafloor spreading system (Mascarene Basin spreading system (MBSS)) had developed between the northeastern margin of Madagascar and the Seychelles Plateau in the north, and the eastern margin of Madagascar and the Laccadive Plateau in the south. The MBSS thus initiated the formation of the Mascarene Basin and separation of Madagascar from SEY + LAX + LCP + SPB + NPB blocks. Based on extents and orientations of the magnetic lineations of chron C34ny, which is the oldest identified magnetic lineation of the Mascarene Basin, we infer that in the northern Mascarene

Basin area (i.e. between Seychelles and northeastern Madagascar, the MBSS was margin parallel. Whereas in the southern Mascarene Basin (i.e. between eastern margin of Madagascar and the Laccadive Plateau) the MBSS at that time was comprised of short, oblique to the margin segments, which were connected by en-echelon short transform offsets. The margin-oblique southern segment of MBSS developed within the thinned continental crust lying between Madagascar and the Laccadive Plateau. With the commencement of oceanic opening, part of that thinned crust got attached to Madagascar as its continental margin and part got attached to Laccadive Plateau as its continental margin. The existence of margin-oblique spreading segments in the southern Mascarene Basin at chron C34ny and a transform fault in the same locale prior to initiation of spreading, perhaps suggest a leaky transform fault origin of that spreading system. Perhaps, the transform fault, that earlier existed east of Madagascar gradually developed into leaky transform fault and then into spreading ridge segments, as the area came under the influence of Marion hotspot in the southern vicinity and the spreading commenced in a direction compatible with the contemporary regional relative plate motion direction.

At this time under the influence of Marion hotspot or due to some other tectonic stress, a northward propagating rift was initiated in the regions between the Laccadive Plateau and the southern Indian Protocontinental block (SPB) and as a result the SPB started slowly sliding north-eastwards with respect to Laccadive Plateau. This sliding probably was accommodated along a pre-existing line of weakness, which later evolved into the Chain-Kairali Escarpment (CKE) on the southwestern continental margin of India. Further southwestward extension of this line of weakness appear to align with a transform offset trend, which in due course will evolve into the Mahanoro FZ of the Mascarene Basin. We would like to mention here that, earlier Yatheesh et al. (2013b) inferred that CKE is a major sheared margin segment of the Indian continental margin along which the continental margin off the nearly straight southeast coast of Madagascar glided past India. Now, we revise that inference slightly to propose that the shear movement across CKE appear to have taken place between southern Laccadive Plateau and SE coast of Madagascar on one side and the ATTC region on the other side. Similar shearing along another pre-existing line of weakness, which was inherited by another transform offset of the Mascarene Basin, might have separated Laccadive Plateau from its northern neighbour of Greater Seychelles.

4.4 Reconstruction at 68.5 Ma (Within Chron C31n; Late Cretaceous)

The ∼68.5 Ma reconstruction (Fig. 7c) is for a time falling within the normal chron C31n and it corresponds to 14.5 myr younger time than the previous reconstruction. We propose that by this time a ternary rift system (rift-rift-rift) with a triple junction (GNL Triple junction) came into existence off Saurashtra peninsula of western India. Whatever may be the mode of genesis or timing of formation, we propose that at

68.5 Ma the southern arm of this rift system was propagating southward and was causing gradual divergence of the conjoined Seychelles-Laxmi Ridge and the SPB. The eastern arm of this rift system was propagating eastward as the Narmada rift, which was causing gradual divergence of the NPB and SPB. The western arm of this rift system was propagating westward and was causing gradual divergence of the conjoined Seychelles-Laxmi Ridge from NPB. The southern arm of the rift system in due course will give rise to the oceanic Laxmi Basin, hence we refer this rift arm as Laxmi Basin axis of divergence (or Laxmi Basin AoD). The western arm of the rift system in due course will give rise to the oceanic Gop Basin, hence we refer that western rift arm as Gop Basin axis of divergence (or Gop Basin AoD). The Narmada Rift arm of the system in due course will become a failed rift (aulacogen).

By this time the rift between SPB and Laccadive Plateau, referred hereafter as the Laccadive Basin axis of divergence (or Laccadive Basin AoD), also might have propagated some distance further northward and caused further crustal divergence between SPB and the Laccadive Plateau. On the Madagascar side, Marion hotspot moved away southwards and seafloor spreading continued in both the northern and southern Mascarene Basin.

4.5 Reconstruction at Chron C30no (~67.6 Ma; Late Cretaceous)

The chron 30no (∼67.6 Ma) reconstruction (Fig. 7d) corresponds to 0.9 myr younger time than the time of previous reconstruction. At that time on the Indian side, the Laxmi Basin AoD reached the stage of seafloor spreading in its northerly part and thus commenced the formation of the oceanic Laxmi Basin between the continental margins adjacent to the SPB and the NW-SE trending southern segment of the Laxmi Ridge. However, towards south the Laxmi Basin AoD might have still continued as a southward propagating rift. We inferred this situation based on our proposed revised identification (discussed in an earlier section) of the oldest and conjugate seafloor spreading magnetic lineations of chron C30no (∼67.6 Ma) in the Laxmi Basin. Crustal extension and outward propagation might have continued at that time along the Gop Basin AoD and easterly Narmada arm of the rift. On the Madagascar side, seafloor spreading continued in both the northern and southern Mascarene Basin. The Laccadive Basin AoD continued its northward propagation resulting further divergence between SPB and the Laccadive Plateau.

4.6 Reconstruction at Chron C29no (~64.7 Ma; Early Paleocene)

The chron C29no (∼64.7 Ma) reconstruction (Fig. 7e) corresponds to 2.9 myr younger time than the time of previous reconstruction. By this time on the Indian

side, the Gop Basin AoD reached the stage of seafloor spreading and as a result the GNL triple junction has become a ridge-rift-ridge (R-r-R) triple junction. Initiation of spreading in the Gop Basin was preceded by volcanic emplacements on the thinned continental crustal areas northwards of Gop Basin, which was identified by Calvès et al. (2011) as the Saurashtra Volcanic Platform (SVP). The SVP thus forms the conjugate of the east-west trending northerly part of the Laxmi Ridge and presence of SDRs on the southern margin of SVP (Calvès et al. 2011) perhaps indicate this margin was volcanic in nature. By this time in the Laxmi Basin area spreading ridge developed almost up to the northern extremities of the Laccadive Plateau. As the divergence continued along the Laccadive Basin AoD, the Laccadive Basin developed into a triangular shaped basin. The seafloor spreading continued in the southern Mascarene Basin but in the northern Mascarene Basin the spreading appears to have slowed down substantially after chron C30no ($\sim$67.6 Ma). Interestingly this slowing down appears to be contemporaneous with the time of initiation of seafloor spreading in the Laxmi Basin.

4.7 Reconstruction at Chron C28ny (~62.5 Ma; Early Paleocene)

The chron C28ny ($\sim$62.5 Ma) reconstruction (Fig. 7f) corresponds to 2.2 myr younger time than the time of previous reconstruction. According to us, this time corresponds to the oldest magnetic lineation inferred in the Arabian Basin. At this stage two significant developments took place; the Greater Seychelles broke into the Seychelles Plateau and the Laxmi Ridge by development of a new spreading center, while spreading in the northern Mascarene Basin ceased. This new spreading center between the Seychelles Plateau and the Laxmi Ridge will later develop into the Carlsberg Ridge. The basalts drilled at ODP site 707 (dated at 63.7 ± 1.1 Ma) on the Seychelles Plateau perhaps were emplaced shortly before this stage during the period of transition between rifting of Greater Seychelles and the initiation of this spreading center. The break-up between the Laxmi Ridge and the Seychelles Plateau started while seafloor spreading in the Laxmi and Gop basins were still continuing. Probably the proximity of the Réunion hotspot was a reason for these developments. The Seychelles Plateau and the Laxmi Ridge was getting separated by short segments of spreading centers in the westerly part and by short segments of rifts in the easterly part. This system of spreading center/rifts, of the then Carlsberg Ridge, was connected with the spreading system in the southeastern Mascarene Basin by a long transform offset. This was also the time when the first stage of unique spreading ridge propagation commenced along the short segments of the Carlsberg Ridge with a dominant westward propagation direction. Formation of the Laxmi Basin seamounts commenced some time during chron C28n perhaps as result of interaction of the waning Laxmi Basin spreading center with the Réunion hotspot in the proximity.

On the Madagascar side, seafloor spreading continued in the southern Mascarene Basin and divergence continued along the Laccadive Basin AoD.

4.8 Reconstruction at Chron C27ny (~60.9 Ma; Middle Paleocene)

The chron C27ny (∼60.9 Ma) reconstruction (Fig. 7g) corresponds to 1.6 myr younger time than the time of previous reconstruction. By this time some more rift segments in the easterly part of the Carlsberg Ridge spreading center/rifts system developed into oceanic spreading centers, as if the Carlsberg Ridge system was attempting to attain close proximity of the Réunion hotspot, which was near the northern extremity of the Laccadive Plateau. The ridge propagation, which commenced earlier during chron C28ny with a dominant westward propagation direction continued till this time and transferred crust from the Eastern Somali Basin to the Arabian Basin. Continued spreading/rifting across the Carlsberg Ridge by this time created a triangular wedge of oceanic crust between the Laxmi Ridge and the Seychelles Plateau. Based on predicted track of the Réunion hotspot, it appears that the Laxmi Basin spreading axis was in the closest proximity of the hotspot at this time. Therefore increased melt supply might have caused the seamounts to grow rapidly, even to become sub-aerial. On the Madagascar side, seafloor spreading continued in the southern Mascarene Basin and divergence continued along the Laccadive Basin AoD.

4.9 Reconstruction at Chron C26no (~57.9 Ma; Late Paleocene)

The chron C26no (∼57.9 Ma) reconstruction (Fig. 7h) corresponds to 3.0 myr younger time than the time of previous reconstruction. We consider this was the time when the waning phase of seafloor spreading, with very slow spreading rate, commenced in both the Gop and Laxmi basins spreading centers, while spreading developed along the full length of the Carlsberg Ridge. The ridge propagation along the Carlsberg Ridge continued during this time but sometime during chron C26r the propagation direction appears to have changed. At the time of C26no the Carlsberg Ridge had a long western segment and several short easterly segments and the propagation direction along these segments was broadly eastward. Since chron C27ny lineations were the youngest lineations observed on both flanks of the southern Mascarene Basin, therefore we assume that spreading in the Mascarene Basin ceased some time between chron C27ny and chron C26no. After cessation of spreading in the entire Mascarene Basin area, the spreading center probably jumped north between the southern end of the Laccadive Plateau and the northern boundary

of the Mascarene Basin. This way the Mascarene Basin spreading center relocated itself closer to Réunion hotspot. Perhaps in due course of time around 45 Ma, this relocated spreading center will further relocate itself over the Réunion hotspot and will cause the formation of the Saya de Malha Bank. With cessation of spreading, the Mascarene Basin together with Seychelles Plateau became part of the African plate. Although spreading ceased in the Mascarene Basin, it continued in the Madagascar Basin. Perhaps at that time the spreading center between the Laccadive Plateau and the northern boundary of the Mascarene Basin was connected with the Madagscar Basin and Carlsberg Ridge spreading centers by long offset transform faults. The divergence continued along the Laccadive Basin AoD.

4.10 Reconstruction at Chron C25no (~56.4 Ma; Late Paleocene)

The chron C25no ($\sim$56.4 Ma) reconstruction (Fig. 7i) is our last reconstruction and it corresponds to 1.5 myr younger time than the time of previous reconstruction. We choose this time, because we infer that sometime during the preceding reverse geomagnetic polarity period (i.e. within C25r period (57.554 Ma–56.391 Ma)); (i) seafloor spreading in the Gop Basin ceased and the extinct spreading center of the Palitana Ridge came into existence, (ii) seafloor spreading in the Laxmi Basin ceased and the extinct spreading center of the Panikkar Ridge came into existence, (iii) the extension regimes in the Narmada Rift zone stopped and it became a failed rift (aulacogen), and (iv) the crustal divergence regime in the Laccadive Basin stopped. Stoppage of these divergence regimes caused stoppage of the drifting away of the Laccadive Plateau and the Laxmi Ridge from India and both these continental fragments reached their present position relative to India and got welded with the Indian plate. Volcanism along the Laxmi Basin seamounts also had stopped simultaneously with the extinction of Laxmi Basin spreading center during chron C25r and the Laxmi Basin area started gradually subsiding. The eastward ridge propagation which commenced at chron C26no along the Carlsberg Ridge continued in the same directional sense till this time.

4.11 Some Unresolved Problems and Demerits of the Model

The evolutionary model of WCMI-ADOB region presented in this study accommodated most of the available dependable information and integrated separate ideas into a framework of the early evolution of the region. We hope this model will stimulate further research, particularly those leading towards understanding of the processes related to the genesis and evolution of the WCMI-ADOB region. This model is also expected to provide useful constraints for improving the evolutionary

model of the Indian Ocean region as a whole. This model being quantitative, can also become a very useful tool for the researchers for various related studies, such as; (i) to examine the validity of the juxtaposition of various onshore tectonic elements which are inferred as conjugate, and (ii) to study the spatial and temporal evolution of sedimentary units of the offshore basins of the region in detail. However, despite these advantages and improvements in knowledge, we also observe that there remain some crucial knowledge gaps that need to be filled. Therefore, in the following paragraphs we specifically mention the knowledge gaps about few such important tectonic elements and also mention some thinkable demerits of this model. We hope these mentions will help developing appropriate investigations in future that can fill the required knowledge gaps and achieve a better understanding of the early evolution of the study area.

4.11.1 The Age of the Laxmi and Gop Basins Oceanic Crusts

As mentioned earlier, there is a broad agreement that the Laxmi and Gop basins are underlain by oceanic crust and they contain linear magnetic anomalies, which can be equated to two-limbed seafloor spreading sequences across extinct spreading centers. However, there is considerable difference of opinion regarding the identification of those anomalies and thereby the ages related to seafloor spreading history of these basins. These age constraints are not only required for correct plate tectonic reconstructions, they are also important requirements to understand the processes related to the fragmentation of the involved continental blocks. The existence of large Deccan Flood Basalt province, which is assumed to represent the impingement of Réunion hotspot in the vicinity, appear to show bias towards implication of this hotspot while explaining the genesis and geodynamic evolution of various tectonic features of the WCMI-ADOB region. The short sequences surely are making it difficult to unambiguously identify the magnetic anomalies in terms of geomagnetic polarity time scale. Establishing the age of the underlying oceanic crust by dating the basement rocks collected at some locations through deep sea drilling can help identification of those magnetic anomalies. An alternate approach for identification of these anomalies perhaps would be to use high resolution magnetic data collected by deep tow magnetic systems. The high resolution magnetic data can provide characteristic signatures of the anomalies which can aid their identification. Until such age constraints are obtained, the early geodynamic history of the WCMI-ADOB region cannot be established in proper temporal framework.

4.11.2 Nature of Crust of the Laccadive Plateau and Laccadive Basin

One of the significant aspects of the evolutionary model of the WCMI-ADOB region presented by us is that we have considered the Laccadive Plateau as a continental fragment. As discussed earlier, the understanding about the genesis of

Laccadive Plateau is still ambiguous, and possibility of it being a continental sliver cannot be ruled out. Recent reporting (Ajay et al. 2010) of the presence of SDRs on the western edge of the Laccadive Plateau perhaps adds more credence to the continental sliver genesis of the Laccadive Plateau. Nevertheless our assumption is in variance with the commonly held belief that the Laccadive Plateau area represents the volcanic trace of the Réunion hotspot. Admittedly, we are not the first to assume Laccadive Plateau as a continental fragment for any plate-tectonic reconstruction. Earlier, Yatheesh et al. (2006) demonstrated that Laccadive Plateau can be accommodated as an intervening continental fragment in an India–Madagascar juxtaposition in immediate pre-drift scenario and Laccadive Plateau was included as a continental fragment in a model of early opening of the Arabian Sea proposed by Yatheesh (2007). Laccadive Plateau was also considered by Ganerød et al. (2011) and Torsvik et al. (2013) as a continental fragment in their reconstructions of the Western Indian Ocean that were made in different contexts. We believe, our reconstructions suggest that Laccadive Plateau as a continental sliver can be reasonably accommodated in the framework of the early evolution of the WCMI-ADOB region. Further, it can be seen from different reconstructions presented by us, that the predicted track of the Réunion hotspot passes through the region covered by the Laccadive Plateau. We believe, this situation do not contradict the continental sliver genesis of the Laccadive Plateau, because a continental sliver region, even if comes over a plume, will have volcanic emplacements, and if the plume trail covers a considerable stretch of the sliver, then the emplaced volcanics may even show age progression. A similar situation is evident in the DFB province of the western Indian peninsula, where the volcanics were emplaced over the continental basement as it passed over the Réunion hotspot and gradual younger volcanics were emplaced from north to south of the region. We agree that our model does not confirm the continental sliver genesis of the Laccadive Plateau. That confirmation has to await further studies to establish the structure and nature of the crust of the region. Till then our model can be the basis for an alternate line of thinking for further research on geodynamics of the region.

As discussed earlier, the Laccadive Basin is the narrow triangular shaped basin that lies between the Laccadive Plateau and the southwestern continental slope of India. If Laccadive Plateau is a continental sliver, then Laccadive Basin will obviously be the region of crustal divergence that separated Laccadive Plateau from southern Indian peninsula. As of now, the meagre published information do not allow to ascertain whether this region of crustal divergence of the Laccadive Basin is only an extended continental crust or it reached the stage of oceanic spreading as has been observed in the neighbouring Laxmi and Gop basins in the north. Yatheesh et al. (2013b) have demonstrated by gravity anomaly modelling, that the crust in the Laccadive Basin region could either be a much thinned continental crust or an anomalously thick oceanic crust. Our proposed evolutionary model considered this divergence, but could not resolve the ambiguity about the nature of the crust underlying Laccadive Basin. Establishing the nature of the crust of the Laccadive Basin is thus a requirement. Moreover, if an oceanic crust underlies the Laccadive Basin and that contains identifiable seafloor spreading magnetic

anomalies, then we may also get some time constraints for opening of the region, which is not available at present.

4.11.3 Demerits of the Presented Evolutionary Model

Our model assumed that the Laccadive Plateau and the Laxmi Ridge are continental slivers. As discussed earlier (in Sect. 2.2), although evidences are emerging in support of a continental sliver nature of the Laccadive Plateau region, still this aspect awaits to be firmly established. Similarly, although many observations support the general belief that the Laxmi Ridge is a continental sliver, still a recent study (Misra et al. 2015) inferred that the Laxmi Ridge is composed of oceanic crust and represents an extinct spreading center. Admittedly, our model will not remain valid in its entirety, in case future studies firmly disprove the continental sliver nature of the Laccadive Plateau or confidently establish the extinct oceanic spreading center genesis of the Laxmi Ridge as a whole. Further, the Euler rotation parameters used for our quantitative reconstructions were estimated from the inferred locations and ages of various conjugate features. These rotation parameters may have to be re-estimated in case studies in future identify newer and better constrained conjugate features/piercing points or provide improved time constraints (e.g. revised ages of the magnetic lineations of the Laxmi and Gop basins). In other words the quantitative reconstructions presented in this study are sensitive to locations and age constraints of the conjugate points used for estimation of rotation parameters. We hope some future studies will carry out sensitivity analysis of such reconstruction models in relation to these variables.

In a recent study Torsvik et al. (2013) proposed the existence of 'Mauritia'—a Precambrian micro-continent between Madagascar and southern India prior to the commencement of India–Madagascar break up during Cretaceous. They (ibid.) opined that during Cretaceous-Cenozoic times this 'Mauritia' micro-continent thinned, fragmented and dispersed to give rise to the present day sub-volcanic crust of Mauritius and continental fragments from the Southern Mascarene Plateau (e.g. parts of Saya de Malha, Nazareth and Cargados-Carajos Banks) and the Laccadives, Maldives and Chagos areas adjacent to Indian margin. Mauritia micro-continent is an interesting proposition and one cannot rule out such a possibility. However, in our model we have included only the Laccadive Plateau part of that proposed Mauritia mainly because, we believe the evidence of continental affinity in this region is relatively better constrained as compared to the Mauritius and southern Mascarene plateau. Further, our model suggested that the Mauritius—southern Mascarene Plateau part of Mauritia, if formed by fragmentation of Mauritia micro-continent, could have commenced only sometime between chron C27ny and chron C26no, when the spreading center from southern Mascarene Basin jumped north within a thinned continental crust zone between the southern end of the Laccadive Plateau and the northern boundary of the Mascarene Basin. Possibly this thinned continental crust region was the parental material from where at least part of Mauritius and southern Mascarene plateau region could have formed. Therefore, we

believe our model retains scope to accommodate the genesis of Mauritius and southern Mascarene plateau region as continental sliver, but due to poor constraints presently we refrained from much speculation on this aspect.

5 Conclusions

This paper synthesises information from various published and unpublished studies to develop reconstructions describing the early plate-tectonic evolution of the WCMI-ADOB region from the time of initiation of the India-Madagascar break-up ($\sim$88.0 Ma; Late Cretaceous) till chron C25no ($\sim$56.4 Ma; Late Paleocene). These reconstructions provided a new view about the dispersals of Madagascar, Seychelles and India, during their early drift period wherein the Laxmi Ridge and the Laccadive Plateau have been accommodated as intervening continental slivers. The main conclusions from these reconstructions are as follows:

- Around 88.0 Ma (Late Cretaceous) the continental blocks/slivers involved in the evolution of the WCMI-ADOB region were juxtaposed in their immediate pre-drift configuration while a wide continental rift zone of hitherto obscure origin existed between the larger continental blocks of India and Madagascar.
- Shortly before chron C34ny ($\sim$83.0 Ma), the Mascarene Basin spreading system developed between the northeastern Madagascar and the Seychelles Plateau in the north, and the eastern Madagascar and the Laccadive Plateau in the south. This spreading system initiated the formation of the Mascarene Basin and separation of Madagascar from conjoined SEY + LAX + LCP + SPB + NPB blocks. Some time between 88.0 and 83.0 Ma a regime of crustal divergence also commenced between the Laccadive Plateau and the SPB.
- Around 68.5 Ma (within chron C31n) a ternary rift system came into existence off Saurashtra peninsula of western India and that system initiated divergence of the conjoined SEY + LAX from NPB and SPB. Continuation of this divergence caused commencement of seafloor spreading in the Laxmi and Gop basins around 67.6 Ma and around 64.7 Ma respectively. Seafloor spreading in the northern Mascarene Basin substantially slowed down after the commencement of spreading in the Laxmi Basin.
- Around chron C28ny ($\sim$62.5 Ma), the Greater Seychelles broke into the Seychelles Plateau and the Laxmi Ridge by development of a new spreading center (ancestor of the Carlsberg Ridge), while spreading in the northern Mascarene Basin ceased but spreading at very slow rate continued in the Laxmi and Gop basins. This was also the time of commencement of; (i) the unique spreading ridge propagation along the short segments of the then Carlsberg Ridge, and (ii) the formation of the Laxmi Basin seamounts.
- Around chron C27ny ($\sim$60.9 Ma), more rift segments in the easterly part of the then Carlsberg Ridge spreading center/rift system developed into oceanic spreading centers and continued divergence along that system created a

triangular wedge of oceanic crust between the Laxmi Ridge and the Seychelles Plateau. The Laxmi Basin spreading center, being in the closest proximity of the Réunion hotspot at that time, might have received increased melt supply and as a result the Laxmi Basin seamounts grew rapidly even to the extent of becoming sub-aerial.

- Around chron C26no ($\sim$57.9 Ma) the waning phase of seafloor spreading commenced in both the Gop and Laxmi basins spreading centers and spreading developed along the full length of the then Carlsberg Ridge. Spreading in the southern Mascarene Basin ceased some time between chron C27ny ($\sim$60.9 Ma) and chron C26no ($\sim$57.9 Ma) and the spreading center jumped north between the southern end of the Laccadive Plateau and the northern boundary of the Mascarene Basin, probably to relocate itself closer to Réunion hotspot.
- Some time during chron C25r (57.554–56.391 Ma); (i) the seafloor spreading in the Gop and Laxmi basins and volcanism along the Laxmi Basin seamounts ceased (ii) the Narmada Rift zone became a failed rift, and (iii) the crustal divergence regime in the Laccadive Basin stopped. With the cessation of these divergence regimes, the Laccadive Plateau and the Laxmi Ridge reached their present position relative to India and got welded with the Indian plate.

References

Ajay KK, Chaubey AK, Krishna KS, Gopala Rao D, Sar D (2010) Seaward dipping reflectors along the SW continental margin of India: evidence for volcanic passive margin. J Earth Syst Sci 119(6):803–813

Baksi AK (2005) Evaluation of radiometric ages pertaining to rocks hypothesized to have been derived by hotspot activity, in and around the Atlantic, Indian and Pacific oceans. In: Foulger GR, Natland JH, Presnall DC, Anderson DL (eds) Plates, plumes and paradigms, geological society of America special paper 388, pp 55–70

Bastia R, Reeves C, Pundarika-Rao D, D'Silva K, Radhakrishna M (2010) Paleogeographic reconstruction of East Gondwana and evolution of the Indian continental margin. DCS-DST Newslett 20(2):2–8

Basu AR, Renne PR, Dasgupta DK, Teichmann F, Poreda RJ (1993) Early and late igneous pulses and high 3He plume origin for the deccan flood basalts. Science 261:902–906

Batiza R (1977) Petrology and chemistry of Guadalupe Island: an alkalic seamount on a fossil ridge crest. Geology 5:760–764

Bernard A, Munschy M (2000) Le bassin des Mascareignes et le bassin de Laxmi (ocen Indien occidental) se sont-ils formes a I'axe d'un meme centre d'expansion? Comptes Rendus de I'Academie des Sciences - Series IIA - Earth and Planetary Science 330(11):777–783

Besse J, Courtillot V (1988) Paleogeographic maps of the continents bordering the Indian Ocean since the Early Jurassic. J Geophys Res 93(B10):11791–11808

Bhattacharji S, Chatterjee N, Wampler JM (1996) Timing of Narmada-Tapti rift reactivation and Deccan volcanism: geochronological and geochemical evidence. Gondwana Geological Magazine Special Volume 2:329–340

Bhattacharya GC, Chaubey AK (2001) Western Indian Ocean—a glimpse of the tectonic scenario. In: Sengupta R, Desa E (eds) The Indian Ocean—a perspective, vol 2, pp 691–729. Oxford & IBH Pub. Company Ltd., Delhi

Bhattacharya GC, Subrahmanyam V (1986) Extension of the Narmada-Son lineament on the continental margin off Saurashtra, Western India, as obtained from magnetic measurements. Mar Geophys Res 8:329–344

Bhattacharya GC, Yatheesh V (2013) Software package "ROTPXY" for carrying out quantitative plate tectonic reconstruction. Copyright application filed, 046CR2013

Bhattacharya GC, Chaubey AK, Murty GPS, Gopala Rao D, Scherbakov VA, Lygin VA, Philipenko AI, Bogomyagkov AP (1992) Marine magnetic anomalies in the northeastern Arabian Sea. In: Desai BN (ed) Oceanography of the Indian Ocean. Oxford-IBH, New Delhi, pp 503–509

Bhattacharya GC, Chaubey AK, Murty GPS, Srinivas K, Sarma KVLNS, Subrahmanyam V, Krishna KS (1994a) Evidence for seafloor spreading in the Laxmi Basin, northeastern Arabian Sea. Earth Planet Sci Lett 125:211–220

Bhattacharya GC, Murty GPS, Srinivas K, Chaubey AK, Sudhakar T, Nair RR (1994b) Swath bathymetric investigation of the seamounts located in Laxmi Basin, Eastern Arabian Sea. Mar Geodesy 17:169–182

Bhattacharya GC, Dyment J, Chaubey AK, Royer JY, Srinivas K, Yatheesh V (2001) Paleogene tectonic fabric and evolution of the Arabian and Eastern Somali basins, NW Indian Ocean. EOS Trans Am Geophys Union 82(47), Fall Meeting Supplement abstract T11A-0842

Bhattacharya GC, Chaubey AK, Royer JY, Dyment J, Srinivas K, Ramprasad T (2003a) Opening of the Western Indian Ocean: a revised model based on a new compilation. Paper presented at the European Geophysical Society-American Geophysical Union-European Union of Geosciences Joint Assembly, Nice, 06–11 Apr 2003

Bhattacharya GC, Dyment J, Chaubey AK, Royer JY, Srinivas K, Yatheesh V (2003b) Paleo-propagating ridges and the plate tectonic evolution of the Arabian and Easter Somali Basins, Northwest Indian Ocean. Project completion report submitted to the Indo-French Centre for the Promotion of Advanced Research (IFCPAR), New Delhi

Bissessur D, Dyment J, Deplus C, Yatheesh V (2009) A triple junction trace beneath Reunion Island? Insight from marine magnetic anomalies. European Geosciences Union, Geophysical Research Abstracts 11, EGU2009-6383

Biswas SK (1982) Rift basins in western margin of India and their hydrocarbon prospects with special reference to Kutch Basin. Am Assoc Pet Geol Bull 66:1497–1513

Biswas SK (1987) Regional tectonic framework, structure and evolution of the western marginal basins of India. Tectonophysics 135:307–327

Biswas SK (ed) (1988) Structure of the western continental margin of India and related igneous activity, Memoir 3. Deccan flood basalts. Geological Society of India, Bangalore

Biswas SK (1989) Hydrocarbon exploration in western offshore basins of India. In: Recent geoscientific studies in the Arabian Sea off India. Geological Survey of India, Special Publication 24, pp 185–194

Biswas SK, Singh NK (1988) Western continental margin of India and hydrocarbon potential of deep-sea basins. In: 7th Offshore Southeast Asia conference, 1988, pp 170–181

Boyden JA, Müller RD, Gurnis M, Torsvik TH, Clark JA, Turner M, Ivey-Law H, Watson RJ, Cannon JJ (2011) Next-generation plate-tectonic reconstructions using GPlates. In: Baru C,

Keller GR (eds) Geoinformatics: cyberinfrastructure for the solid earth sciences. Cambridge University Press, Cambridge, pp 95–114

Burke K, Dewey JF (1973) Plume-generated triple junctions: key indicators in applying plate tectonics to old rocks. J Geol 81:406–433

Calvès G, Schwab AM, Huuse M, Clift PD, Gaina C, Jolley D, Tabrez AR, Inam A (2011) Seismic volcanostratigraphy of the western Indian rifted margin: the pre-Deccan igneous province. J Geophys Res 116(B01101). doi:10.1029/2010JB000862

Cande SC, Kent DV (1995) Revised calibration of the geomagnetic polarity time scale for the Late Cretaceous and Cenozoic. J Geophys Res 100:6093–6095

Carmichael SM, Akhter S, Bennett JK, Fatimi MA, Hosein K, Jones RW, Longacre MB, Osborne MJ, Tozer RSJ (2009) Geology and hydrocarbon potential of the offshore Indus Basin, Pakistan. Petrol Geosci 15:107–116

Chatterjee S, Rudra DK (1996) KT events in India: impact, rifting, volcanism and Dinosaur extinction. Mem Queensland Mus 39(3):489–532

Chatterjee S, Guven N, Yoshinobu A, Donofrio R (2006) Shiva structure: a possible KT boundary impact crater on the western shelf of India. Spec Publ Mus Texas Tech Univ 50:1–39

Chatterjee S, Goswami A, Scotese CR (2013) The longest voyage: tectonic, magmatic, and paleoclimatic evolution of the Indian plate during its northward flight from Gondwana to Asia. Gondwana Res 23:238–267

Chaubey AK, Bhattacharya GC, Murty GPS, Desa M (1993) Spreading history of the Arabian Sea: some new constraints. Mar Geol 112:343–352

Chaubey AK, Bhattacharya GC, Rao DG (1995) Seafloor spreading magnetic anomalies in the southeastern Arabian Sea. Mar Geol 128:105–114

Chaubey AK, Bhattacharya GC, Murty GPS, Srinivas K, Ramprasad T, Rao DG (1998) Early Tertiary seafloor spreading magnetic anomalies and paleo-propagators in the northern Arabian Sea. Earth Planet Sci Lett 154:41–52

Chaubey AK, Dyment J, Bhattacharya GC, Royer JY, Srinivas K, Yatheesh V (2002a) Paleogene magnetic isochrons and palaeo-propagators in the Arabian and Eastern Somali basins, NW Indian Ocean. In: Clift PD, Croon D, Gaedicke C, Craig J (eds) The tectonic and climatic evolution of the arabian sea region, special publication 195, pp 71–85. Geological Society, London

Chaubey AK, Rao DG, Srinivas K, Ramprasad T, Ramana MV, Subrahmanyam V (2002b) Analyses of multichannel seismic reflection, gravity and magnetic data along a regional profile across the central-western continental margin of India. Mar Geol 182(3–4):303–323

Chenet AL, Quidelleur Z, Fluteau F, Courtillot V, Bajpai S (2007) ^{40}K–^{40}Ar dating of the main Deccan large igneous province: further evidence of KTB age and short duration. Earth Planet Sci Lett 263:1–15

Collier JS, Minshull TA, Kendall J-M, Whitmarsh RS, Rumpker G, Joseph P, Samson P, Lane CI, Sansom V, Vermeesch PM, Hammond J, Wookey J, Teanby N, Ryberg T, Dean SM (2004) Rapid continental breakup and microcontinent formation in the western Indian Ocean. EOS Trans Amer Geophys Union 85(46):481, 496

Collier JS, Sansom V, Ishizuka O, Taylor RN, Minshull TA, Whitmarsh RB (2008) Age of Seychelles-India break-up. Earth Planet Sci Lett 272:264–277

Collier JS, Minshull TA, Hammond J, Whitmarsh RB, Kendall J-M, Sansom V, Lane CI, Rumpker G (2009) Factors influencing magmatism during continental break-up: new insights from a wide-angle seismic experiment across the conjugate Seychelles-Indian margins. J Geophys Res 114:B03101. doi:10.1029/2008JB005898

Corfield RI, Carmichael S, Bennett J, Akhter S, Fatimi M, Craig T (2010) Variability in the crustal structure of the West Indian Continental Margin in the Northern Arabian Sea. Petrol Geosci 16 (3):257–265

Ganerød M, Torsvik TH, Van Hinsbergen DJJ, Gaina C, Corfu F, S. W, Owen-Smith TM, Ashwal LD, Webb SJ, Hendriks BWH (2011) Palaeo-position of the Seychelles microcontinent in relation to the Deccan Traps and the Plume Generation Zone in Late Cretaceous-Early Palaeogene time. In: Van-Hinsbergen DJJ, Buiter SJH, Torsvik TH, Gaina C, Webb SJ (eds)

The formation and evolution of Africa: a synopsis of 3.8 Ga of Earth History, special publication 357, pp 229–252. Geological Society, London

Courtillot VE, Renne PR (2003) On the ages of flood basalt events. CR Geosci 335:113–140

Courtillot V, Besse J, Vandamme D, Montigny R, Jaeger JJ, Capetta H (1986) Deccan flood basalts at the Cretaceous/Tertiary boundary? Earth Planet Sci Lett 80:361–374

Courtillot V, Feraud G, Maluski H, Vandamme D, Moreau MG, Besse J (1988) Deccan flood basalts and the Cretaceous/Tertiary boundary. Nature 333:843–846

Crawford AR (1978) Narmada-Son lineament of India traced into Madagascar. J Geol Soc India 19 (4):144–153

Devey CW, Stephens WE (1991) Tholeiitic dykes in the Seychelles and the original spatial extent of the Deccan. J Geol Soc London 148:973–983

DGH (2014) Directorate General of Hydrocarbons (DGH), Noida, India web page: Kerala Konkan Basin. http://www.dghindia.org/15.aspx. Accessed 29 Oct 2014

Duncan RA (1981) Hotspots in the Southern Oceans—an absolute frame of reference for the motion of the Gondwana continents. Tectonophysics 74:29–42

Duncan RA, Hargraves RB (1990) ^{40}Ar/^{39}Ar Geochronology of basement rocks from the Mascarene Plateau, the Chagos Bank, and the Maldives Ridge. In: Duncan RA, Backman, J, Peterson C, et al. (ed) Proceedings of ODP scientific results, vol 115, pp 43–51. Ocean Drilling Programme, College Station, TX

Dyment J (1991) Structure et évolution de la lithosphère océanique dans l'océan Indien: apport des anomalies magnétiques. Université Louis Pasteur, Strasbourg, Thèse de Doctorat, pp 374

Dyment J (1998) Evolution of the Carlsberg Ridge between 60 and 45 Ma: ridge propagation, spreading asymmetry, and the Deccan-Reunion hotspot. J Geophys Res 103:24067–24084

Dyment J, Chaubey AK, Royer JY (2001) Long lived "super propagators" on the Carlsberg Ridge between Chrons 26–20 (58–42 Ma). 11th meeting of the European Union of Geosciences, Strasbourg, France, 8–12 Apr 2001

Eagles G, Wibisono AD (2013) Ridge push, mantle plumes and the speed of the Indian plate. Geophys J Int 194(2):670–677

Gaedicke C, Schlutter HU, Roeser HA, Prexl A, Schreckenberger B, Meyer H, Reichert C, Clift P, Amjad S (2002) Origin of the northern Indus Fan and Murray ridge, Northern Arabian Sea: interpretation from seismic and magnetic imaging. Tectonophysics 355:127–143

Gibbons AD, Whittaker JM, Muller RD (2013) The breakup of East Gondwana: assimilating constraints from Cretaceous ocean basins around India into a best-fit tectonic model. J Geophys Res-Solid Earth 118(3):808–822

Gombos AM, Powell WG, Norton IO (1995) The tectonic evolution of western India and its impact on hydrocarbon occurrences—an overview. Sed Geol 96(1–2):119–129

Gunnell Y (2001) Dynamics and kinematics of rifting and uplift at the western continental margin of India: insight from geophysics and numerical models. In: Gunnell Y, Radhakrishna BP (eds) Sahyadri The great escarpment of the Indian subcontinent, Geological Society of India. Memoir 47, pp 475–496. Geological Society of India, Bangalore

Gunnell Y, Harbor D (2008) Structural underprint and tectonic overprint in the Angavo (Madagascar) and Western Ghats (India)—implications for understanding scarp evolution at passive margins. J Geol Soc India 71:763–779

Hey R (1977) A new class of "pseudofaults" and their bearing on plate tectonics: a propagating rift model. Earth Planet Sci Lett 37:321–325

Hey RN, Duennebier FK, Morgan JP (1980) Propagating rifts on midocean ridges. J Geophys Res 85:3647–3658

Hofmann C, Feraud G, Courtillot V (2000) ^{40}Ar–^{39}Ar dating of mineral separates and whole rocks from te Wesern Ghats lava pile: further constraints on duration and age of the Deccan Trap. Earth Planet Sci Lett 180:13–27

Hooper PR (1999) The winds of change. In: Subbarao KV (ed) The deccan traps: a personal perspective. Memoir 43 (1), pp 153–165. Geological Society of India, Bangalore

IOC-IHO-BODC (2003) Centenary edition of the GEBCO digital atlas. CD-ROM on behalf of the Intergovernmental Oceanographic Commission and the International Hydrographic

Organization as Part of the General Bathymetric Chart of the Oceans, British Oceanographic Data Centre, Liverpool, UK

Ishwar-Kumar C, Windley BF, Horie K, Kato D, Hokada T, Itaya T, Yagi K, Gouzu C, Sajeev K (2013) A Rodinian suture in western India: new insights on India-Madagascar correlations. Precambr Res 236:227–251

Jacob J, Dyment J, Yatheesh V (2014) Revisiting the structure, age, and evolution of the Wharton Basin to better understand subduction under Indonesia. J Geophys Res Solid Earth 119:169–190

Jerram DA, Widdowson M (2005) The anatomy of Continental Flood Basalt Provinces: geological constraints on the processes and products of flood volcanism. Lithos 79,:385– 405

Katz MB, Premoli C (1979) India and Madagascar in Gondwanaland based on matching Precambrian lineaments. Nature 279:312–315

Khanna M, Walton EK (1992) Petrological studies of Karoo sandstones, Western shelf, Seychelles. In: Plummer PhS. (ed.) First Indian Ocean Petroleum Seminar, Proc. UN Sem., Seychelles 1990, pp 291–305

Kolla V, Coumes F (1990) Extension of structural and tectonic trends from the Indian subcontinent into the Eastern Arabian Sea. Mar Pet Geol 7:188–196

Kothari V, Waraich RS, Baruah RM, Lal NK, Zutshi PL (2001) A reassessment of the hydrocarbon prospectivity of Kerala-Konkan deep water basin, western offshore, India. Paper presented at the International Conference and Exhibition PETROTECH-2001

Krishna KS, Rao DG, Sar D (2006) Nature of the crust in the Laxmi Basin (14°–20°), western continental margin of India. Tectonics 25, TC1006. doi:10.1029/2004TC001747

Krishna KS, Abraham H, Sager WW, Pringle MS, Frey F, Gopala Rao D, Levchenko OV (2012) Tectonics of the Ninetyeast Ridge derived from spreading records in adjacent oceanic basins and age constraints of the ridge. J Geophys Res 117:B04101. doi:10.1029/2011JB008805

Kroner A, Brown L (2005) Structure, composition and evolution of the South Indian and Sri Lankan Granulite Terrains from deep seismic profiling and other geophysical and geological investigations: a LEGENDS initiative. Gondwana Res 8(3):317–335

Kumar A, Pande K, Venkatesan TR, Bhaskar Rao YJ (2001) The Karnataka late Cretaceous dykes as products of the Marion hotspot at the Madagascar—India breakup event: evidence from $^{40}Ar/^{39}Ar$ geochronology and geochemistry. Geophys Res Lett 28:2715–2718

Laughton AS, Matthews DH, Fisher RL (1970) The structure of the Indian Ocean. In: Maxwell AE (ed) The Sea, vol 4. Wiley-Interscience, New York, pp 543–586

Lawver LA, Gahagan LM, Dalziel WD (1998) A tight fit-Early Mesozoic Gondwana, a plate reconstruction perspective. In: Motoyoshi Y, Shiraishi K (eds) Origin and evolution of continents, special issue 53. Memoir, National Institute of Polar Research, Tokyo, pp 214–229

Mahoney JJ, Duncan RA, Khan W, Gnos E, McCormic GR (2002) Cretaceous volcanic rocks of the South Tethyan suture zone, Pakistan: implications for the reunion hotspot and Deccan Traps. Earth Planet Sci Lett 203:295–310

Malod JA, Droz L, Mustafa Kamal B, Patriat P (1997) Early spreading and continental to oceanic basement transition beneath the Indus-deep sea fan: northeastern Arabian Sea. Mar Geol 141:221–235

Matthews KJ, Muller RD, Wessel P, Whittaker JM (2011) The tectonic fabric of the ocean basins. J Geophys Res-Solid Earth 116. doi:10.1029/2011jb008413

McKenzie D, Sclater JG (1971) The evolution of the Indian Ocean since the Late Cretaceous. Geophys J Royal Astron Soc 25:437–528

Melluso L, Sheth HC, Mahoney JJ, Morra V, Petrone CM, Storey M (2009) Correlations between silicic volcanic rocks of the St. Mary's Islands (southwestern India) and eastern Madagascar : implications for Late Cretaceous India-Madagascar reconstructions. J Geol Soc London 166:283–294

Menon RD, Santosh, M. (ed) (1995) A Pan-African gemstone province of East Gondwana, vol 34. India and Antarctica during the Precambrian. Geological Society of India, Bangalore

Miles PR, Roest WR (1993) Earliest seafloor spreading magnetic anomalies in the north Arabian Sea and the ocean-continent transition. Geophys J Int 115:1025–1031

Miles PR, Munschy M, Segoufin J (1998) Structure and early evolution of the Arabian Sea and East Somali Basin. Geophys J Int 15:876–888

Minshull TA, Lane CI, Collier JS, Whittmarsh RB (2008) The relationship between rifting and magmatism in the northeastern Arabian Sea. Nat Geosci 1:463–467

Misra AA, Bhattacharyya G, Mukherjee S, Bose N (2014) Near N–S paleo-extension in the western Deccan region, India: Does it link strike-slip tectonics with India–Seychelles rifting? Int J Earth Sci 103:1645–1680

Misra AA, Mukherjee S (2015) Tectonic inheritance in continental rifts and passive margins. SpringerBriefs in Earth Sciences (in Press)

Misra AA, Sinha N, Mukherjee S (2015) Repeat ridge jumps and microcontinent separation: insights from NE Arabian Sea. Mar Pet Geol 59:406–428

Morgan WJ (1972) Deep mantle convection plumes and plate motions. Am Assoc Pet Geol Bull 56:203–213

Morgan WJ (1981) Hotspot tracks and the opening of the Atlantic and Indian Oceans. In: Emiliani (ed) The sea, vol 7, pp 443–487. Wiley Interscience, New York

Mukhopadhyay R, Karisiddaiah SM, Ghosh AK (2012) Geodynamics of the Amirante Ridge and Trench Complex, Western Indian Ocean. Int Geol Rev 54(1):81–92

Murty AVS, Arasu RT, Dhanawat BS, Subrahmanyam VSR (1999) Some aspects of deepwater exploration in the light of new evidences in the western Indian offshore. In: Third international petroleum conference and exhibition. PETROTECH, pp 457–462

Mutter JC, Talwani M, Stoffa PL (1982) Origin of the seaward-dipping reflectors in oceanic crust off the Norwegian margin by "subaerial sea-floor spreading. Geology 10:353–357

Naini BR (1980) Geological and Geophysical study of the continental margin of Western India, and the adjoining Arabian Sea including the Indus cone. PhD thesis, Columbia University, USA

Naini BR, and Talwani, M. (1982) Structural framework and the evolutionary history of the continental margin of Western India. In: Watkins JS, Drake CL (eds) Studies in continental margin geology, vol 34, pp 167–191. American Association of Petroleum Geologists

Naqvi SM (2005) Geology and evolution of the Indian plate. Capital Publishing, New Delhi

Norton IO, Sclater JG (1979) A model for the evolution of the Indian Ocean and the break-up of Gondwanaland. J Geophys Res 84(B12):6803–6830

Owen-Smith TM, Ashwal LD, Torsvik TH, Ganerød M, Nebel O, Webba SJ, Werner SC (2013) Seychelles alkaline suite records the culmination of Deccan Traps continental flood volcanism. Lithos 182–183:33–47

Pande K (2002) Age and duration of the Deccan Traps, India: a review of radiometric and paleomagnetic constraints. Proc Indian Acad Sci (Earth Planet Sci) 111(2):115–123

Pande K, Sheth HC, Bhutani R (2001) ^{40}Ar–^{39}Ar age of the St. Mary's Islands volcanics, southern India: record of India—Madagascar break-up on the Indian subcontinent. Earth Planet Sci Lett 193:39–46

Pepper JF, Everhart GM (1963) The Indian Ocean: the geology of its bordering lands and the configuration of its floor. In: Miscellaneous Geologic Investigations. U.S. Geological Survey, pp 1–33

Planke S, Symonds PA, Alvestad E, Skogseid J (2000) Seismic volcanostratigraphy of large-volume basaltic extrusive complexes on rifted margins. J Geophys Res 105(B8):9335–19351

Plummer PS (1995) Ages and geological significance of the igneous rocks from Seychelles. J Afr Earth Sci 20(2):91–101

Plummer PS (1996) The Amirante ridge/trough complex: response to rotational transform rift/drift between Seychelles and Madagascar. Terra Nova 8:34–47

Plummer PS, Belle ER (1995) Mesozoic tectono-stratigraphic evolution of the Seychelles microcontinent. Sed Geol 96:73–91

Rabinowitz PD, Coffin MF, Flavey D (1983) The separation of Madagascar and Africa. Science 220(4592):67–69

Radhakrishna BP (2001) The Western Ghats of the Indian Peninsula. In: Gunnell Y, Radhakrishna BP (eds) Sahyadri—the great escarpment of the Indian subcontinent, Memoir 47, pp 133–144. Geological Society of India, Bangalore

Radhakrishna T, Joseph M (2012) Geochemistry and paleomagnetism of Late Cretaceous mafic dikes in Kerala, southwest coast of India in relation to large igneous provinces and mantle plumes in the Indian Ocean region. Geol Soc Am Bull 124(1/2):240–255

Radhakrishna BP, Vasudev VN (1977) The early Precambrian of southern Indian shield. J Geol Soc India 18:525–541

Raju ATR, Sinha RN, Ramakrishna M, Bisht HSN, VM (1981) Structure, tectonics and hydrocarbon prospects of Kerala-Laccadive Basin. In: Rao P (ed) Geological interpretation of geophysical data, pp 123–127. Oil and Natural Gas Commission, Dehra Dun, India

Randrianaloso A, Zimmermann J-L, Rambeloson R, Ratsimba G (1981) Précisions sur l'âge de la première sedimentation marine au-nord-est de Madagascar en liason avec la dislocation de bloc Sechelles-Indes-Madagascar. Comptes Rendus Academic Sciences Series 2:1039–1042

Rao RP, Srivastava DC (1981) Seismic stratigraphy of west Indian offshore. In: Rao RP (ed) Workshop on geological interpretation of geophysical data. ONGC, Dehradun, pp 1–9

Rao GSP, Tewari HC (2005) The seismic structure of the Saurashtra crust in northwest India and its relationship with the Reunion Plume. Geophys J Int 160:318–330

Rao DG, Ramana MV, Bhattacharya GC, Subba Raju LV, Kamesh Raju KA, Ramprasad T (1992) Marine geophysical studies along a transect across the continental margin off Bombay, India. In: Desai BN (ed) Oceanography of the Indian Ocean. Oxford & IBH, New Delhi, pp 493–501

Ratheesh-Kumar RT, Ishwar-Kumar C, Windley BF, Razakamanana T, Nair RR, Sajeev K (2014) India–Madagascar paleo-fit based on flexural isostasy of their rifted margins. Gondwana Res, in press. doi:10.1016/j.gr.2014.06.008

Raval U, Veeraswamy K (2003) India-Madagascar separation: breakup along a pre-existing—mobile belt and chipping of the craton. Gondwana Res 6(3):467–485

Reeves C, Leven J (2001) The evolution of the west coast of India from a perspective of global Tectonics. J Geophys 22(1):17–23

Roberts G, Harmer C, Rutherford K, O'Brien C (2010) Deep water west coast India—the opening of a new play beneath the Deccan Basalts. Spectrum Geo Technical paper Ref 20549

Royer JY, Schlich R (1988) Southeast Indian Ridge between the triple junction and the Amsterdam and Saint-Paul Islands: detailed kinematics for the past 20 m.y. J Geophys Res 93 (B11):13524–13550

Royer JY, Chaubey AK, Dyment J, Bhattacharya GC, Srinivas K, Yatheesh V, Ramprasad T (2002) Paleogene plate tectonic evolution of the Arabian and Eastern Somali basins. In: Clift PD, Croon D, Gaedicke C, Craig J (eds) The tectonic and climatic evolution of the Arabian Sea Region, special publication 195, pp 7–23. Geological Society, London

Sahabi M (1993) Un Modele generele de d'evolution de l'ocean Indien. Ph.D. thesis, Universite de Bretagne Occidentale, France

Salisbury MH, Keen CE (1993) Listric faults imaged in oceanic crust. Geology 21:117–120

Sandwell DT, Müller RD, Smith WHF, Garcia E, Francis R (2014) New global marine gravity model from CryoSat-2 and Jason-1 reveals buried tectonic structure. Science 346:65–67

Santosh M, Yang QY, Shaji E, Tsunogae M, RamMohan M, Satyanarayanan M (2014) An exotic Mesoarchean microcontinent: the Coorg, Block, southern India. Gondwana Res, in press. doi:10.1016/j.gr.2013.10.005

Schlich R (1982) The Indian Ocean: aseismic Ridges, spreading centres and basins. In: Nairn AEM, Stehli FG (eds) The ocean basins and margins, vol 6. Plenum Press, New York, pp 51–147

Sen G (2001) Generation of Deccan trap basalt. Proc Indian Acad Sci 110:409–431

Sharma RS (2009) Cratons and fold belts of India, 127. Lecture notes in earth sciences. Springer, Berlin

Sheth HC (2005) From Deccan to Reunion: no trace of a mantle plume. In: Foulger GR, Natland JH, Presnall DC, Anderson DL (eds) Plates, Plumes, and Paradigms, special paper 388, pp 477–501. Geological Society of America

Siawal A, Samal JK, Kaul AK (2014) A note on identification of SDR's in Laxmi Basin of Arabian Sea region. ONGC Bulletin 49(1):45–50

Singh D, Alat CA, Singh RN, Gupta VP (1997) Source rock characteristics and hydrocarbon generating potential of Mesozoic sediments in Lodhika area, Saurashtra basin, Gujarat, India, In: Proceedings of 2nd international petroleum conference and exhibition, pp 205–220. Petrotech-97, New Delhi

Srinivas K (2004) Seismic reflection and bathymetric study over deep offshore regions off the central west coast of India. PhD thesis, Goa University, Goa, India, 180 pp

Sriram K, Gupte SS, Kothari V, Bisen M, Waraich RS (2006) Structure and evolution of Saurashtra Arch in Kutch-Saurashtra deepwater area, Western India. In: 6th International conference & exposition on petroleum Geophysics, Kolkata, 2006, pp 21–25

Storey M, Mahoney JJ, Saunders AD, Duncan RA, Kelley SP, Coffin MF (1995) Timing of hotspot related volcanism and the breakup of Madagascar and India. Science 267(5199):852–855

Subrahmanya KR (2001) Origin and evolution of the Western Ghats and the West Coast of India. In: Gunnell Y, Radhakrishna BP (eds) Sahyadri—the great escarpment of the Indian subcontinent, Memoir 47, pp 463–473. Geological Society of India, Bangalore

Talwani M, Reif C (1998) Laxmi Ridge- a continental sliver in the Arabian Sea. Mar Geophys Res 20:259–271

Todal A, Eldholm O (1998) Continental margin off western India and Deccan large igneous province. Mar Geophys Res 20:273–291

Torsvik TH, Tucker RD, Ashwal LD, Carter LM, Jamtveit V, Vidyadharan KT, Venkataramana P (2000) Late cretaceous India—Madagascar fit and timing of breakup related magmatism. Terra Nova 12:220–224

Torsvik TH, Amundsen H, Hartz EH, Corfu F, Kusznir N, Gaina C, Doubrovine PV, Steinberger B, Ashwal LD, Jamtveit B (2013) A Precambrian microcontinent in the Indian Ocean. Nat Geosci 6(3):223–227

Valsangkar AB, Radhakrishnamurthy C, Subbarao KV, Beckinsale RD (1981) Paleomagnetism and Potassium–Argon age studies of acid igneous rocks from the St. Mary Islands, Memoir 3, pp 265–275. Geological Society of India, Bangalore

Vandamme D, Courtillot V, Besse J, Montigny R (1991) Paleomagnetism and age determination of the Deccan Traps (India): results of a Nagpur-Bombay traverse and review of earlier work. Rev Geophys 29:159–190

Walker JD, Geissman JW, Bowring SA, Babcock LE (2013) The Geological Society of America geologic time scale. Geol Soc Am Bull 125(3–4):259–272

Wessel P, Smith WHF (1995) New version of the Generic Mapping Tools released. EOS, Trans Amer Geophys Union 76:329

Whitmarsh RB (1974) Some aspects of plate tectonicsin the Arabian Sea. Initial reports of the deep sea drilling project, vol 23. US Government Printing Office, Washington, pp 35–115

Whitmarsh RB, Weser OE et al (1974) Site 219. initial reports of the deep sea drilling project, vol 23. US Government Printing Office, Washington, pp 35–115

Windley BF, Razafiniparany A, Razakamanana T, Ackermand D (1994) Tectonic framework of the Precambrian of Madagascar and its Gondwana connections. Geol Rundsch 83:642–659

Yatheesh V (2007) A study of tectonic elements of the western continental margin of India and adjoining ocean basins to understand the early opening of the Arabian Sea, PhD thesis, Goa University, Goa, India, pp 212

Yatheesh V, Bhattacharya GC, Mahender K (2006) The terrace like feature in the mid-continental slope region off Trivandrum and a plausible model for India-Madagascar juxtaposition in immediate pre-drift scenario. Gondwana Res 10(1–2):179–185

Yatheesh V, Bhattacharya GC, Dyment J (2009) Early oceanic opening off Western India-Pakistan margin: the Gop Basin revisited. Earth Planet Sci Lett 284:399–408

Yatheesh V, Dyment J, Bhattacharya GC, Muller RD (2013a) Deciphering detailed plate kinematics of the Indian Ocean and developing a unified model for East Gondwanaland reconstruction: an Indian-Australian-French initiative. DCS-DST Newslett 23(1):2–9

Yatheesh V, John Kurian P, Bhattacharya GC, Rajan S (2013b) Morphotectonic architecture of an India-Madagascar breakup related anomalous submarine terrace complex on the southwest continental margin of India. Mar Pet Geol 46:304–318

Yoshida M, Rajesh HM, Santosh M (1999) Juxtaposition of India and Madagascar: a perspective. Gondwana Res 2(3):449–462

Rift Grabens and Crustal Architecture of the Offshore North East Coast-Mahanadi Basin, Eastern Continental Margin of India

Somali Roy, Mainak Choudhuri and Pankaj Gupta

Abstract The rift system in North East Coast-Mahanadi (NEC-MND) basins has been developed during the separation of India and Antarctica, similar to those in Krishna-Godavari (KG) and Cauvery (CY) basins. The rift architecture is well established in the KG and CY basins, both in the onshore as well as offshore. Few publications have reported the presence of rift systems in offshore Mahanadi basin, but very little is known about the continued presence of the rift system to the north of the Mahanadi Basin, in the NEC Basin. The present article has documented the continuation of the rift systems in the offshore NEC Basin, based on interpretation of 2D and 3D seismic reflection data. The internal architecture of the rift grabens have been interpreted and thickness maps been generated to show the distribution of the sediments within the grabens. Seismic velocity data and 2D forward gravity model has also been used to bring out additional informations about the basement and crustal structure.

Keywords India · East coast · Rift · Bengal basin · Mahanadi basin · 3D seismic mapping · RMS amplitude

1 Introduction

Study of coastal tectonics is of interest in regional geoscientific studies (Misra et al. 2014, 2015; Misra and Mukherjee 2015). The North East Coast-Mahanadi (NEC-MND) basin lies in the northern-most part of East Coast of India. Like the Krishna-Godavari (KG) and Cauvery (CY) basins, this basin is also a pericratonic, passive margin basin along the east coast. The wide and stable shelf in this part of the east coast is made up from the heavy discharge of the Ganga-Brahmaputra system in the Bengal basin to the north and from somewhat lesser effects of the rivers like

S. Roy (✉) · M. Choudhuri · P. Gupta
Reliance Industries Limited, Petroleum (E&P), Navi Mumbai, India
e-mail: roysomali29@gmail.com

Fig. 1 Tectonic Evolution of East Coast of India; the figure showing the separation of India and Antarctica around 145 Ma (modified from Reeves 2007, unpublished report for RIL)

Brahmani and Subarnarekha, depositing sediments in and around the study area. The formation of the NEC-MND basin is coeval with that of the KG and CY basins, during the Early Cretaceous breakup between India and Antarctica (Fig. 1), and is well documented in literatures (Rao 2001; Nemčok et al. 2007, 2012). Rift grabens in the onshore NEC-MND area have been documented by Oil India Limited (e.g., Fuloria et al. 1992). The main challenge in this area is to interpret the detailed architecture of rift grabens in the offshore area and continue the structural trend of the basin with other basins in East Coast of India.

The study area lies mostly in the NEC Basin, covering only parts of the Mahanadi basin, between latitude 18.5°N–21.4°N and longitudes 87.2°E–89.5°E (Fig. 2), at water depth between 60 and 2300 m . It is covered by a grid of regional 2D reflection seismic data, with 3D reflection seismic data covering a small part in the NW. Wells drilled by petroleum exploration companies have been correlated and published by Fuloria et al. (1992), which have been considered in the integration of this article. Additionally satellite gravity data is available over the entire area, which has been used to analyze broad basement features. Seismic stacking velocity is available along the seismic data coverage, which is used to clarify the rift signatures in the seismic data.

1.1 Tectonic Framework

The crustal domains along the east coast of India has been taken from Nemčok et al. (2012), where the continent-ocean transition has been divided into a continental-proto-oceanic crust boundary, and a proto-oceanic–oceanic crust boundary, based on interpretations along regional GXT seismic lines and forward gravity modeling.
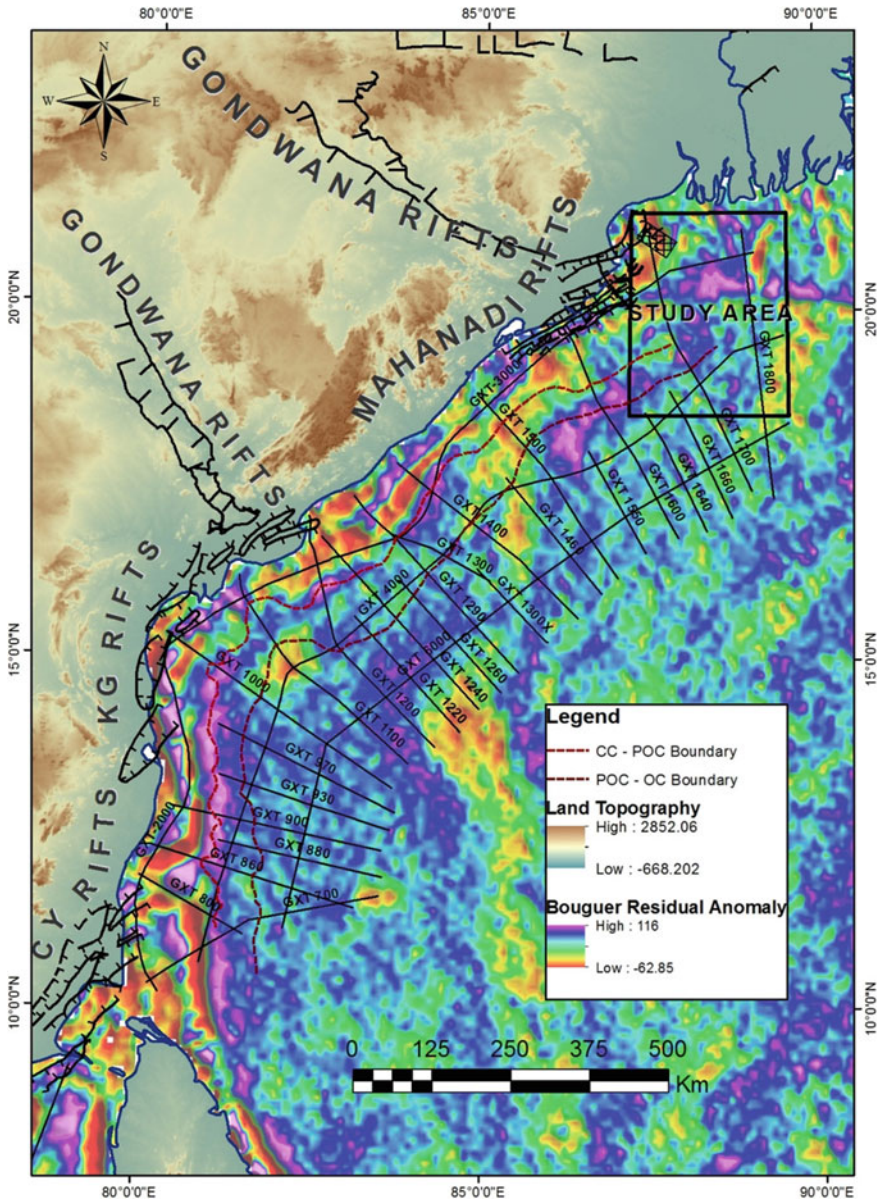
Fig. 2 The figure primarily shows the location of the study area with respect to the other basins of the East Coast (EC) of India basins. The map mainly represents the land topography and the Bouguer residual gravity anomaly in the offshore. The navigation lines mainly orthogonal and few along the coastline are the locations of the GXT seismic profiles across EC of India. The cross-hatched rectangle within the study area is the 3D area. The continental boundaries shown in this figure has been referred from Nemčok et al. (2012). The onland rifts orthogonal to the present day coastline is the Permo-Triassic rifts or Gondwana rifts
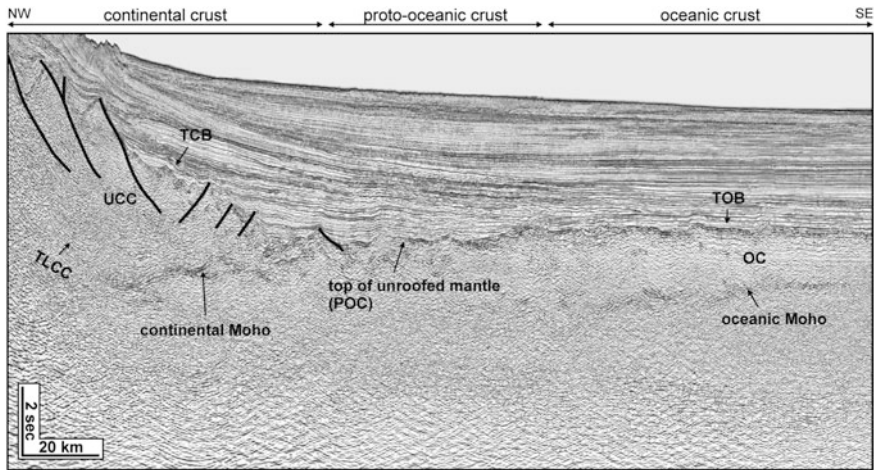
Fig. 3 Seismic line GXT-1000, which runs through the Krishna basin, shows typical section of different crustal types. Nemčok et al. (2012). The line of section is shown in Fig. 2

Their work is mostly concentrated in the KG and CY basins, which has been considered as reference for explaining the structures in the NEC-MND region.

The crustal architecture in the east coast of India is best visualized in the GXT-1000 line in the KG basin, as shown in Fig. 3 (same as Fig. 5 of Nemčok et al. 2012). The figure shows an overall passive margin geometry thinning towards the oceanic side. The presence of rifts in the NW indicates the presence of extended brittle upper continental crust (UCC). The top of basement underneath the sediments is the top of continental basement (TCB). The lower continental crust (LCC) is more ductile than the upper crust, and is shown to contain sub-parallel layering in contrast to chaotic reflections in the UCC; its top is marked as Top Lower Continental (TLCC). Towards SE, the continental crust (CC), eventually, thins out and mantle gets exposed. The exposed mantle in contact with seawater gets serpentinized, forming Proto-Oceanic Crust (POC). The oceanic crust (OC) is formed to the SE of the POC, the top of which is shown as high reflectivity layer termed the top oceanic basement (TOB), while the oceanic Moho is observed below the OC as a diffused layer of higher reflectivity. The CC-POC and POC-OC boundaries from Nemčok et al. (2012) are shown in Fig. 2.

2 Data Used

A synergic approach using reflection seismic data and satellite gravity data has been used to infer the rift signature and crustal domains within the study area.

2.1 Reflection Seismic Data

The multiclient GXT IndiaSpan seismic data, acquired by Simpson et al. (2006) for regional geological study in the east coast of India, form the primary seismic database of this study (Fig. 2). Phase I of IndiaSpan covers the entire offshore eastern India and comprises about 13,574 km of 2D data acquisition. It was acquired with a 10 km long offset, 100-fold coverage and 18 s record length and a 2 millisecond (ms) sample rate, with source strength of approximately 200 bar m peak-to-peak power. The imaging depth was about 25 km, which is sufficient to image the entire crust down to Mohorovicic (Moho) discontinuity, together with the different crustal types and their disposition. In the current study, the total data quantum in the east coast of India is 11,587 km (8087 + 3500 km) including both Phase-1 and Phase-1 infill data. The average length of each profile from shelf to ultra-deep water is more than 300 km (Simpson et al. 2006). The data are available in both pre-stack time-(PSTM) and pre-stack depth-migrated (PSDM) formats.

3D seismic data used in this study was recorded by PGS in 2008. 3D seismic is acquired using 6 streamers of 6000 m length and 2 sources (3090 cu in) configuration, which provided surface sampling of 12.5 m along the line and 25 m along the trace. 3D Pre-Stack time migration processing is carried out by WesternGeco. Full fold data covers about 1876 km area and trace length is 9100 ms with 2 ms record length. Stacking velocity information is available at 100 by 100 m grid size.

2.2 Satellite Gravity Data

The study uses public domain satellite free-air gravity anomaly data, available from http://topex.ucsd.edu/WWW_html/mar_topo.html as a global 1-arc minute grid compilation (Sandwell and Smith 2009, V. 20.1). The data is generated by merging marine radar altimetry data from dedicated with EGM2008 global gravity model, available from National Geospatial-Intelligence Agency (NGA), USA, to produce a seamless merged dataset covering the entire Earth. The data is suitable for analysis within a wavelength band of 15–200 km (Sandwell and Smith 1996, 2009) with an error limit of 2−3 mGal (Sandwell and Smith 2009).

The free-air gravity data has been used to create a Bouguer Residual anomaly map using a Bouguer slab density of 2.0 $gmcc^{-1}$ and a 10 km upward continuation filter, to infer the major crustal features, as shown in Fig. 2. Two sharp bands of negative anomaly, separated by a sharp positive anomaly, are observed running parallel to the coastline. The landward band of negative anomaly of about −10 mGal is produced by the rifted half grabens, and the basinward negative band of −10 mGal, adjacent to a positive peak of about 10 mGal, has been interpreted to be due to the crustal transition from continental to proto-oceanic crust. In this data, individual grabens are not clear due to the limited spatial resolution. However there

is a broad zone of low gravity within the 3D area, which is taken to represent the cumulative signature of the grabens in the gravity data. A strike-slip fault, separating the MND and NEC basin, as mentioned by Fuloria et al. (1992) cannot be clearly identified from the gravity anomaly map.

3 Seismic Interpretations

3.1 Crustal Interpretations

An attempt to interpret the crustal domains marking the CC-POC and POC-OC boundaries is made in NEC-MND region as shown in a representative seismic line GXT-1700 that passes through the study area (Fig. 4). In this figure, the TCB and TOB are well observed, as they show higher reflectivity (hard topped) with respect to the sediments above. Though major faults are not observed within the continental crust in this particular seismic section, but some ruggedness are definitely observed which may be formed due to sub-seismic faults and fractures. A subtle reflection is observed below the TCB within thick chaotic reflections, which is interpreted as the TLCC. Moving towards the SE, the continental Moho rises towards the basement top, but is not observed to reach the basement.

The oceanic crustal domain is observed to the SE, with the presence of a well-developed oceanic Moho. The oceanic Moho shows a subtle, but uninterrupted amplitude continuation. The top of oceanic crust is the TOB, with very strong reflection beneath the sediments.

In between the CC and the OC lies a diffused zone without any Moho signature, which has been taken as the POC. The observation is substantiated by the presence of contorted reflections patterns, indicating the deformed nature of this zone, which have been taken as further point in favor of a POC (Karner 2008; Nemčok et al. 2012).
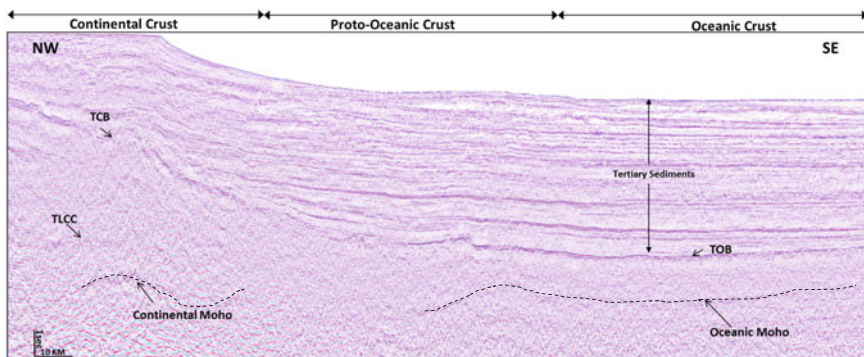

Fig. 4 Regional seismic line GXT-1700 that runs through the study area, north of Mahanadi basin, shows the continental Moho and the oceanic Moho is interpreted at about 11 s

Thus, the ocean-continent transition is interpreted as a diffused zone with two boundaries—(1) a CC-POC boundary, where the upper crust tapers to the surface (though not clearly visible in this section), and it represents the end of the continental crust and (2) a POC-OC boundary defined by the beginning of oceanic Moho and representing the beginning of the oceanic crustal domain. Figure 5 shows the likely position of CC-POC (red cross) and POC-OC (yellow cross) boundaries within the study area as interpreted from the seismic data. The boundaries mapped in the study area shows a landward shift from what interpreted in Nemčok et al. (2012). Further north, the boundaries could not be extended due to absence of deep seismic data.

Figure 5 also shows the position of the extracted profile for gravity modeling and the tentative position of the CC-POC boundary, as discussed later.
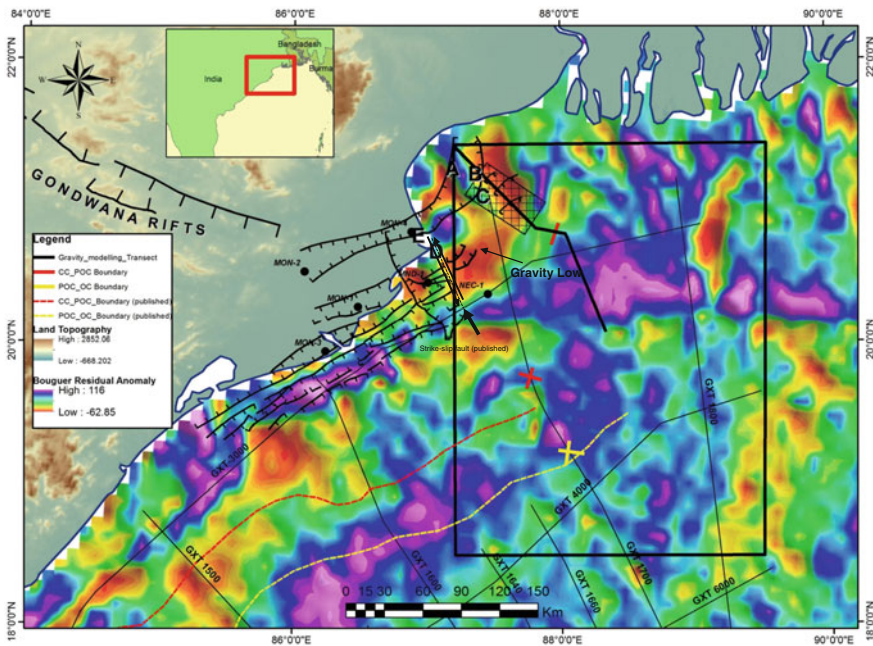

Fig. 5 The zoomed part of Fig. 1. The rift-grabens in the Mahanadi basin are acknowledged from Fuloria et al. (1992). The numbered rift-grabens in the study area are the part of the present paper. The grabens A-C are dipping basinward, whereas the grabens D and E are dipping landward. The black bold line across the grabens A-C is the gravity modeling transect. The *red* and *yellow dashed lines* are the CC-POC and POC_OC boundaries respectively from Nemčok et al. (2012). The *red* and *yellow* crosses are the interpretations from seismic section Fig. 4. The *red line* segment on the gravity modeling transect is the CC-POC boundary at a distance of 106.4 km from the beginning of the line. Unroofing of the mantle is not evident in the model, so the boundary is taken at the point where the where the continental crust reached it thinnest. POC-OC boundary is not present in the section, probably is goes through just outside the model limit. The strike-slip fault shown in the figure is taken from Fuloria et al. (1992)

3.2 Rift Signature Interpretation

Seismic mapping has been done for the most prominent reflectors and major chrono-stratigraphic horizons in both the 2D and 3D seismic data. Three major grabens have been identified from 3D seismic data in the northern part of the study area, marked as A, B and C in Fig. 6. The bounding faults of these grabens dip towards the basin margin. Balasore graben is present in the NW as small grabens, with the bounding faults getting reactivated in Tertiary.

For the purpose of establishing the rift architecture, three horizons have been interpreted from 2D seismic data and correlated throughout the study area:

(a) Basement top (Red horizon)
(b) Post-rift top (top of rift-related sediments, Yellow horizon)
(c) Top of Post rift volcanics (Magenta horizon)

The rift packages are identified from their growth geometry towards the bounding fault and truncation at their top at the break-up unconformity. The rift patterns show orientation parallel to the coast line and are related to the India-Antarctica break-up similar to the rift grabens on the adjacent offshore Mahanadi graben and KG and CY basin further south. The mapped synrift base/basement horizon, marked with red color, is shown in Fig. 7a, together with the location of the three main grabens, A, B and C and the Balasore graben towards NW. The colors red-yellow and green-purple in the map indicate lower and higher TWT (two-way-time in milliseconds) values, which represent the shallower and deeper basement depths, respectively. Figure 7b shows the map of the post-rift top, marked
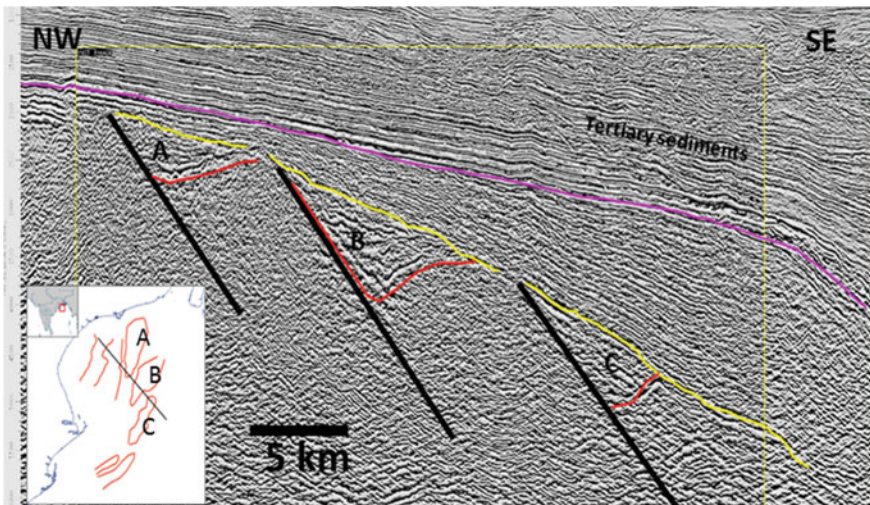

Fig. 6 Seismic section through the study area, showing the key surfaces and the interpreted grabens. Vertical scale is in ms TWT (two-way-time)
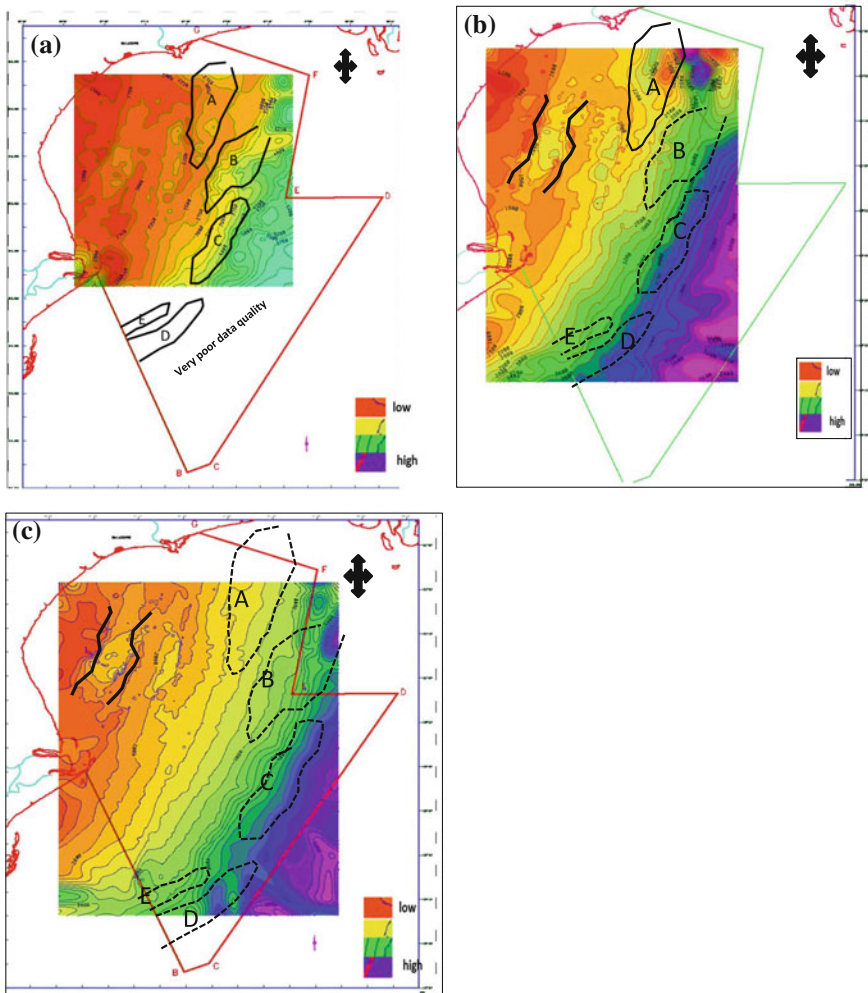
Fig. 7 a TWT structure map of basement top (syn-rift base) in the study area. The colours *red* and *yellow* are low values and *blue* and *purple* are high values. The data quality of 2D seismic lines are very poor, thus the map could not be extrapolated till grabens D and E. **b** TWT structure map of post-rift top in the study area. **c** TWT structure map of top of post-rift volcanics

with yellow in Fig. 6. The graben geometry is difficult to identify from this map, except for graben A. Figure 7c shows the map of the post-rift volcanics, with the topography mimicking the present day sea floor.

Five 2D seismic profiles are shown for details of the individual grabens in the NEC-MND basin (Figs. 8, 9, 10, 11 and 12), together with the interpreted key seismic reflectors. Figure 8 shows the grabens A and B; graben B is further sub-divided into B' and B", based on a subsidiary fault within the main depocentre. In this and the subsequent figure, the reflectors below the red horizon are chaotic in

Fig. 8 Seismic section through the study area, showing the key surfaces and the interpreted grabens. Vertical scale is in ms TWT
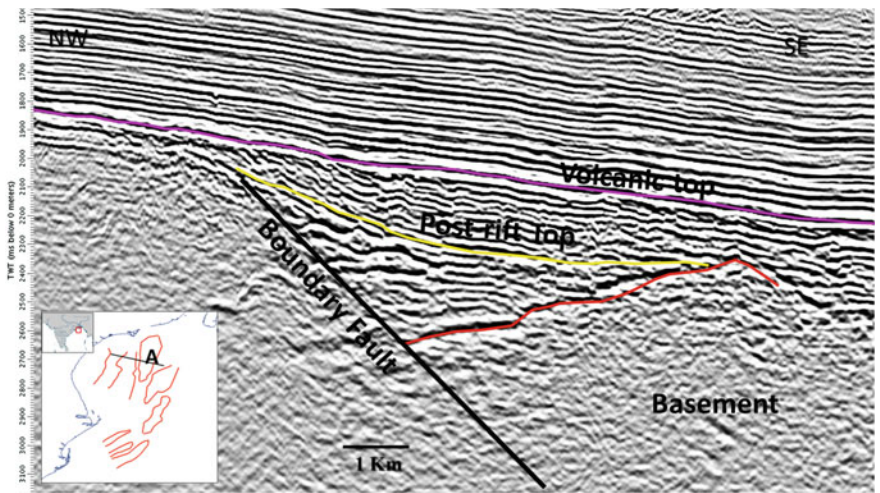
Fig. 9 Seismic section through the study area, showing the key surfaces within graben A. Vertical scale is in ms TWT

nature and show no proper pattern, and are interpreted as the basement. Seismically similar correlatable package has been drilled by OIL and ONGC Ltd. in MON-4 (onland) and MND-1(offshore) in Mahanadi basin, indicating the presence of basement. Thus the red horizon is interpreted as the basement top. The black lines are the faults observed within the basement. The reflectors above the red horizon show growth patterns typical of synrift package. The top of this sediment package is the yellow horizon above which no growth patterns are observed. Above the synrift package (yellow horizon), show bright amplitude and low frequency, and are
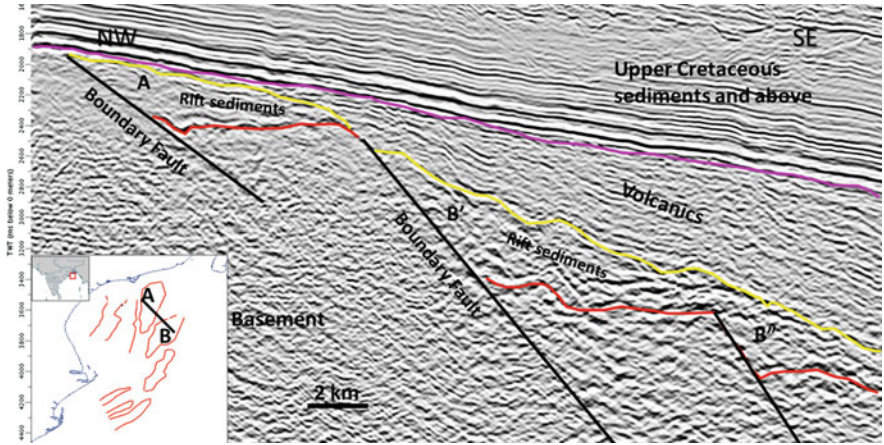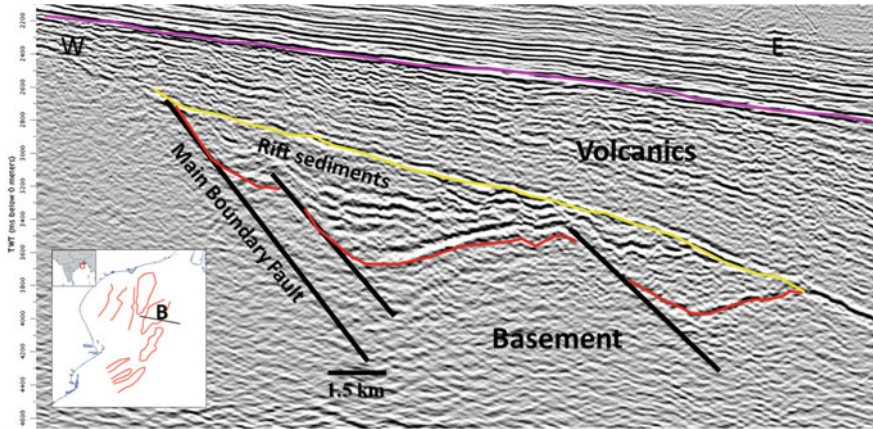
Fig. 10 Seismic section through the study area, showing the key surfaces for Graben B. Vertical scale is in ms TWT
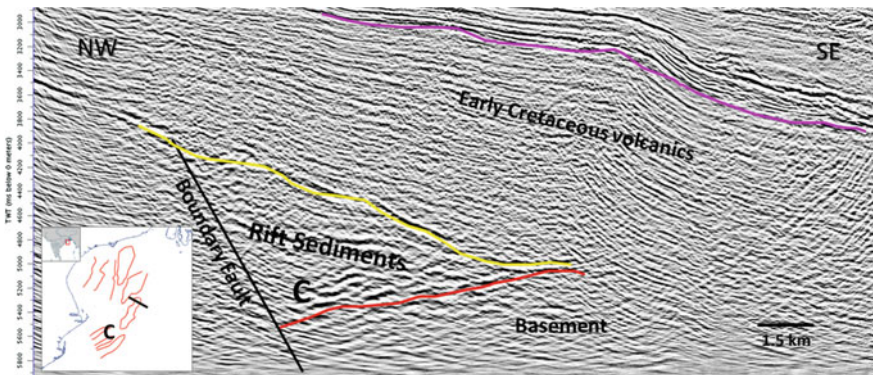
Fig. 11 Seismic section through the study area, showing the key surfaces for Graben C. Vertical scale is in ms TWT

interpreted as lava-flows. This package has been drilled in the offshore well NEC-1, whose location is shown in Fig. 5, in other part of Mahanadi basin, confirming the lithology. These lava flows are probably related to late Early Cretaceous volcanism associated with Rajmahal traps and 85°E Ridge volcanism, based on similar time of formations (Bakshi 1995) and geographical closeness. The palynological assemblage recorded in these basalts is related to Rajmahal Traps and 85°E Ridge which is reported by Interra Exploration Company (India) Private Ltd. Figures 9, 10 and 11 show the geometry of the individual grabens A, B and C in detail. Note that in Fig. 11, the Early Cretaceous volcanics become thicker on top of graben C, which lies more towards the CC-POC boundary, compared to that in grabens A and B. Apart from the major grabens, A, B and C, two minor grabens, D and E lies outside
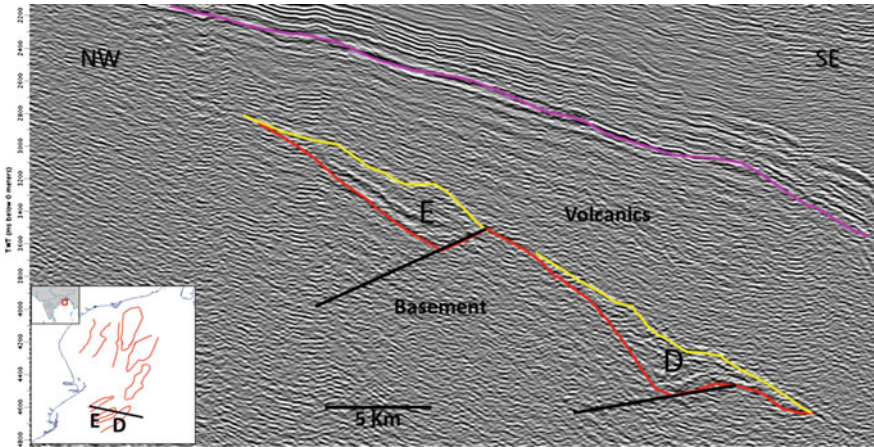
Fig. 12 Seismic section through the study area, showing the key surfaces for grabens D and E. Vertical scale is in ms TWT

the 3D area, in the southern part of the study area (Fig. 12). The bounding faults in these grabens dip landwards.

3.2.1 3D Seismic Mapping

3D seismic data enables us to identify the sedimentation history within the synrift grabens in much detail, and consequently, four horizons have been mapped within the synrift packages from in 3D seismic volume as shown in Fig. 13:
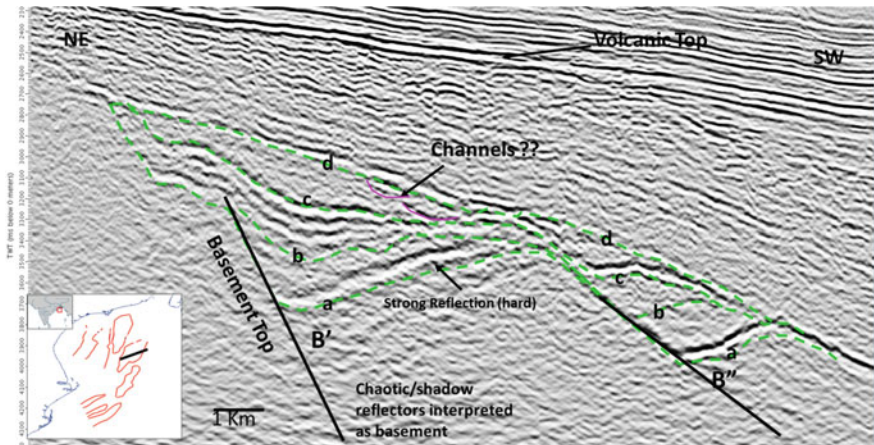
Fig. 13 The figure showing the detailed interpretation in an arbitrary line across the graben B in TWT (ms)

(a) Syn-rift base (Basement top)
(b) Early Synrift top
(c) Late Synrift top (Synrift top)
(d) Sag phase top (Post-rift top)

The horizons mapped from the 3D seismic data are present locally and we have not been able to correlate them across the different grabens. An illustrated example of these subdivisions of the synrift package has been shown for graben B, whose seismic imaging is better than those of grabens A and C. Figure 13 shows an arbitrary seismic profile across graben B with the horizons interpreted in 3D seismic volume. The reflector 'a' is very prominent and it demarcates the interface between the chaotic reflectors below and the wedge forming reflectors above. Thus the reflector 'a' indicates the basement top. The top of 'a' shows wedge-pattern reflectors with thickening sediments near the faults marked in black, indicating growth pattern characteristics of synrift deposits. This sediment package shows an absence of layering and reflection continuity, and is indicative of sudden influx of locally derived sediments within the synrift, probably representing alluvial fans and fan deltas. This may indicate the beginning of syn-rift phase, the top of which, and reflector 'b'; is taken as the end of early rift sedimentation. The reflectors above 'b' show high reflectivity with parallel sediment patterns, typical of calm lacustrine environment (Morley and Wescott 1999), the top of which is marks the end of synrift sedimentation, and is indicated by the reflector 'c'. The reflectors above 'c' are parallel to sub-parallel and also show concave-up reflections indicative of local accommodation during post rift sedimentation, and are taken to represent sag-phase deposits. The reflector'd' mark the top of the sag phase post-rift sediments. Above the sag phase deposits, the reflectors are of high amplitude and low frequency, with some chaotic patters, and are taken to represent the Early Cretaceous volcanics, as discussed in the earlier section.

Figure 14a shows the time-structural map of horizon 'a' at the synrift base. In this figure, two grabens are observed: B' and B", along which the accommodation spaces are created during various phases of rifting. These are individual rift systems having their respective basin bounding faults forming two isolated basins. The dimension of graben B' is larger than that of B". The overall extents of the rift grabens are unknown due to limited data extent. Figure 14b, shows the 3D perspective view of the same time structure map.

Figure 15a shows the time-structure map of horizon 'c' at the top of synrift. Figure 15b, shows the RMS (Root Mean Squared) amplitude map of the late synrift top. The red dashed boundary marked around the high amplitude response shows a narrow head and broaden end, and may represent a lobate feature associated with a channelized flow system. The direction of the flow is orthogonal to the fault displacement.

Figure 16a shows the time-structure map of horizon'd', the top-most horizon in the rift basin marking the end of sag phase sedimentation. Figure 16b shows the RMS amplitude map of the same, extracted in a window along the horizon with
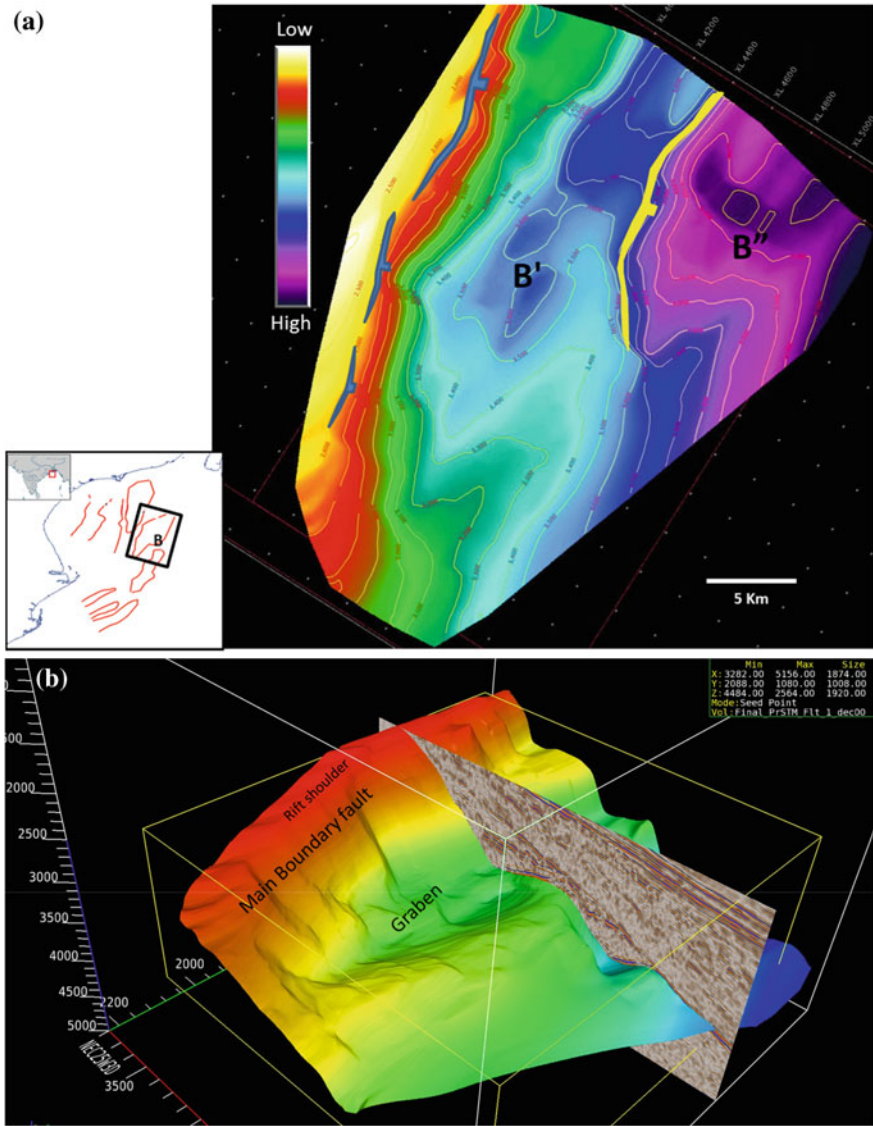
Fig. 14　a Time-structure map view of the base of synrift. **b** 3D view of base of the synrift base. *Red* and *yellow* colours show shallow depth and *green* and *blue* colours show deeper depth

30 ms top and below to it. The high amplitude in the figure may indicate the presence of coarse-grained sediments.

Figure 17 shows the TWT thickness map between the synrift base and the synrift top. In this figure some prominent depocentres are present, corresponding to the grabenal geometry. The thickest sediments are along the bounding faults, indicating growth nature of the fills.
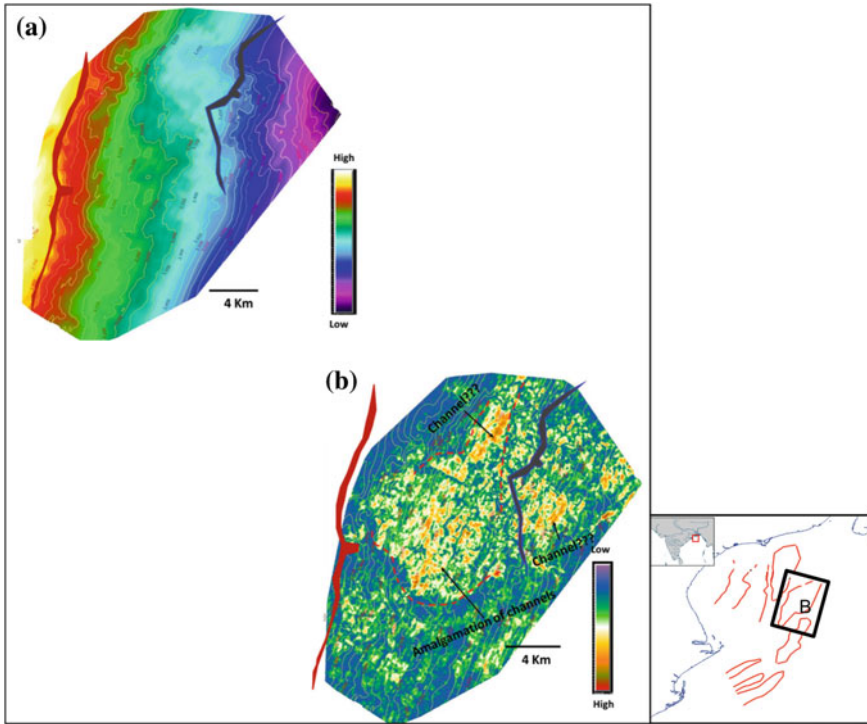
Fig. 15 **a** Time structure map of top of early syn-rift phase; **b** amplitude map overlaid by TWT contours. The location of the maps is shown in the *inset*

Seismic velocity analysis has been performed to support the interpreted graben geometry, which shows a good fit with the interpretation. Figure 18 is a representative velocity profile along graben B, illustrating the fit between the interpretation and velocity variation. Major velocity change is seen at the interpreted basement level where velocity reaches more than 5500 m/s. Figure 19 shows a time-vs-velocity plot along a 1D location shown with dashed line in Fig. 18. It shows that the interval velocity ranges between 4900 and 5400 m/s within the synrift sequence, and increases drastically within the basement. The sediments within post-rift sequence shows a slight velocity inversion, which then increases again within the synrift.

3.3 2D Forward Gravity Modeling

2D forward gravity modeling has been used to validate the interpreted crustal boundaries from seismic data. It involves setting up a model, calculating the gravity anomaly, comparing it with the observed data and iteratively varying the density of
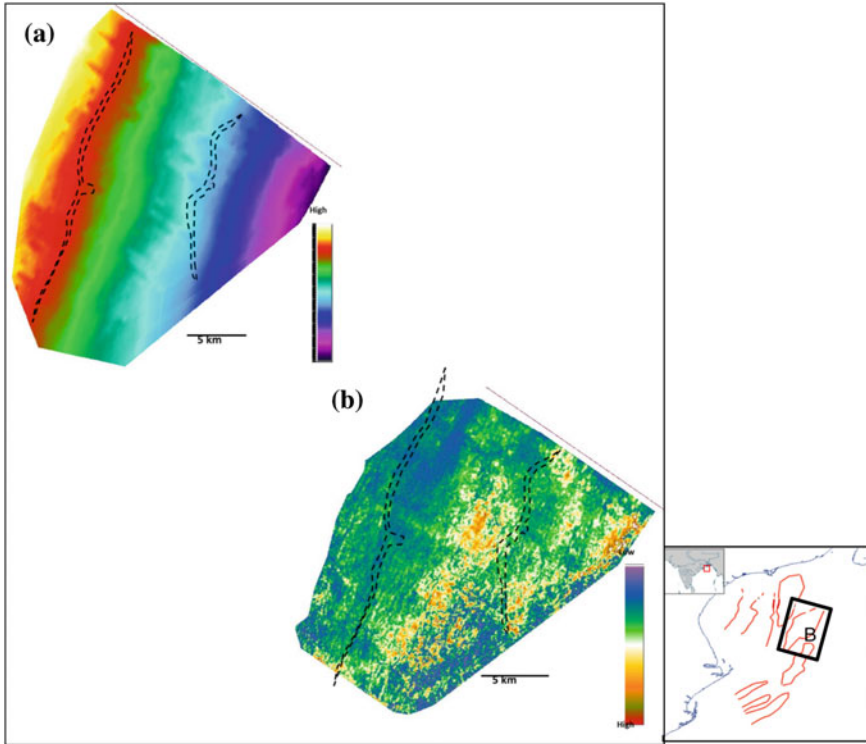
Fig. 16 a Time structure map of top of late syn-rift phase; **b** amplitude map of the syn-rift top

the interpreted layers and modifying the source body geometries until the calculated anomaly matches well with the observed data. The modeling is done in GM-SYS 5.01.10, which is part of Geosoft's Oasis montaj 6.4.2 suite. The densities used for the different layers (e.g. Clark 1966; Touloukian et al. 1981; Christensen and Mooney 1995; Lillie 1999) are shown in Table 1. The software calculates the gravity anomaly response, which is matched with the observed data and a difference is calculated, which needs to be minimized to get a good fit. The methods used to calculate the gravity model response is based on the methods of Talwani et al. (1959), and make use of the algorithms described in Won and Bevis (1987). All the models extend to ± 30,000 km in the −X and +X directions to eliminate edge-effects.

The free-air gravity anomaly includes the gravity effect of the water layer at the water-sediment interface, and shows a strong correlation with bathymetry. In the current study, a profile extracted from the gravity anomaly data is used to interpret the crustal geometry in the study area and is validated by forward gravity modeling. As the seismic section along the extracted profile is only 13 km deep (check depth), the crustal layers were all interpreted based on gravity signature, the last seismically interpreted horizon being the Lower Cretaceous volcanic base over the synrift
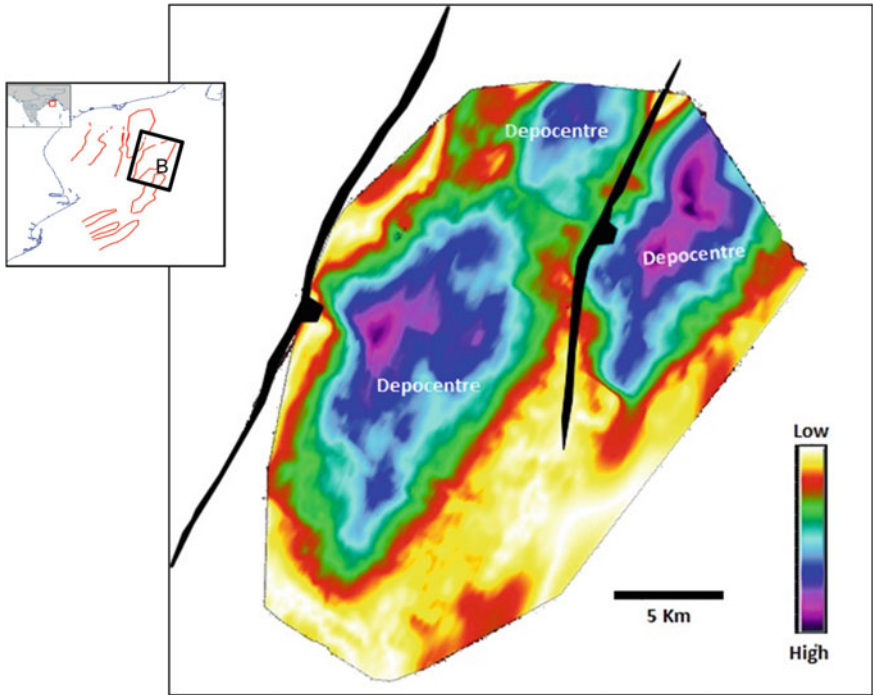
Fig. 17 The figure showing the TWT thickness map (ms) between the Synrift base and the Synrift top
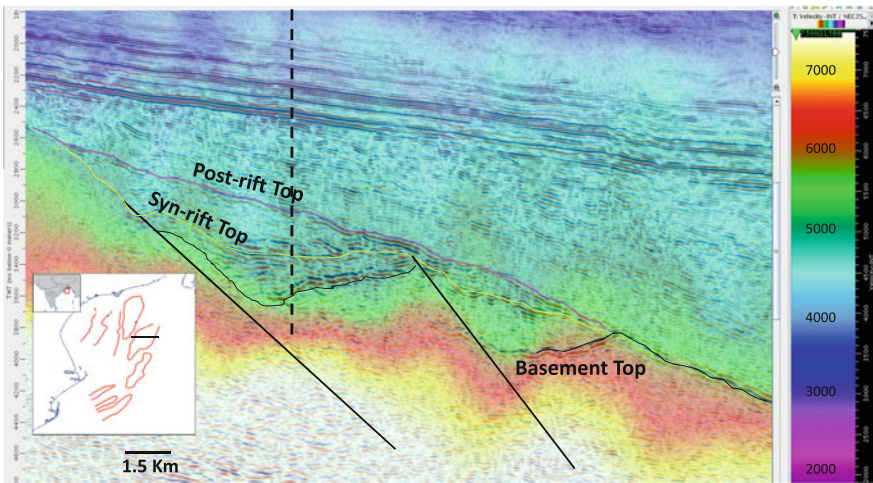
Fig. 18 The figure showing the seismic section overlaid by interval velocity. The *dashed line* is the location for 1D-profile in Fig. 19
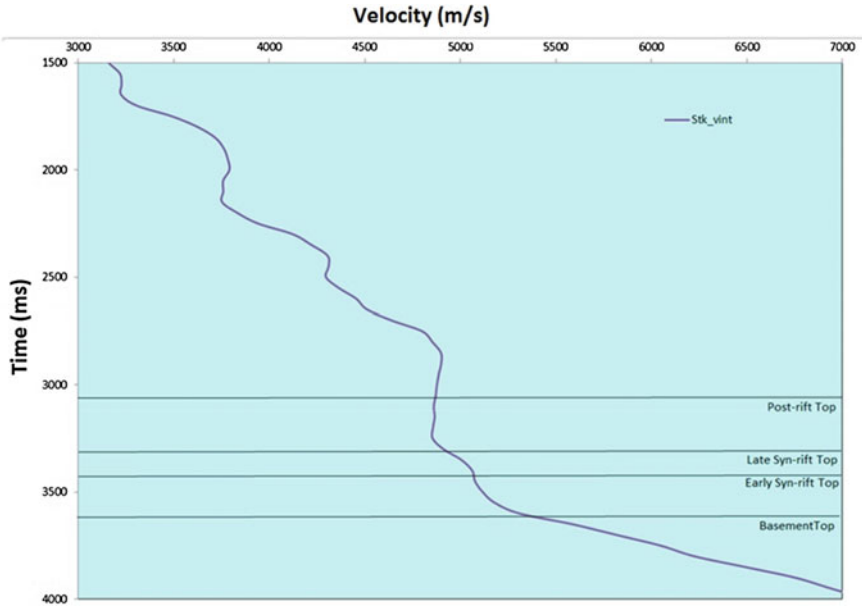
Fig. 19 The figure showing the interval velocity plot at the graben B (the location is shown as *dashed line* in Fig. 18)

Table 1 Densities used in gravity modeling

Layer	Density (g cm^{-3})	Type
Water	1.03	Water
Sediment 1	2.3	Sediment
Sediment 2	2.4	
Sediment 3	2.5	
Sediment 4	2.6	
Volcanics	2.7–2.9	Volcanics
Upper cont. crust	2.63	Crust
Middle cont. crust	2.89	
Lower cont. crust	3.04	
Upper ocn. crust	2.7	
Middle ocn. crust	2.89	
Lower ocn. crust	3.04	
Mantle	3.36	Mantle

Cont—continental and ocn—oceanic

grabens. Gravity data has also been used to check for the presence of low density synrift sequences below the basalt, but because of small dimensions of the individual grabens compared to the spatial resolution of the data points, it was not possible to uniquely isolate the gravity signature of the grabens. The extracted

profile shows moderate negative values between −25 and −45 mGal in the continental side, gently rising to +45 mGal near the shelf break and then rapidly falls to −8 mGal as the basin deepens.

During forward gravity modeling, different models have been tried to match the observed gravity anomaly, and the one that fits the expected crustal architecture in the study area (Nemčok et al. 2007, 2012; Sinha et al. 2010) has been taken. The modeled profiles (Figs. 20, 21 and 22) whose location is shown in Fig. 5 show a thinning of the continental crust towards the basinal side, gradually merging with oceanic crustal rocks, without any definite presence of exhumed mantle zone. This is expected in regions affected by post-rift volcanism, where the gravity signature of the unroofed Moho gets lost in the voluminous magma flows. The same is observed in Fig. 4, where the basinward termination of the continental Moho is unclear, leaving doubt about unroofed mantle. The shallowest mantle comes up at a gravity
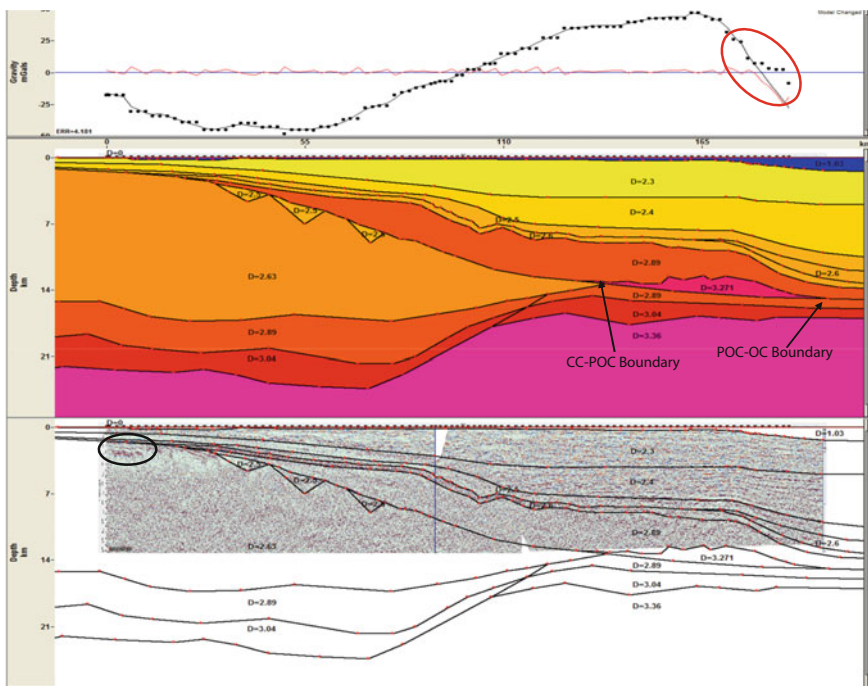
Fig. 20 Forward gravity model along profile extracted across the NEC basin, showing a good match between the observed and calculated gravity anomaly values. The blocks with prescribed density are matched with the seismic interpretation of the main boundaries to prepare the model. *Dotted line*—observed gravity anomaly values, *thin line*—calculated values, *red line* along zero mGal—difference between observed and calculated anomaly values. The extreme end of the data shows a sharp lowering of gravity anomaly value (*red circle*), which has not been modelled. The basinward gravity anomaly high has been explained by the presence of a high density body (of 3.2 g cm^{-3}) below the basalt flows which may represent an intrusive body. Balasore graben is marked in *black*
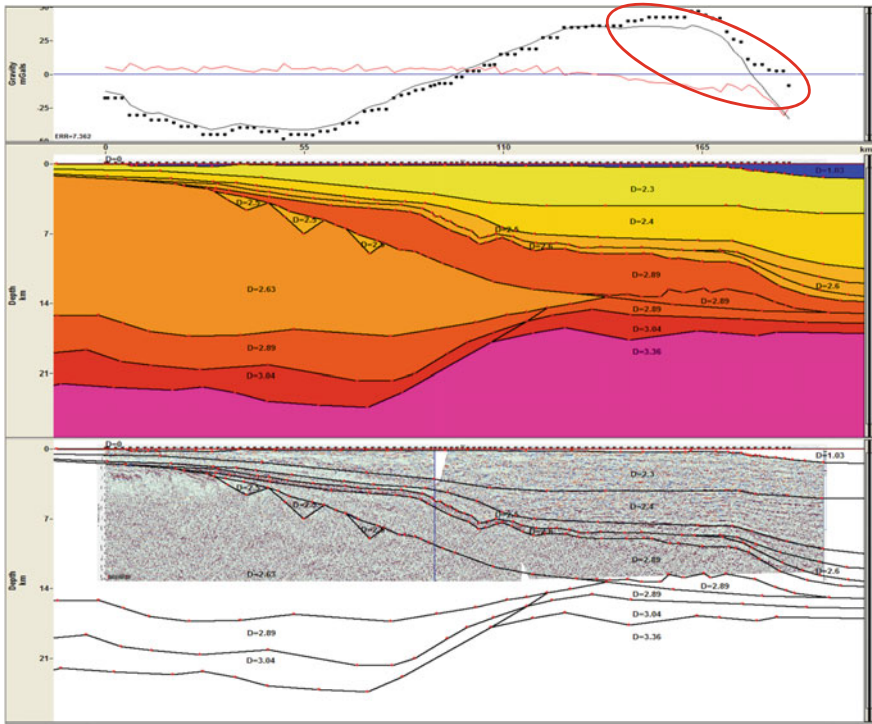
Fig. 21 Same as Fig. 20. Changing the density of the high density body to match that of the basalt/middle crust immediately shows up as a strong localized decrease of the modelled gravity anomaly values (*circled red*)

anomaly value of +33 mGal, while further rise in gravity anomaly requires the inclusion of a high density body (of 3.2 g cm^{-3}) below the basalt flows which may represent an intrusive body (Fig. 20). With the absence of this high-density layer, a strong localized decrease of the modeled gravity anomaly values is observed on the basinward side of the profile (Fig. 21). The extreme basinward end of the data shows a sharp lowering of gravity anomaly values, which from its frequency content, seems to be a shallow level density anomaly within the sedimentary layers, or at the water-sediment interface. It has not been modeled in this study. The synrift grabens observed in seismic image has been assigned a density of 2.5 g cm^{-3}, which when removed shows a negligible change in the calculated gravity anomaly sharing that the spatial resolution at the gravity data is insignificant to properly model the synrift grabens (Fig. 22).
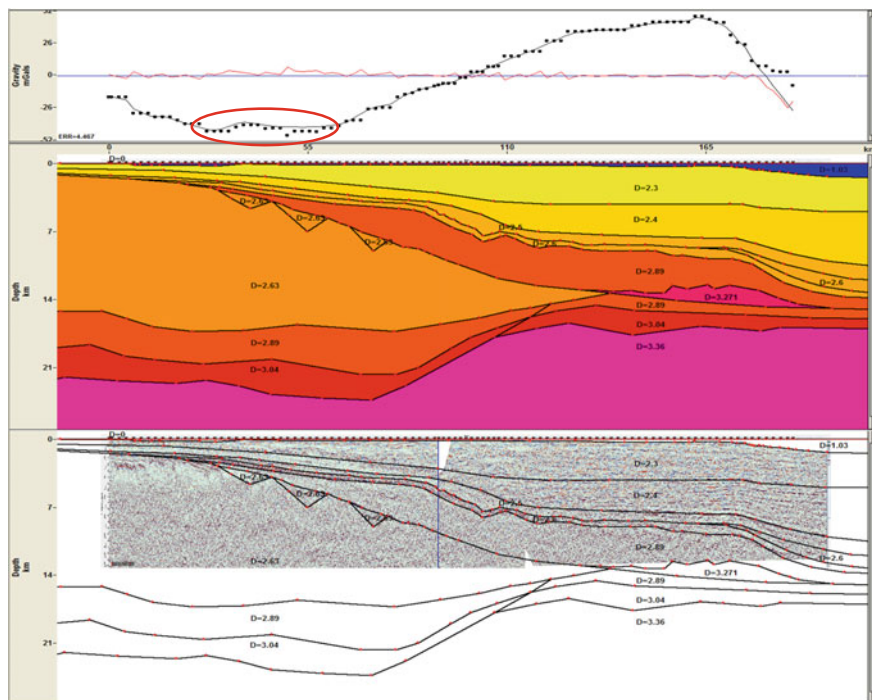
Fig. 22 Same as Fig. 20. Changing the density of synrift grabens to match that of the *upper continental crust* shows up as a gentle increase in the calculated gravity anomaly (*circled red*)

4 Discussions on Synrift Age

The interpretation of rift grabens below Early Cretaceous volcanics has been reported for the first time from the study area. The three major grabens are small and isolated, and may represent the distal end of the rifted continental crust. The rift age is not available in this region. The rift age, as determined biostratigraphically in the Krishna-Godavari basin is from Toarcian to Valanginian. In NEC-MND basin, the rift age is uncertain mainly because of ambiguity between well data (ONGC and OIL drilled wells) and the biostratigraphic report (Interra Exploration Company (India) Private Ltd.) and the absence of seismic data correlating these wells. RIL has not drilled any well in these rift grabens. Four onland wells, earlier drilled by OIL in the grabens shown in Fig. 2 have reported Early Cretaceous as the age of the oldest sediments in these grabens (Fuloria et al. 1992). RIL's in-house interpretations suggest that the synrift sediments drilled in MON-4 and MND-1 well are of Upper Jurassic age, based on the presence of *Callialasporites dampieri*, a key marker of Jurassic age. Further support comes from Adyalkar (1964), who suggest a Liassic age (Lower Jurassic) for the outcrops of Atgarh sandstone near Cuttack, Orissa, believed to be of syn-rift deposits related to India-Antarctica break-up.

5 Conclusions

Based on the above interpretations and discussions the following points have been concluded:

1. The rift system has been observed in the NEC-Mahanadi basin, whose orientation is inline with the rift systems seen in KG and CY basins.
2. Due to limited data control, the CC-POC and POC-OC boundaries can only be interpreted in GXT-1700.
3. The actual presence of a strike slip fault between Mahanadi and NEC rift grabens as mentioned in Fuloria et al. (1992), could not be established from our current dataset.
4. The sedimentary sequences within the synrift succession points towards a well-developed synrift sytem in the NEC-Mahanadi basin.
5. The presence of rifts in the basin cannot be interpreted from 2D Gravity modelling.

References

Adyalkar P (1964) Sedimentological study of the Atgarh sandstones. Cuttack district, Orissa

Bakshi AK (1995) Petrogenesis and timing of volcanism in the Rajmahal flood basalt province, northeastern India. Chem Geol 73–90

Christensen NI, Mooney WD (1995) Seismic velocity structure and composition of the continental crust: A global overview. J Geophys 9761–9788

Clark SP (1966) Handbook of physical constants. Geol Soc Am Mem 587

Fuloria R, Pandey R, Bharali B, Mishra J (1992) Stratigraphy, structure and tectonics of Mahanadi offshore basin. Geol Surv Ind Spec Publ 29:255–265

Interra Exploration Company (India) Private Ltd. (n.d.). Structural and stratigraphical interpretation of geological and 2D seismic data NEC block, Mahanadi offshore. Interra Exploration Company (India) Private Ltd, Mumbai

Karner GD (2008) Depth-dependent extension and mantle exhumation: an extreme passive margin end-member or a new paradigm? In: Central atlantic conjugate margin conference. Halifax, Canada

Lillie RJ (1999) Whole earth geophysics: an introductory textbook for geologists and geophysicists, 1st edn. Prentice Hall, Upper Saddle River, pp 251–277

Misra AA, Bhattacharyya G, Mukherjee S, Bose N (2014) Near N–S paleo-extension in the western Deccan region, India: Does it link strike-slip tectonics with India–Seychelles rifting? Int J Earth Sci 103:1645–1680

Misra AA, Mukherjee S (2015) Tectonic inheritance in continental rifts and passive margins. SpringerBriefs in Earth Sciences (in Press)

Misra AA, Sinha N, Mukherjee S (2015) Repeat ridge jumps and microcontinent separation: insights from NE Arabian Sea. Mar Pet Geol 59:406–428

Morley CK, Wescott WA (1999) Sedimentary environments and geometry of sedimentary bodies determined from subsurface studies in East Africa. AAPG Stud Geol 44:211–231

Nemcok M, Sinha S, Stuart C, Welker C, Choudhuri M, Sharma S et al (2012) East Indian margin evolution and crustal architecture: integration of deep reflection seismic interpretation and gravity modeling. Geological Society, London, Special Publications, London

Nemcok M, Stuart C, Welker C, Smith S, Yalamanchili S, Srivastava DC et al (2007) Crustal types, structural architecture and plate configurations study of Reliance east coast region. EGI for Reliance Industries Limited, Navi Mumbai

Rao GN (2001) Sedimentation, stratigraphy, and petroleum potential of Krishna-Godavari basin, east coast of India. Am Assoc Pet Geol 85:1623–1643

Sandwell DT, Smith WF (1996) Global bathymetry prediction for ocean modeling and marine geophysics. http://topex.ucsd.edu/marine_topo/text/topo.html

Sandwell DT, Smith WF (2009) Global marine gravity from retracked Geosat and ERS-1 altimetry: ridge segmentation versus spreading rate. J Geophys 114 BO1411

Simpson K, Plummer J, Brink R (2006) Report on contractor performance during the 'INDIASPAN' 2D marine seismic reflection survey offshore India. Survey by Scan Geophysical ASA onboard the M/V Geo Searcher for GX Technology Corporation

Sinha ST, Nemcok M, Choudhuri M, Misra AA, Sharma SP, Sinha N et al (2010) The crustal architecture and continental break up of East India passive margin: an integrated study of deep reflection seismic interpretation and gravity modeling. AAPG Annual Convention & Exhibition, New Orleans

Talwani M, Heirtzler JR (1964) Computation of magnetic anomalies caused by two dimensional bodies of arbitrary shape. In: Parks GA (ed) Computers in the mineral industries, part 1, Stanford University. Publications, Geological Sciences, pp 464–480

Talwani M, Worzel JL, Landisman M (1959) Rapid gravity computations for two dimensional bodies with application to the Mendocino submarine fracture zone. J Geophys Res 64:49–59

Touloukian YS, Judd WR, Roy RF (1981) Physical properties of rocks and minerals. McGraw-Hill, New York, pp 230–411

Won IJ, Bevis M (1987) Computing the gravitational and magnetic anomalies due to a polygon: algorithms and fortran subroutines. Geophysics 52:232–238

Study of CO$_2$ EOR in a Sector Model from Mature Oil Field, Cambay Basin, India

Ravi Prakash Srivastava, Nimisha Vedanti, Idar Akervoll, Per Bergmo, Ramesh Chandra Yerramilli, Sanjay Surya Yerramilli and V.P. Dimri

Abstract Among various Enhanced Oil Recovery (EOR) methods, gas injection has been proven to be one of the effective ways of enhancing oil recovery from mature fields. The field under study has approached the economic limit of production under conventional recovery methods (primary and secondary recovery). Since start of production in sixties, the field has produced 48.5 % of the initial oil in place and the water cut has increased to 89 % in April 2011. Responding to the industry needs, initially a comprehensive study was performed to evaluate the potential of immiscible CO$_2$ injection for the recovery of residual oil after water flooding in this mature field. This paper presents the preliminary results of immiscible CO$_2$ injection on the basis of laboratory studies and detailed compositional simulations carried out on a sector model of the field. Based on the results obtained from laboratory studies it was found that CO$_2$ injection yields significant incremental recovery. Simulation results show significant increase in field oil production, essentially from 200 to 1100 m^3/day and considerable decrease in water cut were observed. In addition, detailed PVT simulations were carried out to obtain

R.P. Srivastava · N. Vedanti (✉) · R.C. Yerramilli · S.S. Yerramilli · V.P. Dimri
CSIR-National Geophysical Research Institute, Hyderabad, India
e-mail: nimisha@ngri.res.in; nim.ved@gmail.com

R.P. Srivastava
e-mail: ravi_prakash@ngri.res.in

R.C. Yerramilli
e-mail: yslsrchandra@gmail.com

S.S. Yerramilli
e-mail: sanjaysurya@gmail.com

V.P. Dimri
e-mail: vpdimri@ngri.res.in

I. Akervoll · P. Bergmo
SINTEF Petroleum Research, Trondheim, Norway
e-mail: Idar.akervoll@sintef.no

P. Bergmo
e-mail: Per.Bergmo@sintef.no

an equation of state (EOS) that would better describe the phase changes in the reservoir. These results would form the basis for carrying out CO_2 EOR simulations on a field scale.

Nomenclature

CO_2	Carbon dioxide
WAG	Water alternating gas
EOR	Enhanced oil recovery
PVT	Pressure volume temperature
EOS	Equation of state
NNW-SSE	North north west—south south east
ONGC	Oil and natural gas corporation
OWC	Oil water contact
TVD	True vertical depth
TPD	Tons per day
N_2	Nitrogen
HC	Hydrocarbon
HCPV	Hydrocarbon pore volume
TVDSS	True vertical depth sub sea
MW	Molecular weight
MMP	Minimum miscibility pressure

1 Introduction

Enhanced Oil Recovery (EOR) by CO_2 injection is an attractive option because it has the potential to increase the oil recovery of producing fields. In the recent years, CO_2 injection for EOR has received a great attention due to multifold benefits such as reduction of global warming effects caused by greenhouse gas, enhancing oil recovery and high tax savings in some countries, earning carbon credit by practicing CO_2 EOR which could eventually culminate in CO_2 sequestration and storage. In response to these reasons, CO_2 EOR has attracted many policy makers and industries to implement it. Gas and oil reservoirs are considered as safe storage sites due to their historic record of trapping buoyant fluids for millions of years. Long term deposition capacity in oil reservoirs is limited, but petroleum reservoirs represent significant sinks for CO_2 (Holt et al. 2000).

The sour gas produced from offshore fields was processed to separate CO_2 in a processing plant and is delivered through a pipeline infrastructure which is about 70 km away from the implementation site. The field under study has been subjected to massive water flooding, however; still residual oil is left either as bypassed oil zones or as capillary trapped residual oil, which encourages the use of tertiary recovery methods as future options to increase the recovery. An EOR module for

immiscible CO$_2$ and water injection at alternate intervals [often termed as water alternating gas (WAG), in this case CO$_2$—WAG] was developed and preliminary calculations using this module and limited data indicated that the oil recovery potential for CO$_2$-WAG is more efficient than the continuous CO$_2$ injection; however this needs further study and simulation of continuous gas injection scenario in details.

CO$_2$-WAG EOR process involves efficient displacement of oil towards the production wells by overriding gas and under riding water fronts. The oil in this reservoir is not miscible with the pure CO$_2$ at reservoir conditions. In case CO$_2$ develops miscibility in the displacement front with the oil while propagating through the reservoir, then miscible displacement of capillary trapped residual oil occurs (Akervoll and Bergmo 2010). However, the swelling in the oil due to pure CO$_2$ injection is about 1.2 times of the volume (Dimri et al. 2012). This will enable efficient displacement of bypassed oil after water flooding. The density of CO$_2$ at reservoir conditions is in most cases lesser than the water (Hartai 2012) and may therefore reach other parts of the reservoir and consequently improve the sweep efficiency. Petrophysical and fluid composition properties in the reservoir model are populated by using results of laboratory and log data. We evaluate different injection schemes including CO$_2$ injection with and without recirculation of CO$_2$ breakthrough gas and CO$_2$-WAG.

2 Geological Setting

Cambay basin trending in NNW-SSE direction is an intracratonic rift basin in western India, which has proven hydrocarbon reserves. It contains thick sedimentary column that includes paleogene sediments, which corresponds syn-rift stage of deposition. The sediments in this basin usually range in age from Paleocene to recent, which were deposited over the Deccan basaltic basement (Mehdizadeh et al. 2010). Reactivation of such basement produced horst and graben structures, within which deposited sediments serve as hydrocarbon reservoirs. The thick sequences include shale sequences inter bedded with trap-wacke. Trap conglomerate and thin coal layers are also deposited above the trap. It is believed that the entire area subsided during Early Eocene resulting in deposition of Cambay shale, which is considered to be the main source rock. Subsequent to subsidence, several progradational and retrogradational sequences developed in the reservoir sediments during upper to mid Eocene period, which marks the reservoir. It can be further divided into four main members, comprising shales and sands. Telwa and Kanwa shale members form the cap rock in the reservoir. Further, the reservoir sands are often composed of thin alterations of sands and shales. In total 11 layers (S_A–S_K) were identified. Sands S_A to S_E, represent the middle sand group and sands S_F to S_K represent the upper sand group. The potential layers for CO$_2$ injection are S_C and S_D layers that are clubbed together in the simulation model and are referred as S_{C+D} in the following sections.

3 Reservoir Description

The length of the reservoir structure is about 17 km and the width is about 3 km. Structural map of the reservoir is shown in Fig. 1. The North—Western flank has gentle dip of less than 8° whereas South-Eastern flank is steeper with maximum of 18° dip. Faulting and lateral variations in continuity of the layers and reservoir properties appear to be the main controlling factors for oil distribution. Also, the layers are not continuous throughout the reservoir and some pinchouts were observed in between, which pose production challenges. The formation thickness of the target layers (S_{C+D}) is around 30 m. The average porosity and permeability of the target layers are 23 % and 1000 mD respectively. The reservoir parameters are summarized in Table 1. The oil water contact (OWC) was found to vary between
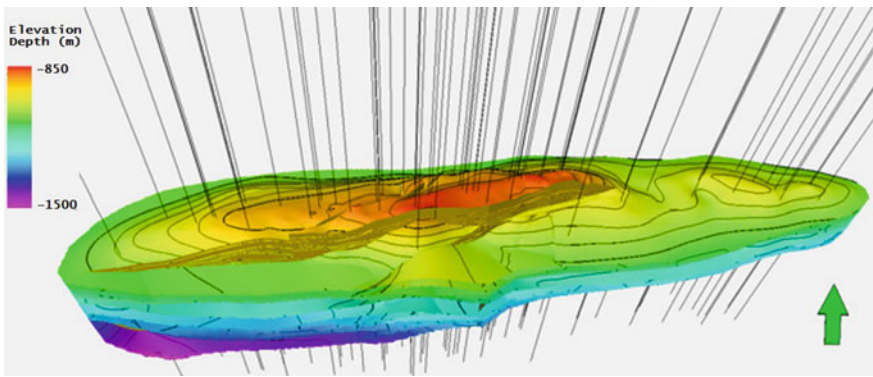
Fig. 1 Structural map of the reservoir being studied with wells penetrated in different layers. Legend shows depth where *red* is shallow and *magenta* is deeper. Faults are cutting structural contours

Table 1 Reservoir properties of the field (operator report)

Field/input data	Units	Values
Reservoir temperature	°C	78
Reservoir pressure	Bar	113.7
Saturation pressure	Bar	102.41
Depth	M	1113
Oil viscosity	Cp	0.36
Water viscosity	Cp	0.343
Density of stock tank oil	kg/Sm^3	820
GOR	Sm^3/Sm^3	80
B_o	Rm^3/Sm^3	1.44
Gas density	kg/Sm^3	0.739

1190 and 1214 m True Vertical Depth (TVD) and gas oil contact is at 1050 m TVD. A gradual lowering of the OWC in the north-east and eastern direction is due to the structural setting of the reservoir.

4 Objective of Present Study

Sand S_{C+D} is the major oil bearing sand in reservoir holding 552 MMbbls oil in-place. The field has produced around 48.5 % of the original oil in place till date since start of production in sixties. The sand was exploited initially using a well spacing of 500–600 m. A plateau oil production rate of 4400–4500 ton per day (TPD) was attained during 1968–1978 with the help of 65–73 production wells. From 1979, a decline in oil production and a steady increase in water cut were observed. As of 2011, the field is producing at an oil rate of 391 TPD with an average water cut of 88 %, which is uneconomical to operate. Further, laboratory studies indicated that the recovery could be increased by CO_2 injection. So, as per industry needs, a feasibility study was performed to evaluate the potential of immiscible water alternating gas (WAG), injection for the recovery of residual oil in this mature field. The gas in this case is CO_2.

5 Laboratory Studies

To evaluate the feasibility of tertiary gas injection for EOR in this mature oil field, laboratory experiments using representative cylindrical core samples were carried out by the operator. Experiments using CO_2, N_2 and HC gases at an injection rate of 1 cc/h were tested. CO_2 injection resulted in incremental oil recovery over water flood of around 11.8 % of hydrocarbon pore volume (HCPV) while HC gas injection resulted in 4.0 % of HCPV. Therefore, it was decided to go for CO_2 EOR study in the reservoir. In order to choose an optimum CO_2 injection rate, a series of experiments using CO_2 at different flow rates (5 cc/h and 1 cc/h) were conducted. From the experimental results it was found that repeated injection of CO_2 at 1 cc/h followed by a one week closure resulted in highest incremental recovery after water flood, which was around 15.71 % of HCPV. The detailed results of the experiments are presented in Tables 2 and 3 respectively. Inputs provided for simulation are as follows:

1. **Reservoir Model**: In this study, we have chosen the most productive layer (S_{C+D}) of the reservoir and a sector penetrated by 60 injectors (water and gas) and 106 producers to study the effect of CO_2-WAG on tertiary recovery. Geologically the model is E-W trending doubly plunging anticline, cut by reverse fault at southern flank (Fig. 2). The areal extent of the model is 9400 m in length and 5780 m in width. Structural contour and thickness maps were made available by

Table 2 Oil recovery at various CO_2 injection rates (operator report)

Stages of oil recovery	Experiment-I (CO$_2$ injection @ 5 cc/h)	Experiment-II (CO$_2$ injection @ 1 cc/h)	Experiment-IIa (Repeated CO$_2$ injection @ 1 cc/h after 1 week closure)
Oil recovery after water flood, % of HCPV	56.11	59.88	–
Oil recovery after tertiary gas injection, % of HCPV	64.67	72.65	75.59
Incremental oil recovery over water flood, % of HCPV	8.56	12.77	15.71

Table 3 Oil recovery for various gas injections at a flow rate of 1 cc/h (operator report)

Stages of oil recovery	Experiment-I (CO$_2$ injection @ 1 cc/h)	Experiment-II (N$_2$ injection @ 1 cc/h)	Experiment-IIa (HC injection @ 1 cc/h)
Oil recovery after waterflood, % of HCPV	64.8	55.5	57.7
Oil recovery after tertiary gas injection, % of HCPV	76.6	60.3	61.7
Incremental oil recovery over waterflood, % of HCPV	11.8	4.8	4.0

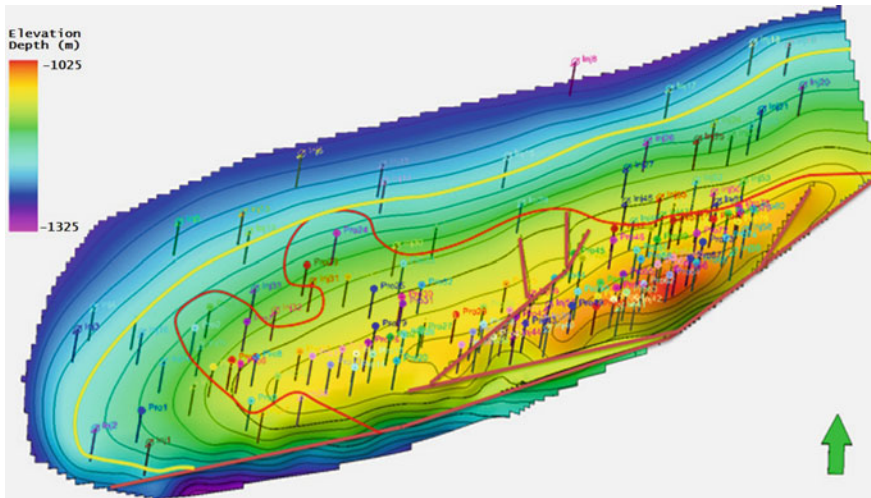**Fig. 2** Geometry of the reservoir model with the injectors (open circles) and producers (closed circles) in depth domain. The OWC is set at 1200 m (*yellow contour*). The *green arrow* at the bottom right indicates geographical north. The crest of the structure is towards southeast dominated by faults (*brown lines*). The area enclosed by the *red line* is dominated by production wells

Table 4 Reservoir rock properties for sub-layers within S3+4 (operator report)

Parameters/layers	S4-1	S4-2	S4-3	S4-4	S3-1	S3-2
Effective thickness, m	3.19	3.69	6.85	3.65	4	3.8
Porosity, %	24.7	24.9	23.5	23.5	23.9	21.7
Permeability, mD	540	1013	938	630	945	1953

the operator. In total 10 faults were modeled from the available fault sticks with the major ones running in northeast-southwest direction. A representative geological model was constructed from the available contour and thickness maps considering 11 layers within the productive horizon. The whole model consists of two main geologies, sand layers separated by the shale layers. The average distance between the wells is around 500 m. The injector wells can be used either as water injector or as a gas injector. The depth of the reservoir model extends from 1009 to 1342 m TVDSS.

2. **Rock Properties**: In this study, all the reservoir properties like porosity, permeability, rock compressibility etc. were obtained from the operator. The total thickness of the reservoir sand layers is 26 ± 1.5 m. The reservoir sands had an average porosity of 23 % and permeability of 1000 mD. The porosity and permeability assigned to the individual sub-layers are summarized in Table 4. The shale layers were assigned 100 % water saturation and zero permeability. The rock compressibility was taken as 2.16e-5 psi. The relative permeability functions are derived by use of Corey relative permeability correlations. The oil-water and gas-oil relative permeability curves are presented in Fig. 3.

3. **Fluid Properties**: The oil composition, mol-fraction and the molecular weight (MW) of each component, and the density of the liquid components of the live reservoir oil are presented in Table 5. The density and viscosity, formation volume factor of oil (B_o) and formation volume factor of gas (B_g) of the reservoir oil as a function of increasing pressure are presented in Table 6. These
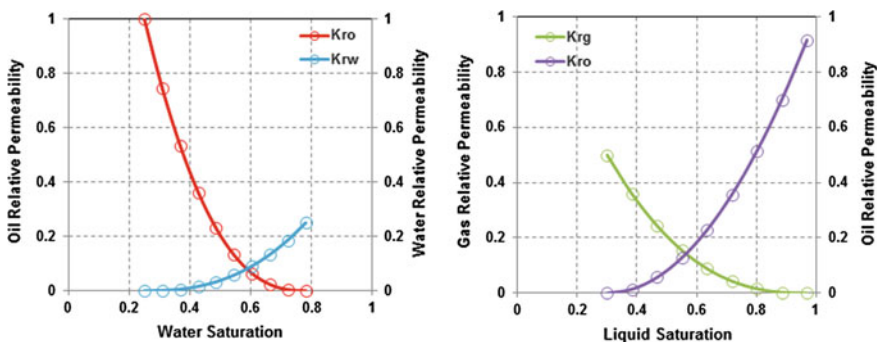
Fig. 3 Oil-Water (*left*) and Gas-oil (*right*) relative permeability curves used for simulation

Table 5 Composition, mol-fraction and molecular weight of each component and density of liquid components (operator report)

Component	Mol-fraction	Molecular weight (g/mol)	Liquid density (g/cm^3)
N$_2$	2.280	28.014	0.2600
CO$_2$	0.850	44.010	0.4200
C1	79.310	16.043	0.2600
C2	7.480	30.070	0.3580
C3	5.980	44.097	0.5076
iC4	1.120	58.124	0.5633
nC4	1.580	58.124	0.5847
iC5	0.75	72.151	0.6246
nC5	0.75	72.151	0.6309
C6	15.98	86.178	0.6635
C7	16.36	96.000	0.7380
C8	13.73	107.000	0.7650
C9	8.10	121.000	0.7810
C10	6.03	133.000	0.7920
C11	4.29	145.000	0.7960
C12	4.10	158.000	0.8100
C13	3.53	171.000	0.8250
C14	2.86	185.000	0.8360
C15	2.05	198.000	0.8420
C16	1.56	209.000	0.8490
C17	1.54	226.000	0.8450
C18	0.95	242.000	0.8480
C19	0.80	251.000	0.8580
C20+	3.545	407.000	0.9000

Table 6 Differential liberation study at reservoir temperature from one of the wells

Pressure (kg/cm^2)	Oil density (g/cm^3)	Oil viscosity (cP)	Oil FVF (B$_o$)	Gas FVF (B$_g$)
107.59	0.6987	0.48	1.347	–
106.19	0.6983	0.48	1.348	–
87.90	0.7048	0.51	1.319	11.80
70.32	0.7129	0.57	1.285	15.10
52.74	0.7223	0.62	1.250	20.70
35.16	0.7332	0.68	1.213	31.80
18.28	0.7477	0.79	1.166	61.52
0.0	0.7561	1.10	1.080	–
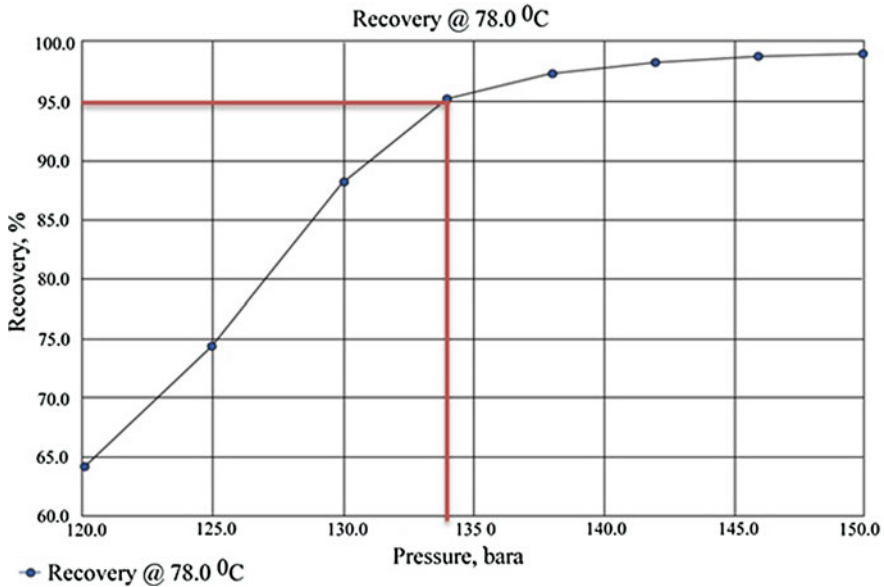
Fig. 4 MMP calculation using slim tube simulation. The pressure corresponding to 95 % recovery shows MMP value, which is 134 bar

fluid (oil and gas) properties are obtained from the differential liberation test. Soave-Redlich-Kwong (SRK) equation-of-state EOS is used to compute the phase behavior, physical properties, and composition of the gas and liquid phases present in the reservoir at relevant pressure and temperature conditions. PVT simulations were carried out using PVTSim (Calsep 2010) to generate the pseudo-components for reservoir simulation and for obtaining the minimum miscibility pressure (MMP) for the reservoir fluids. The result of the MMP calculation is shown in Fig. 4. The MMP is around 134 bar for the pure CO$_2$, which suggests that miscible CO$_2$ injection is not feasible in this field, since reservoir pressure is significantly less (104 bar) than the MMP. Therefore, in order to achieve miscible CO$_2$ injection in this field, the MMP was reduced by mixing HC components with CO$_2$.

4. Well Conditions and Development Strategy: All the wells used in the simulation study are vertical with an effective wellbore radius of 10.2 in. The skin factor at the wellbore was assigned zero value. The well placement pattern followed by the operator was adopted initially (Fig. 2). All the wells were kept on production rate control from the beginning of the simulation. Some of the injection wells were drilled selectively, keeping in view the permeability variation and heterogeneity of reservoir sands. Water injection was planned simultaneously for all the layers within S$_{C+D}$ unit in spite of their varying permeability.

5. **Grid System**: The productive layers in the reservoir are separated by impermeable beds (shales) that do not allow vertical fluid flow. Following the

combination-elimination procedure, the layers, which belong to the same rock type, are combined into one layer. A thickness weighted average of both porosity and permeability was calculated for the combined layer. It was assumed that the vertical fluid flow in thin reservoirs is not significant. A reservoir simulation grid with 187 × 110 grid cells and 11 geological layers was used for simulation. The resolution of the simulation grid blocks in horizontal x-direction is 50 m, y-direction is 47 m and grid cell height is 0.9 m in the entire model.

Model Validation The model is initialized for reservoir simulation with undersaturated oil (no gas-cap) and enclosed aquifer with the OWC at 1200 m TVDSS as illustrated in Fig. 2. The model is tuned to match the reported initial oil in place of 552 MMbbls.

6 Simulation Results and Discussion

Schlumberger's commercial reservoir simulator Eclipse 2012 was used for simulating the CO2-WAG displacement studies. The simulation runs were conducted using black oil simulator 'E100' of Eclipse 2012 (Schlumberger 2012). However, the simulation results shown in this paper are from the conceptual model. The model was built based on only S_{C+D} surfaces, and no well tops were available, neither well data was available. In the absence of required information from this old field, we couldn't do proper history matching but we managed to mimic the production curve based on random choice of producers and injectors. The interesting
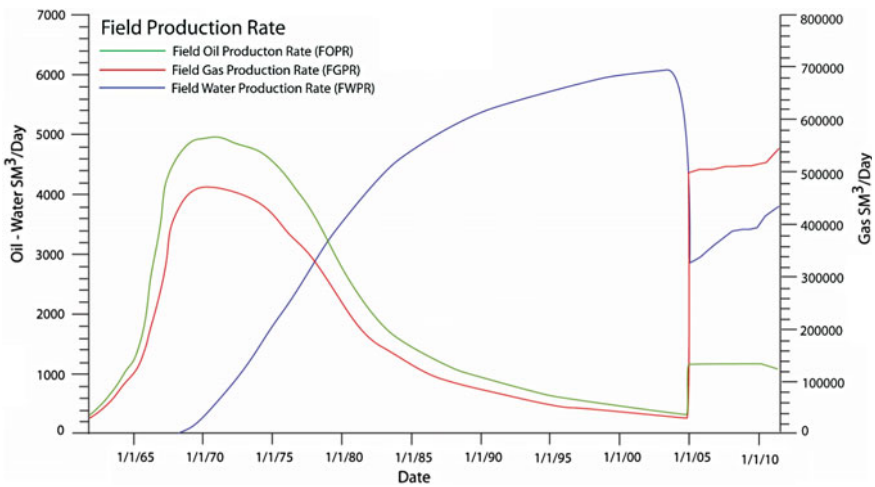
Fig. 5 Simulation of S_{C+D} layered reservoir model with CO_2 injection since Oct. 2004, to understand the effect of CO_2—EOR in a light oil field

Fig. 6 Pressure profile in sand S_{C+D}

part was that when we used CO_2-WAG, the recovery increased significantly, and hence we concluded that CO_2-WAG could be a good choice for the field but it needs further investigation.

The results of the simulation are shown in Fig. 5. It is interesting to note that there is significant increase in field oil production after CO_2-WAG, from 200 to 1100 Sm^3/day, and water production is also decreased considerably from 5800 to 3000 Sm^3/day. Increased oil production maintains a plateau for period of five years before declination in 2010; however water production increases steadily after initial drop in 2005 (Fig. 5). Pressure profile of major pay sand is shown in Fig. 6. We can see that EOR has provided good pressure support.

7 Concluding Remarks

The study shows interesting and encouraging effect of CO_2 potential to enhance the oil recovery from a light oil field (45–47° API). With immiscible CO_2 flooding EOR results are very encouraging. A mixture of injection gas with 40 % CO_2 and 60 % light hydrocarbons gives miscible displacement. However, 60 % of light hydrocarbons are too high to practically implement, hence research is underway to find the possibility of miscible CO_2 EOR by improving the mixture of injection gas.

The field being studied is an old oil field with old installations. CO_2 being corrosive in nature, the operator has to assess the cost of well work-overs and CO_2 transport compared with the gain due to incremental oil recovery.

References

Akervoll I, Bergmo PE (2010) CO_2-EOR from representative North Sea oil reservoirs. In: SPE Annual International Conference on CO_2 Capture, Storage and Utilization, SPE 139765

Calsep (2010) PVT simulation package. www.calsep.com

Dimri VP, Srivastava RP, Vedanti N (2012) Fractal models in exploration geophysics: application to hydrocarbon reservoir, vol 41. Elsevier Science, Amsterdam. ISBN: 978-0-08-045158-9

Hartai E (2012) Carbon dioxide storage in geological reservoirs, report published online (www.dnr.sc.gov) downloaded from. http://fold1.ftt.uni-miskolc.hu/~foldshe/co2geol.pdf

Holt T, Lindenberg E, Taber JJ (2000) Technologies and possibilities for large scale CO_2 seperation and underground storage. In: SPE Annual Technical Conference and Exhibition, SPE 63103

Mehdizadeh H, Srivastava RP, Vedanti N, Landro M (2010) Seismic monitoring of an insitu combustion process in a heavy oil field. J Geophys Eng 7(1):16–29

Schlumberger (2012) Eclipse reservoir simulation software v.2012.2. www.slb.com

Organic Properties and Hydrocarbon Generation Potential of Shales from Few Sedimentary Basins of India

Devleena Mani, D.J. Patil and A.M. Dayal

Abstract Shales form the principal source rock for most of the conventional and unconventional petroleum systems. In India, both the prolific and prospective sedimentary basins have excellent to fair development of shales that range in age from the Proterozoic to Cenozoic. Deposition, preservation and maturation of organic content in shales define the source rock characteristics and its hydrocarbon generation potential, leading to a prolific/non prolific oil and gas play. Useful insight on development and hydrocarbon generation potential of shales and other organic rich source rocks is obtained through the geochemical study of sedimentary organic matter. In the present work, organic richness, kerogen type and thermal maturity of potential shales from few sedimentary basin of India, namely—Vindhyan, Krishna-Godavari, Kutch, Cambay and Jammu and Kashmir have been studied, to understand their effectiveness as source rocks in the particular basins. The studied shales show high Total organic carbon (TOC) content and contain dominantly Type III kerogen with partial contributions from Type II, in varying stages of hydrocarbon generation from immature to post mature, depending upon the thermal history of respective basins. Quantitative approaches involving the use of kinetic parameters for thermal cracking of organic matter (kerogen) into hydrocarbons, in conjunction with the source rock quality can account for improved understanding of the hydrocarbon resources in these basins.

Keywords India · Shale · Source rocks · Organic geochemistry · Hydrocarbons

1 Introduction

Shales form the principal source rock for most of the conventional and unconventional petroleum systems around the globe (Hunt 1996). In India, both the producing as well as the frontier basins exhibit excellent to fair development of

D. Mani (✉) · D.J. Patil · A.M. Dayal
CSIR-National Geophysical Research Institute, Hyderabad 500007, India
e-mail: devleenatiwari@ngri.res.in

shales that range in age from the Proterozoic to Cenozoic. The source potential of shale rocks depends primarily upon the organic facies, which has been defined as 'a mappable subdivision of a designated stratigraphic unit, distinguished from the adjacent subdivisions on the basis of the character of its organic constituents, without regard to the inorganic aspects of the sediment' (Jones and Demaison 1982; Jones 1983). Palynological studies of the organic facies in source rocks has been used since earlier days to investigate the organic matter content, source input and depositional environment. However; the geochemistry of source rocks was developed in relatively recent times, and it added a precise quantitative hand to the palynological and sedimentological studies of the source rocks. Advances in disciplines like molecular and stable isotope geochemistry have led to infer reliably on abundance, origin, type and maturity of organic matter, which are key controls in development of petroleum source rocks.

In India, hydrocarbons occur across a large temporal range of geological setup from Cambrian (Bikaner-Nagaur), Permian (Krishna-Godavari), Mesozoic (Cauvery; Krishna-Godavari; Jaisalmer; Barmer-Sanchor), to Cenozoic (Assam-Arakan, Cambay, Mumbai offshore; Krishna-Godavari), with majority of production coming from the Cenozoic sediments (Bhowmick and Misra 2012; DGH 2014). The Mesozoics, despite of sufficient sedimentary thicknesses in basins like Kutch and Saurashtra, have added meagerly to the Indian hydrocarbon reserves due to inherent challenges in understanding of their sub-basaltic petroleum generative aspects. Gondwana sequences are now being targeted in basins like Krishna-Godavari, Assam, and Damodar Valley. About 80 % of the Indian sedimentary cover is under different stages of initial exploration (DGH 2014). Petroleum geochemistry essentially adds to the much needed information towards determining of the presence and properties of hydrocarbons trapped in the source rocks or the potential to generate such hydrocarbon (Chandra et al. 2001; Eden and Mungo 2013; Mani et al. 2011a, b; Peters et al. 2005). Useful insights on basic source rock characterization, genetic correlations of oil and gas and kinetic parameters of thermal cracking of hydrocarbons can be obtained though the properties of organic content and/or hydrocarbon components.

Giving an overview on the transformation of sedimentary organic matter into hydrocarbons, we present the organic geochemical characteristics of shales, an important source rock in majority of oil and gas plays from few sedimentary basins of India, namely—Vindhyan, Kutch, Cambay, Jammu and Kashmir and Krishna-Godavari. The results presented include the qualitative and quantitative aspects of shale's total organic carbon (TOC) content and thermal maturity of the different kerogen types. Also, the kinetic parameters derived from the cracking of kerogen into hydrocarbons are discussed for the shales from the Kutch region.

2 Organic Matter, Source Rock Development and Hydrocarbon Generation

Of less than 0.1 % of the carbon that escapes the carbon cycle only to get incorporated in the sediments and in later stages, under given conditions of sufficient thermal exposure and burial, matures to generate the hydrocarbons (Mani et al. 2013). Photosynthesis has been the basis for mass production of organic carbon and its preservation in sedimentary basins is governed by the paleo depositional environments and oxygenation conditions, sedimentation rates and grain size (Tissot and Welte 1984). Successive burial of organic matter to different depths causes the physical and chemical transformations and evolution of kerogen into hydrocarbons (Fig. 1).

Initially, diagenetic processes operate in recently deposited sediments at shallow depths and low temperatures (typically <50 °C). The biopolymers such as proteins and carbohydrates progressively evolve into geopolymer—the kerogen. Successive deposition of sediments with time results in burial of previous beds and exposure of sediments to subsurface conditions of increasing temperature ($\sim$50–150 °C) and pressure ($\sim$300–1000 bars) depending on the overburden sedimentary column and tectonic activity (Hunt 1996). Thermal degradation of kerogen leads to generation of liquid petroleum, wet gas and condensate. With still higher temperature ranges (150–200 °C), organic molecules are cracked to gas in the process of metagenesis (Fig. 1). The last stage of evolution of sediments is metamorphism resulting in greenschist and amphibolite facies (Tissot and Welte 1984).

Around 10–20 % of the petroleum is formed directly from the hydrocarbons synthesized by the once living organisms. These include C_{15+} compounds with recognizable biological structures (biomarkers or the chemical fossils), which get trapped in sediments with no or minor changes during the diagenesis processes
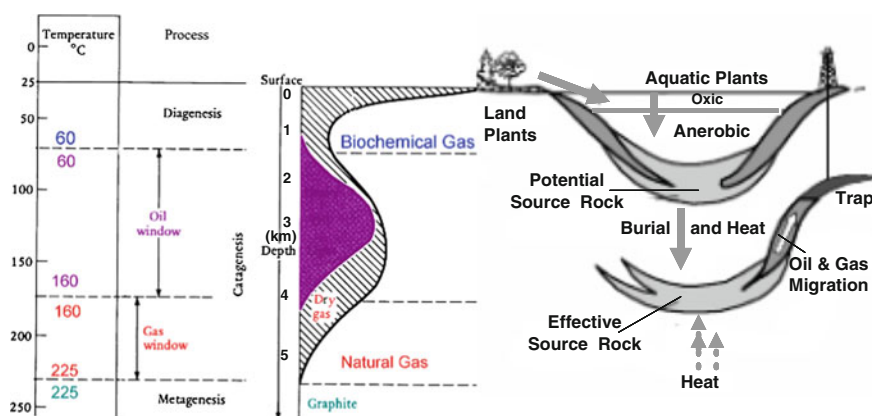

Fig. 1 Generalized evolution of sedimentary organic matter upon increasing burial and temperature (not to scale) (after, Mani et al. 2013)

associated with sedimentation. These are easily soluble in the organic solvents and constitute the bitumen fraction of organic matter. It represents the first source of hydrocarbons. The second and the major source (80–90 %) of hydrocarbons involve the conversion of the lipids, proteins and carbohydrates of living organisms into organic matter of sedimentary rocks or the kerogen. When buried deeper at high temperatures kerogen cracks to bitumen, which degrades to give oil and gas (Hunt 1996; Tissot and Welte 1984).

The organic richness and maturity of sedimentary organic matter are directly related to the hydrocarbon generation potential of a source rock. Those having TOC greater than 2 % are considered very good source rocks; and that of <0.5 % are considered to be poor with very low to negligible hydrocarbon generation potential. Depending upon the source organic input and depositional environment, the carbon (C), hydrogen (H) and oxygen (O) contents of the kerogen differs, resulting its classification into Type I, II, III and IV (van Krevelen 1961; Hunt 1996; Tissot and Welte 1984). Where the depositional and early diagenetic environment is highly oxygenated, the total-organic-carbon (TOC) content is low. The remaining kerogen contains large quantity of oxygen with a negligible generative capacity for hydrocarbons, despite a relatively high hydrocarbon/TOC ratio in the immature state. An anoxic depositional, early diagenetic environment can result in the preservation of organic-rich, fine-grained sediments that can develop into excellent source rock. Thermal maturity, which is the extent of temperature time driven reactions that convert the sedimentary organic matter or kerogen to oil and gas, is equally important for generation of hydrocarbons. In general, thermally immature source rocks do not have pronounce effect of temperature ($\sim$60 °C; 0.2–0.6 % Ro). The bacterial and plant organic matter is converted to kerogen and bitumen and biogenic methane is generated. Thermally mature kerogen generates oil ($\sim$60–160 °C; 0.6–1.35 % Ro) where as the post mature kerogen (>160 °C; >1.35 % Ro) is in wet condensate and dry gas zones (Tissot and Welte 1984; Peters and Casa 1994).

The petroleum evaluation in a sedimentary basin involves a quantitative approach, taking into account the amount of oil and gas generated by primary cracking of kerogen when temperature increases through time (Fig. 2; Tissot and Espitalie 1975). The degradation of kerogen into hydrocarbons is described by a series of n parallel chemical reactions, each of which obey a first order kinetics, characterized by Arrhenius Law.

$$dX_i/dt = A^{(-E_i/RT)} \cdot X_i \tag{1}$$

dX_i/dt	hydrocarbon generation rate
A	arrhenius constant
E_i	activation energy
R	molar gas constant
T	absolute temperature
X_i	residual petroleum potential
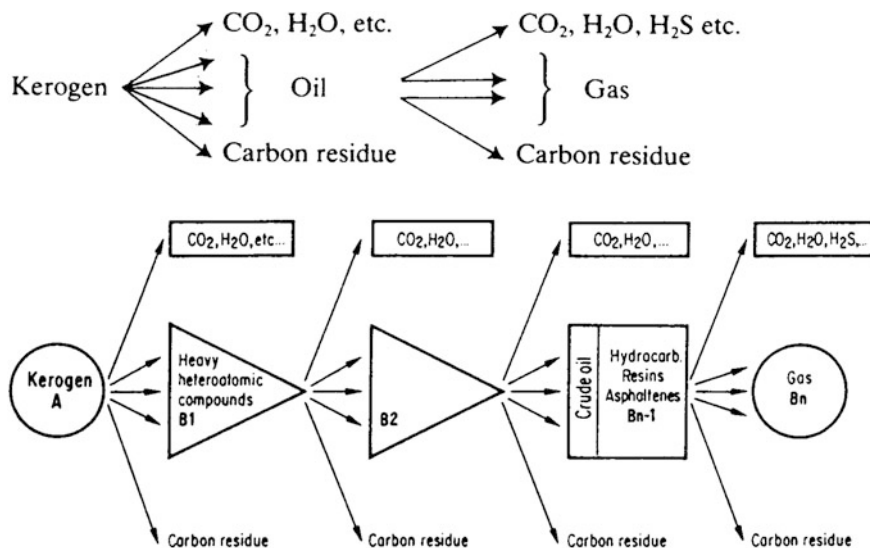
Fig. 2 General scheme of kerogen degradation (after, Tissot and Espitalie 1984)

The total initial petroleum potential of kerogen (Hydrogen Index) HI in mg HC/gTOC is expressed by $HI = \sum_{i=1}^{n} Xi_o$. Thus, the amount Q of generated hydrocarbons is (mg HC/gTOC) is

$$Q = \sum_{i=1}^{n} (Xi_o - Xi) \tag{2}$$

The kinetic parameters so obtained are used in basin modelling to predict the amount and timing of generated hydrocarbons as function of time and temperature (Tissot and Espitalie 1975).

3 Analytical Procedures

An array of geochemical screening and follow up analyses of organic rich source rocks using advanced techniques such as programmed pyrolysis, biomarker separation and analysis, and compound specific stable isotopic composition measurements are used to understand the source rock's quality and quantitative hydrocarbon generation.

3.1 Rock Eval Pyrolysis

Rock Eval pyrolysis is one of the most basic organic geochemical screening methods and is used to estimate the petroleum potential of rocks by open system

cracking of kerogen according to a programmed temperature pattern (Behar et al. 2001). The complete process takes place in the two ovens, pyrolysis and oxidation (combustion), respectively of Rock Eval pyrolyzer. The pyrolyzed hydrocarbons are monitored by a flame ionization detector (FID), forming the so-called peaks S_1 (thermovaporized free hydrocarbons) and S_2 (pyrolysis products from cracking of kerogen). The method is completed by combustion of the residual rock recovered after pyrolysis up to 850 °C, under artificial air (N_2/O_2). During pyrolysis and combustion, released CO and CO_2 are monitored on line by means of an infra-red cell. This complementary data acquisition enables determination of the organic and mineral carbon content of samples, labelled TOC and MinC, respectively. The T_{max} value is a maturity parameter. It corresponds to the temperature at which maximum amount of hydrocarbons are released from the thermal degradation of kerogen, i.e. the temperature at which S_2 peak reaches its maximum. Among various calculated parameters of Rock Eval, the hydrocarbon potential or hydrogen index, (HI) is defined by $100 \times S_2/TOC$. The oxygen index (OI) is defined as $100 \times S_3/TOC$, where S_3 is the CO_2 released during the pyrolysis. These indices help in defining kerogen types and maturation. Details on Rock Eval functioning, parameters acquired, and interpretive guidelines have been discusses by several workers (Behar et al. 2001; Espitalie et al. 1987; Lafargue et al. 1988; Peters 1986; Peters and Cassa 1994).

3.1.1 Operational Parameters for Rock Eval

Pyrolysis of shales was carried out using the Rock Eval 6 pyrolyser, Turbo version (Vinci Technologies). After obtaining a stable signal for the detectors, the instrument was calibrated in standard mode using the IFP standard, 160000 (T_{max} = 416 °C; S_2 = 12.43). The samples were weighed in pre-oxidized crucibles depending upon the organic matter content (~ 50–70 mg of shale; and 8–15 mg of coaly shale). The shale samples were run under analysis mode using the bulk rock method and basic cycle of Rock Eval 6 and the data was reported on dry weight basis (Mani et al. 2014).

3.2 Gas Chromatography (GC)

Gas Chromatography is an instrumental technique for the qualitative and quantitative identification of chemical compounds (Grob 2004). The separation and identification of the chemical mixture takes place in a gas chromatograph, which consists of three main components (i) an injector: it is a port meant for injecting the samples into the system, (ii) a column: where the analyte gets separated into its components depending upon its affinity with the stationary phase and the mobile carrier gas phase and (iii) the detector: where the qualitative and quantitative determination of the analyte takes place. The technique is based on the partitioning

of the molecules between the stationary phase of the column and the mobile phase of the carrier gas. A carrier gas is usually an inert or un-reactive gas such as helium or nitrogen that carries the sample through the column to the detector. The column consists of the stationary phase made up of polymeric material and is contained in a heated oven to maintain the column temperature. Depending upon the nature of analyte, columns of different types such packed or capillary columns with specific polymer are used. The mobile phase elutes the components to reach the detector at different time, which is very specific for each component under a particular condition of pressure and temperature and is called the retention time (Rt) of respective component. The flame ionization detector (FID) is used for the detecting the hydrocarbon concentration. In an FID, the organic compounds are burnt in a flame of hydrogen and air and the electrons produced are collected over a collecting electrode. The resulting current is the response of the detector in the form of series of signal peaks and is recorded using peak area or peak height as basis (Grob 2004).

3.2.1 Operational Parameters for GC

Varian CP-3380 gas chromatograph was used for the determination of concentration of gaseous hydrocarbons. Nitrogen, with a flow rate of 30 ml/min, was used as a carrier gas. The temperature of injector port was maintained at 120 °C. The GC was equipped with packed column: Porapak 'Q' of length 1.8 m and diameter: $1/8'' \times 2.0$ mm. The column oven program is given in Table 1. The temperature of the detector (FID) was maintained at 200 °C. The fuel gases used to burn the flame at FID were hydrogen and zero air with flow rate of 300 ml/min. Star Workstation was used for the data acquisition. The calibration of the gas chromatograph was done using external standard (BOC standard gas mixture), comprising of methane, ethane, propane, *i*-butane, *n*-butane, *i*-pentane and *n*-pentane, of four different concentration levels (Mani et al. 2012a).

3.3 Organic and Isotope Ratio Mass Spectrometry

3.3.1 Organic/Gas Chromatography-Mass Spectrometry (GC-MS)

GC-MS is used to detect and quantify organic compounds using relative gas chromatographic retention times, elution patterns, and the mass spectral fragmentation patterns characteristic of their structures (Sneddon et al. 2007). A typical GC-MS system performs (1) compound separation by gas chromatography; (2) transfer of

Table 1 Column Oven program for GC

Temp. (°C)	Rate (°C/min)	Hold (min)	Total (min)
60	–	3	3
120	20	18	24

separated compounds to the ionizing chamber of the mass spectrometer; (3) ionization; (4) mass analysis; (5) detection of the ions by the electron multiplier; (6) acquisition, processing, and display of the data by computer (Sneddon et al. 2007). As the individual organic compounds elute from the GC, they enter the MS, typically and most common is the electron ionization detector. Here, they are bombarded by a stream of electrons causing them to fragment. The mass of the fragment divided by the charge is the mass charge ratio (m/z). Almost always the charge is +1, and m/z ratio represents the molecular weight of the fragment. In case of a quadrupole GC-MS, a group of four electromagnets (a quadrupole), focus each fragment through a slit into the detector. These quadrupoles are programmed by a computer to direct only certain fragments, one at a time (scan) until the range of m/z is recovered. This produces the mass spectrum, which is a graph of signal intensity (relative abundance) versus m/z ratios (essentially molecular weight). Each compound has a unique fingerprint and software is readily available to provide a library of spectra for unknown compounds (Sneddon et al. 2007).

Solvent Extraction

Prior to the analysis of organic compounds on GC-MS, the total organic matter is extracted from the sediments through the use of organic solvents at raised temperature and pressure. Extraction of organic matter from selected shale samples was carried out using Buchi Speed Extractor E-914. 3 g of sample was mixed with 3 g of sand and placed between the top and bottom layers of 1.5 g sand each, in 40 ml extraction cell. The extraction was done in atmosphere of nitrogen with maximum temperature and pressure of 100 °C and 100 psi, respectively using dichloromethane (DCM) and methanol in ratio of 9:1. The Speed Extractor was programmed for three extraction cycles. The collected organic extracts were reduced to about 1 ml on the Buchi Rotavap V-855. n-pentane was added to the extract for the separation of asphaltene, following which the HCl treated Cu turning were added for the removal of sulphides. The extracts were cleaned up using silica column chromatography and separate fractions of the extracts, saturate and aromatic, were analyzed for the n-alkane and PAH components (Mani et al. 2015).

Operational Parameters for GC-MS

A Varian 320 Quadrupole Mass Spectrometer coupled to Varian CP-3800 Gas Chromatograph, equipped with Br-5 MS column (30 m × 0.25 mm × 0.25μm) was used to analyze the organic extracts for the n-alkanes and PAH in full scan and selective ion monitoring (SIM) modes, respectively. In the SIM mode, the GC oven was programmed at 70 °C with a hold time of 4 min and increased to 300 °C @20 °C/min with a hold time of 15 min. The MS was operated under 70 eV with source temperature at 240 °C and transfer line at 280 °C. The manifold was maintained at 40 °C. In the full scan mode, the column oven was programmed at

40 °C with a hold time of 1 min and increased to 310 °C @5 °C/min with a hold time of 15 min. The calibration for *n*-Alkanes was done using C_{14}–C_{32} (even carbon numbered homologues + pristine/phytane) standard from Chiron AS and that of PAH standard from Accustandard (PAH mix). The sample spectra and retention times were compared with characteristic published spectra (Philp 1985a, b; Peters and Moldowan 1993) and/or procured standard spectra (Mani et al. 2012b, 2015).

3.3.2 Isotope Ratio Monitoring Spectrometry (IRMS)

IRMS are widely used to determine the ratio of stable isotopes of Carbon (C) and Oxygen (O), i.e. $^{13}C/^{12}C$ and $^{18}O/^{16}O$, respectively in geological samples. With the advancement of hyphenated techniques, the separation power of gas chromatograph has been coupled to the mass spectrometer along with introduction of sample combustion interface into the gas chromatograph-isotope ratio mass spectrometer (Platzner 1997). The separated products of the sample mixture in the stream of helium at the output of the gas chromatograph are passed through an oxidation/ reduction reactor and then introduced into the ion source of mass spectrometer for precise concentration determination. The basic mass spectrometer comprises of the (i) ion source for fragmentation of sample molecule into ions and (ii) mass analyzer for separating the ion beam according to the mass of the respective ions. The open split-coupling device ensures that only a part of the sample/reference gas containing carrier gas is fed into the ion source of the MS. In this way, pulse injection of sample gas can be analyzed, reducing the volume constraints and sample size (Platzner 1997).

Continuous Flow-IRMS is a generic term for IRMS instruments that are coupled on-line to preparation lines or instruments. This includes the (i) Gas Chromatography-Combustion-IRMS (GC-C-IRMS), used for the compound specific analysis of hydrocarbon components. (ii) Gas Bench-IRMS (GB-IRMS), used for the C and O isotope ratio determinations on carbonates. (iii) Elemental Analyzer-IRMS (EA-IRMS), used for the determination of coexisting organic matter in shale samples, with IRMS, being common to all the above mentioned peripherals.

GC-C-IRMS

The $\delta^{13}C$ analysis of gaseous hydrocarbons was carried out using GC-C-IRMS. An Agilent 6890 GC coupled to a Finnigan-Delta Plus^{XP} IRMS via a GC combustion III interface was used for the determination of carbon isotope ratios. One ml of the ortho-phosphoric acid desorbed gas (Horvitz 1985) was injected into the GC, equipped with "Pora Plot Q" capillary column 25 m in length and a diameter of 0.32 mm, in splitless mode with helium as carrier gas at a fixed oven temperature of 28 °C. The chromatographically separated hydrocarbon gases after eluting from GC column enter a pre-oxidized Cu-Ni-Pt combustion reactor maintained at 960 °C,

where they get converted into carbon dioxide and water. The water was removed using Nafion membrane tube prior to their entry into the mass spectrometer. The purified CO_2 after combustion enters into the mass spectrometer for $^{13}C/^{12}C$ ratio measurement of the respective hydrocarbon component. The GC-C-IRMS was calibrated to the international standard Vienna Pee Dee Belemnite (VPDB) using Natural Gas Standard (NGS-1) mixture (Mani et al. 2011a).

4 Case Studies

Of the twenty six sedimentary basins in India, shales of varied age and lithology are prolific source rocks in six basins, whereas there are several frontier basins in which the potential source rocks are yet being characterized at different stages of exploration. Geochemical attributes such as organic richness, kerogen type and thermal maturity of shales are important parameters, which define a potential source rock and provide useful insights onto the geological processes under which the carbonaceous sediments got deposited and were well preserved, leading to generation of hydrocarbons. Organic geochemical parameters studied for the shales from some of the sedimentary basins of India are described below.

4.1 Vindhyan Basin

The Proterozoic Vindhyan basin consists of more than 5000 m thick sedimentary sequence, which is characterized by the presence of rich fossil assemblage, organic rich black shales containing microbial mats and stromatolitic limestones. The existence of Infra-Cambrian reservoir sequences, source–seal relationships and the widespread presence of carbonaceous shale and stromatolitic carbonate render promising opportunities for hydrocarbons in the basin (DGH 2014; Ojha 2012). The Vindhyan succession is divided into the Lower Vindhyan (Semri Group) which is overlain unconformably by the Upper Vindhyan (Kaimur, Rewa, and Bhander Groups) (Banerjee et al. 2002, 2006; Dutta et al. 2006; Sharma 2006; Sastri 1984). Evaluation of organic matter in the outcrop shale samples from the Semri and Kaimur Groups of Vindhyan basin was carried out using Rock Eval pyrolysis, wherein thirty-two rock samples from the Khachhuhar, Murlipahar, Banjari (Rohtas Formation, the Semri Group) and Amjhore (Bijaigarh Formation, the Kaimur Group) were studied for their organic richness and kerogen type (Fig. 3) (Dayal et al. 2014).

The Total Organic Carbon (TOC) content in shales ranges between 0.04 and 1.43 %. The S_1 (thermally liberated free hydrocarbons) values range between 0.01 and 0.09 mg HC/g rock (milligram hydrocarbon per gram of rock sample), whereas the S_2 (hydrocarbons from cracking of kerogen) show the values between 0.01 and 0.14 mg HC/g rock. The HI and T_{max} correlation, which is a modified form of van
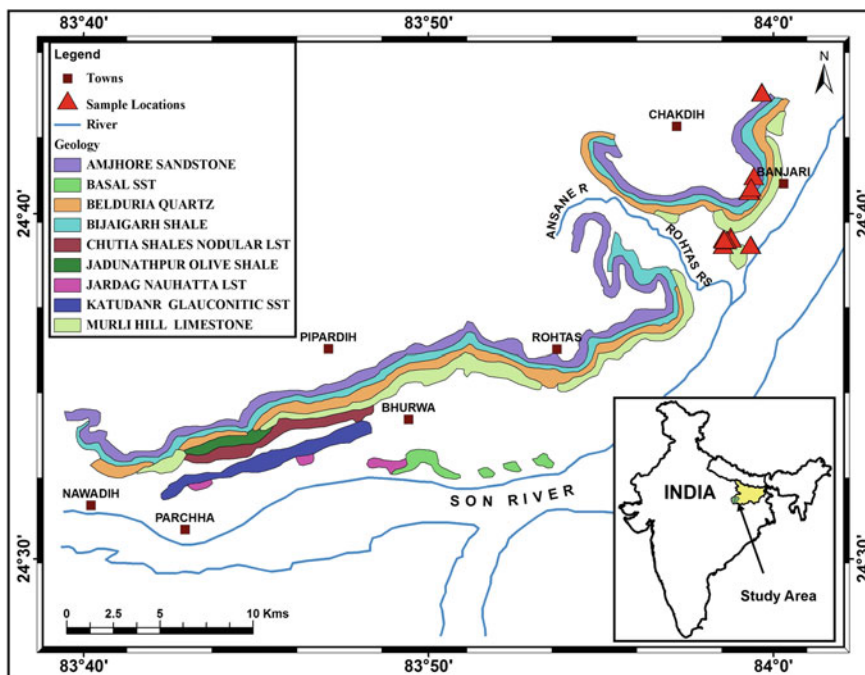
Fig. 3 Geological map of the Vindhyan basin showing the outcrops of the Semri and Kaimur rocks along with the sample locations (after, Dayal et al. 2014)

Krevelen diagram (Hunt 1996; Tissot and Welte 1984; van Krevelen 1961) is used here to determine the quality and maturity of kerogen from Semri and Kaimur Groups of rocks (Fig. 4). In general, T_{max} values lower than 435 °C indicate immature stage of kerogen. T_{max} values between 435 and 455 °C indicate "oil window" conditions (mature kerogen). Values between 455 and 470 °C are considered transitional. A T_{max} higher than 470 °C represents the wet-gas zone and

Fig. 4 Hydrogen Index (HI) versus T_{max} (temperature at highest yield of S2) plot of shales from the Semri and the Kaimur Groups, Vindhyan basin (after, Dayal et al. 2014)
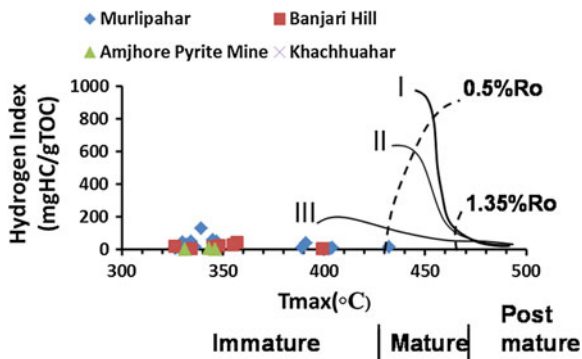
over mature kerogen (Peters 1986). The thermal maturity of the shales from Semri Group of rocks is between immature to mature range, whereas the shales from the Muralipahar and Banjari hills are thermally more mature compared to the Amjhore. The kerogen is characterized by Type III gas prone kerogen (Dayal et al. 2014).

The Semri Group of rocks was deposited in marine environment and show profuse development of organo-sedimentary structure, the microbialites (Sharma 2006). These shales, as indicated by their Rock Eval data, suggest good to excellent gas generation potential (Dayal et al. 2014). The presence of elevated concentrations of adsorbed light gaseous hydrocarbons (methane, ethane, propane) in the near surface sediments of Vindhyan basin (Dayal et al. 2014) indicates that hydrocarbons have been generated in the subsurface. The adsorbed soil gas, CH_4 (C_1), C_2H_6 (C_2), C_3H_8 (C_3) and nC_4H_{10} (nC_4), concentrations measured in the soil samples from the eastern part of Vindhyan basin (Son Valley) vary from 0 to 186 ppb, 0 to 4 ppb, 0 to 5 ppb, and 0 to 1 ppb, respectively (Dayal et al. 2014; Ojha 2012). The light hydrocarbon concentrations (C_1–C_4) in near surface soils of the western Vindhyan basin around Chambal Valley have been reported to vary between 1–2547 ppb, 1–558 ppb, 1–181 ppb, 1–37 ppb and 1–32 ppb, respectively with high concentrations around Baran-Jhalawar-Bhanpur-Garot regions (Kumar et al. 2006). The microseepage of light hydrocarbons of thermal origin is indicated by the compound specific isotopic analysis of C_1 and C_2 compounds (−45.7‰ to −25.2‰ and −35.3‰ to −20.19‰; VPDB) (Fuex 1977; Dayal et al. 2014). The organically rich shales with sufficient thermal maturity might be the source for these hydrocarbons.

4.2 Krishna-Godavari Basin

The Krishna-Godavari (KG) on the eastern coast of India occupies an important place amongst the Gondwana basins. The basin evolved from the rifting of the Gondwanaland along the eastern continental margin of India during the Early Mesozoic (Sastri et al. 1981; Veevers 2004). Gondwana sediments along with the Tertiary sequences form rich source rocks, making KG one of the most promising petroliferous provinces of India. The Raghavapuram (R), Gollaplli (G), and Tirupati (T), form a dominant Cretaceous petroleum system R-G-T-R (!) with Razole (R) acting as basaltic caprock in the west of KG basin. Ten carbonaceous shales were collected from the exposed Raghavapuram Formation spanning the top, middle and bottom sections of the hillock, near Ramnujampuram village (Fig. 5) (Mani et al. 2012a, 2015). Organic geochemical studies comprising of TOC, Rock-Eval pyrolysis, and biomarker separation and analysis were carried on the Raghavapuram shales to understand their paleo and depositional environment and its implications toward hydrocarbon generation in the basin (Mani et al. 2012a, 2015).

The TOC content varies between 0.01 and 0.5 % in the shales. Rock Eval pyrolysis studies of the selected shales show the S_1 values to range between 0.01 and 0.06 mg HC/g rock, whereas, the S_2 values vary between 0.01 and 0.05 mg HC/g
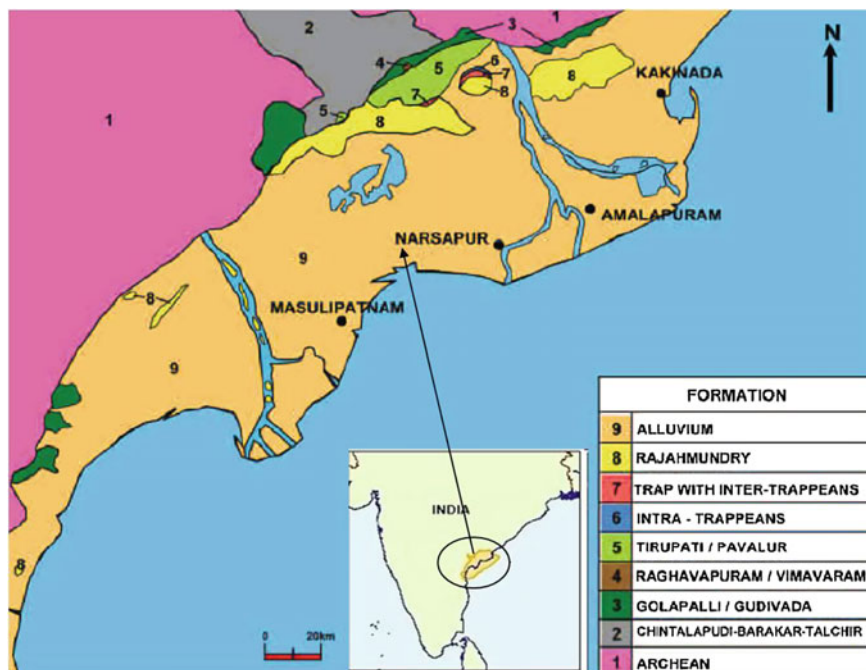
Fig. 5 Geological map of Krishna-Godavari basin showing the exposures of Raghavapuram shales (after, Gupta 2006)

rock. The thermal maturity parameter, T_{max} ranges between 302 and 497 °C. The hydrogen index (HI) is between 50 and 500 mg HC/g TOC. The HI versus T_{max} plot for the majority of shales studied here indicate a Type III kerogen with immature to post mature stage of hydrocarbon generation (Fig. 6). Type-III kerogen with low H/C range (H/C = 0.7 to 1.0) generates primarily gas, condensates and some waxes and contains mostly condensed poly-aromatics and oxygenated functional groups, with minor aliphatic chains. The organic matter is mostly derived from terrestrial higher plants. This is in agreement with the paleoecological conditions which existed during the deposition of the Raghavapuram sediments (Bhalla 1968; Lakshminarayana 2002; Mani et al. 2015).

The extractable organic matter from the Raghavapuram shales was used to study the polyaromatic and n-alkanes hydrocarbons. The PAH analysis on GC—showed the presence of naphthalene, acenapthene acenaphthylenes, phenanthrene, anthracene, fluoranthene, pyrene, benzoanthracene and chrysene; however the alkylated homologues are not present in significant measurable concentration (Table 2) (Mani et al. 2012a, 2015). Distribution of PAHs is often used as an indicator for depositional environment and lithology (Simoneit 1992; Simoneit and Fetzer 1996). Two types of PAHs, those derived from combustion and those sourced from land plant have been proposed (Killops and Massoud 1992). Phenanthrene and chrysene
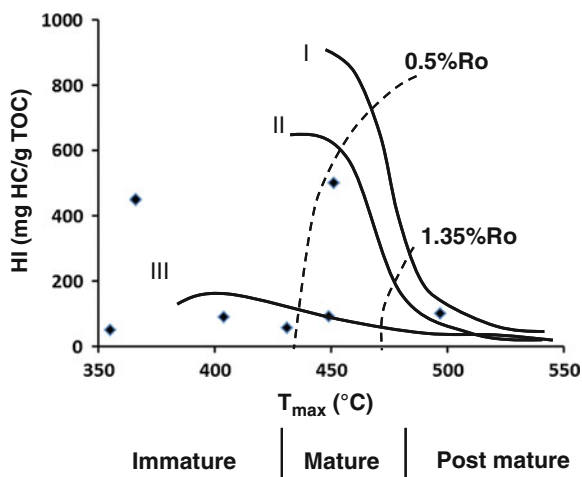
Fig. 6 HI versus T_{max} plot indicating the kerogen type in the Raghavapuram shale, KG basin (after, Mani et al. 2015)

Table 2 PAH concentration (ppb) in the extracted organic matter from Raghavapuram shales, KG, basin (after, Mani et al. 2015)

	RGRPM-26	RGRPM-29	RGRPM-31	RGRPM-32	RGRPM-33	RGRPM-34	RGRPM-35
Naphthalene	229.7	309.4	465	276	178.7	128	411.7
Phenanthrene	84.93	180.1	120.4	148	90.3	69.1	178
Anthracene	86.74	100.4	123.5	151.4	92.2	70.5	124
Fluoranthene	17.38	56.7	17.02	32.6	nd	nd	202
Pyrene	36.88	34.3	21.2	32.8	28.8	35.2	269
Benzoanthrrene	43.9	26.7	18.3	17.7	15.2	12.9	228
Acenaphthene	nd	21.6	464.6	nd	nd	26.8	nd
Acenapthylene	nd	66.7	202.9	nd	nd	55.9	nd
Chrysene	nd	23.1	17.9	17.31	23.2	45.9	278

may arise in recent sediments through both combustion and diagenetic processes, probably from terpenoids (Jiang et al. 1998). The high phenanthrene and chrysene concentrations observed in the Raghavapuram shales indicate high terrestrial source organic matter input. Benzoanthracenes, acenapthenes and acenapthylenes are present in three samples in significant concentrations. These compounds are present naturally in bituminous fossil fuels, such as coal and crude oil deposits, as a result of diagenesis, which involves low temperature (100–150 °C) transformation of organic material over a significant span of time.

The Raghavapuram shales are characterized by the presence of n–C_{11}–C_{18}, including n-tricosane and phytanes (Table 3) (Mani et al. 2012a, 2015). Alkane

Table 3 *n*-alkane distribution (ppb) in the extracted organic matter from Raghavapuram shales, KG basin (after, Mani et al. 2015)

	RGRPM-26	RGRPM-29	RGRPM-31	RGRPM-32	RGRPM-33	RGRPM-34	RGRPM-35
n-undecane	56.9	89.5	45.8	62.9	34.8	76.9	23.1
n-tridecane	69.7	69.7	58.9	63.9	63.8	33.4	56.2
n-pentadecane	76.1	87.9	65.9	163.8	78.9	35.9	110.2
n-octadecane	55.6	67.6	73.4	86.7	45.7	77.9	17.9
Phytane	65.2	89.2	87.2	91.5	56.2	89.4	27.5
n-Tricosane	43.4	44.2	87.1	73.5	65.8	95.9	62.1

biomarkers have been widely applied to study the source, paleoenvironmental conditions and maturity of sedimentary organic matter (Allan and Douglas 1977; Philip 1985a, b). The *n*-alkanes from the organic matter in sedimentary rocks originate from lipids in bodies of plants and animals. The source of organic input in sediments can be inferred through the odd and even predominance of *n*-alkanes (Peters and Moldowan 1993; Peters et al. 2005). Input of terrigenous source material is indicated by a strong predominance of high molecular weight odd-numbered alkanes ($n–C_{25}$ to $n–C_{31}$), which are associated with leaf waxes (Brooks and Smith 1967). The *n*-alkanes, C_{11} to C_{23}, obtained in the organic matter extracts from the Raghavapuram shales indicate marine inputs to the sedimentary organic matter. Pristane, phytane (Pr/Ph) ratio has been proposed as an indicator of redox potential of source sediments by Didyk et al. (1978). It has been widely utilized in many studies to infer oxicity or anoxicity of depositional environments and source of organic matter. The mass spectra of the extracted organic matter from Raghavpuram shales show the occurrence of phytanes, indicating the oxygen low conditions during the deposition and preservation of these sediments (Mani et al. 2015).

The organic geochemical proxies indicate the source organic matter to be derived from near-shore terrestrial environment and its deposition in strongly reducing conditions. The organic matter richness and maturity derived from a favourable depositional setting has its bearing upon the Gondwana sediments globally, and also provides promising petroleum exploration opportunities, particularly in the Raghavapuram sequence of the KG basin (Mani et al. 2012a, 2015).

4.3 Kutch Basin

The Kutch basin in the western margin of Indian subcontinent encompasses one of the best developed and well preserved Cenozoic sequences comprising of organic rich Tertiary shales. The basin has identified hydrocarbon prospectivity (DGH 2014; Patil et al. 2013). Cenozoic sequences comprising of lignite and interbedded carbonaceous shales occur as discrete mappable units in the north western part of Kutch, chiefly at Panandhro, Akrimota, Umarsar Mata-no-Madh, Lakhpat-Dhedhadi in Lakhpat Taluka (Biswas 1992; Dutta et al. 2011). The study area forms part of a condensed stratigraphic section of ~ 900 m thickness, ranging from Paleocene to Pliocene and is exposed in open cast mines of Mata-no-Madh, Panandhro and Umarsar (Fig. 7). Twenty five shale samples were collected from the interbedded shale horizons within the lignite sequences to determine the TOC content and kerogen type in the shales using Rock-Eval pyrolysis (Misra et al. 2013a; Dayal et al. 2013).

The Total Organic Carbon (TOC) content from Mata-no-Madh shales ranges between 0.35 and 30.99 %. The S_1 values range between 0.01 and 3.71 mg HC/g. The S_2 values range between 0.02 and 74.01 mg HC/g. The T_{max} values lie between 383 and 428 °C respectively. The hydrogen index (HI) is ranging in values between 3 and 312 mg HC/g TOC, where as the oxygen index (OI) shows variegated values
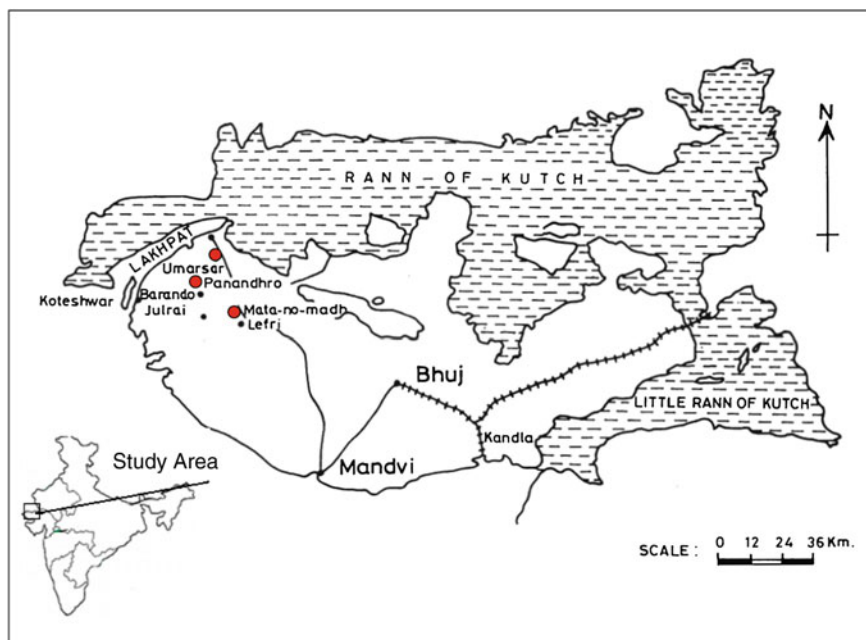
Fig. 7 Map of Kutch basin along with the location of lignite mines (after, Misra et al. 2013a)

ranging between 18 and 151 mg CO_2/g TOC (Misra et al. 2013a). For the Umarsar shales, the TOC varies between 0.79 and 25.43 %. The S_1 values are between 0 and 3.05 mg HC/g Rock and the S_2 values range between 0.24 to 91.13 mg HC/g Rock. The T_{max} varies between 421 and 426 °C, whereas the HI values vary between 30 and 258 mg HC/g TOC. The OI values range between 29 and 58 mg CO_2/g TOC (Misra et al. 2013a).

The Panandhro shales shows TOC content ranging between 1.08 and 1.35 %. The S_1 values range between 0.05 and 0.34 mg HC/g Rock, S_2 values between 0.65 and 1.56 mg HC/g Rock. T_{max} varies between 423 and 452 °C. The HI and OI values range between 53–116 mg HC/g TOC and 40–214 mg CO_2/g TOC respectively. The mineral carbon content lies between 0.09 and 3.96 % (Misra et al. 2013a).

The gas generation potential of the shales depends upon the organic richness, basically TOC, and its thermal maturity. A TOC content (wt%) <0.50 is considered poor; 0.50–1.0 as fair; 1.0–2.0 as good and that >2.0 as excellent for the source rocks (Hunt 1996; Peter and Cassa 1994). In general, the shales from Mata-no-Madh and Umarsar area have TOC >2 %. These values indicate good source rock potential.

The Tertiary shales from the Kutch basin show a higher hydrogen index from the samples belonging to the Mata-no-Madh and Umarsar areas, where as the Panandhro shales show comparatively lower HI values (Misra et al. 2013a; Dayal

et al. 2013). The HI values vary linearly in positive direction with the TOC content, whereas the OI values show a negative correlation. This is an accepted trend for the variation of hydrogen and oxygen indices with the TOC for hydrocarbon source rocks which are deposited in low oxygen conditions and having well preserved organic matter (Tissot and Welte 1984). The HI versus OI correlations for the shales from Mata-no-Madh and Umarsar shows that the kerogen is characterized by Type-II/Type-III and Type-III kerogen, whereas that of Panandhro shales show Type-III kerogen.

The HI versus T_{max} (pyrolysis temperature) plot for the shales from the Kutch Basin indicates the kerogen to be characterized by Type-II/III to Type-III kerogen (Fig. 8) (Misra et al. 2013a; Dayal et al. 2013). The Tertiary shales from the Kutch Basin show an immature stage for the kerogen towards hydrocarbon generation and could possibly be in early diagenetic stage. These shales can be thermally mature with suitable hydrocarbon generation potential if buried deeply elsewhere in the basin. Naredi Formation is reported to have a subsurface extent of about 40 m (Biswas 1992). The subsurface extent of the Formation containing the shale horizons and the petrological and petrophysical details along with the organic geochemical attributes of the shales on subsurface core samples shall help in precise delineation of horizons for the shale gas plays.
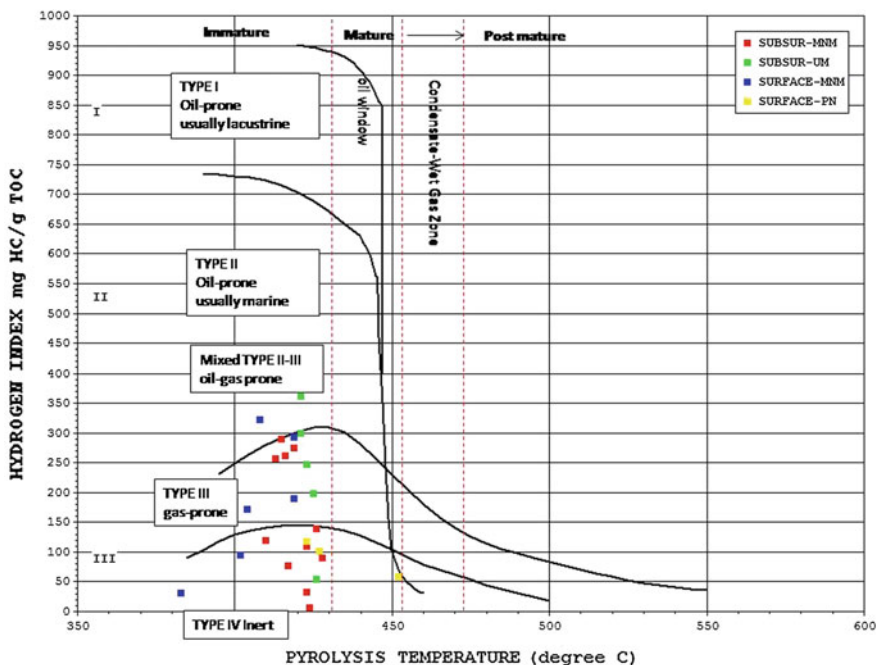
Fig. 8 HI versus T_{max} plot for the shales from Matanomadh, Panandhro and Umarsar, showing the maturity (after, Misra et al. 2013a)

4.4 Cambay

The petroliferous Cambay basin in western India with interbedded carbonaceous shales in its thick Tertiary sequence forms a potential prospect for the shale gas. Organic-rich, fine grained clastic Cambay, Tarapur and other Tertiary shales have sourced the oil and gas for the basin. The interbedded shale formations within the Middle Eocene lignite sequences, referred to as Cambay Formation, (Nagori et al. 2013), in the Tadkeshwar and Rajpardi mines of Surat and Bharuch districts (Fig. 9), respectively, have been sampled to study the organic matter properties (Misra et al. 2013b; Dayal et al. 2013). In general, the shales from Rajpardi area show a high TOC content along with other Rock Eval parameters compared to that of Tadkeshwar. The TOC content from Rajapardi shales ranges between 9.35 and 26.03 %. The S_1 values range between 3.29 and 7.12 mg HC/g rock and are characteristic of the entire sample suit. The S_2 values show an elevated range between 60.6 and 190.11 mg HC/g Rock. The T_{max} ranges between 429 and 435 °C. The HI is high ranging in values between 648 and 754 mg HC/g TOC, whereas OI for all studied samples is near to 15 mg CO_2/g TOC. The mineral carbon content is <0.5 %. The organic matter in shales is characterized by Type II kerogen, suitable for the generation of oil and gas (Fig. 10a) (Misra et al. 2013b).

For the Tadkeshwar shales, the TOC varies between 0.19 and 47.39 %. The S_1 values are between 0.05 and 3.58 mg HC/g Rock and the S_2 values range between
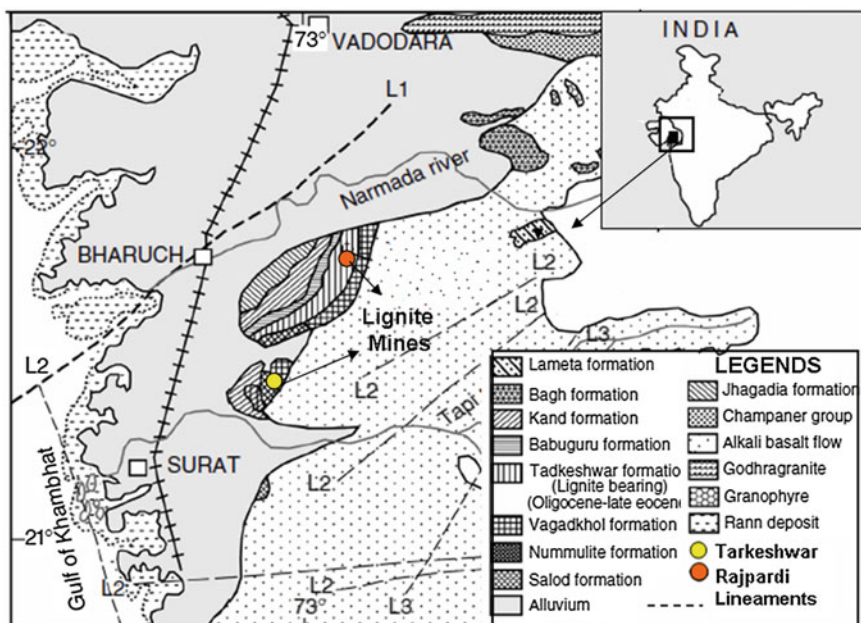
Fig. 9 Geological sample location map of lignite mines in Gujarat (after, Misra et al. 2013b)

Fig. 10 **a** HI versus T$_{max}$ plot for the shales associated with lignites in Tadkeshwar lignite mine, Gujarat (after, Misra et al. 2013b). **b** The HI versus T$_{max}$ plot for the shales associated with lignites in Rajpardi lignite mine, Gujarat (after, Misra et al. 2013b)
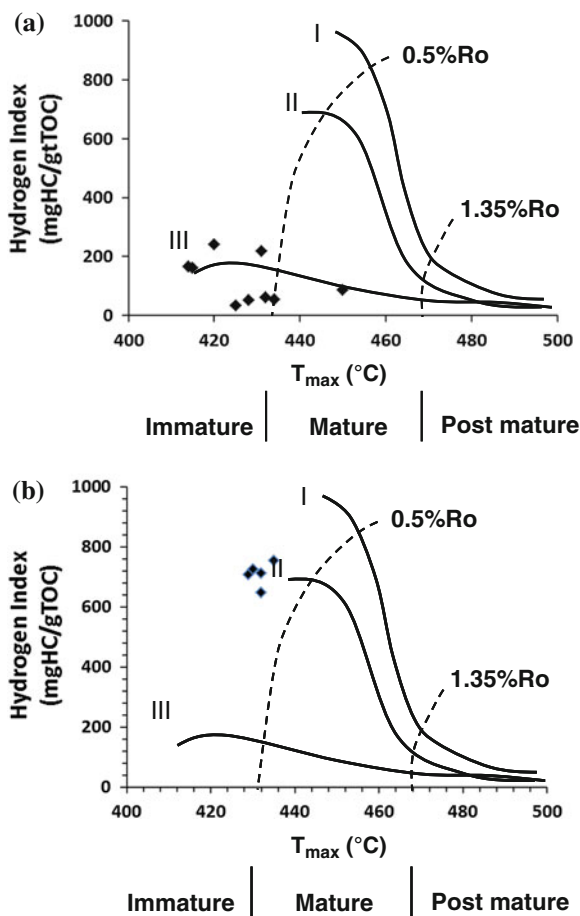
0.14 and 78.84 mg HC/g rock. The T$_{max}$ varies between 342 and 450 °C, whereas the HI values vary between 33 and 241 mg HC/g TOC. The variation of HI versus T$_{max}$ suggests an immature to mature stage for the hydrocarbons. The organic matter in shales is characterized by Type III kerogen, suitable for the generation of gas (Fig. 10b) (Misra et al. 2013b).

4.5 Jammu and Kashmir

The Himalayan Foreland basin is considered prospective for hydrocarbon generation and entrapment, owing to its favorable tectonics and geological setting (DGH, 2014). The Karewa and Spiti-Zanskar basins are categorized potentially prospective due to their analogy with similar hydrocarbon producing basins of the world

(Jokhan Ram 2005; DGH 2014). Organic richness and kerogen properties of the Eocene Subathu shales obtained from the outcrops and underground mines of Jammu region have been evaluated using Rock Eval pyrolysis (Mani et al. 2014). Twenty-nine shales/coaly shales and few coals were collected from the interbedded shale horizons of underground mines in coal fields of Kalakot, Kotla and Mahogla and outcrops at Salal, Kanthan and Kalimitti areas of Jammu for the organic matter characterization (Fig. 11).

The Eocene shales/coaly shales show quite high Total Organic Carbon (TOC) content ranging from 3.2 to 77.8 %. The S_1 values range from 0.01 to 2.6 mg HC/g rock. S_2 shows an elevated value ranging from 0.51 to 71.62 mg HC/g rock. The HI ranges between 2 and 113 mg HC/g TOC, where as the oxygen index (OI) for all studied samples is low (<30 mg HC/g CO_2). A modified van Krevelen diagram (van Krevelen 1961) indicates that organic matter is characterized by Type III kerogen. The T_{max} of the shale samples ranges from 490 to 515 °C suggesting a post mature phase for the hydrocarbons (Fig. 12). The coals and coaly shales have TOC content >30 %, and T_{max} above 550 °C suggesting high levels of maturity as compared to the carbonaceous shales. The organic matter in majority of Subathu samples consists of Type III kerogen and has generation potential for the gaseous hydrocarbons (Fig. 13).

Stratigraphic equivalents of Subathu, the Lower Dharamsala Formation of Himachal Pradesh, indicated gas shows during exploratory drilling (Karunakaran and Rangarao 1979; DGH 2014). The gases of Jwalamukhi and Nurpur wells are methane rich with low nitrogen concentration and are dry and thermogenic in nature (C_{2+} < 2 %) (Mittal et al. 2006). Carbon isotopic composition of methane from these wells suggest a deep over mature source for the gases ($\delta^{13}C_1 \sim -32.0‰$) (Mittal et al. 2006). The knowledge of the distribution, facies, and thickness of the
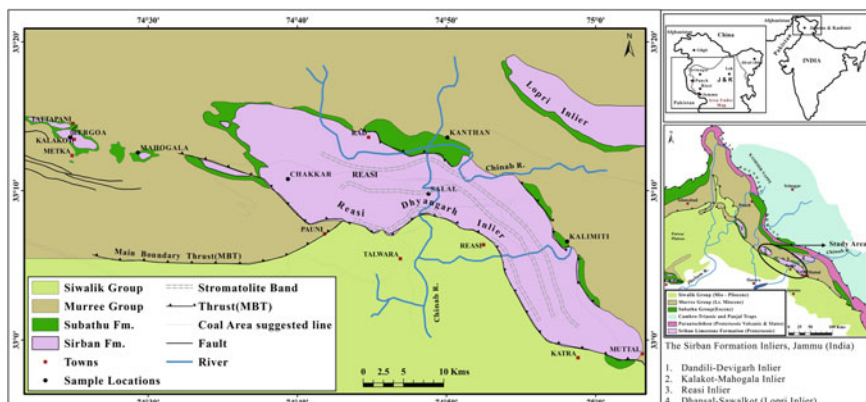
Fig. 11 Geological map of Jammu region showing the sample collection points for the Subathu shales (after, Mani et al. 2014)
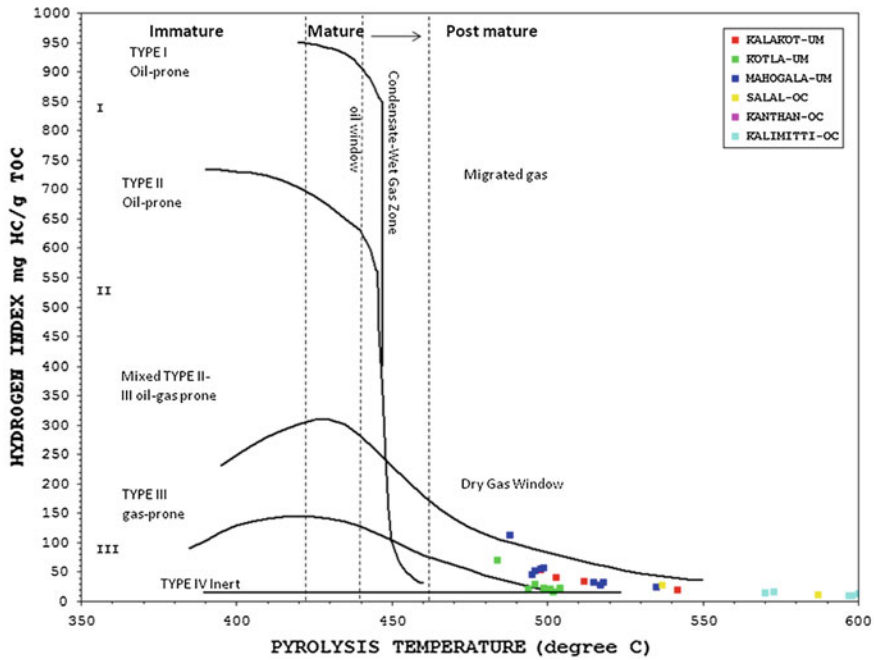
Fig. 12 HI versus T$_{max}$ plot indicating the thermal maturity of kerogen in the Subathu shales, Jammu (after, Mani et al. 2014)
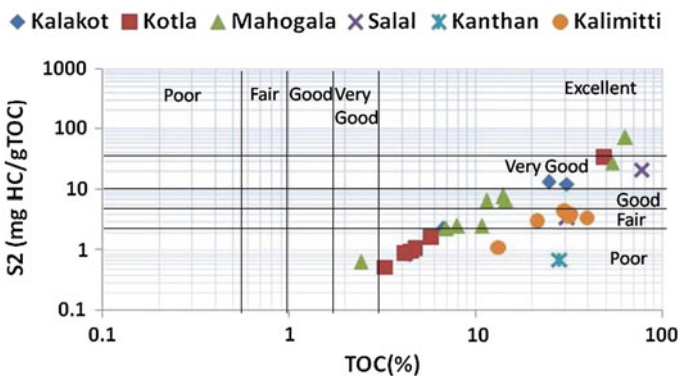
Fig. 13 Source rock characteristics as interpreted by the relationship between remaining hydrocarbon potential (S$_2$) and TOC (wt%) for the Subathu shales from Jammu (after, Mani et al. 2014)

Subathu Group shale put together with petro-physical and lithologic properties and stratigraphic heterogeneity due to faults and fractures can provide criteria for precise defining of the gas shale horizons.

5 Quantitative Approach to Petroleum Potential of a Basin

A mathematical model of petroleum generation based on kinetics of kerogen degradation and utilizing the general scheme of kerogen evolution explicitly for geological time was proposed by Tissot (1969), Tissot and Espitalie (1975). The primary cracking of kerogen is based on several parallel first order reactions obeying Arrhenius law (Fig. 2; Eq. 1). The kinetic parameters (Ei, A, q0i) in these reactions can be determined by optimising the pyrolysis parameters obtained by the open system pyrolysis, such as that of Rock Eval.

An example of quantitative estimates on hydrocarbon generation from the pyrolysis study of Tertiary shales from the Kutch basin is presented through the use of optimization program OPTKIN and Rock Eval parameters—S2, HI, Time, Temperature and heating rate of pyrolysis (5, 15, 30 °C). The representation, for a kerogen, of its activation energies (E1, E2, …, Ei) of cracking is described through a histogram in Fig. 14. With increasing depth and temperature, the various bonds corresponding to successive activation energies are broken, roughly in order of increasing energies. A Type II/III kerogen has a wide distribution of activation energies which are generally unsymmetrical, due to the complex nature of kerogen with lesser aliphatic components and large quantity of aromatic structures.

For each pyrolysis curve used for optimization, a comparison is obtained between:

(i) measured and computed petroleum potential HI (in mg/g TOC); (ii) measured and computed S_2 peak temperature T_{max} (in deg. C); (iii) measured and computed amounts Q of generated hydrocarbon (in mg/g TOC, from 0 to HI); (iv) measured and computed Hydrocarbon generation rates dQ/dt (in mg/g TOC/deg. C); (v) measured and computed transformation ratios TR from Kerogen to Hydrocarbon
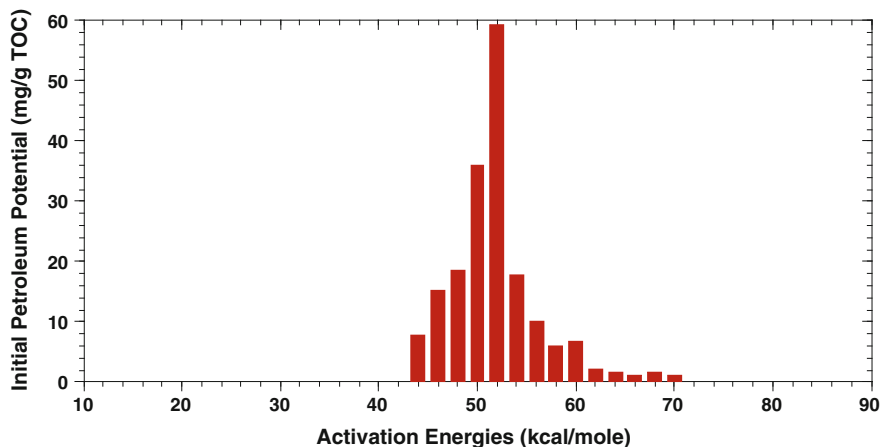
Fig. 14 Activation energy distributions as determined by the open system pyrolysis of Tertiary shales from Kutch basin
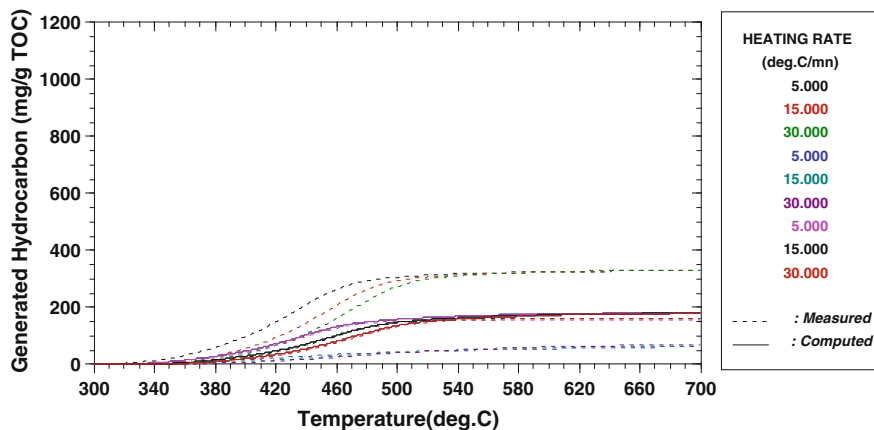
Fig. 15 Amount of hydrocarbon generated as determined by the open system pyrolysis of Tertiary shales from Kutch basin

(in %, from 0 to 100 %); TR = Q/HI. The amount of generated hydrocarbons Q, (Eq. 2) obtained from the computation and optimization of open system pyrolysis parameters of the Tertiary shales is shown in Fig. 15. A good match between the measured and computed values of the generated hydrocarbons, at a maximum value of 180 mg HC/g TOC, is obtained within temperature range between 380 and 490 °C.

The principle use of such calibrated kinetic models of thermal cracking of kerogen into hydrocarbons is that along with thermal and burial history data of a basin, 1D geological basin models can be created, which provide quantitative estimates on oil and gas generated as a function of time. These models help in determination of the timing of petroleum formation for comparison with the age of structural or stratigraphic traps and in general, offer a holistic approach towards evaluation of hydrocarbon potential of a basin.

6 Summary

Organic geochemical characterization of varied age shales from the Vindhyan, Krishna-Godavari, Kutch, Cambay and Jammu and Kashmir basins indicate high TOC content, with dominantly type III kerogen in immature to post mature stage, depending upon the depositional and thermal history of the respective basin. The Raghavapuram shales along with its stratigraphic equivalents, is inferred to be main source rock for much of the prolific KG basin. The extractable organic matter comprising of *n*-alkanes and PAH, along with the kerogen pyrolysis studies suggest promising petroleum opportunities for the Raghavapuram sequence. Amongst the frontier basins, the Semri and Kaimur Group shales from the Vindhyan basin show a gas prone Type III kerogen, where as the Tertiary shales from the Kutch and

Cambay basin show organic rich, mixed Type II and III kerogen. The Subathu shales from Jammu show a post mature Type III kerogen suitable for a late metagenetic gas generation. The frontier basins are characterized by varied geology, age, tectonics, and depositional environments and the potential source rock data controls, in particular, are poor. The studied organic geochemical parameters can be used to map the pod of potential/active source rocks, regional variation in organic facies, and volume of generated hydrocarbons, which are critical in defining a basin's hydrocarbon reserve.

References

Allan J, Douglas AG (1977) Variations in the content and distribution of n-alkanes in a series of carboniferous vitrinites and sporinites of bituminous rank Geochim. Cosmochim Acta 41:1223–1230

Banerjee A, Pahari S, Jha M, Sinha AK, Jain AK, Kumar N, Thomas NJ, Misra KN, Chandra K (2002) The effective source rocks in the Cambay basin. India. AAPG Bull 86(3):433–456

Banerjee S, Dutta S, Paikaray S, Mann U (2006) Stratigraphy, sedimentology and bulk organic geochemistry of black shales from the Proterozoic Vindhyan Supergroup, Central India. J Earth Syst Sci 115(1):37–47

Behar F, Penteado V, Beaumont HL, De B (2001) Rock-Eval 6 technology: performances and developments. Oil Gas Sci Technol—Rev IFP 56(2):111–134

Bhalla SN (1968) Paleoecology of the Raghavapuram Shales (Early Cretaceous), East Coast Gondwanas, India. Palaeogeogr Palaeoclimatol Palaeoecol 5(4):345–357

Bhowmick PK, Misra R (2012) Indian oil and gas potential. In: Banerjee DM, Singhvi AR (eds) Proceedings of the INSA glimpses of geoscience research in India, vol 78, pp 218–228

Biswas SK (1992) Tertiary stratigraphy of Kutch. J Palaeontol Soc India 37:1–29

Brooks JD, Smith JW (1967) The diagenesis of plant lipids during the formation of coal, petroleum and natural gas-I. Changes in the n- paramhydrocarbons. Geochim Cosmochim Acta 31:2389–2397

Chandra K, Raju DSN, Bhandari A, Mishra CS (2001) Petroleum systems in the Indian sedimentary basins: stratigraphic and geochemical perspectives. Bull Oil Nat Gas Corp 38 (1):1–45

Dayal AM, Mani Devleena, Mishra Snigdharani, Patil DJ (2013) Shale Gas prospects of the Cambay Basin, Western India. Geohorizon 18(1):26–31

Dayal AM, Mani D, Madhavi T, Kavitha S, Kalpana MS, Patil DJ, Sharma M (2014) Organic geochemistry of Vindhyan sediments: implications for hydrocarbons. J Asian Earth Sci 91:329–338

Didyk BM, Simoneit BRT, Brassell SC, Eglinton G (1978) Organic geochemical indicators of palaeoenvironmental conditions of sedimentation. Nature 272:216–222

Directorate General of Hydrocarbons (DGH) (2014) Retrieved from www.dghindia.org

Dutta S, Steiner M, Banerjee S, Erdtmann B, JeevanKumar S, Mann U (2006) *Chuaria circularis* from the early Mesoproterozoic Suket Shale, Vindhyan Supergroup, India: insights from light and electron microscopy and pyrolysis–gas chromatography. J Earth Syst Sci 115(1):99–112

Dutta S, Mathews RP, Singh BH, Tripathi SM, Singh A, Saraswati PK, Banerjee S, Mann U (2011) Petrology, palynology and organic geochemistry of Eocene lignite of Matanomadh, Kutch Basin, Western India: Implications to depositional environment and hydrocarbon source potential. Int J Coal Geol 85:91–102

Eden H, Mungo D (2013) Geochemistry-the dark horse upstream. GeoExpro 10(1):22–25

Espitalie J, Marquis F, Sage L (1987) Organic geochemistry of the Paris Basin. In: Brooks J, Glennie K (eds) Petroleum geology of north west Europe. Graham and Totman, London, pp 71–86

Fuex AN (1977) The use of stable carbon isotope in hydrocarbon exploration. J Geochem Explor 7:155–188

Grob RL (2004) Theory of chromatography. In: Grob RL, Barry EF (eds) Modern practice of gas chroamtography, 4th edn. Willy, New York, 743p

Gupta SK (2006) Basin architecture and petroleum system of Krishna-Godavari basin, east coast of India. Lead Edge 25(7):830–837

Horvitz L (1985) Geochemical exploration for petroleum. Science 229(4716):821–827

Hunt JM (1996) Petroleum geochemistry and geology, 2nd edn. W.H. Freeman and company, USA, 715p

Jiang C, Alexander R, Kagi RI, Murray AP (1998) Polycyclic aromatic hydrocarbons in ancient sediments and their relationships to palaeoclimate. Org Geochem 29(5–7):1721–1735

Jokhan Ram J (2005) Hydrocarbon exploration in onland frontier basins of India: perspective and challenges. J Palaeontol Soc India 50(1):1–16

Jones RW, Demaison GJ (1982) Organic facies-stratigraphic concept and exploration tool. In: Salvidar-Sali A (ed) Proceedings of the second ASCOPE conference and exhibition, Manila, Oct 1981, pp 51–68

Jones RW (1983) Organic matter characteristics near the shelf-slope boundary. Soc Econ Paleontol Mineral (SEPM) 33:391–405 (special publication)

Karunakaran C, Ranga Rao A (1979) Status of exploration for hydrocarbon in the Himalayan region—contributions to stratigraphy and structure. In: Proceeding of Himalayan geology seminar, 13–17 Sept 1979. Miscellaneous publications no 41, Part V, vol 1–6(6). Geological Survey of India, New Delhi

Killops SD, Massoud MS (1992) Polycyclic aromatic hydrocarbons of pyrolytic origin in ancient sediments: evidence for Jurassic vegetation fires. Org Geochem 18(1):1–7

Kumar B, Raju SV, Patil DJ, Kalpana G, Vishnu Vardhan C (2006) Integrating surface geochemical expressions with geological, geophysical and remote sensing data: case histories from selected Proterozoic Basins of India. http://www.searchanddiscovery.com/documents/2006/06088houston_abs/abstracts/kumar.htm, downloaded on 16 Dec 2012

Lafargue E, Marquis F, Pillot D (1988) Rock-Eval 6 applications in hydrocarbon exploration, production and soil contamination studies, vol 53(4). In: Juillet-Août (1998). IFP, Pondicherry

Lakshminarayana G (2002) Evolution in Basin Fill Style during the Mesozoic Gondwana Continental break-up in the Godavari Triple Junction, SE India. Gondwana Res 5(1):227–244

Mani D, Patil DJ, Dayal AM (2011a) Stable carbon isotope geochemistry of near surface adsorbed alkane gases in Saurashtra basin. Chemical Geology 280(1–2):144–153

Mani D, Dayal AM, Rasheed MA, Satish Kumar T, Rao TG, Balaram V (2011b) Soil Iodine determination in Deccan Syneclise Basin of India: implications for near surface geochemical hydrocarbon prospecting. Nat Resour Res 20(1):75–88

Mani D, Ratnam B, Patil DJ, Kalpana MS, Dayal AM (2012a) Geochemical proxies for the interpretation of sedimentary paleoenvironment: preliminary results from Krishna Godavari basin, India. In: IGCP-3rd annual symposium response of asian rivers to climate change—past, present and future scenario, 14–16 Nov 2012. CSIR-National Geophysical Research Institute, Hyderabad

Mani D, Patil DJ, Kalpana MS, Dayal AM (2012b) Evaluation of hydrocarbon prospects using surface geochemical data with constraints from geological and geophysical observations in Jamnagar area, Saurashtra Basin, India. J Pet Geol 35(1):67–84

Mani D, Patil DJ, Dayal AM (2013) Evolution of sedimentary organic matter and formation of oil and gas: a geochemical approach. In: International seminar on earth science for society, 7–8 Dec 2012. CSIR-National Geophysical Research Institute, Hyderabad

Mani D, Dayal AM, Patil DJ, Hafiz M, Hakoo N, Bhat GM (2014) Gas potential of Proterozoic and Phanerozoic shales from NW Himalaya, India: inferences from new pyrolysis data. Int J Coal Geol 128–129:81–95

Mani D, Ratnam B, Patil DJ, Kalpana MS, Dayal AM (2015) Elemental and organic matter characteristics of the Gondwana sediments from the Krishna–Godavari Basin, India. Chemie der Erde-Geochemistry (accepted)

Misra SR, Mani D, Kavita S, Kalpana MS, Patil DJ, Vyas DU, Dayal AM (2013a) Organic matter characteristics and gas generation potential of the Tertiary shales from the NW Kutch basin, India. J Pet Sci Eng (under review)

Misra SR, Mani D, Kavita S, Patil DJ, Kalpana MS, Dayal AM (2013b) Pyrolysis results of shales from the South Cambay basin, India: implications for gas generation potential. J Geol Soc India (accepted article)

Mittal AK, Pandey HC, Singh RR (2006) Geochemistry of gas seeps from surface shows and wells of the Himalayan foreland Basin. In: Proceedings of 6th international conference and exposition on petroleum geophysics, Kolkata, pp 235–291

Nagori ML, Khosla SC, Jakhar SR (2013) Middle Eocene Ostracoda from the Tadkeshwar Lignite Mine, Cambay Basin, Gujarat. JGeol Soc India 81:514–520

Ojha PS (2012) Precambrian sedimentary basins of India: an appraisal of their petroleum potential. In: Bhat G, Craig J, Thurow JW, Thusu B, Cozzi A (eds) Geology and hydrocarbon potential of Neoproterozoic–Cambrian Basins in Asia, vol 366. Geological Society, London. doi: 10.1144/sp366.11 (special publications)

Patil DJ, Mani D, Madhavi T, Sudarshan V, Srikarni C, Kalpana MS, Sreenivas B, Dayal AM (2013) Near surface hydrocarbon prospecting in Mesozoic Kutch sedimentary basin, Gujarat, Western India–A reconnaissance study using geochemical and isotopic approach. J Pet Sci Eng 108:393–403

Peters K (1986) Guidelines for evaluating petroleum source rocks using programmed pyrolysis. Am Assoc Pet Geol 70:318–329

Peters KE, Cassa MR (1994) Applied source rock geochemistry. In: Magoon LB, Dow WG (eds) The petroleum system—from source to trap: Tulsa, Okla. Am Assoc Pet Geol Memoir 60:93–117

Peters KE, Moldowan JM (1993) The biomarker guide—interpreting molecular fossils in petroleum and ancient sediments. Prentice Hall, New Jersey

Peters KE, Walters CC, Moldowan JM (2005) The biomarker guide: biomarkers and isotopes in the environment and human history, vol 1. Cambridge Press, Cambridge

Philp RP (1985a) Fossil fuel biomarkers applications and spectra. Elsevier, The Netherlands

Philp RP (1985b) Biological markers in fossil fuel production. Mass Spectrom Rev 4:1–54

Platzner IT (1997) Modern isotope ratio mass spectrometry. Wiley, Chichester

Sastri MVA, Moitra AK (1984) Vindhyan stratigraphy—a review, memoir. Geol Surv India 116 (II):109–148

Sastri VV, Venkatachala BS, Narayanan V (1981) The evolution of the east coast of India. Palaeogeogr Palaeoclimatol Palaeoecol 36:23–54

Sharma M (2006) Late Proterozoic (Statherian) carbonaceous film from the olive (Koldaha shale), Semri Group, Vindhyan Supergroup, India. J Paleontol Soc India 51(2):27–35

Simoneit BRT, Fetzer JC (1996) High molecular weight polycyclic aromatic hydrocarbons in hydrothermal petroleums from the Gulf of California and Northeast Pacific Ocean. Org Geochem 24:1065–1077

Simoneit BRT (1992) Natural hydrous pyrolysis-petroleum generation in submarine hydrothermal systems. In: Whelan JK, Farrington JW (eds) Productivity, accumulation and preservation of organic matter in recent and ancient sediments. Columbia University Press, New York, pp 368–402

Sneddon J, Masuram S, Richert JC (2007) Gas chromatography-mass spectrometry-basic principles, instrumentation and selected applications for detection of organic compounds. Anal Lett 40(6):1003–1012. doi:10.1080/00032710701300648

Tissot B (1969) Premières données sur les mécanismes et la cinetique de la formation du pétroledans les sédiments. Simulation d'un schéma réactionnel sur ordinateur (First data on the mechanisms and kinetics of the formation of petroleum in sediments. Simulation of a reaction scheme on a computer) Revue de Institut Français du Pétrole, vol 24, pp 470–501

Tissot BP, Welte DH (1984) Petroleum formation and occurrence. A new approach to oil and gas exploration. Springer, Berlin, p 538pp

Tissot B, Espitalie J (1975) L'evolution thermique de la matiere organique des sediments; applications d'une simulation mathematique; Potentiel petrolier des basins sedimentaires et reconstitution de l'histoire thermique des sediments: Revue de l'Institut Francais du Petrole et Annales des Combustibles Liquides, vol 30, pp 743–777

Van Krevelen DW (1961) Coal: typology-chemistry-physics-constitution. Elsevier Science, Amsterdam

Veevers JJ (2004) Gondwanaland from 650–500 Ma assembly through 320 Ma merger in Pangea to 185–100 Ma breakup: supercontinental tectonics via stratigraphy and radiometric dating. Earth Sci Rev 68:1–132

Overpressure Zones in Relation to In Situ Stress for the Krishna-Godavari Basin, Eastern Continental Margin of India: Implications for Hydrocarbon Prospectivity

Rima Chatterjee, Suman Paul, Dip Kumar Singha and Manoj Mukhopadhyay

Abstract An analysis for over pressure zone (OPZ) prevailing in parts of the Krishna-Godavari Basin (KG-B) at the Eastern Continental Margin of India (ECMI) is found promising from the viewpoint of its hydrocarbon potentials. Pressure coefficients estimated from pore pressure studies reveal that there is a rather extensive (lateral) OPZ in the study area than hitherto expected with maximum pressure coefficient of 1.31 or more. The stress magnitudes like vertical stress (S_v), minimum horizontal stress (S_h) and pore pressure gradient (PPG) and fracture pressure gradient (FPG) are predicted from well log data for 15 available wells distributed over an area of 6022 km^2 in KG-B. The wells are drilled to depths of 3660 m on-land (#Wells 1–9) and up to 4000 m in offshore (#Wells 10–15). The PPG ranges from 11.85 to 13.10 MPa/km, whereas, the FPG varies from 17.40 to 19.78 MPa/km in sediments penetrated by the wells displaying normal pressured sediment to a significantly higher value of 19.78 MPa/km for the over-pressured sediments. The values of vertical stress gradient (VSG) varies from 14.67 to 23.10 MPa/km, whereas, the values of S_h magnitude varies from 64 to 77 % of the S_v in normally-pressured to over-pressured sediments. VSG, PPG and FPG tend to decrease with corresponding increase in water column for the studied offshore wells. These results are utilized for constructing contour maps for observing the variations in the VSG and in the OPZ-top, also for constructing PPG contour map in 3D along the vertical section connecting all 15 wells extending from onshore to offshore regions. Any significant increase in pore pressure means the decrease of

R. Chatterjee (✉) · D.K. Singha
Department of Applied Geophysics, Indian School of Mines, Dhanbad 826004, India
e-mail: rima_c_99@yahoo.com

S. Paul
Department of Petroleum Engineering, Al Habeeb College of Engineering and Technology, Hyderabad 501503, India

M. Mukhopadhyay
Department of Geology and Geophysics, King Saud University, PO BOX 2455, Riyadh 11451, Kingdom of Saudi Arabia

effective horizontal stress in respect of depth. As a result, the safety windows or safe mud-weight windows (the difference between PPG and FPG corresponding to particular depth interval in a well) will also decrease with the increase of PPG and FPG. Analytical approach adopted above is then critically examined to recommend how a priori steps based on petrophysical characters of a formation are closely monitored in time and optimum mud weight maintained during drilling.

1 Introduction

The KG-B is considered as one of the largest petroliferous basin positioned at the center of ECMI. A number of hydrocarbon potential structures and traps have been identified in the basin over the decades in both onshore and offshore regions and a few of these have already started producing. An enormous thick piles of the Mesozoic to Tertiary sedimentary sequences in KG-B have been delineated from geophysical surveys and the estimated thickness of that sediment is about 8 km (Bastia et al. 2010). Such a thick sediment succession is actually controlled in a vast range of geological settings, such as: coastal basin, shelf-slope apron, deepwater fan complex, deep-sea channel, delta, subsurface horst and graben structures, etc. (Rao et al. 2013) and all these made the basin quite unique. Consequently, the basin has emerged as one of the frontier basins for hydrocarbon exploration and production, in particular, after the multi-trillion cubic feet supergiant gas discovery in current years (http://www.dghindia.org). Substantial hydrocarbon potential exist both in the Tertiary delta as well as in the channel-levee-overbank play types in deepwater (Bastia et al. 2006). High sedimentation rate, thick sediment and buried mobile shale strata favor shale tectonics in KG-B offshore which is exposed in the form of mud diapirs, large extensional growth faults in the shelf and upper slope regions, and toe-thrusts in the deeper parts of the basin; few of the structural elements are buried under the transportation of large scale mass deposits (Dewangan et al. 2008). Interpretation from magnetic anomaly for western part of KG-B offshore helped to delineate a NE-SW trending structural high and its orthogonal fracture zones. Actually, three tectonic features are recognized here between the Eocene shelf-edge inherited at the rifted Indian Shield margin and the slope features under ECMI. The Eocene shelf-edge mostly coincides with the Continent-Ocean-Boundary under offshore KG-B.

The geological sections traversing across the horst or sub-basins of KG-B, such as: Krishna, West Godavari and East Godavari sub-basins and further beyond into the offshore areas describes how the sediments have been deposited with geological time as referred by Rao et al. (2013) in a review. A synoptic view of sediment disposition on the overlying rifted, warped and thinned crust is illustrated in Fig. 2. The geological section is partly described by geophysical surveys (modified after Radhakrishna et al. 2012) and the information regarding drill holes are provided in the present study. The reservoir rocks in KG-B are mostly comprised of siltstone,

silty sandstone, shaly sandstone, sandy siltstone and sandstone where the hydro-carbons are expected to be accumulated in faults, anticlines, unconformities, pinch-outs, lenses or in their combinations. The unconventional stratigraphic traps related to regional sand pinch-outs, channel fills and truncations are supposed to be prominent hydrocarbon accumulators (Gupta 2006; Shanmugam et al. 2009). Synchronous active subsidence and high sedimentation rate have obviously played a considerable role for the development of overpressure zones in KG-B (Anitha et al. 2014). Rao and Mani (1993) are probably the first authors to report on the abnormal pressure regime in the KG-B. The knowledge of pore pressure and fracture pressure is essential for understanding the geometry of basin, developing the basin models, mapping of hydrocarbon traps/seals, analyzing trap configurations and identifying the migration pathways.

It is well documented in literature why reliable estimates on pore pressure and fracture pressure are essential for an optimized casing program design, for risk analysis as well as for avoiding well control problems, such as blowouts. There are several factors for generation of overpressure in sedimentary basins such as: tectonic compression, hydrocarbon generation, disequilibrium compaction, aquathermal expansion, mineral transformation, mineral dehydration, hydrocarbon buoyancy and vertical fluid movement (Osborne and Swarbrick 1997; Bowers 2002; Zhang 2011; Singha and Chatterjee 2014). Precise velocity determination is therefore crucial in geopressure prediction (Dutta 2002; Chopra and Huffman 2006). Overpressures generated by disequilibrium compaction are associated with anomalously high sediment porosity and are thus more readily detectable in sonic log (Sayers et al. 2002; Tingay et al. 2009). An OPZ in KG-B is usually ascribed to higher sonic—derived porosities. Pore pressure gradient (PPG) and fracture pressure gradient (FPG) are by far most significant considerations for evaluating the technical merit as well as the financial aspect in any well-plan. For successful drilling operation it is therefore essential to know accurately the areas of elevated PPG as it may pose drilling difficulty (Fleming et al. 1998). Pore pressure is usually estimated prior to drilling from drilling experience, mud weights, sonic and resistivity measurements in nearby wells and also from local seismic velocity and discrimination of lithology . The pore pressure and fracture pressure gradients together guide the development of the rig selection, wellhead ratings, mud schedule and casing program (Schultheiss et al. 2009). Mainly these considerations lead us in the present study to better delineate the OPZ and to explore relationship between in situ stress and pore pressure from available log data from 15 wells drilled onshore in KG-B and its deep water areas to the north-east.

2 Study Area

The KG-B is broadly described into three sub-basins, namely the Krishna, West Godavari and East Godavari; the latter two are separated by the Bapatla and Tanuku horsts in their respective locales (Bastia et al. 2006; Rao et al. 2013) (Fig. 1). The
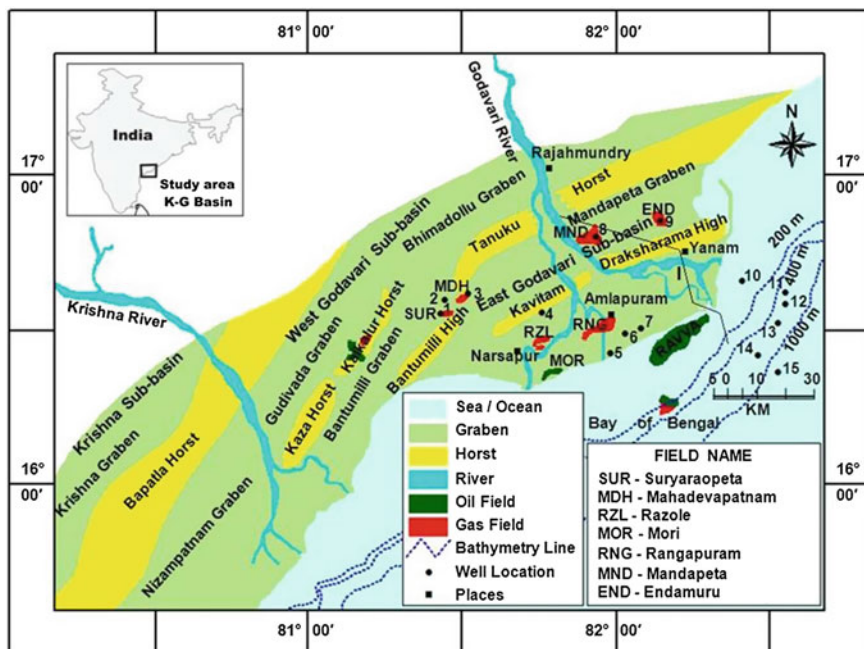
Fig. 1 Prominent horst and graben structures and oil-gas fields mapped in KG-B. Present study is based on 15 wells: 9 onshore and six offshore; distributed over an area of ∼6022 km². Refer text for details. Geologic section I is illustrated on Fig. 2

West Godavari sub-basin is further subdivided into the Gudivada, Bantumilli grabens. The Kaza-Kaikalur horst is separated these grabens. The graben namely, Mandapeta and Kavitam-Draksharama high are located on either side of the Tanuku horst in the East Godavari sub-basin. The grabens are mainly filled up by the Mesozoic sediments which constitute the rift fill sequence tilted landward. The sedimentation pattern changed during the Tertiary periods. Two major rivers, the Krishna and the Godavari drain the clastic sediments to sea shore for initiating the deltaic processes. Variable sedimentation rates are reported for the KG-B; ranging from 0.07 to greater than 2 mm/year (Anitha et al. 2014). High sedimentation, at rates >1 mm/year, is known to generate overpressure in many sedimentary basins around the world (Fertl 1976).

A total number of 15 drilled wells distributed both onshore and offshore, is used in the present study for detection of OPZ in the coastal zone (Fig. 1). Of these, 10 wells are drilled in the KG-B covering an area of ∼5100 km² distributed at the MDP, END, RAN, KAV Gas Fields located in the East Godavari sub-basin and the MDH, SUR Gas Fields in the West Godavari sub-basin, including one well at shallow waters in KG-B offshore namely, KY. The other 5 wells are drilled in deep offshore KG-B. The water depths in these vertical wells are varying from 515 to 1265 m, where, these wells reach up to 3960 m in sediments (Chatterjee et al.
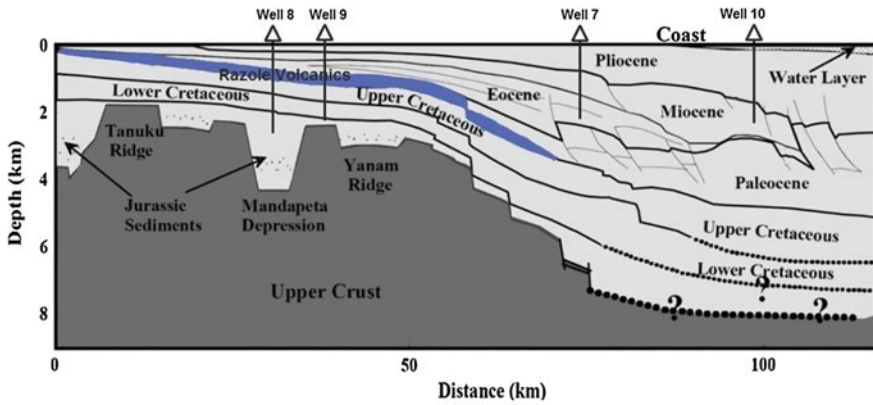
Fig. 2 Synoptic geologic section across KG-B illustrating the rifted and deformed top basement underneath the sediment cover; section line shown on Fig. 1 (modified after Radhakrishna et al. 2012). Wells #7–10 are projected onto the section line. Penetration depths for the wells and pertinent logs for the wells are shown on Figs. 3 and 4
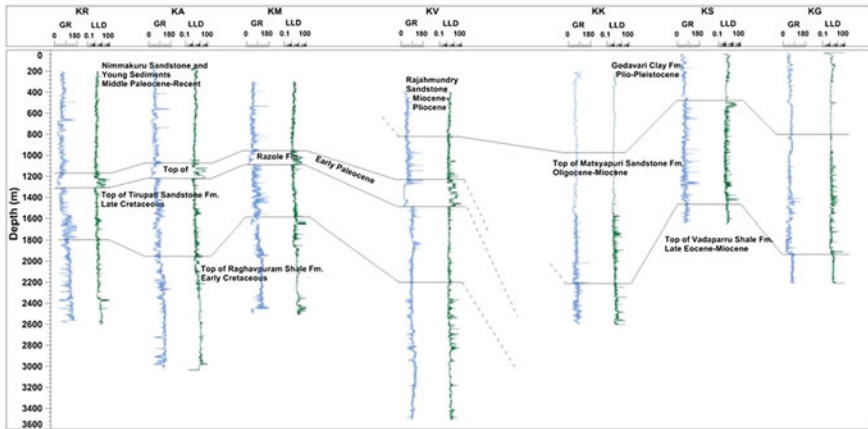
Fig. 3 Well log correlation for seven wells #1–7 drilled in KG-B onshore (modified after Singha and Chatterjee 2014). Formation tops are identified from GR and LLD logs monitored in the wells. Refer text for discussion

2010). Of these, five wells are depicted at their projected sites on the geologic section given on Fig. 2, including Well #7 that refers to the deeper water KG-B. The well correlation in onshore and offshore areas in KG-B is shown in Figs. 3 and 4.
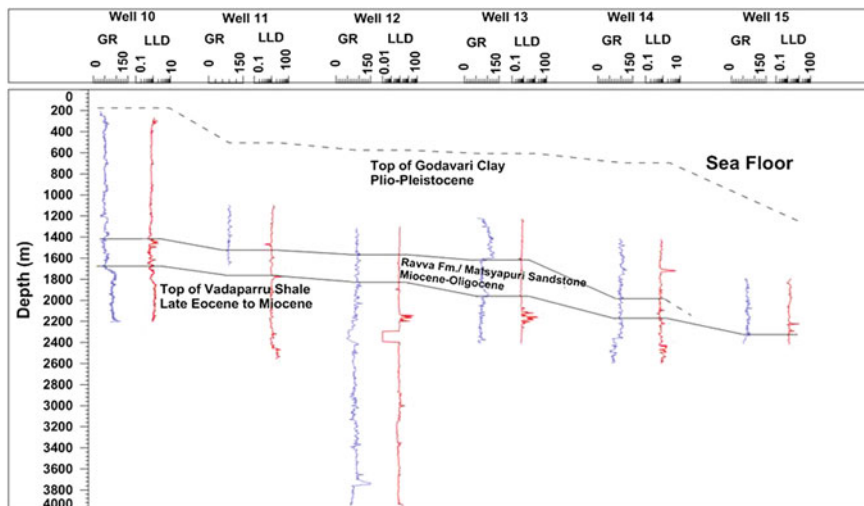
Fig. 4 Well log correlation for six wells #10–15 drilled in KG-B offshore. Formation tops are identified in relation to sea floor

3 Detection of Overpressure Zones

We have argued in a previous study that in sand/shale sequences as observed in the wells of KG-B, the low permeability, e.g. clay prevents the escape of pore fluids at rates sufficient to keep up with the rate of increase in vertical stress (Singha and Chatterjee 2014). The pore fluid begins to carry a large part of the load and pore fluid pressure will increase. This process is referred to as under-compaction or compaction disequilibrium and is considered as a feasible mechanism to explain and quantify overpressure in the KG-B. Sonic logs are popularly used for estimating pore pressure in shale using the Eaton and equivalent depth methods of estimating pore pressure from velocity data in reference to a Normal Compaction Trend (NCT) (Van Ruth et al. 2002). The primary focus in this approach lies in estimating the pore pressure from the sonic logs for establishing the NCT, i.e., the acoustic travel time versus depth for normally pressured sediments. Estimation of vertical stresses are also required for the Eaton and equivalent depth methods that are to be used (Eaton 1972; Sarker and Batzle 2008). Accordingly, we defined the NCT graphically and its deviation in travel time from sonic logs for the wells in KG-B for the purposes of delineation of OPZ. We have reported it before that the overpressure in the KG-B is most likely related to its low permeability sediment and is confined by low permeability media (Chatterjee et al. 2011). NCT represents best possible fitted linear data in the low permeable zone, like shale (Fig. 5a, b) for the two wells namely; #7 and #13 in the KG-B onshore and offshore areas respectively (Fig. 1). Top of the OPZ is detected from deviation of NCT as well as from the separation between density and sonic porosities. Figure 5 illustrates the behavior of
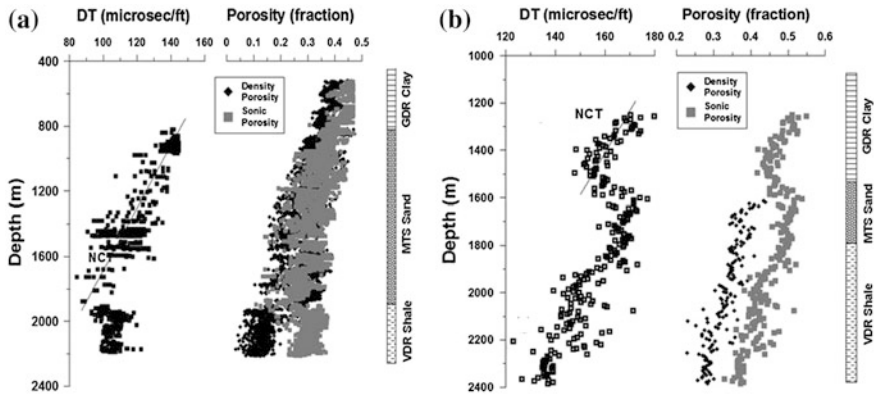
Fig. 5 **a** Display of Normal Compaction trend (NCT) for the onshore well #7 indicating the top of OPZ at 1919.16 m depth. Separate labels for Φd and φs in respect of depth corresponding to the Oligo-Miocene sand. Lithology identification is indicated on the right panel: GDR, Godavari, MTS, Matsyapuri and VDR, Vadaparru, **b** Display of NCT for the offshore well #13 indicating the top of OPZ at 1600.00 m depth corresponding to GDR clay; separate labels for Φd and φs in respect of depth. Lithology identification is indicated on the right panel: GDR, Godavari, MTS, Matsyapuri and VDR, Vadaparru

the porosity trend for the normal-compacted and under-compacted shale formations in KG-B. Pore Pressure (PP) for ten wells is calculated from Eaton's sonic equation (Eaton 1972), while, Miller's sonic equation (Miller 1995) has been used to estimate PP for deep water wells using the magnitude of vertical stress.

Vertical stress (S_v) is calculated from bulk density of the rock which is force per unit area applied by load of overburden rock above the point of measurement. The essential equation given by Plumb et al. (1991) is:

$$S_v = \int_0^z \rho(z) g \, dz \tag{1}$$

where z, $\rho(z)$ and g are the depth at point of measurement, bulk density of the rock as a function of the depth and acceleration due to gravity respectively.

The PP for onshore and shallow offshore wells has been calculated using Eaton's sonic (Eaton 1972) and for deep water wells by Miller's equation (Miller 1995).

$$PP = S_v - (S_v - Ph) * (DTn/DT)^3 \tag{2}$$

$$PP = VSG - \frac{\frac{1}{\lambda} \ln \left\{ \frac{DT}{DT_{ml}} \left(\frac{DT_{ml} - DT_{matrix}}{DT - DT_{matrix}} \right) \right\}}{Depth} \tag{3}$$

where, Ph = hydrostatic pressure ($\int_0^z \rho \, g \, dz$) where ρ = average mud density which is constant, DTn = sonic travel time in low permeable zone calculated from NCT trend, DT = observed sonic travel time. Hydrostatic pressure gradient is taken as 10 MPa/km for all 15 wells in KG-B (Chatterjee and Mukhopadhyay 2002, Chatterjee 2008; Chatterjee et al. 2011). VSG = vertical stress gradient i.e. gradient of S_v, DT_{ml} = Sonic travel time of sediment at mudline i.e. 200 μs/ft, DT_{matrix} = Sonic travel time matrix material i.e. 58 μs/ft and λ = Empirical parameter defining the rate of increase in velocity with effective stress, i.e. 0.000221/psi.

The calculated PP from the vertical stress data and NCT can be validated with the pressure measurement tools like Repeat Formation Tester (RFT), Modular Dynamic Tester (MDT) in permeable and impermeable rocks (Gholami et al. 2014). The pressure estimate from the Eqs. (2) and (3) had already been compared to the pressure measured by RFT and MDT tools for onshore and offshore wells respectively (Singha and Chatterjee 2014; Chatterjee et al. 2011). Previous author e.g. Swarbrick (2002) had discussed the best use of porosity based pore prediction techniques in moderately constant lithology, and in the overpressure zones generated by disequilibrium compaction. Therefore, pore pressure prediction from acoustic log will work well in the KG-B.

The FP has been determined from Matthews–Kelly's equation (Matthews and Kelly 1967):

$$FP = K_i * (S_v - PP) + PP \tag{4}$$

where, K_i = matrix stress coefficient = S_h/S_v and S_h = minimum horizontal stress calculated from the equation (Engelder and Fischer 1994; Hillis 2000)

$$S_h = PP + \sigma^*(S_v - PP)/(1 - \sigma) \tag{5}$$

where σ is Poisson's ratio. We have reported in previous study that σ for rocks in the KG-B ranges from 0.24 to 0.28 (Chatterjee and Mukhopadhyay 2002).

The minimum horizontal stress obtained from above Eq. (5) can be calibrated against direct measurement of leak-off test (LOT) (Yamamoto 2003; Zoback et al. 2003). The estimated S_v, PP, FP and S_h from the respective Eqs. (1)–(5), as well as the top of OPZ, porosity for all 15 wells are listed in Table 1. The gradient S_v for these 15 well is found to vary between 14.67 MPa/km in well #15 and 23.10 MPa/km in well #8. The S_v gradient contour map and its 3D representation for the study area clearly exhibits decreasing gradient in offshore areas (Fig. 6). The top of OPZ covering 14 wells in this study area separately plotted is shown as a contour plot (Fig. 7). The top of OPZ varies between 1200 m corresponding to well #10 in offshore and 2324 m for well # 5 onshore. The OPZ contour map and its 3D animation reflect the variation for the top of OPZ in the Raghavapuram and Vadaparru Shale Formations. The gradient of PP varies in the OPZ from 11.85 to 13.10 MPa/km, whereas, the gradient of FP ranges 14.13–19.78 MPa/km for these 15 wells. It is also observed from Table 1 that

Table 1 Lists the Top of OPZ, S_v gradient, PP gradient, FP gradient, S_h gradient, S_h/S_v and porosities for 15 wells in K-G basin

Well name	Top of OPZ (m)	S_v gradient MPa/km	Predicted PP gradient (MPa/km) In OPZ	Predicted FP gradient (MPa/km)		S_h gradient (MPa/km)		S_h/S_v		Porosity (fraction in OPZ)		Formation	Geologic age
				In OPZ	In normal pressured sediment	In OPZ	In normal pressured sediment	In OPZ	In normal pressured sediment	φd	φs	Name	
1	1830.00	21.60	11.65	18.90	17.89	15.61	14.52	0.72	0.67	0.12	0.24	Raghavapuram shale	Early cretaceous
2	2280.00	22.85	12.30	19.78	18.30	16.20	14.79	0.70	0.64	0.07	0.22	Raghavapuram shale	Early cretaceous
3	1650.00	22.37	12.18	19.42	16.05	16.04	14.75	0.72	0.66	0.12	0.24	Raghavapuram shale	Early cretaceous
	2290.00	21.55	13.10	19.58	17.86	16.52	14.51	0.77	0.67	0.12	0.27	Raghavapuram shale	Early cretaceous
5	2324.00	21.80	12.32	19.00	17.80	15.60	14.40	0.71	0.65	0.17	0.27	Vadaparru shale	Late eocene-miocene
6	1431.46	21.10	12.30	18.75	17.40	15.47	14.08	0.72	0.66	0.17	0.31	Vadaparru shale	Late eocene-miocene
7	1919.16	21.00	12.80	18.85	17.47	15.80	14.16	0.76	0.68	0.13	0.30	Vadaparru shale	Late eocene-miocene
8	–	23.10	–	–	19.51	–	15.65	–	0.67	0.19	0.23	–	–
9	1350.00	21.35	11.27	18.29	17.52	14.97	14.12	0.70	0.68	0.18	0.22	Raghavapuram shale and Tirupati sandstone	Early cretaceous to late cretaceous

(continued)

Table 1 (continued)

Well name	Top of OPZ (m)	S_v gradient MPa/km	Predicted PP gradienl (MPa/km) In OPZ	Predicted FP gradienl (MPa/km)		S_h gradient (MPa/km)		S_h/S_v		Porosity (fraction in OPZ)		Formation	
				In OPZ	In normal pressured sediment	In OPZ	In normal pressured sediment	In OPZ	In normal pressured sediment	φd	φs	Name	Geologic age
10	1200.00	21.50	11.98	18.01	17.90	15.67	14.39	0.73	0.67	0.27	0.30	Matsyapuri sand vadaparru shale	Late eocene to oligocene
11	1320.00	17.37	11.94	15.90	13.68	14.70	12.79	0.71	0.64	0.25	0.31	Vadaparru shale	Late eocene-miocene
12	1700.00	18.38	12.18	17.24	14.02	15.41	13.10	0.75	0.68	0.23	0.33	Vadaparru shale	Late eocene-miocene
13	1600.00	17.55	12.46	15.83	13.72	14.04	12.40	0.73	0.67	0.28	0.36	Matsyapuri sand vadaparru shale	Late eocene to oligocene
14	1420.00	17.01	11.88	15.33	13.37	14.72	12.67	0.70	0.66	0.29	0.37	Godavari Clay vadaparru shale	Late eocene-pliocene
15	2080.00	14.67	12.25	14.13	13.02	12.98	11.34	0.77	0.72	0.24	0.38	Godavari clay vadaparru shale	Late eocene-pliocene

OPZ Over Pressure Zone; S_v Vertical Stress; *PP* Pore Pressure; *FP* Fracture Pressure; S_h Minimum horizontal compressive stress; *φd* Porosity derived from density log and *φs* Porosity derived from sonic log

Φd and φs represent porosities derived from density and sonic logs
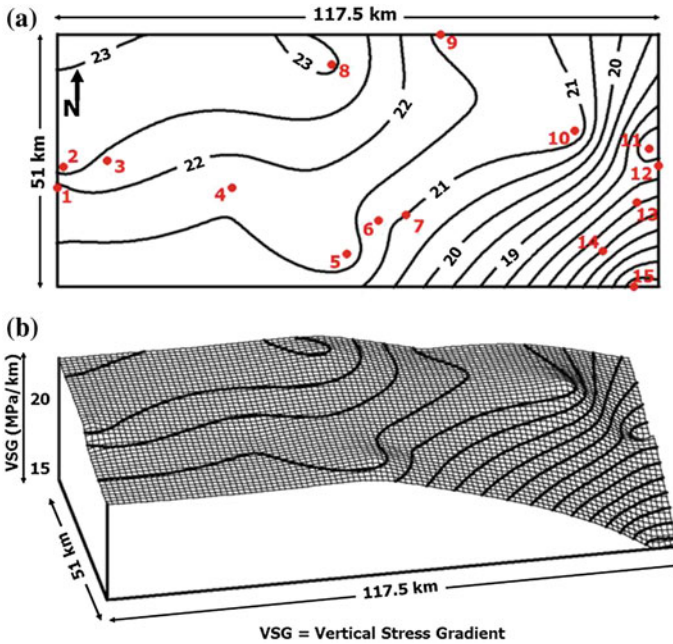
Fig. 6 Distribution of 15 wells across the study area and the vertical stress gradient (VSG) (unit: MPa/km) map. Lower panel illustrates its 3D impression. VSG contours steepen across the continental slope to the southeast

the ratio of S_h/S_v ranges from 0.64 to 0.72 at the normal pressured sediment whereas it is increased and varies from 0.70 to 0.77 at the overpressured sediments. Pore pressure gradient versus depth plot (Fig. 8) along a vertical section from well 1 to 15 shows the increase of gradient from onshore to offshore parts with an exception in well 4 due to presence of OPZ at greater depth. The PP gradient increases from West Godavari sub-basin through coastal part of the East Godavari sub-basin to KG-B offshore, where, it ranges from 11.27 MPa/Km in well #9 to 13.10 MPa/km in well #4.

4 Relationship Between Pore Pressure, Fracture Gradient and In Situ Stress

Stresses acting in formations play an important role in geophysical prospecting and development of hydrocarbon reservoirs. The direction and magnitude of in situ stresses are required in planning for borehole stability during hydraulic fracturing for enhanced production and selective perforation for prevention of sanding during production as well as for directional drilling. So, accurate and reliable assessment of
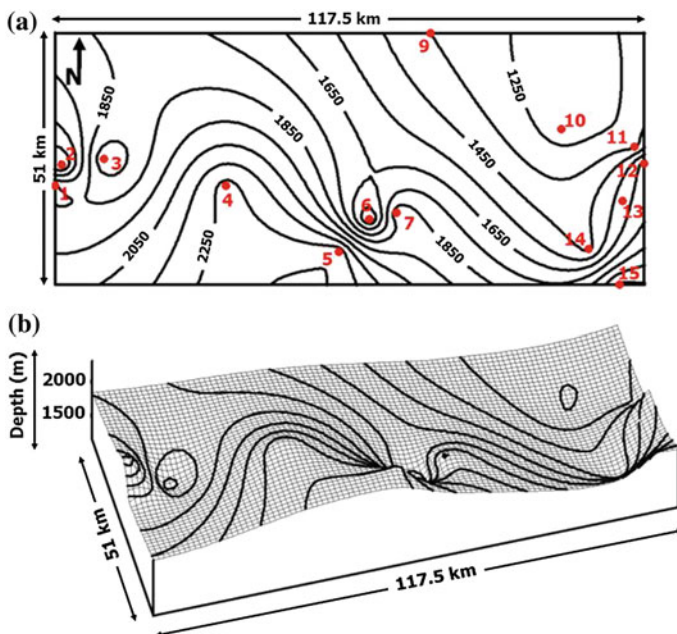
Fig. 7 Contour map of Top of OPZ for the study area and its 3D impression in KG-B
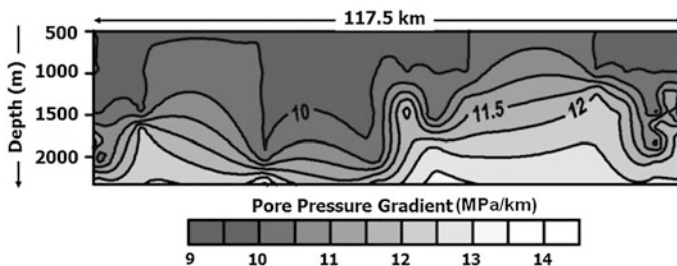
Fig. 8 Variation of pore pressure gradient with depth for a vertical section derived from wells 1 through 15 between onshore to offshore KG-B

horizontal stress magnitudes can provide an early caution of impending drilling problems that may be mitigated by appropriate drilling fluid design and drilling practices (Sinha et al. 2008). The PP gradient increases from the West Godavari sub-basin through the coastal part in the East Godavari sub-basin for KG-B off-shore. This is due to thicker sediment deposition together with the increase of vertical stress. Sand units in the overpressured Formations, like the Raghavapuram and Vadaparru shales, are known to contain gas. Hence, a better delineation of OPZ in the area will be helpful for studies on gas migration as well as borehole stability during depleting the reservoirs in these gas fields. To look after the wellbore

stability in the KG-B, proper mud weight (MW) can be estimated from PP studies. Mud weight selection for pressure control requires information on PPG and FPG. The PPG defines the lower limit of MW while FPG defines the upper limit of MW (cf. Tan and Willoughby 1993; Wang et al. 2008; Singha and Chatterjee 2014).

The abnormal high pressures or overpressures, occurring mostly in the sediments from Cretaceous to Miocene age, have 4 km of thickness deposited in fluvio—deltaic conditions implying for a relatively high rate of sedimentation. The double overpressured configuration lies primarily in the wells 5, 6 and 7 located near the Rangapuram field, Amalapuram area (Singha and Chatterjee 2014). The single overpressure configuration lies primarily in the West Godavari sub-basin. The top of the overpressure zone in Table 1 and these horizons show three important characteristics: (a) Distribution of the pressure coefficient (abnormal pressure/normal hydrostatic pressure) is not uniform. Overpressured zones are characterized by high PP gradient as well as low PP gradient above hydrostatic. (b) Pressure coefficient near the gas fields like RZL and RNG is greater than the pressure coefficient observed in the SUR and MDH field and (c) The maximum pressure coefficient of 1.31 is observed for the well #4 near RZL field. Overpressure in the Shale formation having strong sealing capacity controls hydrocarbon accumulation (refer Li et al. 2008). The overpressure existing in the Raghavapuram or Vadaparru Shale formation can drive hydrocarbon migration from the source rock to the traps (Tang and Lerche 1993; Hao et al. 2002). Enhanced overpressure (pressure coefficient greater than 1.8) can also crack the formation and push the sandstone intrusion into the shale, and responsible for the formation of the sand injectites that create new areas for hydrocarbon exploration and production (Shi et al. 2013; Hurst et al. 2011).

Reservoirs which are depleted exhibit rapidly changing lower PP and horizontal stress magnitude than the overlying shaly formation. Drilling through such reservoirs can result into rigorous fluid loss and drilling induced borehole instability. So, accurate and reliable estimation of VSG, PPG, FPG, effective vertical stress and effective horizontal stress are all necessary for planning of a successful drilling of a well. To alleviate different drilling hazards accurate estimation of effective stress is clearly necessary.

Since all five wells in offshore KG-B are deep-water wells but at variable water depths (515, 585, 603, 706 and 1265 m); the sea-water column clearly exerts increasing overburden pressure as the water column gets deeper. Consequently, the VSG (which is partly dependent on the thickness of the water column) for the well #15 having deepest water is manifested by the lowest VSG trend. Further, with increase in water column (say, well #15) the corresponding values of VSG, PPG and FPG decrease as compared to the VSG, PPG and FPG for other wells. The pore pressure, together with fracture gradient, decides the MW that is required. Too much MW cracks or fractures the rock, too little MW allows formation fluids to get into the well and can instigate blow-outs if not controlled. Low fracture gradient under deepwater unconsolidated sediments suggest that the small increases in formation pressure can initiate rock fractures to occur, destabilising the wellbore and potentially leading to an influx of gas and oil (known as a kick) which if uncontrolled could lead to a blowout (Singh et al. 2014). To avoid the risk of

inducing loses due to the narrow margin between the PPG and FPG low density cement system is required to ensure cement coverage across the zone of interest. This opinion is substantiated by the safety window (the difference between PPG and FPG at a particular depth in a well #15) that decreases as the water column increases. In other words, the formation which is having a smaller safety window can be fractured at low mud pressure as compared to a formation that has larger safety window. For the benefit of safe deep-water drilling in offshore KG-B, it is therefore of largely significant that accurate estimation of PPG, FPG and in situ stress is made in order to diminish geohazards which may occur during drilling. These findings are also corroborated by geological evidences on the Pliocene environments in KG-B which are interpreted to be comparable to the modern upper continental slope with rather large scale mass-transport deposits and submarine canyons (Chatterjee et al. 2011). For instance; Shanmugam et al. (2009) consider that tsunamis, earthquakes, frequent tropical cyclones, shelf-edge canyons with steep-gradient walls and sea-floor fault scarps as favorable factors for triggering submarine mass movements.

5 Conclusions

The OPZ generated by disequilibrium compaction is largely detectable in KG-B by virtue of its intimate association with higher porosity. The porosities obtained from sonic and density logs are found to be separated from one another in OPZ. The pressure coefficients reveal that there is widespread overpressure under the study area of KG-B with maximum pressure coefficient of 1.31 or more. The vertical as well as horizontal stress, pore and fracture pressure have been predicted from 15 available wells in KG-B. The observed abnormal PP gradient in the wells ranges from 11.27 to 13.10 MPa/km, whereas, FP gradient varies from 13.02 MPa/km in normal pressured sediment to 19.78 MPa/km in over-pressured sediments drilled in these wells. Vertical stress gradient is observed to vary from 14.67 to 23.10 MPa/km. The S_h magnitude is found to vary from 64 to 77 % of the S_v in normally pressured to over-pressured sediments. With the increase in water column, vertical stress gradient, PPG and FPG trends decrease. This implies that formation can be fractured at lower mud pressure. The technique imbibed through this study indicates how steps can be taken in time if petrophysical characters of a formation are closely monitored and optimum mud weight is maintained during drilling.

References

Anitha G, Ramana MV, Ramprasad Dewangan, Anuradha M (2014) Shallow geological environment of Krishna-Godavari offshore, eastern continental margin of India as inferred from the interpretation of high resolution sparker data. J. Earth Syst Sci 123(2):329–342

Bastia R, Singh P, Nayak PK (2006) Linking shelf delta to deep water; Krishna-Godavari basin. J Geol Soc India 67:619–628

Bastia R, Radhakrishna M, Srinivas T, Nayak S, Nathaniel DM, Biswal TK (2010) Structural and tectonic interpretation of geophysical data along the eastern continental margin of India with special reference to the deep water petroliferous basins. J Asian Earth Sci 39:608–619

Bowers GL (2002) Detecting high overpressure. Lead Edge 21:174–177

Chatterjee R (2008) Effect of normal faulting on in-situ stress: a case study from Mandapeta field, Krishna-Godavari basin, India. Earth Planet Sci Lett 269(3–4):457–466

Chatterjee R, Mukhopdhyay M (2002) In-situ stress determination using well log data for the oil fields of the Krishna-Godavari basin. Petrophysics 43:26–27

Chatterjee R, Mukhopadhyay M, Paul S (2011) Overpressure zone under the Krishna-Godavari offshore basin: geophysical implications for natural hazard in deeper-water drilling. Nat Hazards 57:121–132

Chopra S, Huffman A (2006) Velocity determination for pore pressure prediction. Lead Edge 25:1502–1515

Dewangan P, Ramprasad T, Ramana MV, Mazumdar A, Desa M, Badasab F (2008) Shale tectonics in the continental slope and rise of Krishna-Godavari basin, Bay of Bengal: implication in gas-hydrate exploration. In: AGU fall meeting 2008, Abstract #0S33A-1313, American Geophysical Union

Dutta NC (2002) Geopressure prediction using seismic data: current status and the road ahead. Geophysics 67:2012–2041

Eaton BA (1972) Graphical method predicts geopressures worldwide. World Oil 182:100–104

Engelder T, Fischer MP (1994) Influence of poroelastic behavior on the magnitude of minimum horizontal stress, S_h, in overpressured parts of sedimentary basins. Geology 22:949–952

Fertl WH (1976) Abnormal formation pressure, implication to exploration, drilling, and production of oil and gas reservoirs. Elsevier, Amsterdam, p 382

Fleming M, Flin R, Mearns K, Gordon R (1998) Offshore workers' perceptions of risk comparisons with quantitative data. Risk Anal 18:103–110

Gholami R, Moradzadeh A, Rasouli V, Hanachi J (2014) Practical application of failure criteria in determining safe mud weight windows in drilling operations. J Rock Mech Geotech Eng 6:13–25

Gupta SK (2006) Basin architecture and petroleum system of Krishna Godavari basin, east coast of India. Lead Edge 25:830–837

Hao F, Li S, Gong Z, Yang J (2002) Mechanism of diapirism and episodic fluid injections in the Yinggehai Basin. Sci China Ser D Earth Sci 45:151–159

Hillis R (2000) Pore pressure/stress coupling and its implications for seismicity. Explor Geophys 31:448–454

Hurst A, Scott A, Vigorito M (2011) Physical characteristics of sand injectites. Earth Sci Rev 106:215–246

Li W, Xie J, Gao XH, Zhang LH, Yu F (2008) Characteristics of Jurassic mudstone overpressure and its control on oil and gas accumulation in Turpan depression. Pet Explor Dev 35:28–33 (in Chinese with English abstract)

Matthews WR, Kelly J (1967) How to predict formation pressure and fracture gradient. Oil Gas J 65:92–106

Miller TW (1995) New insights on natural hydraulic fractures induced by abnormally high pressure. Am Assoc Pet Geol Bull 79(7):1005–1018

Osborne MJ, Swarbrick RE (1997) Mechanisms for generating overpressure in sedimentary basins: a reevaluation. AAPG Bull 81:1023–1041

Plumb RA, Evans KF, Engelder T (1991) Geophysical log responses and their correlation with bed-to-bed stress contrasts in Paleozoic rocks, Appalachian plateau, New York. J Geophys Res 96:14509–14528

Radhakrishna M, Twinkle D, Nayak S, Bastia R, Rao SG (2012) Crustal structure and rift architecture across the Krishna Godavari basin in the central eastern continental margin of India based on analysis of gravity and seismic data. Mar Pet Geol 37:129–146

Rao GN, Mani KS (1993) A study on generation of abnormal pressures in Krishna-Godavari basin, India. Indian J Pet Geol 2:20–30

Rao KN, Subraelu P, Nagakumar KCV, Demudu G, Hema Malini B, Rajawat AS, Ajai (2013) Geomorphological implications of the basement structure in the Krishna-Godavari deltas, India. Zeitschrift für Geomorphologie 57(1):25–44

Sarker R, Batzle M (2008) Effective stress coefficient in shales and its applicability to Eaton's equation. Lead Edge 27:798–804

Sayers CM, Johnson GM, Denyer G (2002) Predrill pore-pressure prediction using seismic data. Geophysics 67:1286–1292

Schultheiss P, Holland M, Humphrey G (2009) Wireline coring and analysis under pressure: recent use and future development of the HYACINTH system. Sci Drill 7:44–50. doi:10.2204/iodp. sd.7.0.7.2009

Shanmugam G, Srivastava SK, Das B (2009) Sandy debrites and tidalites of Pliocene reservoir sands in upper-slope canyon environments, offshore Krishna-Godavari Basin (India): implications. J Sedi Res 79(9):736–756

Shi W, Xie Y, Wang Z, Li X, Tong C (2013) Characteristics of overpressure distribution and its implication for hydrocarbon exploration in the Qiongdongnan basin. J Asian Earth Sci 66:150–165

Singh J, Ojha A, Kumar N, Palange SN, Indhankar JN, Rana LB (2014) Successful drilling of india's deepest deepwater exploratory well using advanced while-drilling measurements, abstract. In: 11th middle east geosciences conference and exhibition, March 10–12, Manama, Bahrain

Singha DK, Chatterjee R (2014) Detection of overpressure zones and a statistical model for pore pressure estimation from well logs in the Krishna-Godavari basin, India. Geochem Geophys Geosyst 15(4):1009–1020

Sinha B, Bratton T, Cryer J, Nieting S, Ugueto G, Bakulin A, Hauser M (2008) Estimation of near-wellbore alteration and formation stress parameters from borehole sonic data. SPE Reservoir Eval Eng 11:478–486

Swarbrick RE (2002) Challenges of porosity-based pore pressure prediction. CSEG Recorder, Canada, pp 74–77

Tan CP, Willoughby DR (1993) Critical mud weight and risk contour plots for designing inclined wells. In: 68th annual technical conference and exhibition of the society of petroleum engineers held in Houston, Texas, 3–6 October

Tang J, Lerche L (1993) Geopressure evolution, hydrocarbon generation and migration in the Beaufort-Mackenzie basin, Canada: results from two dimensional quantitative modeling. Mar Pet Geol 10:373–393

Tingay MRP, Hillis RR, Swarbrick RE, Morley CK, Damit AR (2009) Origin of overpressure and pore-pressure prediction in the Baram province, Brunei. AAPG Bull 93:51–74

Van Ruth PJ, Hillis RR, Swarbrick RE (2002) Detecting overpressure using porosity-based techniques in the Carnarvon basin, Australia. APPEA J 42: 559–569

Wang H, Soliman MY, Towler BF, Mukai D (2008) Avoiding drilling problems by strengthening the drillbore while drilling. In: 42nd US rock mechanics symposium and 2nd U.S.-Canada rock mechanics symposium, held in San Francisco, June 29–July 2, Paper no ARMA 08-200

Yamamoto K (2003) Implementation of the extended leak-off test in deep wells in Japan. In: Sugawra K (ed) Proceedings of the 3rd international symposium on rockstress. A.A. Balkema, Rotterdam, pp 225–229

Zhang J (2011) Pore pressure prediction from well logs: methods, modifications, and new approaches. Earth Sci Rev 108:50–63

Zoback MD, Barton CA, Brudy M, Castillo DA, Finkbeiner T, Grollimund BR, Moos DB, Peska P, Ward CD, Wiprut DJ (2003) Determination of stress orientation and magnitude in deep wells. Int J Rock Mech Min Sci 40(7/8):1049–1076

Estimation of In-situ Stress and Coal Bed Methane Potential of Coal Seams from Analysis of Well Logs, Ground Mapping and Laboratory Data in Central Part of Jharia Coalfield—An Overview

Prabir Kumar Pal, Suman Paul and Rima Chatterjee

Abstract Well log data of thirty (30) boreholes from central part of Jharia coalfield have been analysed for estimation of petrophysical and rock mechanical properties of coal seams to facilitate assessment of Coal Bed Methane (CBM) reservoir potentiality of those coal seam. Wells from Jharia area showed 18 major correlatable seams, intersected between 214 and 1324 m depth. The resistivity, density and natural gamma ray log data from the wells of the study area have been utilized for:

(a) Estimation of permeability of coal seams from resistivity log data;
(b) Computation of in-situ stress magnitudes—vertical stress, effective vertical stress and effective horizontal stress at seam horizons;
(c) Establish relationship between in-situ stress and permeability;
(d) Estimation of gas content of coal seams and identification of most potential zones for CBM exploration.

It is observed that the permeability values ranging from 0.82 to 1.12 md with average gas content of 11.50 to 11.75 cc/gm. By comparing gas content, coal seam thickness as well as coal bed permeability of these major coal seams, the most viable CBM potential zone is mapped for this area.

Keywords CBM potential · Jharia coalfield · In-situ stress · Well log application

P.K. Pal
Integrated Coal Mining Limited, Kolkata, India

S. Paul
Department of Petroleum Engineering, Al Habeeb College of Engineering & Technology, Hyderabad 501 503, India

R. Chatterjee (✉)
Department of Applied Geophysics, Indian School of Mines, Dhanbad 826004, India
e-mail: rima_c_99@yahoo.com

143

1 Introduction

At present, methane is produced from coal beds in a number of sedimentary basins in Canada and USA, whereas in some other countries like China, Australia and India. Coal Bed Methane (CBM) is one of the exploration targets of the upstream petroleum sectors. Methane from coal represents a promising energy resource that has significant long-term prospective for discovery and development. On a global scale, the CBM potential of most major coal-bearing regions has been estimated to be 89–269 trillion m^3 of gas in-place (Charles and Bai 1998). India having the fourth largest proven coal reserves and also being the third largest coal producer in the world, holds noteworthy prospects for profitable recovery of CBM. Coalfields of India are mainly divided into two groups namely; Gondwana (Permo-Carboniferous) and Tertiary coalfields. More than 98 % of the coal outputs of India are from Gondwana coalfields. These coalfields are distributed mainly in the river valleys of Damodar (West Bengal–Jharkhand), Pranhita Godavari (Maharasthra–Andhra Pradesh), Mahanadi (Orissa), Narmada (Madhya Pradesh) and Son (Madhya Pradesh). Geographical distribution of the major coal basins of India is shown in Fig. 1.

The performance of CBM reservoirs is extensively controlled by the density and aperture of natural fractures, particularly cleats in coalbeds and joints and in intervening shale and sandstone units (Pashin 1998; Pashin and Groshong 1998; Pitman et al. 2003). The development of joints and cleats in the coal bearing Formation is the product of regional tectonic stresses as well as internal stresses, generated by devolatilization of coal during thermal maturation (Close 1993; Law 1993; Laubach et al. 1998). It is, therefore, apparent that the geomechanical properties and permeability parameters need to be assessed for evaluating the economic potential of natural gas from coal seams of Jharia coalfield and the successful commercial production and exploration sites will be decided by those factors only.

Recent studies by different workers had indicated that India has an estimated resource base of virgin CBM (outside the mining areas) to the tune of 1.0–1.5 TCM (Hazra et al. 2003). The Jharia coalfield is the most important coalfield in India because in India this coalfield is now the sole repository of prime coking coals, i.e. coals which, with or without beneficiation, would on carbonization at high temperature, produce coke for metallurgical purposes. Hence, this coalfield has been extensively explored and exploited. This coalfield is still the leading contributor to India's coal production. Exploration for coal bed methane in Jharia Coalfield (JCF) has been going on for more than one decade.

Characterization and identification of coal seams in deep (more than 300 m) wells are generally considered as useful to evaluate CBM gas potential. The high methane reservoir potential of coal seams is due to the sub-optimum packing of its organic structure during coalification process. The density of pure carbon is approximately 2.23 gm/cc, whereas anthracite has around 1.35 gm/cc and bituminous coal 1.29 gm/cc (Li et al. 2003). This density contrast is almost completely

Fig. 1 Schematic diagram showing the locations of Gondwana coalfields and tertiary coal/lignitefields, India
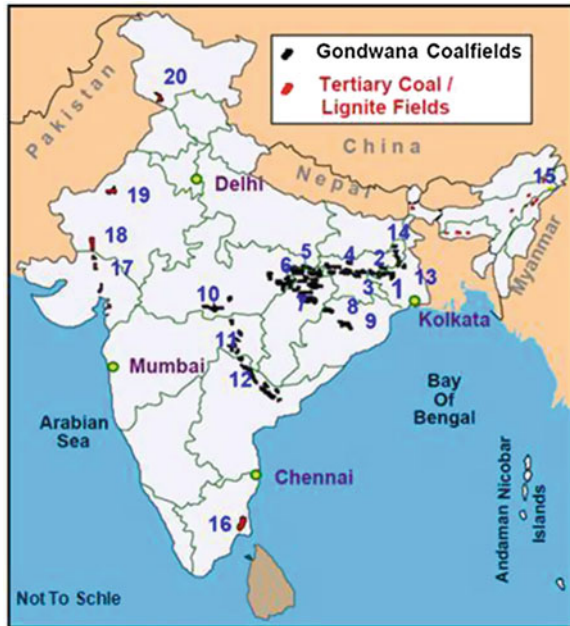
GONDWANA COALFIELDS			
1.	Raniganj	2.	Jharia
3.	Bokaro	4.	North Karanpura
5.	Singrauli	6.	Sohagpur
7.	Korba	8.	Ib-valley
9.	Talchir	10.	Satpura
11.	Wardha	12.	Godavari
13.	Birbhum	14.	Rajmahal
TERTIARY COAL / LIGNITE FIELDS			
15.	Assam-Mehgalaya	16.	Neyveli
17.	Cambay	18.	Barmer-Sanchor
19.	Bikaner	20.	Jammu and Kashmir

due to the micro-porosity created by the packing structure of the organic coal compounds. Harpalani and Schraufnagel (1990) reported that free methane, stored in the coal cleat network/fractures and joints, accounts for less than 10 % of the total gas enclosed in the coal and remaining 90 % plus of methane is physically adsorbed onto the surface of the pores of the coal.

It is claimed by the previous authors (Bell and Bachu 2003) that the worldwide resources of methane trapped within the porous coal system are greater than the total resources of all known conventional gas field. The commercial successes of CBM in the USA, Canada, Australia and China have also led to geophysical prospecting of the coal seams both in the mining and natural gas industry. In Indian scenario, the Gondwana coal seams of Damodar Valley are the prime targets for

CBM exploitation. Application of seismic survey for CBM prospecting to predict CBM content, estimation of mine pressure and other related aspects have been very limited in Indian mining industry. Therefore, the use of well logs in Jharia coalfield for estimation of the rock mechanical and petrophysical properties of coals and for in-situ stress analysis is a significant step to assess CBM potential of the coal seams and to identify high potential zones for CBM exploration and exploitation. Owing to the increasing importance of CBM production from gas reservoirs for coalbed methane extraction from target area like Jharia coalfield, the knowledge of coal bed permeability, in-situ stress magnitude, fracture orientation are essential for planning exploration and development because of their influence on recovery of methane, and the local and regional flow of methane gas and water within coal reservoirs.

To assess the potential of CBM reservoir, coal or non-coal core samples and well logs like density, gamma ray, and resistivity from wells have been used for quantitative estimation of petrophysical and rock mechanical parameters. In India, very few studies have been carried out to establish correlation of stress and permeability in CBM basins. In view of above, a fresh attempt has been made to develop a new methodology to decipher the in-situ stress direction acting at major coal seams from the available multiparametric well log data.

2 Study Area

The Jharia coalfield is situated in the eastern part of India, i.e. in Dhanbad district, Jharkhand and is located about 260 km northwest of Kolkata, West Bengal in the heart of Damodar Valley. The longer axis of this roughly sickle shaped coalfield is running northwest-southeast (Fig. 2). The Jharia coal basin located at the Singhbhum craton extends for about 38 km in an east-west direction and a maximum of 18 km in north-south direction covering an area of about 456 km^2. Its regional strike is ENE to WSW in the western part which slowly swings to E-W in the middle and then to almost N-S towards eastern part of the coalfield. The dip of the Formation in general is southerly (10°). The general stratigraphic succession of Jharia coalfield is given in Table 1 (after Chandra 1992). Coal seams of Jharia coal basin occur in Barakar (Lower Permian) and Raniganj (Upper Permian) Formations within Lower Gondwana sequence (Chatterjee et al. 1990). The most important Barakar Formation (Lower Permian) of Jharia coalfield containing coal seams, consisting of fluviatile deposits as the lowermost member. The basement rocks mainly metamorphics are overlain by the Talchir Formation followed by the Barakar Formation which is the major coal-bearing horizon. The Barren Measures is overlying the Barakar formation followed by the coal bearing Raniganj Formation. The coal seams of the present study belong to Barakar Formation which does not show any evidence of high intensity tectonic deformation except normal gravity faults of different magnitudes—both minor (thrown less than 10 m) and major (thrown 10 m to greater than 100 m) (Ghosh and Mukhopadhyay 1985; Sengupta 1980). Out of total 30 major coal seams 18 are under Barakar Formation
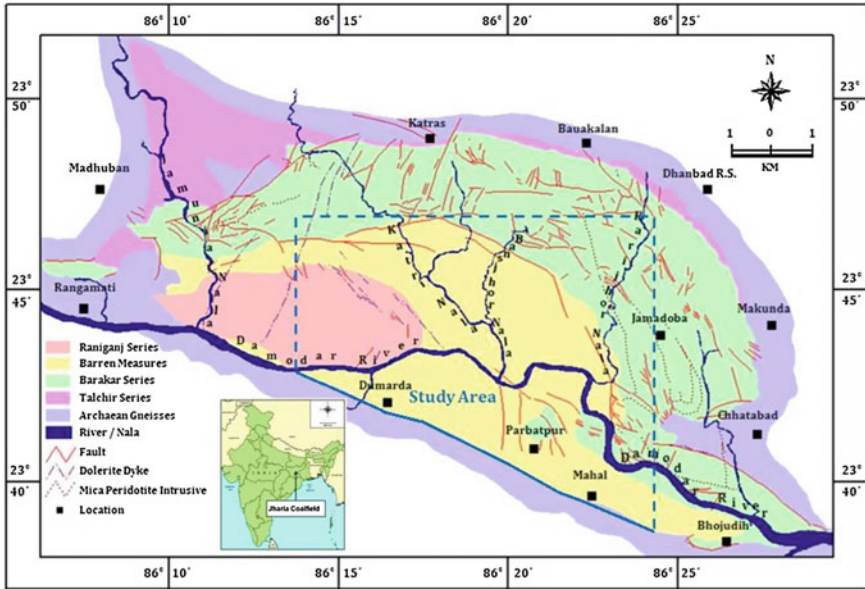
Fig. 2 Structural and stratigraphic map of Jharia coalfield, India (after Sengupta 1980) showing present study area

and the remaining 12 are under Raniganj Formation (Chandra 1992). It is important to note that Jharia coalfield is the only coalfield of India where source coal seams are of prime coking rank. The Barakar Formation consists of coal seams, conglomerates, shales, carbonaceous shales, coarse grained sandstones and siltstones. Data concerning organic petrology and thermal maturity of Barakar and Raniganj Formations are of considerable importance in determining the CBM potential in the Jharia coal basin. The vitrinite macerals are foremost in the shallower coals of Barakar Formation (Lower Permian) and range from 40 to 80 %, whereas exinite content vary in the range of 1–4 % and vitrinite reflectance value ranges from 0.83 to 1.69 % in Barakar coal seams of Jharia (Hazra et al. 2003). The volatile matters on dry ash free basis indicate that the Barakar coals of Jharia are high volatile bituminous to low volatile bituminous in rank (Rudra and Hazra 2009). It has been observed that generally ash content increases with consequent decrease in vitrinite content and increase in inertinite content for the Barakar coals of Jharia Coalfields. The inertinite content for deeper coals in Jharia is varying from 35 to 80 % and vitrinite content range from 20 to 62 % (Hazra et al. 2003).

The present study area, consisting of Singra, Kapuria, Barki, Dumarda, Parbatpur and Moonidih (Extension)/Jarma blocks covering an area of about 38 km^2 is located in the south-central part of Jharia coalfield (Fig. 2). Available well logs, litho-logs and core samples of total 30 exploratory wells have been considered for present study. Figure 3 displays locations of 30 exploratory wells in the study area.

Table 1 Generalized stratigraphic sequence of Jharia coalfield, India

Age	Group	Formation	Litho-type	Max. thickness (m)
Recent and sub-recent		Weathered	Alluvium, sandy soil, clay, gravel etc.	30
Unconformity				
Jurassic		Deccan trap and other igneous activity (intrusives)	Dolerite dykes, mica lamprophyre dyke and sills	
Unconformity				
Upper Permian	D A M U D A	Raniganj	Fine grained feldspathic sandstones, shales with coal seam	800
Middle Permian		Barren measure	Buff colored sandstone, shales and carbonaceous shales	730
Lower Permian		Barakar	Buff colored coarse to medium grained feldspathic sandstones, grits, shales, carbonaceous shales and coal seam	+1250
Upper Carboniferous		Talchir	Greenish shale and fine grained sandstones	245
Unconformity				
Archaean			Metamorphics	

After Chandra (1992)

The 30 wells, namely, S1, S2, S4, S5, S7, S8, S10, S13, S14, K1, K4, K5, K8, K10, K11, K12, K14, K16, K17, K19, J1, J2, J3, J4, J6, J7, J8, M1, M2 and M3 (Fig. 3) have been considered for estimation of stress magnitude and permeability from well log data. Physical properties of coal like permeability and porosity have generally been determined from limited sample volumes such as plugs or cores. There is no published data available on the physical properties of the coal seams in and around the study area. Therefore a methodology has been proposed for estimation of permeability of the coal seams with macro-cleat system from the well log-derived porosity and from known cleat spacing of the coal seams around the study area. Well log data, coal core samples and geological litho-logs of these boreholes recorded occurrence of 18 major/consistent coal seams, namely, seam A, B, C, D, E, F, G, H, I, J, K, L, M, N, O, P, Q and R of Barakar Formation at different depths varying between 214.58 m (in seam R for well K4) and 1354.24 m (in seam J for well J4) in the study area.

It is necessary to correlate the major seams encountered in the wells to evaluate seamwise properties from 30 wells, distributed over the study area (Fig. 3). A schematic regional cross-section along the section K8-S8 (Chatterjee and Paul 2013) traversing the seven wells; K8, K10, K1, J3, J4, S5 and S8 (Fig. 4) show the correlation of the major seams considering both geophysical logs and geological
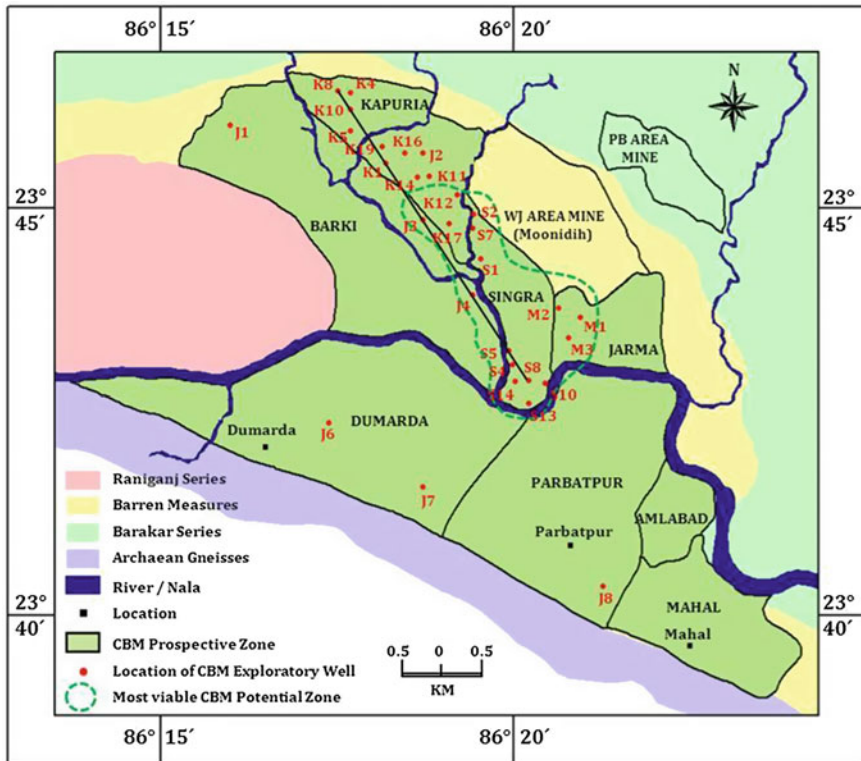
Fig. 3 Showing locations of 30 numbers of wells are distributed in Singra, Kapuria, Jarma, Parbatpur, Dumarda and Barki areas and also locations of WJ area and PB area underground coal mines of Jharia coalfield

litholog data. This cross section across the study area reveals the structural lay out of the seams in the study area. The structure of whole Jharia coal basin had been reported by previous workers like Sengupta (1980) and Chandra (1992).

3 Proximate Analysis of Coal in Laboratory

About 141 coal core samples were collected from the 10 wells, such as: wells S4, S5, S9, S15, S21 from Singra block and wells K9, K10, K16, K19 and K24 from Kapuria block of the Jharia coalfield (Fig. 3). Coal samples were collected following the Indian Standard procedure (IS 436 (Part 1/Section 1) 1991). Proximate analysis based on the Indian Standard procedures (IS 1350 (Part 1) 2003) was carried out in the Fuel and Mineral Engineering (FME) Laboratory of Indian School of Mines, Dhanbad. Table 2 provides the seam-wise proximate analysis results from
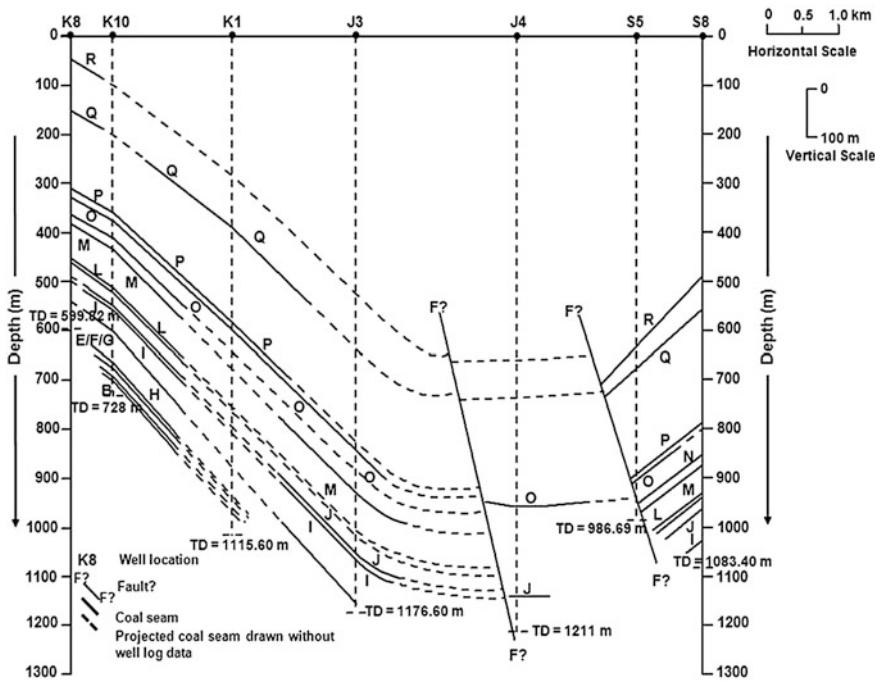
Fig. 4 Displaying schematic regional cross-section along section line K8-S8 (refer Fig. 3) in the Jharia coalfield, India (Chatterjee and Paul 2013). *TD* indicates total depth of well

Table 2 Seam-wise proximate analysis results for 10 wells of Jharia coalfield, India

Seam name	Proximate analysis results (weight %)			
	Moisture (%)	Ash (%)	Volatile matter (%)	Fixed carbon (%)
R	1.05–1.21	17.86–26.38	19.50–24.84	50.41–55.09
Q	1.03–1.13	22.31–27.39	18.92–24.43	50.51–54.40
P	0.80–1.18	17.45–29.73	17.48–23.52	50.77–58.91
O	0.78–1.15	20.83–30.26	17.27–23.28	49.52–54.82
N	0.75–1.13	21.31–30.87	17.15–22.67	49.96–54.95
M	0.82–1.09	18.52–31.35	16.38–22.30	50.01–58.31
L	0.72–1.01	21.70–33.75	15.89–21.42	49.48–55.93
K	0.75–0.98	24.85–30.90	15.45–20.91	50.42–54.10
J	0.84–0.94	19.20–26.63	18.55–20.34	53.30–59.56
I	0.79–0.90	24.85–30.82	18.39–20.13	53.24–59.76
H	0.81–0.86	25.43–26.63	18.38–19.78	53.45–54.62
E/F/G	0.72–0.93	25.71–27.85	17.87–18.74	52.52–54.73
D	0.68–0.89	25.79–29.92	17.18–18.69	52.02–54.73
C	0.70–0.87	26.68–31.72	16.77–17.61	50.65–53.84
B	0.85	27.83	17.28	54.04

laboratory experiments. It can be inferred from proximate analysis that the moisture and volatile matter contents of coals gradually decreases with the increase of depth. The volatile matter content on dry ash free basis estimated by Rudra and Hazra (2009) indicates that the Barakar coals of Jharia coal basin are high volatile 'A' bituminous to low volatile bituminous in rank.

4 Petrographic Analysis of Coal in Laboratory

Coal petrographic analysis for 16 samples from 5 wells, namely, S15, K10, K16, K19, and K24 were carried out at the Central Institute for Mining and Fuel Research, Dhanbad following the Indian Standards (IS 9127 (Part 2) 2002; IS 9127 (Part 3) 2002; IS 9127 (Part 5) 2004). The seam-wise petrographic analysis results are presented in Table 3.

Figure 5 displays the cross-plot between vitrinite reflectance (VRo%) and depth of coal seams. On the basis of the available data, it is found that for the same coal seam VRo% values increases with increasing depth (as in seams I and M) and the VRo% values of coals in same well increases from younger to older coal seams (as in Wells S15, K10, K19 and K24).

Barakar coal seams are generally characterized by high vitrinite content although some coal seams are rich in inertinite content (Navale and Saxena 1989). For coal seam to hold and produce economic quantity of methane it should have vitrinite more than 45 % and VRo% should be more than 0.80 % along with low percentage of mineral matter and moisture (Kumar et al. 2010). From the present petrographic study and from the published data it is observed that vitrinite macerals are the major constituent of the coal of Jharia coal basin (Chatterjee et al. 1990; Mishra et al. 1990; Mishra and Cook 1992).

5 Estimation and Analysis of In-situ Stress

The magnitude of vertical stress/overburden load (S_v) at any depth is produced by the pressure exerted by the rocks above that particular point. The stresses (S_v) are computed by integrating density log values for wells where the hydrostatic pressure gradient with mud density 1.1 gm/cc is considered standard in the studied wells, drilled in both onshore and offshore areas. The pore pressure is assumed equal to the hydrostatic pressure at any particular depth during the estimation of effective stress. In this tectonically relaxed basin (Ghosh and Mukhopadhyay 1985), the effective minimum horizontal stress (S_h) has been estimated using the equation (Chatterjee and Pal 2010) provided below. From the present study it is possible to know the vertical stress magnitude at the roof of the individual coal seams.

Table 3 Laboratory derived coal petrography analysis results for 5 wells of Jharia coalfield, India

Seam name	Well name	Coal core recovery depth interval (m)	Petrographic analysis results (volume % as received basis)					Mean VRo (%)
			Vitrinite (%)	Semi-vitrinite (%)	Liptinite (%)	Inertinite (%)	Mineral matter (%)	
R	S15	512.05–512.20	60.20	3.40	1.80	25.40	9.20	1.27
Q	K19	477.45–477.55	65.50	2.90	1.80	25.10	4.70	1.21
P	S15	834.57–834.76	50.50	2.30	1.10	37.60	8.50	1.56
O	K16	729.65–729.55	52.30	2.70	0.00	39.70	5.30	1.46
O	K19	696.04–696.14	63.40	2.60	0.90	29.60	3.50	1.41
N	S15	964.25–964.35	44.40	1.23	1.00	40.60	12.77	1.75
M	K10	624.80–624.95	61.60	2.40	1.20	29.80	5.00	1.40
M	K24	663.25–663.65	58.80	6.40	1.90	24.40	8.50	1.41
L	K24	737.75–737.85	60.70	1.90	0.30	30.70	6.40	1.48
K	K10	712.65–712.75	58.90	2.10	0.80	33.80	4.40	1.48
J	K24	790.30–790.40	46.30	5.60	0.40	39.50	8.20	1.49
I	K10	747.45–747.55	57.50	1.90	0.60	35.80	4.20	1.51
I	K16	886.75–886.85	46.30	2.10	0.30	48.20	3.10	1.61
H	K24	822.95–823.10	42.10	5.10	0.20	45.40	7.20	1.54
C	K16	1074.55–1074.70	44.60	1.10	0.20	51.80	2.30	1.67
B	K10	895.85–896.00	16.10	1.10	0.00	69.70	13.10	1.71

VRo vitrinite reflectance

Fig. 5 Illustrates the plot of vitrinite reflectance versus depth

Vitrinite Reflectance (%)

y = 1006.x - 745.2
R² = 0.90
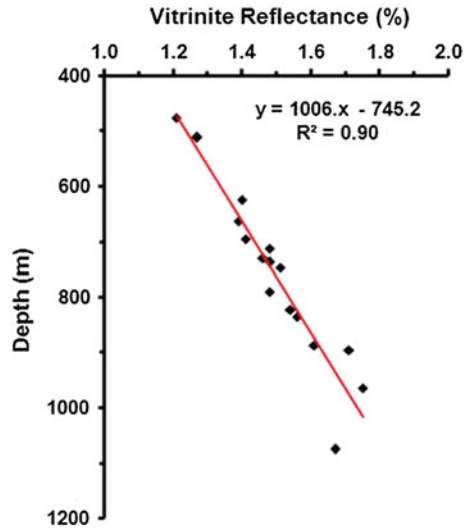
$$S_h = \gamma(S_v - P)/(1 - \gamma) \tag{1}$$

where 'P' is the pore pressure equivalent to hydrostatic pressure and 'γ' is the Poisson's ratio of coal (0.32). It is known that Poisson Ratio for coal has variation with degree of cleating and it responds to stress field. From log data acquired in some wells penetrating Lower Gondwana coals in Jharia, Poisson'sratio is computed generally varying in the range of 0.33–0.44 as a dynamic modulus for full observed range of degree of cleating. The value of 0.32 has been taken from laboratory studies. Owing to lack of fast shear and slow shear data, stress ratio determination is not possible.

Well logs of 30 wells from Jharia coalfield have been considered to determine the magnitudes of in-situ stresses of 16 major coal seams (considered seams E, F and G as a single E/F/G combined seam) of study area (Chatterjee and Paul 2013). Due to thin partings between seam E and F and seams F and G, these seams are considered as a single seam E/F/G during in-situ stress estimation. The magnitudes of S_v, effective vertical stress and effective horizontal stress are estimated and plotted against depth for the study area (Fig. 6).

A decrease in stress gradient is observed inside the coal seams (Fig. 7). The variation in stress gradient is dependent on density of rocks. It is also observed in few wells that the variations in stress gradients are also due the presence of high-density igneous intrusive rocks. The overall trend of the vertical stress increases linearly with depth with a slope of about 45°. This pattern is similar to that in the other coalfields of India and foreign coal basins (Mucho and Mark 1994; Townend and Zoback 2000). The estimated vertical stress, effective vertical stress and effective horizontal stress magnitudes are provided in Table 4 and vary between 5.31–32.71 MPa, 3.51–19.75 MPa and 1.35–9.29 MPa respectively within

Showing magnitudes of vertical stress, effective vertical stress and effective horizontal stress against depth for 30 wells in Jharia coalfield
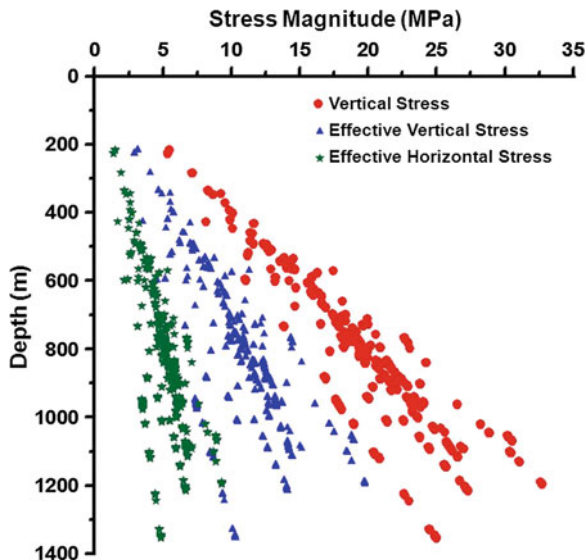
214.58–1345.04 m depth in the study area. The large variation of stress magnitude as observed, may be due to the high density igneous intrusive occurring close to the coal beds.

The variation in vertical stress magnitude values are also observed in each seam. The vertical stress magnitude contour maps are prepared for seams O, P, Q and R (Fig. 8). Four numbers of coal seams were selected for contour plotting, since
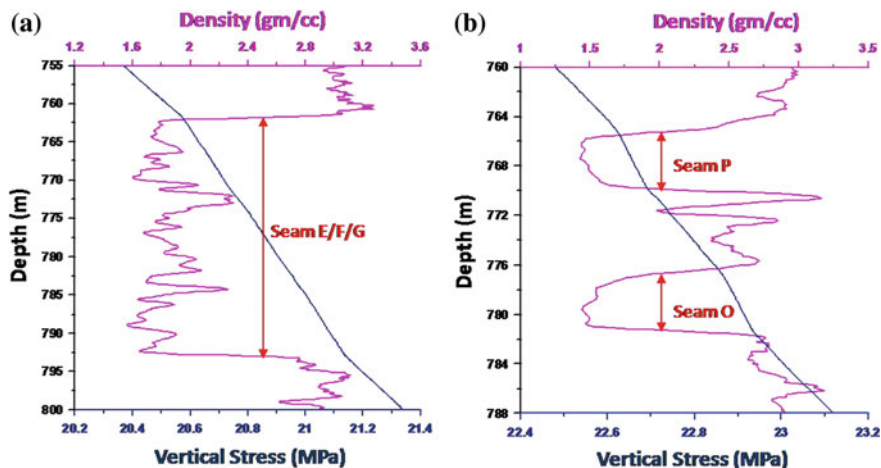

Fig. 7 Relationship between depth and vertical stress for **a** seam E/F/G in well K4 and **b** seam O and seam P in well K1

Table 4 The values of vertical stress, effective vertical stress, effective horizontal stress, coal bed permeability and gas content of study areas from Jharia coalfield, India

Coalfield name	Seam name	Depth* (m)		VS (MPa)		EVS (MPa)		EHS (MPa)		CBP (md)			GC (cc/gm)	
		Min	Max	Min	Max	Min	Max	Min	Max	Min	Max	Avg	Min	Max
Jharia	A	1214.52	1215.72	27.27	27.29	14.11	14.13	6.64	6.66	NE	NE	NE	NE	NE
Jharia	B	842.28	1210.12	20.80	27.17	11.67	14.05	5.49	6.61	NE	NE	NE	11.20	11.51
Jharia	C	831.18	1185.22	20.53	26.65	11.52	13.83	5.42	6.51	0.67	0.71	0.69	11.12	11.59
Jharia	D	802.28	1137.17	19.84	26.54	11.15	14.44	5.25	6.80	0.69	0.75	0.72	11.21	11.52
Jharia	E/F/G	762.08	1327.05	17.60	26.15	7.35	14.24	3.46	6.70	0.70	0.98	0.84	11.11	11.71
Jharia	H	720.58	788.07	17.98	24.84	10.07	13.62	4.74	6.41	0.76	0.80	0.78	11.23	11.69
Jharia	I	674.88	1244.05	16.85	32.71	9.47	19.75	4.46	9.29	0.60	0.85	0.73	11.21	11.89
Jharia	J	663.78	1345.04	16.60	31.05	9.33	18.80	4.39	8.85	0.64	0.97	0.81	11.12	11.91
Jharia	K	639.88	1102.86	15.98	30.43	9.04	18.46	4.26	8.69	0.69	0.88	0.79	11.23	11.72
Jharia	L	631.48	1098.46	15.80	30.38	8.96	18.44	4.22	8.68	0.74	0.92	0.83	11.21	11.61
Jharia	M	561.28	1100.95	14.00	28.85	7.92	17.52	3.73	8.24	0.76	1.05	0.91	11.17	11.72
Jharia	N	540.92	1019.46	13.54	28.23	7.66	17.16	3.61	8.08	0.77	0.98	0.88	11.28	11.86
Jharia	O	426.54	1117.04	8.14	30.52	3.51	18.93	1.65	8.91	0.65	1.25	0.95	11.12	11.75
Jharia	P	490.08	1052.67	12.30	30.26	6.61	18.80	3.11	8.85	0.72	1.08	0.90	11.12	11.67
Jharia	Q	282.78	837.47	7.10	24.22	4.04	15.13	1.90	7.12	0.81	1.13	0.97	11.14	11.68
Jharia	R	214.58	796.07	5.31	23.05	8.87	14.42	1.35	6.78	0.91	1.24	1.08	11.27	11.90

*Depth** = depth of occurrence of coal seam; *VS* = vertical stress; *EVS* = effective vertical stress; *EHS* effective horizontal stress; *CBP* = coal bed permeability; *GC* = gas content; *Min* minimum; *Max* maximum; *Avg* average and *NE* not estimated due to non-availability of well log data
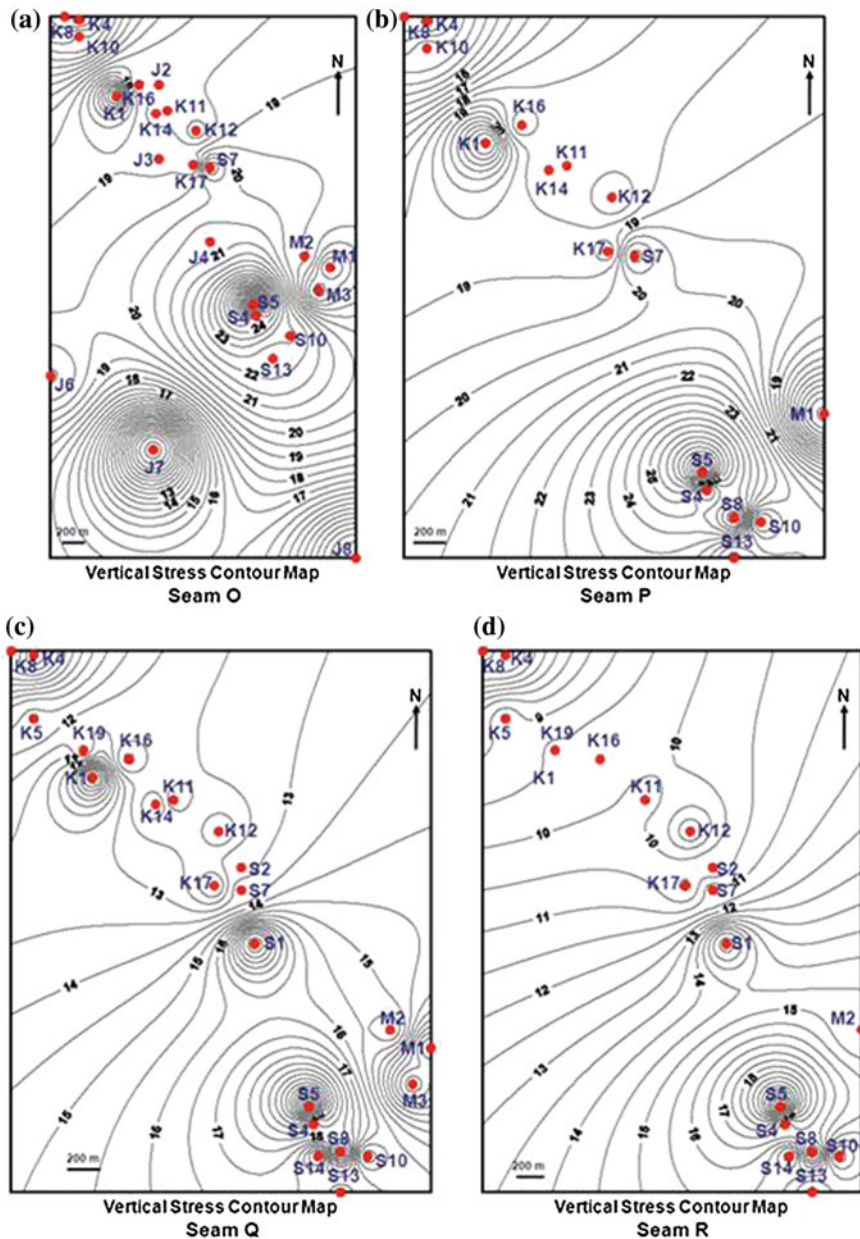
Fig. 8 Displaying vertical stress contour maps for **a** seam O, **b** seam P, **c** seam Q and **d** seam R. Vertical stress contour interval are considered as 0.5 MPa for all seams

majority of wells (sixteen to twenty three numbers of well) had penetrated these seams. The vertical stress magnitude for seam O increases from NNW to the centre part of the area and then decreases from the centre towards the SSE part of the area. This is due to the presence of greater sediment thickness as observed for the wells S4, S5, S10 and S13 located at the centre part of the basin. Vertical stress magnitude increases from NNW to SSE of the study area along the downdip direction and again increases from the central part of the basin along the updip direction. Stress magnitude for seams P, Q and R are increasing from NNW to SSE due to increase in sediment thickness and also due to the dipping coal beds in the same direction. Vertical stress magnitudes reach maximum at the central part of the study area where the wells like; S4, S5, S8, S10, S13 and S14 are located. Stress magnitude values decrease from the central part to the surrounding areas having lesser sediment thickness. The zones, marked by concentric high stress gradient, are generally separated by nala/river which are topographic manifestation of structural discontinuities like faults.

Cleats and fractures in coal of Barakar Formation in Jharia coalfield have already been mapped from coal outcrops from 21 opencast and 2 underground coal mines (Paul and Chatterjee 2011b). Face cleat orientation within same seams such as: B, C, D, E/F/G, H, I, J, K/L, N and O varies from NE–SW to NW–SE in different mining areas, distributed from NW to SE of the basin (Paul and Chatterjee 2011b). In-situ stress (S_H) orientation is parallel to the face cleat direction and has two prominent directions of N25°E and N25°W respectively. The S_H orientation is strongly related with the orientation of faults in this basin, between the major regional lineations, the face cleat and the joint direction (Paul and Chatterjee 2011b).

6 Estimation and Analysis of Coal Bed Permeability

Coal bed permeability (CBP) is almost due to cleat systems which are approximately orthogonal and are normal to the bedding plane. Cleat spacing ranges from millimeter to centimeter range. Coal permeability depends on the internal system of macroscopic (cleat) and microscopic (matrix), fractures, which are dependent on coal composition, coal rank, and timing of formation. Coal permeability depends not only on the volume of pores and fissures but also on the nature of their interconnections. Any factor, that influences the geometry of pores and fissures, influences the permeability.

Coal seams are normally characterized by high electrical resistivities (500–4000 Ω-m). It had been observed that the resistivity measured by shallow resistivity logging tool across the coal seam decreases substantially in wellbores filled with high salinity fluids compared to wells with low salinity fluids (Yang et al. 2006). This indicated that the borehole fluid had replaced pore fluid in the cleats

(invasion zone). The cleat volume/porosity of cleated coal is given by the previous authors (Chatterjee and Pal 2010) as,

$$\text{Cleat volume or Porosity}(\Phi) = 100 \times (0.65/\text{Resistivity})^{0.6} \qquad (2)$$

Using the matchstick model of cleating, initial porosity and initial permeability of coal in any coalfield area can be expressed as a function of cleat spacing and aperture (Harpalani and Chen 1995).

$$\text{Porosity}(\Phi) = 2b/s \quad \text{and} \quad \text{Permeability}(K) = b^3/12s \qquad (3)$$

where 'b' and 's' are the cleat aperture and cleat spacing respectively.

This is the simplest possible model for estimating permeability. The formula used is the direct extension of permeability from flow between parallel plates extended to sets of them. Cleat spacing of 2 mm have been based on laboratory observation. Due to absence of correlating hydraulic aperture and cleat aperture (rugosity of cleat surface) we have assumed the equality between hydraulic aperture and cleat aperture (Gu and Chalaturnyk 2010).Cementation Exponent of 1.6 [1/ 1.6 = 0.6 in Eq. (2)] in porosity estimation from resistivity log is based on laboratory based correlations between resistivity index and saturating fluid resistivity from core samples in other wells in the area.

Short normal resistivity logs of the 16 wells namely; S1, S2, S4, S5, S7, S8, K1, K4, K5, K8, K12, J1, J3, J4, J7 and J8 have been considered for computation of permeability of 14 major coal seams, namely, seams C, D, E/F/G, H, I, J, K, L, M, N, O, P, Q and R. Resistivity log data for seams A and B are not available. During the field survey, the spacing between the mega face cleats were measured and found to be around 2–3 mm at the underground mines of West Jharia (WJ) and Putkee Balihari (PB) areas (Paul and Chatterjee 2011a). Sahay (2009) had reported CBM gas emission from three wells, located in the extension area (Jarma block) of Moonidih. The coal bed permeability of the major seams, like K to R, in these three wells in the Moonidih area is reported less than 1 md (Sahay 2009). The interconnected cleated network has provided the coal bed permeability for fluid flow in the CBM reservoir for these wells under the study area. Therefore Eq. (3) has been used for computation of permeability from log derived cleat volume/porosity for the above mentioned 14 major coal seams of 16 wells with a cleat spacing of 2 mm. The estimated coal bed permeability is plotted against depth for the study area and it is observed that it decreases with increasing depth (Fig. 9).

The estimated coal bed permeability values of 16 wells in Jharia coalfield are predicted in Table 4. The average coal bed permeability of the study areas varies from 0.69 to 1.08 md in Jharia coalfield.

Fig. 9 Showing coal bed permeability against depth for 16 wells in Jharia coalfield
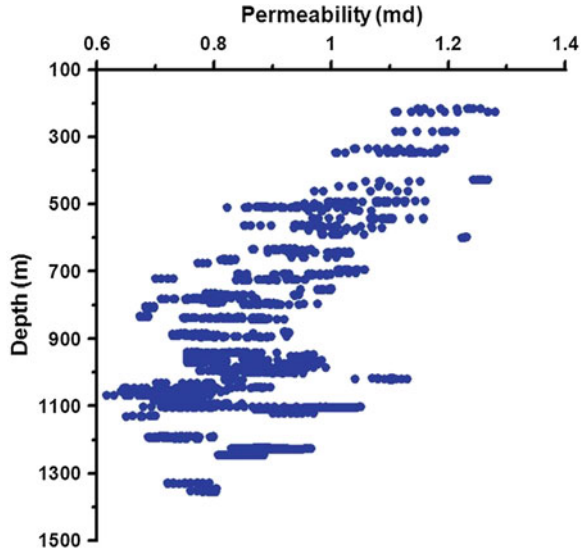
7 Relationship Between In-situ Stress and Coal Bed Permeability

The permeability of coal is affected by the strata stress, gas pressure and temperature of coal seam. The permeability change with respect to a reference state can be obtained from Eqs. (2) to (3) as proposed by several authors (e.g. Palmer and Mansoori 1998; Cui and Bustin 2005).

$$(K/K_0)^3 = (\Phi/\Phi_0)^3 \tag{4}$$

where the subscript 0 refers to the reference state and the matrix size change due to swelling/shrinkage and mechanical forces such as compression is considered as negligible compared to porosity change (Cui and Bustin 2005).

Cui and Bustin (2005) had defined the following stress-permeability relationship assuming constant pore compressibility and bulk compressibility ≪ pore compressibility as

$$K = K_0 \exp(-3C_p\sigma_e) \tag{5}$$

where C_p = pore compressibility and σ_e = vertical effective stress.

It is a simplification to assume pore compressibility as stress-independent, but is reasonable in absence of laboratory data when regressions between effective vertical stress and permeability are confined seam wise and when large variation in vertical stress is absent. The above approach does not take into account variation in cleat space morphology in stressed state with respect to that in unstressed state. The

stress affecting on tortuosity is also not considered due to non-availability of relevant data. The type of resistivity measurement is likely to reflect mega cleats effects predominantly and also will be sensitive to both vertical and horizontal resistivity. In the given the data set of Jharia coalfield the approach is reasonable and the regression provides the relationship between coal bed permeability with effective vertical stress.

In Jharia coalfield, the relation between coal bed permeability and effective vertical stress magnitude for each of 4 wells namely; S7, S8, K4 and K12 has been illustrated in Fig. 10. These 4 wells have been chosen for plotting because these wells penetrated the major coal seams. The depth intervals for penetrated coal seams of wells S7, S8, K4 and K12 are 515.58–1092.68 m, 657.06–1195.96 m, 214.58–846.38 m and 345.76–970.26 m respectively. The goodness of fit (R^2) for best fit exponential curve between permeability and effective vertical stress for these 4 wells varies between 0.72 and 0.79.

Next, the coal bed permeability for four major seams (E/F/G, I, J, K) out of 14 seams are plotted with the effective vertical stress to display the variation pattern of permeability with effective vertical stress within the same seam. These seams were encountered in minimum of 3 wells. The change in permeability within the same coal seams with effective vertical stress are shown in Fig. 11a–d for seams E/F/G, I, J and K. Permeability of each coal seam decreases exponentially with the in-situ effective vertical stress. The R^2 values for the best fit exponential curve between permeability and effective vertical stress vary between 0.72 and 0.95.

Since no study on relationship between coal bed permeability and in-situ stress of coal seams of Jharia coalfield is found in public domain/available publications, till date, an attempt has been made to establish the same from this study. The permeability of all major coal seams for all 16 wells has been considered to decipher the relationship between coal bed permeability and effective vertical stress. A total of 3110 numbers of permeability and effective vertical stress data have been plotted to establish the best fit regression relationships. The exponential relationship between permeability and effective vertical stress has a correlation coefficient (r) of −0.80 and R^2 of 0.71 indicates reasonably good fit of the regression equation for this part of Jharia coalfield (Fig. 12). The cross-plot of permeability versus effective vertical stress in Fig. 12 represents the best fit regression equation for the central part of Jharia coalfield as:

$$y = 71.37e^{-2.22x}, \quad r = -0.80 \quad \text{and} \quad R^2 = 0.71 \tag{6}$$

where, y = permeability and x = well log derived effective vertical stress values.

Average coal bed permeability contour maps have been prepared for four seams namely; O, P, Q and R as displayed in Fig. 13. The four seams are chosen for permeability contour plotting because minimum of eight to maximum of eleven wells had penetrated these seams. The contour plots indicate the lateral variation of coal bed permeability of four seams. Average permeability data for coal seams O, P, Q and R indicate the anisotropic behavior of coal bed permeability. Figure 13a reveals predominant direction of the increase in permeability is along NNW-SSE.
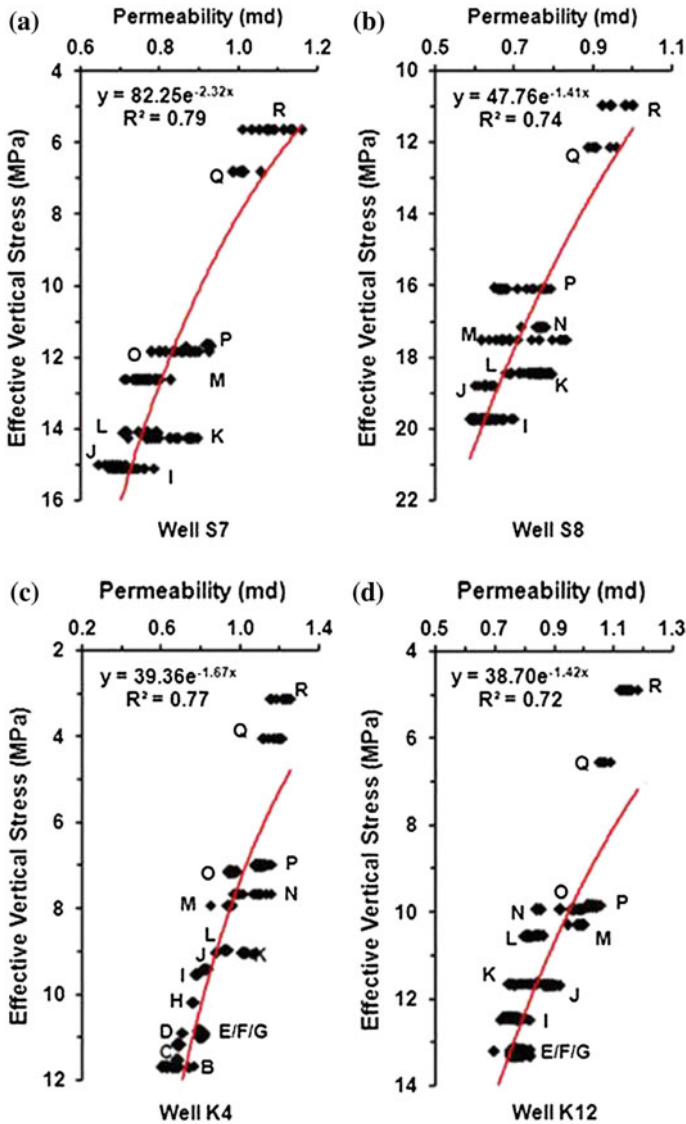
Fig. 10 Coal bed permeability versus effective vertical stress plots for **a** well S7, **b** well S8, **c** well K4 and **d** well K12. Name of the coal seams encountered are marked against respective wells

In case of seam O, a secondary direction of anisotropy was found along NE-SW direction (Fig. 13a). Average coal bed permeability for seam O increases towards updip direction from the central part of the area. The other Fig. 13b–d shows one dominant and another sub-dominant direction towards SSE-NNW and SSW-NNE direction respectively. The coal bed permeability depends on the cleat network
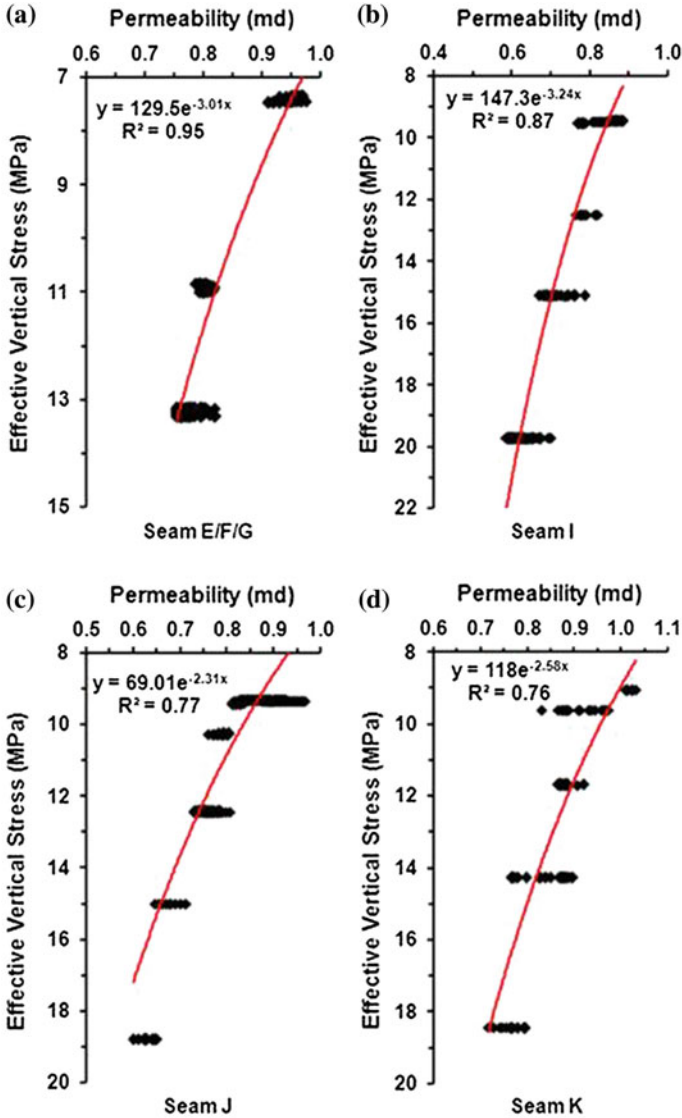
Fig. 11 Coal bed permeability versus effective vertical stress plots for **a** seam E/F/G, **b** seam I, **c** seam J and **d** seam K encountered in 16 wells distributed within Jharia coalfield

within these coal seams. In general fluid flow direction will follow the face cleat direction of the coal seams. Previously authors Paul and Chatterjee (2011a, b) had discussed the relation between cleat network and fluid flow directions at the Moonidih (WJ area mine) and Putkee-Balihari (PB area mine) underground mines and the adjoining areas of Jharia coalfield. The Moonidih and Putkee-Balihari underground mines are located very near to this study area (Fig. 3). The seam

Fig. 12 Coal bed permeability versus effective vertical stress plots considering all major coal seams encountered in 16 wells distributed within Jharia coalfield
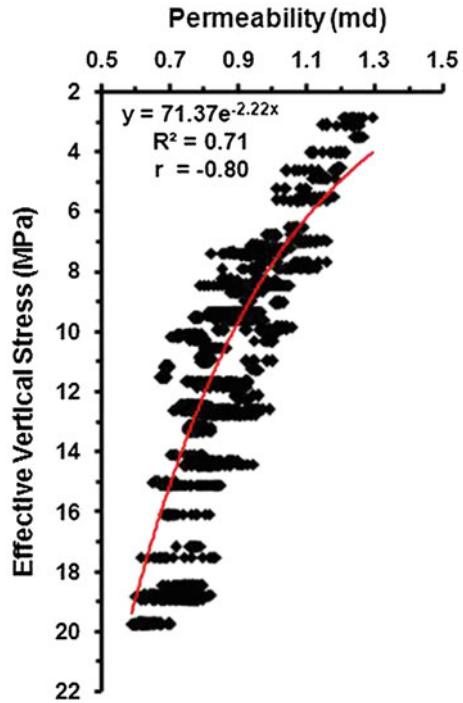
permeability is higher along face cleat orientation of the major seams under study. The previous authors had also observed that the resultant face cleat and butt cleat orientations at these mines are aligned towards N15°W and N75°E respectively. The lineament study based on satellite imagery in Jharia coalfield and the directional analysis of lineaments in Moonidih area had indicated the most dominant trend towards NNW–SSE and secondary trend towards ENE-WSW (Tiwari and Rai 1996; Verma et al. 1989). Ali et al. (2008) had also observed that the face cleat orientation from formation micro- imagery (FMI) log in Parbatpur area is directed towards NW-SE direction, varying between N30°W and N60°W (Paul and Chatterjee 2011a). The present observation from the permeability contour plots for four seams conforms well with the previous studies. The coal bed permeability of the study area shows prominent increasing trend along SE-NW with maximum fluid flow direction from SE to NW.

8 Estimation of Gas Content from Well Logs

Sorption of gas by coal is considered as an extremely important area of research to enhance successful gas recovery from coal seams and to assist the understanding of gas-related problems in underground coal mining (Crosdale et al. 1998). Sorption of

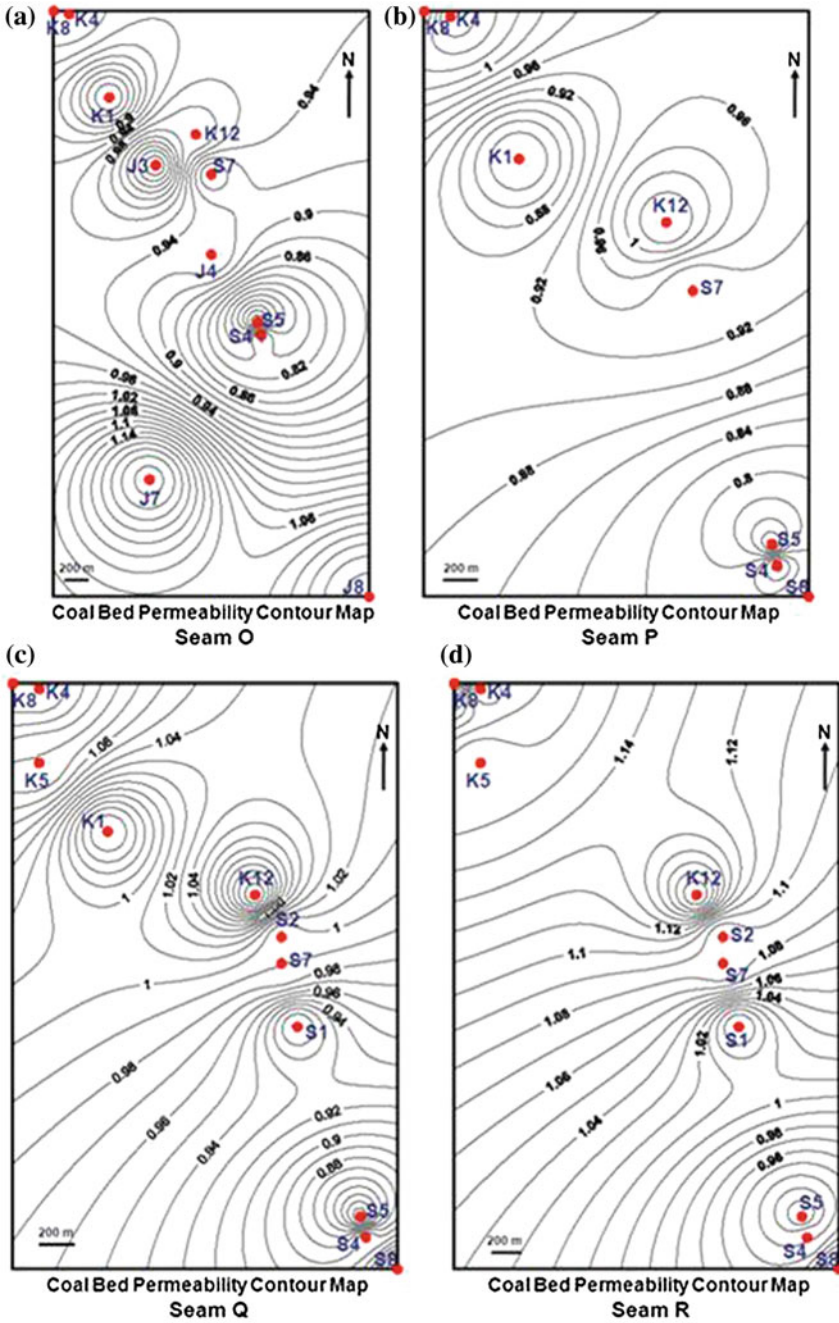**Fig. 13** Displaying coal bed permeability contour maps for **a** seam O, **b** seam P, **c** seam Q and **d** seam R. Coal bed permeability contour interval are considered as 0.02 md for seams O and P and 0.01 md for seams Q and R

gas by coal is robustly related with physical and chemical properties of coal (Crosdale et al. 1998). Gas in coal is adsorbed on the internal surface of micropores and varies directly with pressure and inversely with temperature. Previous authors like Bertard et al. (1970), Kissel et al. (1973), McKulloch et al. (1975), Diamond and Levine (1981), Feng et al. (1984) and Banerjee (1987) has proposed different direct methods for determination of methane adsorbed in coal beds. Gas content can also be estimated indirectly from any of the published global equations provided by Kim (1977), Mavor et al. (1993, 1995), Mullen (1988, 1991).

The above mentioned standard techniques/equations are mostly field-specific, so they alone may not be applicable for high confidence estimation of gas content of whole Jharia coalfield. Total gas in place (GIP) equals the product of tonnage of coal and gas content per unit weight of coal. By using density in g/cc units and gas content in cc/g units, the formula for the GIP calculation simplifies to the product of the volume of coal and a constant. The constant is different for each type of coal and is calculated as the product of the density in gm/cc and the gas content in cc/gm (for example, for a coal with density of 1.4 gm/cc and gas content of 4 cc/g, this constant is 5.6). Consequently, the formula we used is,

$$GIP(\text{Gas In Place}) = \text{Constant} \times \text{Volume}$$

where, Constant = Density (in g/cc) × Gas content (in cc/g).

The following equation is generally used to estimate the total initial adsorbed gas in a CBM reservoir:

$$G = 1359.7 \, Ah\rho_{ac}G_{ac}$$

where, G = Gas-in-Place in scf, A = Reservoir Area in acres, h = Thickness in feet, ρ_{ac} = Average In-situ Coal Density in gm/cc, G_{ac} = Average In-situ Gas Content in scf/ton.

Coal is a rock consisting largely of decomposed organic matter. Unlike most rock core, a coal core has a large internal surface area because it contains very small open pores within its structure. Most of the gas trapped within the coal adheres to the surfaces of the pores, and an estimation of the total internal surface area is useful for determining the potential for gas adsorption by the coal. Gas content per cc is a factor of microposity of coal, shape factor and is given by:

Gas content per cc = A ∗ surface area per cc of coal = A ∗ Available Microporosity of coal ∗ shape factor of micropores ∗ (1/micropore radius) = A ∗ B ∗ (Vitrinite Content/Factor of Degradation of microporosity due to blockage by mineral content) ∗ shape factor of micropores ∗ (1/micropore radius).

Degradation Factor is proportional to mineral content and can be considered as $C * P_e * GR$. This is so because mineral content will be of fine silt to clay size and radioactive and also will be containing elements having significant atomic number contrast with organics including volatiles.

Vitrinite content influences sonic slowness (Δt). It can be considered that

$$\text{Vitrinite content} = V * \Delta t$$

Adsorbed gas content per unit volume of coal can then be thought of as equaling $A * B * C * V * \Delta t / (P_e * GR) * (\alpha/r)$ where A, B, C, V are constants and α is shape factor of micro pores and r is micropore-radius, P_e = Photo-electric absorption index and GR = gamma ray response.

If ρ_c stands for coal density specific volume is given by $(1/\rho_c)$. Total gas content per unit mass of coal would be above plus non-adsorbed gas content say E, gas content per unit mass of coal is therefore given by

Gas content per unit mass of coal $= E + (A * B * C * V) * (\alpha/r) * (\Delta t / (P_e * GR * \rho_c))$ which has the form of the relation used in the paper as Eq. (4).

Parameter B changes with coal rank when same is higher than medium volatile bituminous. Dimension r also changes (decreases) with increasing coal rank. When coal rank is higher than medium volatile bituminous for the low values of radius of micropore and possible proximity of dimensions of mineral matter and micropores Factor C the damage factor increases with increasing rank. When coal rank is less than medium volatile bituminous then C tends to be fairly independent of mineral matter fraction and above formula holds good. Increasing mineral matter content is accompanied by decrease of gas capacity of coal for a given vitrinite content. Factor C increasing with increasing rank implies gas capacity of coal reducing with reducing mineral matter because as rank increases proximity of mineral matter size to micropore size increases, more than offsetting gain in available microporosity for lower mineral matter content.

Thus, the formula above is best suited for coal ranks equal to or lower than medium volatile bituminous rank. For higher ranks segmented parameterization of gas cc/gm of coal may give better estimates when such segmentation is carried out on the basis of vitrinite and ash content, and the form of parameterization would be expected to be different from Eq. (7).

Barakar coals of Jharia are high volatile bituminous to low volatile bituminous in rank. Coal seam wise regression will be useful with form above (since (α/r) can be different for different seams too) relation given in a concise form with the value of $(A * B * C * V*) * (\alpha/r)$ and of E based on regression data carried, as per reference cited by Bhanja and Srivastava (2008) in the following Eq. (7).

Bhanja and Srivastava (2008) had proposed the methodology to predict gas content from well logs in Jharia coalfield in absence of the direct measurement of gas content data of coal samples. No gas adsorption data was available to know the gas content of the major seams encountered in the wells under study. Bhanja and Srivastava (2008) had established the relation between the well log parameters and gas adsorption data from the southern part of the Jharia coalfield. They had estimated the gas content for coal seams of Jharia coalfield from sonic, density, photo electric absorption index (P_e) and gamma ray logs from the following equation:

$$V = 0.767\{\Delta t/(\rho_c \times GR \times P_e)\} + 10.67 \qquad (7)$$

where

V	Volume of gas (cc/gm)
Δt	Sonic log response for coal = 120 µs/ft (for Jharia coalfield)
ρ_c	Density log value for coal seam (gm/cc)
GR	Gamma ray response for coal (cps)
P_e	Photo-electric absorption index value for coal [1.8 barns/electron (for Jharia coalfield)]

For the present study, sonic log data were available for only 5 wells (J1, J3, J4, J7 and J8) adjacent to the Singra and Kapuria blocks and no photoelectric absorption index log (P_e) records were available for this study. Gas content has been estimated from the average sonic log response of 120 µs/ft and an assumed P_e values from well log data for 30 wells (such as: S1, S2, S4, S5, S7, S8, S10, S13, S14, K1, K4, K5, K8, K10, K11, K12, K14, K16, K17, K19, M1, M2, M3, J1, J2 J3, J4, J6, J7 and J8) of Jharia coalfield. Table 4 lists the estimated range of average gas content values for 15 coal seams from these wells of Jharia coalfield. Gas content values range from 11.11 to 11.91 cc/gm for these seams.

9 Delineation of Most CBM Potential Zone

Comprehensive analysis and integrated study, as presented above, demonstrates that the present study area around central Jharia coalfield may be considered as a CBM potential zone in view of the reasonably high gas content values as estimated from well logs and merits consideration for further development. Since no directly measured gas adsorption data was available from within the study area, it is difficult to validate the log-derived gas contents with the actual gas content of these seams. To delineate major CBM potential zones gas content and coal seam thickness contour maps have been prepared for the seams O, P, Q and R only. In previous section coal bed permeability contour maps for the same four coal horizons have been explained. These four seams were selected for this study because these seams were penetrated by the maximum numbers of wells. Figures 14 and 15 represent the variation of gas content and coal seam thickness contour maps. By comparing gas content, coal seam thickness as well as coal bed permeability of these major coal seams, it is observed that the area containing the wells J3, J4, K12, S1, S2, S4, S5, S7 and S8 is having the coal bed permeability values ranging from 0.82 to 1.12 md with average gas content of 11.50–11.75 cc/gm. This zone is also situated in the deeper part of this study area as established in the previous section. Therefore, this zone may be considered as the most potential CBM zone (Fig. 3) and this zone may be targeted for further CBM exploration and production. It is to be noted that this zone is also adjacent to the Moonidih area containing wells M1, M2 and M3 and

Fig. 14 Gas content contour maps for **a** seam O, **b** seam P, **c** seam Q and **d** seam R of Jharia coalfield, India. Gas content contour interval are considered as 0.02 cc/gm for all seams
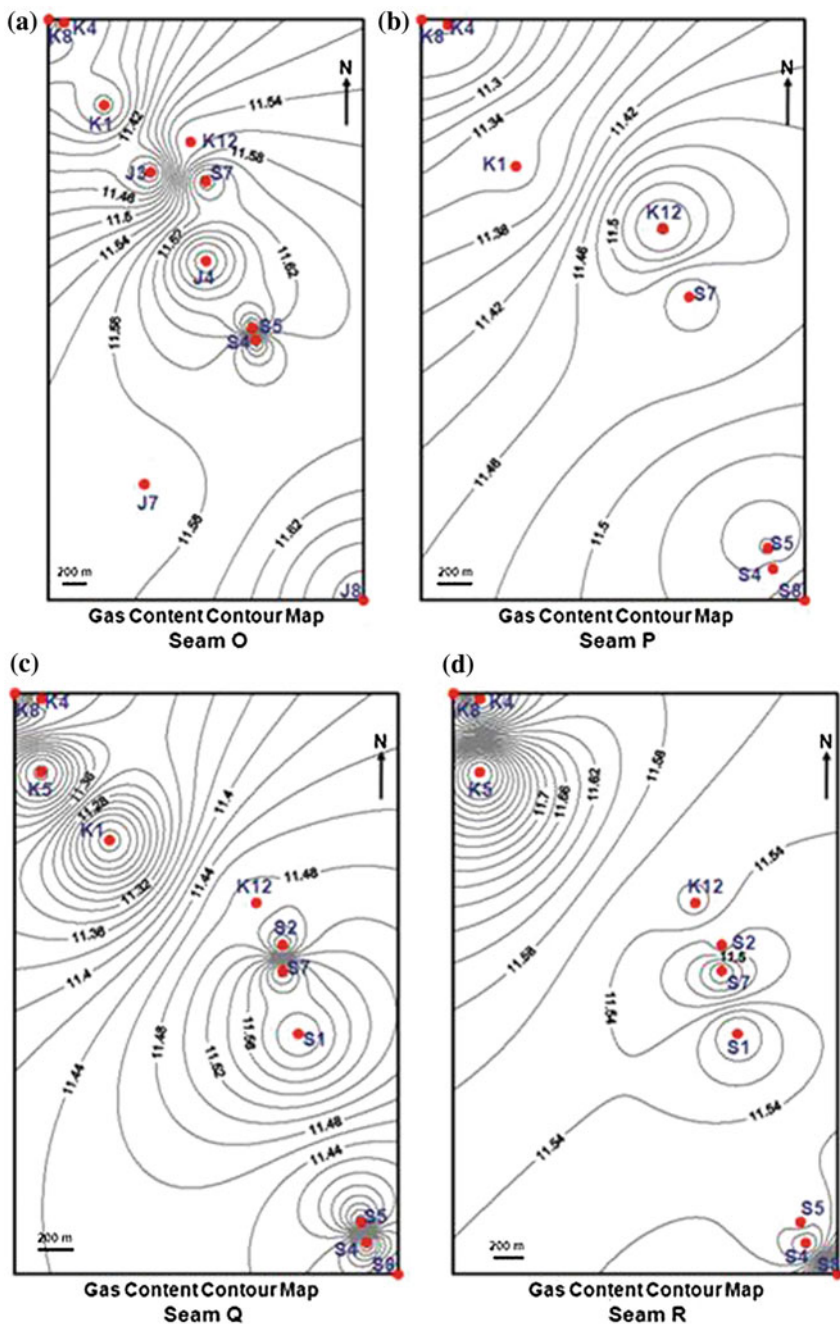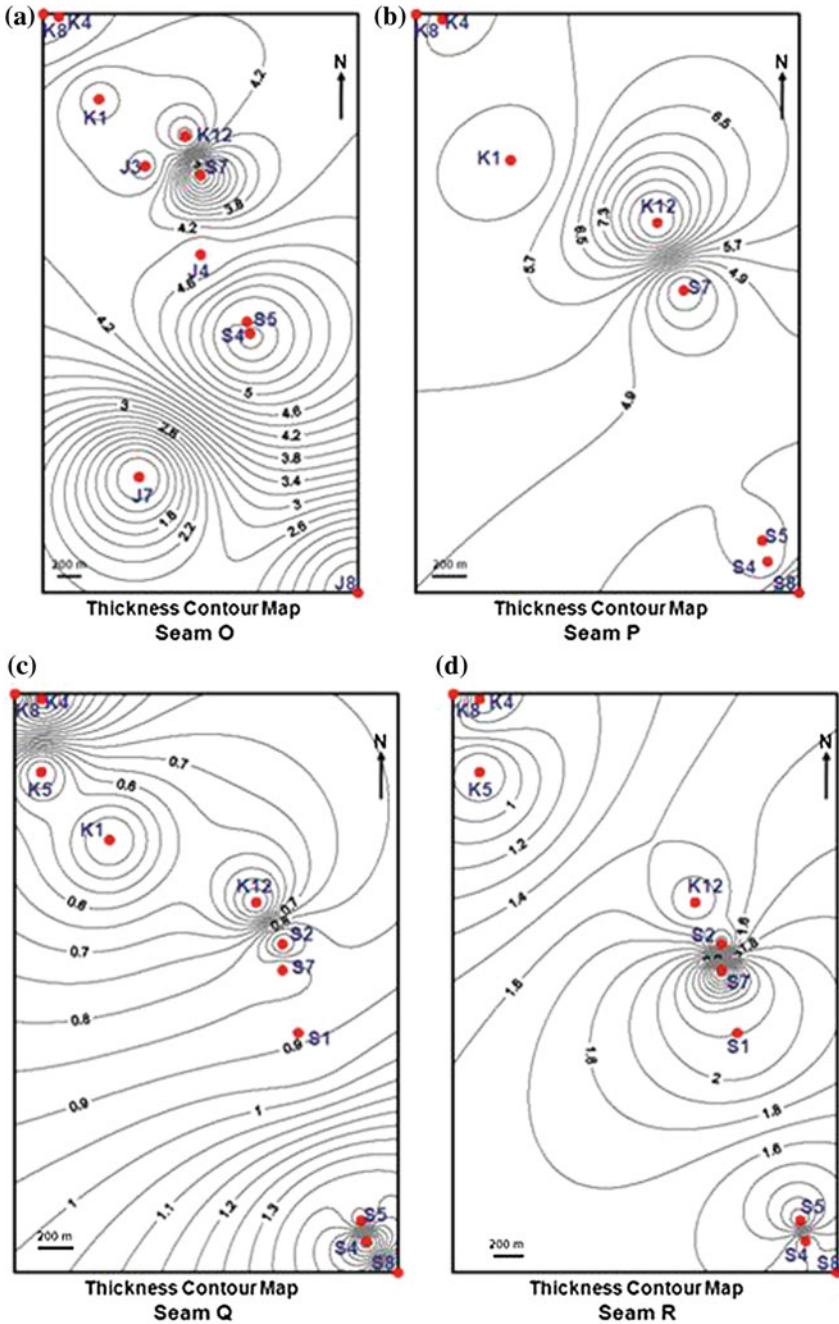
Fig. 15 Coal bed thickness contour maps for **a** seam O, **b** seam P, **c** seam Q and **d** seam R of Jharia coalfield, India. Coal bed thickness contour interval are considered as 0.20, 0.40, 0.10 and 0.10 m for seams O, P, Q and R respectively

Sahay (2009) had reported that the wells located in Moonidih area are producing CBM commercially. Therefore, it is inferred that the zone delineated from the present study may be taken up as the target for additional CBM investigation and potential production area.

10 Conclusions and Remarks

An integrated analysis has been carried out involving geological and geophysical well log data from 30 wells of the study area (Central Jharia coal basin), in combination with the data on proximate analysis, coal petrography, field mapping of cleat structures and lineaments of the area. The study aimed to estimate the critical reservoir parameters of coal seams as CBM reservoir and also to identify the most potential zone for CBM development. The findings for the study area are summarised below:

The stress magnitudes have been computed from the well log data and relationships between depth and vertical stress, effective vertical stress and effective horizontal stress have been established. All the values show increasing trend with depth with varying gradient (Fig. 6; Table 4).

It is observed that the gradient of effective vertical stress reduces within the coal seams due to change in density compared to the roof and floor rocks (Fig. 7). Vertical stress contour maps at the seam roofs show that the stress increases towards the dip of the inclined strata, i.e., towards the deeper or central part of the basin (Fig. 8). The vertical stress contour maps also reveal that the primary direction of stress anisotropy is along NW-SE direction (Fig. 8). It is also observed that the occurrence of high gradient anomalous zones are associated with the major geological structural discontinuities and local lineament pattern.

Coal bed permeability was calculated for each major coal seam from matchstick model using available standard equations. The coal bed permeability values range between 0.69 and 1.08 md. The plots of permeability values against depth show a linear decreasing trend with increasing depth (Fig. 9). The relationship between effective vertical stress (EVS) and permeability is also established and an empirical equation (Eq. 6) has been derived where the correlation co-efficient is 0.71. It is also established that the coal seam permeability progressively decreases with increasing EVS (Figs. 10, 11 and 12).

In order to delineate the CBM potential zones and direction of higher permeability, contour maps for four major coal seams have been generated. The direction of higher permeability lies to the NW and predicted direction of gas flow in from SE to NW. A secondary direction along ENE to WSW has also been found (Fig. 13) and these results are showing close consistency with some previous regional studies.

Gas content values were computed from sonic, density, gamma ray log and photo-electric absorption index logs (Eq. 7; Table 4). Gas content estimated are found to vary between 11.11 and 11.91 cc/gm. Considering the critical parameters

for CBM reservoir such as permeability, stress orientation and gas content, the area encompassing wells—J3, J4, K12, S1, S2, S4, S5, S7 and S8 is found to be most potential (Fig. 3). It may be considered as target for further CBM exploration and production project around this area.

A richer well log data suite including electrical high resolution images: radial and azimuthal delineated shear slowness, Stoneley waveform inversion, energy attenuation and nuclear magnetic resonance (NMR) supported by elemental dry weight logs help filling the vital knowledge gaps for characterization at wells and focused mapping. These further would guide not only locations for sinking wells but also type of wells, well trajectory design, stimulation where required and completion strategies needed for maximizing economic benefits and sustained gain.

References

Ali M, Sarkar A, Sagar R, Klimentos T, Basu I (2008) Cleat characterization in CBM wells for completion optimization. In: SPE indian oil and gas technical conference and exhibition, Mumbai, India, 4–6 March 2008 (Paper Id. SPE 113600)

Banerjee BD (1987) A new approach to the determination of methane content of coal seams. Int J Min Geol Eng 5:369–376

Bell JS, Bachu S (2003) In-situ stress magnitude and orientation estimates for Cretaceous coal-bearing strata beneath the plains area of central and southern Alberta. Bull Can Pet Geol 51 (1):1–28

Bertard C, Bruyet B, Gunther J (1970) Determination of desorbable gas concentration of coal (direct method). Int J Rock Mech Min Sci 7:43–65

Bhanja AK, Srivastava OP (2008) A new approach to estimate CBM Gas Conten from well logs. In: SPE Asia Pacific oil and gas conference and exhibition, Perth, Australia, 20–22 Oct 2008 (Paper Id. SPE 115563)

Chandra D (1992) Jharia coalfield. Mineral Resources of India, Geological Society of India, Bangalore, pp 1–149

Charles MBII, Bai Q (1998) Methodology of coalbed methane resource assessment. Int J Coal Geol 35(1–4):349–368

Chatterjee R, Pal PK (2010) Estimation of stress magnitude and physical properties for coal seams of Rangamati area, Raniganj coalfield, India. Int J Coal Geol 81:25–36

Chatterjee R, Paul S (2013) Classification of coal seams for coal bed methane exploitation in central part of Jharia coalfield, India—a statistical approach. Fuel 111:20–29

Chatterjee CN, Ghose S, Chandra D (1990) Micropetrographic characteristics of certain Lower Permian coal seams of India with special reference to their mode of formation. Int J Coal Geol 14:295–308

Close JC (1993) Natural fractures in coal. In: Law BE, Rice DD (eds) Hydrocarbons from coal. AAPG studies in geology, vol 38, pp 119–132

Crosdale PJ, Beamish BB, Vlix M (1998) Coalbed methane sorption related to coal composition. Int J Coal Geol 35:147–158

Cui X, Bustin RM (2005) Volumetric strain associated with methane desorption and its impact on coalbed gas production from deep coal seams. AAPG Bull 89(9):1181–1202

Diamond WP, Levine JR (1981) Direct method determination of the gas content of coal: procedures and results. US Bureau of Mines report of investigations, RI 8515

Feng KK, Cheng KC, Augsten R (1984) Preliminary evaluation of the methane production potential of coal seams at Greenhills Mine, Elkford, British Columbia. CIM Bull 77:56–60

Ghosh SK, Mukhopadhyay A (1985) Tectonic history of the Jharia Basin—an intracratonic Gondwana basin of Eastern India. Q J Geol Min Metall Soc India 57:33–58

Gu F, Chalaturnyk RJ (2010) Permeability and porosity models considering anisotropy and discontinuity of coalbeds and application in coupled simulation. J Petrol Sci Eng 74(3–4):113–131

Harpalani S, Chen G (1995) Estimation of changes in fracture porosity of coal with gas emissiom. Fuel 74(10):1491–1498

Harpalani S, Schraufnagel RA (1990) Shrinkage of coal matrix with release of gas and its impact on permeability of coal. Fuel 69:551–556

Hazra PN, Rudra M, Guha S, Kar MK, Basumatary JK, Kumar A. (2003) Geochemical characterization of Coalbed Gas of jharia & Raniganj Basins and its implications. In: Proceedings of international conference, Mussauri, India

IS 1350 (Part 1) (2003) Indian standard methods of test for coal and coke. Part 1: proximate analysis. Bureau of Indian Standards, 2nd revision, pp 1–28

IS 436 (Part 1/Section 1) (1991) Indian standard methods for sampling of coal and coke, Part 1: sampling of coal, Section 1: manual sampling. Bureau of Indian Standards, 8th reprint, pp 1–28

IS 9127 (Part 2) (2002) Indian standard methods for the petrographic analysis of bituminous coal and anthracite. Part 2: method of preparing coal samples. Bureau of Indian Standards, 1st revision, pp 1–8

IS 9127 (Part 3) (2002) Indian standard methods for the petrographic analysis of bituminous coal and anthracite. Part 3: method of determining maceral group composition. Bureau of Indian Standards, 1st revision, pp 1–6

IS 9127 (Part 5) (2004) Indian standard methods for the petrographic analysis of bituminous coal and anthracite. Part 5: method of determining microscopically the reflectance of Vitrinite. Bureau of Indian Standards, 1st revision, pp 1–12

Kim AG (1977) Estimating methane content of bituminous coal beds from adsorption data. U.S. Bureau of Mines, RI 8245, pp 1–22

Kissell FN, McCulloch CM, Elder CH (1973) The direct method of determining methane content of coal beds for ventilation design. US Bureau of Mines Report of Investigations, RI 7767

Kumar A, Singh SK, Datta GC (2010) Petrographic characteristics of Gondwana coals of Barakar formation of Bokaro CBM block, Jharkhand, India—implications on certain critical parameters. In: Proceedings of 9th international oil & gas conference and exhibition (PETROTECH 2010), New Delhi, India, 31 October–3 Nov 2010 (Paper Id 20100094)

Laubach SE, Marrett RA, Olson JE, Scott AR (1998) Characteristics and origins of coal cleat: a review. Int J Coal Geol 35:175–207

Law BE (1993) The relation between coal rank and cleat spacing: implications for the prediction of permeability in coal. Proceedings of international coalbed methane symposium II:435–442

Li H, Ogawa Y, Shimada S (2003) Mechanism of methane flow through sheared coals and its role on methane recovery. Fuel 82:1271–1279

Mavor MJ, Close JC, McBane RA (1993). Formation evaluation of exploration coalbed methane wells. SPE/CIM joint international meeting, Calgary, 10–13 June (Paper Id. SPE 21589)

Mavor MJ, Pratt TJ, Nelson CR (1995) Quantify the accuracy of coal seam gas content. Petrol Eng Int 68(10):37–42

McCulloch CM, Levine JR, Kissell FN, Deul M (1975) Measuring the methane content of bituminous coal beds. US Bureau of Mines report of investigations RI 8043

Mishra HK, Cook AC (1992) Petrology and thermal maturity of coals in the Jharia Basin: implications for oil and gas origins. Int J Coal Geol 20(3–4):277–313

Misra BK, Singh BD, Navale GKB (1990) Resino-inertinites of Indian Permian coals—their origin, genesis and classification. Int J Coal Geol 14:277–293

Mucho TP, Mark C (1994) Determining horizontal stress direction using stress mapping technique. In: Proceedings of 13th international conference on ground control in mining, Morgantown, pp 277–289

Mullen MJ (1988) Log evaluation in wells drilled for coal-bed methane. Rocky Mountain Association of Geologists, pp 113–124

Mullen MJ (1991) Coalbed methane resource evaluation from wireline logs in northeastern San Juan Basin: a case study. SPE joint rocky mountain regional/low permeability reservoirs symposium and exhibition, Denver, Colorado, 6–8 March, pp 161–172 (Paper Id. 18946)

Navale GKB, Saxena R (1989) An appraisal of coal petrographic facies in Lower Gondwana (Permian) coal seams of India. Int J Coal Geol 12:553–588

Palmer I, Mansoori J (1998) How permeability depends on stress and pore pressure in coalbeds, a new model. SPE Reservoir Eval Eng 1(6):539–544

Pashin JC (1998) Stratigraphy and structure of coalbed methane reservoirs in the United States: an overview. Int J Coal Geol 35:209–240

Pashin JC, Groshong RH Jr (1998) Structural control of coalbed methane production in Alabama. Int J Coal Geol 38:89–113

Paul S, Chatterjee R (2011a) Determination of in-situ stress direction from cleat orientation mapping for coal bed methane exploration in south-eastern part of Jharia coalfield, India. Int J Coal Geol 87:87–96

Paul S, Chatterjee R (2011b) Mapping of cleats and fractures as an indicator of in-situ stress orientation, Jharia coalfield, India. Int J Coal Geol 88:113–122

Pitman JK, Pashin JC, Hatch JR, Goldhaber MB (2003) Origin of minerals in joint and cleat systems of the Pottsville Formation, Black Warrior basin, Alabama: implications for coalbed methane generation and production. AAPG Bull 87(5):713–731

Rudra M, Hazra PN (2009) Isotopic composition of coalbed methane desorbed from Barakar coals of Damodar valley Gondwana coalfields and its implication. In: Proceedings of petrotech, 11–15 Jan, New Delhi, India

Sahay AN (2009) CMM demonstration project at Moonidih: a path finder for CMM development in Indian geo-mining scenario. MineTech 30(4):11–17

Sengupta N (1980) A revision of the geology of the Jharia coalfield with particular reference to distribution of coal seams. Ph.D. thesis, Indian School of Mines, Dhanbad

Tiwari A, Rai B (1996) Hydromorphogeological mapping for groundwater prospecting using landsat-MSS images—a case study of part of Dhanbad District, Bihar. Journal of the Indian Society of Remote Sensing 24(4):281–285

Townend J, Zoback MD (2000) How faulting keeps the crust strong. Geology 28:399–402

Verma RP, Jaipuriar AM, Paul PR (1989) Compendium on updated and revised geology of Jharia coalfield (excluding TISCO). Central Mine Planning and Designing Institute Ltd., Ranchi, pp 1–282

Yang Y, Peters M, Cloud TA, Van Kirk CW (2006) Gas productivity related to cleat volumes derived from focused resistivity tools in coalbed methane (CBM) fields. Petrophysics 47 (3):250–257

Calcareous Algal-Rich Carbonate Sediments from Assam Shelf, N-E India: An Overview of the Palaeoenvironmental Implications

Suman Sarkar

Abstract Assam Shelf in north-east India is one of the best studied sedimentary basins of the Indian subcontinent with respect to hydrocarbon exploration. Calcareous algae are common biogenic components of the Palaeogene carbonates outcropping in Meghalaya, Assam Shelf. They occur as encrusting and compact thalli, maerls and fragments in lagoonal to proximal outer shelf facies. The relative abundance of calcareous algae increase gradually from late Palaeocene to middle Eocene and is correlated to the evolution of a reefal environment also characterized by rich quantities of benthic foraminifera. The population dynamics of calcareous algae in the carbonate units of the Sylhet Limestone Group indicate an overall shallow bathymetry, mesotrophic nutrient regime and moderate species diversity. Abundance of mastophoroid and sporolithacean corallines points towards a tropical palaeoenvironment. The Palaeocene-Eocene time period featured critical, globally significant events such as the Indo-Asian plate collision and Palaeocene-Eocene Thermal Maximum (PETM). This factor adds to the importance of reef evolution and the constituent biogenic assemblages in NE India during this period.

Keywords Calcareous algae · Assam shelf · Sylhet limestone group · Palaeoenvironment · Benthic foraminifera · India

1 Introduction

Assam Shelf stands out as one of the premiere hydrocarbon basins of India (Raju and Mathur 1995; Borgohain et al. 2010). Several petroleum systems are present within the Assam geologic province, including the Assam Shelf (Kent et al. 2002). Regular systematic exploration activities by geological survey organizations and oil companies like the Oil and Natural Gas Corporation Limited (ONGCL) and Oil

S. Sarkar (✉)
Birbal Sahni Institute of Palaeobotany, 53 University Road, Lucknow 226 007, India
e-mail: suman763@gmail.com

India Limited (OIL) in the shelf horizons of Assam and Meghalaya have generated valuable surface as well as subsurface data related to petroleum and coal resources over the decades. The oil prospects of Assam Shelf and its adjoining parts have been dealt in detail by a number of workers (Murty 1983; Rao and Rajkumar 1987; Kumar et al. 2001). Despite continuous efforts for better hydrocarbon yields, the volume of production is satisfactory but not very significant in comparison to the international standards. There is a need for greater analyses pertaining to the fossil components of Assam Shelf which are bound to be beneficial in deeper understanding of the basin as a whole, thereby adding to the prospects of hydrocarbon exploration.

Calcareous algae are important biogenic components of late Palaeocene-middle Eocene carbonate sediments of the Sylhet Limestone Group, Meghalaya, Assam Shelf (Misra et al. 2002, 2011; Sarma and Ghosh 2006, 2007; Ghosh and Sarkar 2013). This time period is very significant due to events like the Palaeocene-Eocene Thermal Maximum (PETM) affecting almost all the organisms worldwide and collision of Indo-Asian plates that resulted in a wide array of palaeogeographic changes at the global scale (Scheibner and Speijer 2008; Afzal et al. 2011). The Sylhet Limestone Group is a carbonate ramp/tidal flat setting (Tewari et al. 2010a, b). Till date, the phycological studies from the Sylhet Limestone have mainly emphasized on taxonomy and largely neglected the palaeoenvironmental interpretations as a whole. Calcareous algal assemblages are persistent throughout the Cenozoic and have found increasing application in the evaluation and interpretation of a multitude of ecological parameters (Nebelsick et al. 2005, 2013; Brandano et al. 2009). Most coralline algal taxa are excellent bathymetric indicators (Braga and Aguirre 2004). Calcareous algae are also economically important by virtue of their application in reconstruction of depositional palaeoenvironmental models and contribution as important building blocks in numerous carbonate hydrocarbon reservoirs and reefs (Wray 1977; Kundal 2011).

In this paper, the palaeoenvironment of calcareous algal assemblages characterizing the carbonate units of the Sylhet Limestone Group is analyzed. Calcareous algae are well suited to such an approach because their differential diagnostic characteristics can be readily distinguished in thin-section along with their growth-form and taphonomic features (Braga et al. 1993; Nebelsick and Bassi 2000; Ghosh and Sarkar 2010).

2 Geological Setting

The Assam Shelf is the north-eastern extension of the Indian Craton and includes Jaintia, Khasi, Garo, Mikir Hills, Shillong Plateau and the upper Assam Valley. A series of activities along the fault zones of the Assam Shelf (formed by movements in the Himalayan and Arakan-Yoma regions) and the Indo-Asian plate collision controlled the depositional regime in the area (Jauhri and Agarwal 2001; Tewari et al. 2010b). Platform conditions were set up during the Late Cretaceous with

advent of sandstone deposition. The clastic sedimentation continued till the late early Palaeocene but a late Palaeocene modification in the tectonic regime lowered the subsidence rates, leading to a major reduction in the clastic supply. This event finally resulted in platform development upon which the carbonate sequences of the Sylhet Limestone Group got deposited. The carbonate platform existed until the late middle/late Eocene when another alternation in the tectonic regime brought about an increase in the terrigenous clastic input. This resulted in the deposition of thicker clastic sequences during the Late Palaeogene and Neogene (Jauhri and Agarwal 2001). The study area was created during Late Cretaceous by formation of a gulf in a shelf environment due to rifting along the Indo-Burmese orogen (Banerji 1981). The gulf opened eastward to oceanic realm and graded westward into continental environments; its basinal equivalents were, however consumed in the process of subduction following the Indo-Asian collision, though they are occasionally preserved as thin slices in the pile of folded Palaeogene sequences of the Naga Hills (Acharyya 1997).

An extensive and prolonged marine transgression phase laid down the deposits of the Sylhet Limestone Group. However, the carbonate deposition was occasionally interrupted due to a rise in clastic supply and phenomenon of shallowing (Jauhri and Agarwal 2001). The depositional process occurred in carbonate platform environment which tended to become reefal throughout the course of deposition of the Sylhet Limestone (Ghose 1976; Jauhri and Agarwal 2001). The Sylhet Limestone Group includes three carbonate units viz., Lakadong Limestone, Umlatdoh Limestone and Prang Formation in ascending order intercalated with Lakadong Sandstone and Narpuh Sandstone (Misra et al. 2011). The Sylhet Limestone is underlain by the late early to middle Palaeocene Therria Sandstone and overlain by shale/sandstone alternations of the late Eocene Kopili Formation (Jauhri and Agarwal 2001; Jauhri et al. 2006).

3 Materials and Methods

The studied carbonate samples were collected during fieldwork in a number of limestone quarries on the Jowai-Badarpur Road (NH-44) near Lumshnong, Meghalaya (Fig. 1). Detailed sections of the carbonate successions were examined taking into account important features such as lithology and the biogenic assemblages. The analysed carbonate successions were bound on the base and top by carbonate-siliciclastic mixed beds that have been excluded from the present study. In order to study the algal assemblages, standard thin sections ($\sim 3.5 \times 5.0$ cm) were prepared. Based on the incidence, abundance and frequency of various taxa, corresponding palaeoecological factors were evaluated with an overview of the palaeoenvironment. Calcareous green algae and non-geniculate coralline red algae were identified in thin section at the most precise taxonomic level possible. The thickness of individual algal thalli and encrusting coralline algae were also measured for estimation of the hydrodynamic energy levels. Apart from these,
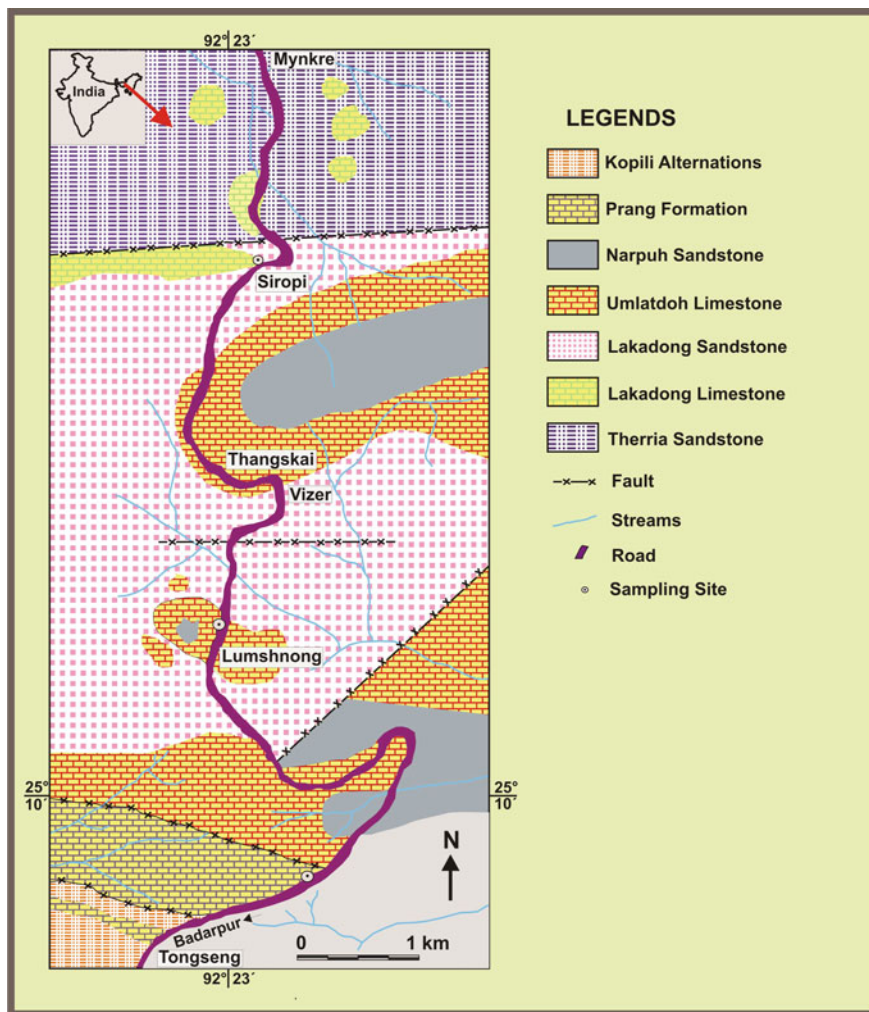
Fig. 1 Geological map showing an overview of the study area and sites of sampling (modified after Dutta and Jain 1980)

geniculate corallines were mostly identified at the generic level due to disarticulation in all the specimens. The species-level identification of the geniculates was further restricted due to severe abrasion in most of the forms and complete absence of reproductive organs (conceptacles). Abundance of various groups of calcareous algae, smaller and larger benthic foraminifera, and other biotic constituents as a whole across all the carbonate successions has been given special emphasis in this work (Fig. 2). Relative abundance of calcareous algae was estimated in thin-section by measuring the proportional area occupied by each taxon relative to the total algal
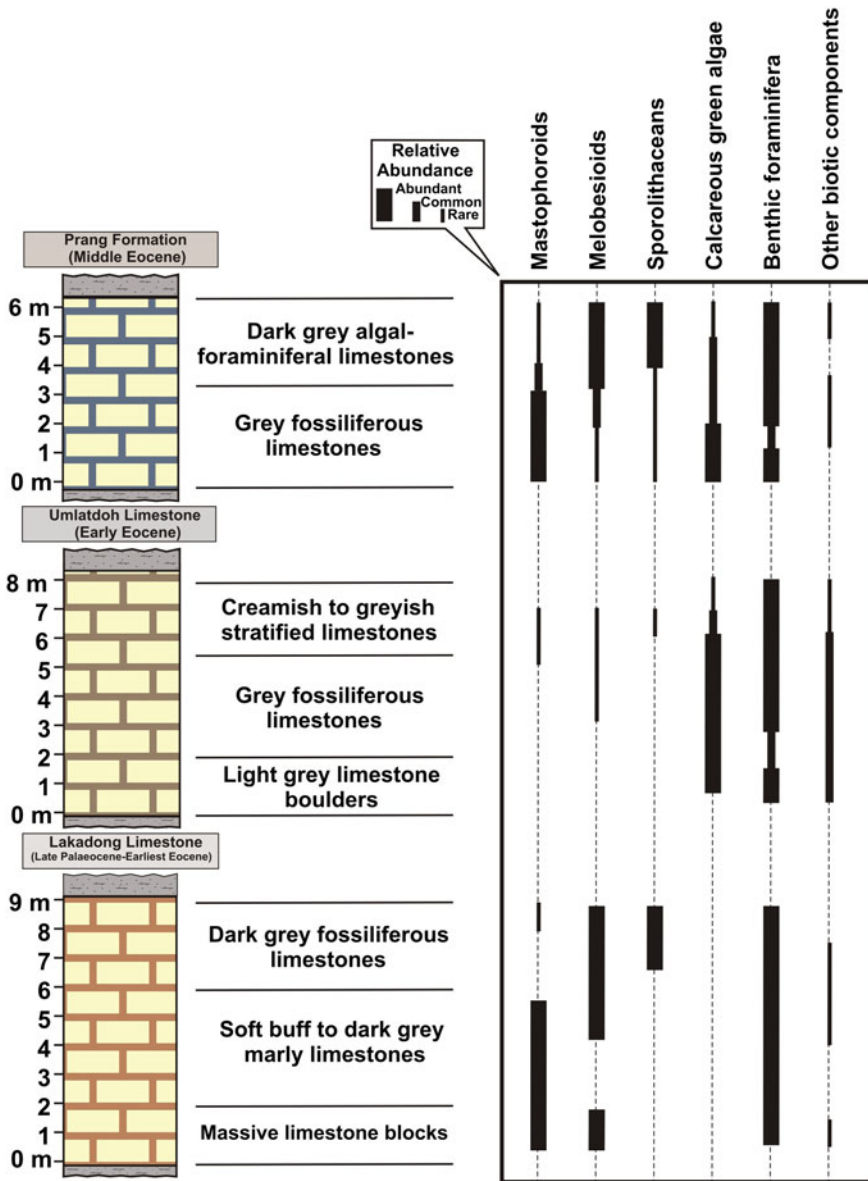
Fig. 2 Relative abundance of the major biotic constituents with respect to the studied sections

as well as biogenic population (Perrin et al. 1995). Coralline algal growth-form terminology follows Woelkerling et al. (1993). Taphonomy has been analyzed following Nebelsick and Bassi (2000). Thin sections were studied with Olympus BX 50 plane light microscope.

4 Results

Following the qualitative as well as quantitative analysis of the calcareous algae, three major algal assemblages have been distinguished. Benthic foraminifera (especially the larger forms) are also principal biogenic components of the studied foralgal reef sediments. Echinoderms, gastropods and molluscs etc. are the subordinate biogenic constituents. Negligible occurrence of corals nullifies the possibility of a coralgal reef environment. Calcareous algae have fair abundance in all the samples except few rare ones dominated by smaller miliolid foraminifera including *Quinqueloculina*, *Spiroloculina*, *Periloculina*, *Triloculina* and *Biloculina* etc. and larger foraminifera like *Nummulites*, *Alveolina*, *Miscellanea* and *Ranikothalia* etc. Across the various successions of the Sylhet Limestone Group pertaining to different time slices, major changes are witnessed in the larger benthic foraminiferal assemblages. Thanetian sediments (late Palaeocene; lower part of Lakadong Limestone) are enriched in *Miscellanea* (*M. juliettae*, *M. yvettae*) and *Glomalveolina* (*G. primaeva*, *G. levis*). Ilerdian sediments (earliest Eocene; upper part of Lakadong Limestone) are rich in *Miscellanea miscella*, *Ranikothalia nuttalli*, *Lockhartia haimei*, *Operculina* spp., *Rotalia* spp., *Assilina* spp., *Glomalveolina* spp., *Alveolina* spp. and smaller *Nummulites* spp. Rare *Orbitolites* and *Orbitosiphon* are also observed in the upper part of the Lakadong Limestone. In the Ypresian sediments (early Eocene) pertaining to the Umlatdoh Limestone, species of *Textularia*, *Daviesina*, *Alveolina*, *Nummulites* and *Lockhartia* are common to abundant. A conspicuous difference between the nummulitid assemblages of Lakadong and Umlatdoh Limestone is that the former is dominated by smaller tests while the latter is rich in larger forms. Lastly, the middle Eocene Prang Formation is dominated by larger *Nummulites* and *Alveolina*. Species of smaller miliolids and rotaliids, *Borelis*, *Operculina*, *Rotalia*, *Discocyclina*, *Orbitolites*, *Textularia* and *Lockhartia* are secondary in occurrence.

5 Mastophoroid Coralline Red Algal Assemblages

These assemblages are dominated by members of the subfamily Mastophoroideae. *Lithoporella melobesioides* is the most common species and dominates the algal populations in some samples of all the carbonate successions. *Spongites* spp. can also be identified in few samples. Abrasion and bioerosion are observed in some mastophoroid thalli. Unconsolidated, encrusting and fruticose growth-forms are observed in case of the mastophoroids. Geniculate corallines including *Corallina* and *Jania* are found in close vicinity of these taxa indicating lagoonal to inner shelf environmental setting. Geniculate corallines are observed only in form of disarticulated intergenicula with lack of conceptacles. Geniculate coralline algae are rare to common in the Lakadong Limestone, very rare in Umlatdoh Limestone but abundant in the Prang Formation. In case of geniculate forms, arborescent (tree-

like) growth-form can be assumed by comparison with the living counterparts. A number of unidentifiable thin, laminar thalli of mastophoroid corallines are also observed in all the sections. Maerls of melobesioid coralline algae (genera *Lithothamnion* and *Mesophyllum*) are abundant in the mastophoroid assemblages of the Lakadong and Prang units with absence to very rare occurrence in the Umlatdoh Limestone.

6 Calcareous Green Algal Assemblages

These assemblages are dominated by species of green algal genera *Halimeda*, *Ovulites* and *Acicularia* mostly characteristic of lagoonal to inner shelf environment. They are completely absent in the Lakadong Limestone succession but very abundant in both the Umlatdoh and Prang carbonates (latter is particularly rich in halimeds). Absence of green algae in the Lakadong Limestone can be attributed to lack of suitable substrate and environmental setting (adverse nutrient levels or possible competition for space and light with geniculate coralline algae/foraminifera) during the depositional period. As the carbonate platform evolved over time, the green algae probably succeeded in establishing themselves and dominated the benthic environment thereafter. *Halimeda* is represented by *Halimeda fragilis*, *H. cylindracea* and *H. tuna*, that are the dominating species. *Ovulites arabica*, *O. pyriformis* and *O. margaritula* are the dominating species of *Ovulites*, while *Acicularia robusta* and *A. valeti* are the common acicularids. Geniculate corallines (*Corallina matansa* and *Jania occidentalis*) are subordinate components of these assemblages in Prang Formation. *Lithoporella melobesioides, lithophylloids* and unidentifiable corallines with very thin laminar thalli are also minor components of the algal assemblages locally. Dasycladalean calcareous algae including species of *Dissocladella* are observed rarely in the Umlatdoh Limestone.

7 Melobesioid-Sporolithacean Coralline Red Algal Assemblages

Species belonging to the subfamily Melobesioideae and family Sporolithaceae are the major components of these algal assemblages. Both melobesioids and sporolithaceans are common to abundant in the Lakadong Limestone and Prang Formation depicting middle to proximal outer shelf environment. However, they are rare in the Umlatdoh Limestone with few specimens limited to the upper portion of the section. These assemblages include varying proportions of *Mesophyllum* and *Lithothamnion* species, and other unidentifiable melobesioids commonly observed in unconsolidated, encrusting, warty and lumpy growth-forms. Species of *Sporolithon* are also common to abundant in these assemblages and mainly show

warty/lumpy growth-forms. Several indeterminate melobesioids are observed in these assemblages that cannot be given a generic status due to absence of diagnostic multiporate conceptacles. *Lithoporella melobesioides* and other unidentifiable mastophoroids are also present in some samples, accounting for minor proportions of these algal assemblages.

Apart from these algal assemblages, Lakadong Limestone is characterized by encrusting coralline algae forming 4–5 mm-scale laminations upon larger foraminiferal skeletons. These forms are not identifiable but ascertained to be coralline red algae. In both the Umlatdoh and Prang units, thinner encrusting corallines are present very rarely (0.7–1 mm). Except for these encrusting coralline algae, it is difficult to estimate whether the algal forms grew where they appear (autochthonous deposits) or brought to location of deposition by hydrodynamic waves and/or tumbled downslope from higher topographic settings prior to or after death (allochthonous deposits). Action of storms/cyclones in the marine environment playing an action during the deposition of Sylhet Limestone calcareous algae cannot be ruled out either. Maerls are obviously allochthonous, but the extent of their displacement from their growing place is hard to estimate.

8 Discussion and Conclusions

The petroleum systems of the Assam Shelf most likely are genetically and temporally related to some of the gas-prone petroleum systems of the Bengal Basin (Wandrey et al. 2000). Constant efforts are being made to better define the relationship between source and reservoir rocks in the Assam Shelf (Mathur et al. 2001). However, multiple stacked source and reservoir rock sequences, and extensive fault systems allow mixing of hydrocarbons, making it difficult to distinguish individual petroleum systems. Till date, the Sylhet limestones have not been exploited well for commercial hydrocarbon production. The sediments within the Sylhet Group possess fair to good source rock characteristics and are marginally mature (Pahari et al. 2008). Thermal maturity values range from R_o 0.5 to 0.62 % in the Sylhet Limestone Group. The maturity value is expected to show an increase with depth to the southeast towards the Naga thrust fault and possibly be even higher in the subthrust zone. The reservoir rocks of the Assam Shelf also include the Sylhet Group limestones (Pahari et al. 2008). Contribution from algal and other marine precursors are bound to play an important role in n-Alkane distribution patterns in the oils of Assam Shelf. Algal-rich facies are generally suitable source rocks for hydrocarbons. Calcareous algae are critical biogenic components of several Cretaceous and early Cenozoic carbonates recorded from some of the major oil fields of the world (Wray 1977; Jauhri et al. 2006). Sirte Basin of Libya is one such highly yielding oil horizon where reef and other carbonate accumulations of Palaeocene age are the principal oil and gas reservoirs (Burwood et al. 2003). This basin encompasses banks of coralline algae and larger benthic foraminifera. Porosities are found to be the highest in the algal-foraminiferal member of this

reefal domain, averaging about 27 %, and 20–25 % throughout much of the overlying coral-algae reef limestone. The Intisar A reef of the Sirte Basin is a 400 m thick bioherm composed mainly of corals and coralline algae that has proven to be a highly productive oil field (Wray 1977). The Intisar reef was deposited within a part of a larger shelf province favourable for reef growth, and the site of accumulation was apparently controlled by a local dome in the sea floor that localized growth of corals and algae. Devonian carbonate deposits of central Alberta, Canada and late Palaeozoic phylloid algal limestones in the United States are important petroleum reservoirs and consist of different classes of algae (Wray 1977; Dix 1990). In all these, oil production results from the porous and permeable zones within the algal build-ups. Likewise, the Sylhet Limestone Group also projects an early Palaeogene reefal environment comprising calcareous algae as one of the dominating biogenic components. The δ^{13}C and δ^{18}O isotope data has recently been obtained from the Lakadong Limestone (Tewari et al. 2010a) and indicate a shallow marine depositional environment. It correlates well with the Palaeocene stable carbon and oxygen isotope data at the global scale (Tewari et al. 2007; Urrutia and Cruz 2008). The isotopic values recorded from the Lakadong Limestone suggest that the water temperature ranged $\sim$27–30 °C which relates very well to the biological productivity of the calcareous algae reported in the present study. As the Tertiary carbonates belonging to the Sylhet Limestone Group are rich in algae, research on calcareous algae correlated with limestone porosity and permeability is indeed a lucrative proxy for advanced hydrocarbon exploration in the carbonate deposits of Meghalaya and Assam Shelf as a whole.

Palaeocene-Eocene time period is significant in the geological time scale due to important events like the Indo-Asian plate collision and PETM, which had a major impact on the palaeogeography and palaeoclimate pertaining to various groups of flora and fauna globally including the larger benthic foraminifera (Scheibner and Speijer 2008; Afzal et al. 2011). There have been major changes in the benthic foraminiferal assemblages viz., abundance of *Miscellanea*, *Glomalveolina* and *Ranikothalia* in the Lakadong Limestone, that is gradually replaced by dominating larger *Nummulites* and *Alveolina* assemblages in the Prang Formation. In this regard, the algal assemblages have shown good degree of persistence. Most calcareous algal taxa have long geological ranges extending to the present (Kundal 2011). In the Sylhet Limestone Group, the mastophoroid, melobesioid and sporolithacean genera recorded right from the late Palaeocene to middle Eocene sediments, also extend to the present-day marine environmental settings worldwide (Maneveldt et al. 2008). Green calcareous algae also are observed both in fossil as well as living state (Hillis-Colinvaux 2001; Granier 2012). This proves that these calcareous algal forms have withstood the adverse environmental conditions and continue to evolve since a long geological time period.

Mastophoroid algal assemblages are characteristic of tropical, very shallow-water settings (Adey 1979; Minnery 1990; Iryu et al. 1995; Braga and Aguirre 2004). *Lithoporella* and *Sporolithon* are both tropic-indicating coralline algal genera (Pomar et al. 2004). Rare occurrence of *Lithophyllum* and other lithophylloids (indicative of sub-tropical and temperate conditions) further advocates for

a tropical depositional environment. Melobesioid coralline algae are scarce in very shallow-water frameworks and only occur as thin encrusting plants on corals and other corallines. The melobesioids dominate the coralline algal assemblages at deep tropical and shallow to deep temperate environments, reaching depths as high as 120 m (Adey 1979; Adey et al. 1982; Iryu et al. 1995; Lund et al. 2000; Braga and Aguirre 2004). *Sporolithon* usually occurs in association with melobesioids in deep bathymetric settings in low altitude areas. In present-day environmental settings, melobesioids and *Sporolithon* are observed in the below 15 m zone across a wide array of locations globally (Lund et al. 2000; Braga and Aguirre 2004). In the present case study, mastophoroids and melobesioids are consistently found in close association with larger benthic foraminifera which cannot survive at deeper levels due to association with their algal endosymbionts (light-dependent). Therefore, depth in excess of 40–45 m cannot be inferred for any of the Sylhet Limestone units (Umlatdoh is rather shallower due to dominance of halimeds and other calcareous green algae). This relatively broad bathymetric setting inferred from the carbonates of the Sylhet Limestone Group in Meghalaya, N-E India is very much contrasting with the restricted depth range of several corallines common in the present day Indo-Pacific reefs (Braga et al. 2009). Most living plants of *Hydrolithon onkodes*, probably the most abundant of the extant reef-building corallines, occur in the shallowest 5–10 m depth interval (Adey et al. 1982; Cabioch et al. 1999). Several other mastophoroid species also are limited to the upper, highest illumination 10 m zones of the present day reefs (Adey et al. 1982; Iryu et al. 1995; Littler and Littler 2003).

Calcareous algae are commonly reported from oligotrophic to mesotrophic depositional environments in both modern as well as fossil settings (Brandano et al. 2009). Excess of nutrients/eutrophic nutrient regime is detrimental for healthy growth of halimeds and other calcareous algae. The Umlatdoh Limestone and Prang Formation are rich in halimeds, other green calcareous algae and non-geniculate coralline red algae. Filter-feeding organisms like barnacles, balanids and serpulids typical of high-nutrient conditions are rare to absent across all the studied carbonate units. Oligotrophy marker z-corals and dasyclads are very rare in the thin-sections of the studied samples. Corals in particular are very sparse and found only in form of tiny fragments (no carpets/blocks/reef framework). Dasyclads are limited only to a few samples in the Umlatdoh Limestone. The calcareous algal and benthic foraminiferal assemblages across the carbonate units of the Sylhet Limestone are indicative of mesotrophic nutrient conditions with minor fluctuations towards oligotrophy and eutrophy. In all the studied carbonates, a symbiotic relationship between several calcareous algae and larger benthic foraminifera was observed. This association is assumed to have played a major role in the nutrient assimilation rates of both the groups, thereby determining the overall nutrient regime of the shallow marine environment.

Species diversity is an important parameter for any floral or faunal group irrespective of the surrounding environment. In the present study, species diversity of calcareous algae increases steadily from the late Palaeocene-earliest Eocene Lakadong Limestone to the middle Eocene Prang Formation (Fig. 3). This can be
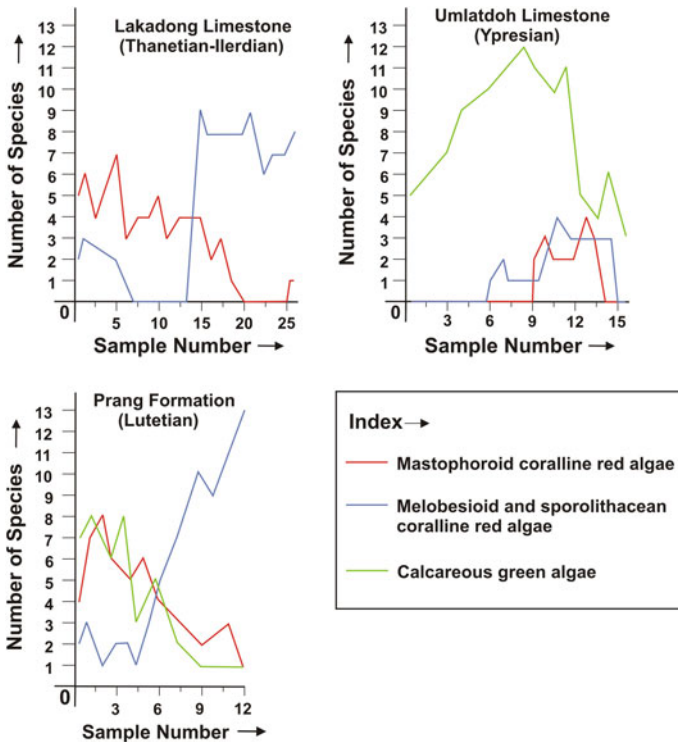
Fig. 3 Species diversity of different classes of calcareous algae recorded from different carbonate units of the Sylhet Limestone Group

attributed to the gradual evolution of the reefal environment that paved way for improved species constitution over the geological time scale (Fig. 4). Prang Formation, rich in all classes of calcareous algae and benthic foraminifera, probably presents the phase in which the reef development was complete/nearly complete and the algal flora flourished in the benthic environment. Overall, the calcareous algal species diversity in the Sylhet Limestone Group is moderate. Greater abundance of larger benthic foraminifera was perhaps the reason for calcareous algae not attaining higher diversity and abundance in the studied carbonate successions. However, fair level of algal abundance in the Lakadong Limestone and fair to abundant algal assemblages in the Umlatdoh Limestone and Prang Formation present healthy prospective for application in hydrocarbon industry by examining limestone porosity and permeability in the carbonate sediments. As calcareous algae are cosmopolitan in character ranging in a wide array of sedimentary basins worldwide, applied phycological research can prove to be a cheaper and beneficial aspect in petroleum exploration.

Lutetian (middle Eocene)

Developed reef setting dominated by mastophoroids, melobesioids, *Sporolithon*, halimeds, *Nummulites*, *Assilina* and various alveolinids

Bathymetry 20–40 m

Ypresian (early Eocene)

Foralgal reef dominated by calcareous green algae including abundant *Halimeda* and *Acicularia*, smaller miliolids, *Nummulites*, *Alveolina*, *Assilina* and echinoids

Bathymetry 15–25 m

Ilerdian (earliest Ypresian)

Domination of mastophoroids, melobesioids, sporolithaceans, larger rotaliids, *Ranikothalia*, *Lockhartia*, alveolinids, different species of *Miscellanea*, first instance of nummulitids and assilinids

Bathymetry 30–45 m

Thanetian (late Palaeocene)

Reefal system dominated by mastophoroids, melobesioids, smaller miliolids, smaller and larger rotaliids, *Miscellanea* and *Glomalveolina*

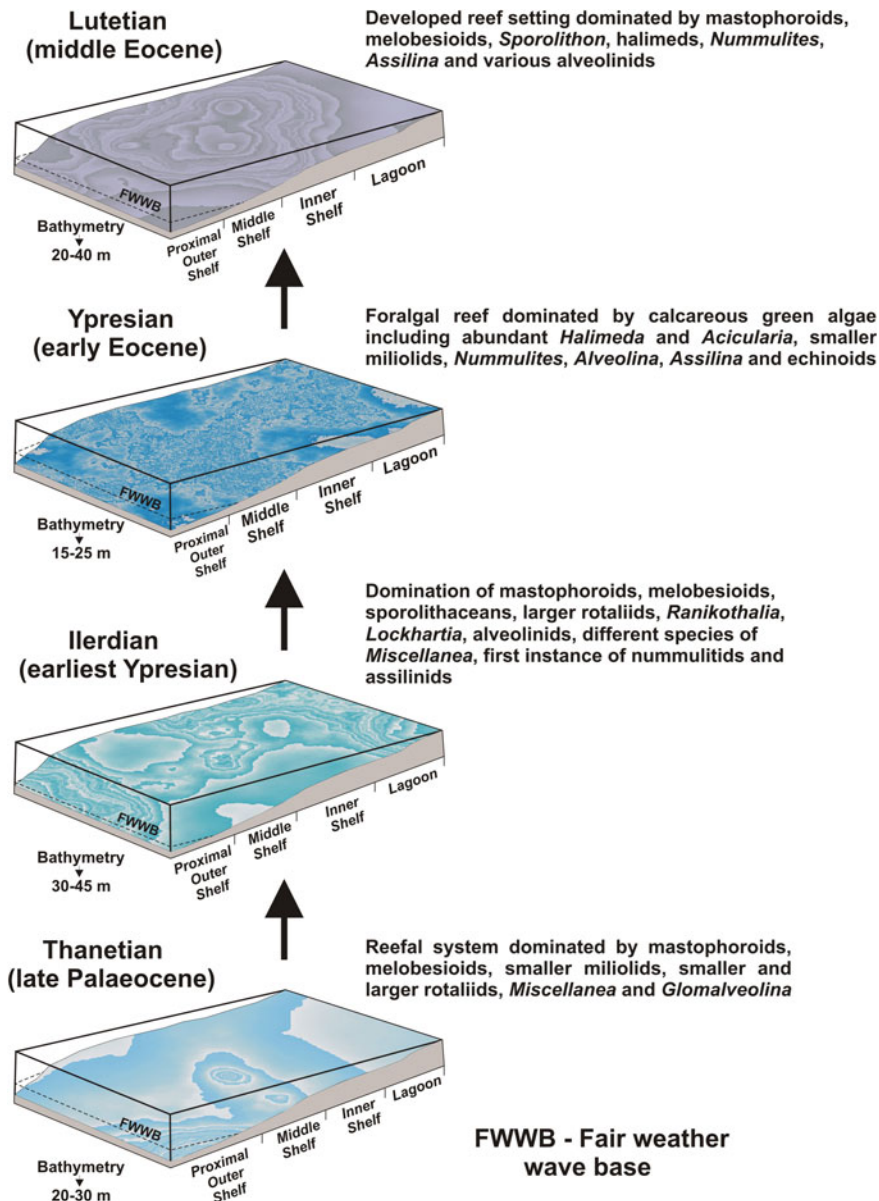Bathymetry 20–30 m

FWWB - Fair weather wave base

Fig. 4 Conceptual models showing the evolution of foralgal reef system in Assam Shelf with gradual changes in biogenic assemblages and approximate bathymetric ranges

References

Acharyya SK (1997) Stratigraphy and tectonic history and reconstruction of the Indo-Burma-Andaman mobile belt. Indian J Geol 69:211–234

Adey WH (1979) Crustose coralline algae as microenvironmental indicators in the Tertiary. In: Gray J, Boucot AJ (eds) Historical biogeography, plate tectonics and the changing environment. Oregon University Press, Corvallis, pp 459–464

Adey WH, Townsend RA, Boykins WT (1982) The crustose coralline algae (Rhodophyta: Corallinaceae) of the Hawaiian Islands. Smithson Contrib Mar Sci 15:1–74

Afzal J, Williams M, Leng MJ, Aldridge RJ (2011) Dynamic response of the shallow marine benthic ecosystem to regional and pan-Tethyan environmental change at the Paleocene-Eocene boundary. Palaeogeogr Palaeoclimatol Palaeoecol 309:141–160

Banerji RK (1981) Cretaceous-Eocene sedimentation, tectonism and biofacies in Bengal Basin, India. Palaeogeogr Palaeoclimatol Palaeoecol 34:57–85

Borgohain P, Borah C, Gilfellon GB (2010) Sandstone diagenesis and its impact on reservoir quality of the arenaceous unit of barail group of an oilfield of upper Assam shelf, India. Curr Sci 98:82–88

Braga JC, Aguirre J (2004) Coralline algae indicate Pleistocene evolution from deep, open platform to outer barrier reef environments in the northern great barrier reef margin. Coral Reefs 23:547–558

Braga JC, Bosence DWJ, Steneck RS (1993) New anatomical characters in fossil coralline algae and their taxonomic implications. Palaeontology 36:535–547

Braga JC, Vescogni A, Bosellini FR, Aguirre J (2009) Coralline algae (Corallinales, Rhodophyta) in western and central Mediterranean messinian reefs. Palaeogeogr Palaeoclimatol Palaeoecol 275:113–128

Brandano M, Frezza V, Tomassetti L, Cuffaro M (2009) Heterozoan carbonates in oligotrophic tropical waters: the attard member of the lower coralline limestone formation (upper oligocene, malta). Palaeogeogr Palaeoclimatol Palaeoecol 274:54–63

Burwood R, Redfern J, Cope MJ (2003) Geochemical evaluation of East Sirte Basin (Libya) petroleum systems and oil provenance. Geol Soc Lond Spec Publ 207:203–240

Cabioch G, Montaggioni LF, Faure G, Ribaud-Laurenti A (1999) Reef coralgal assemblages as recorders of paleobathymetry and sea-level changes in the Indo-Pacific province. Quatern Sci Rev 18:1681–1695

Dix GR (1990) Upper Devonian (Frasnian) non-calcified Algae, Alberta: geological relevance to leduc platforms and petroleum source rocks. Bull Can Pet Geol 38:429–439

Dutta SK, Jain KP (1980) Geology and palynology of the area around lumshnong, Jaintia Hills, Meghalaya, India. Biol Mem 5:56–81

Ghose BK (1976) Palaeogene reef rock-complex of Meghalaya and its oil potentialities. Sci Cult 42:248–253

Ghosh AK, Sarkar S (2010) Contemporary taxonomic perspectives of fossil coralline red algae: their possible origin and evolution. Palaeobotanist 59:107–119

Ghosh AK, Sarkar S (2013) Palaeoecological implications of corallinacean red algae and halimedacean green algae from the prang formation of south Shillong Plateau. J Geol Soc India 81:531–542

Granier B (2012) The contribution of calcareous green algae to the production of limestones: a review. Geodiversitas 34:35–60

Hillis-Colinvaux L (2001) The calcareous reef alga *Halimeda* (Chlorophyta, Bryopsidales): a Cretaceous genus that diversified in the Cenozoic. Palaeogeogr Palaeoclimatol Palaeoecol 166:89–100

Iryu Y, Nakimori T, Matsuda S, Abe O (1995) Distribution of marine organisms and its geological significance in the modern reef complex of the Ryukyu Islands. Sediment Geol 99:243–258

Jauhri AK, Agarwal KK (2001) Early Palaeogene in the south Shillong Plateau, NE India: local biostratigraphic signals of global tectonic and oceanic changes. Palaeogeogr Palaeoclimatol Palaeoecol 168:187–203

Jauhri AK, Misra PK, Kishore S, Singh SK (2006) Larger foraminiferal and calcareous algal facies in the Lakadong formation of the south Shillong Plateau, NE India. J Palaeontol Soc India 51:51–61

Kent WN, Hickman RG, Dasgupta U (2002) Application of a ramp/flat-fault model to interpretation of the naga thrust and possible implications for petroleum exploration along the Naga thrust front. Am Assoc Pet Geol Bull 86:2023–2045

Kumar M, Mandal J, Dutta SK, Bhuyan D, Das B, Saikia B (2001) Palynostratigraphy of the subsurface sediments of upper Assam Basin, India. Geobios 34:241–251

Kundal P (2011) Generic distinguishing characteristics and stratigraphic ranges of fossil corallines: an update. J Geol Soc India 78:571–586

Littler DS, Littler MM (2003) South Pacific reef plants. A diver's guide to the plant life of South Pacific coral reefs. Offshore Graphics, Inc, Washington, pp 332

Lund MJ, Davies PJ, Braga JC (2000) Coralline algal nodules off Fraser Island, Eastern Australia. Facies 42:25–34

Maneveldt GW, Chamberlain YM, Keats DW (2008) A catalogue with keys to the non-geniculate coralline algae (Corallinales, Rhodophyta) of South Africa. S Afr J Bot 74:555–566

Mathur N, Raju SV, Kulkarni TG (2001) Improved identification of pay zones through integration of geochemical and log data—a case study from Upper Assam basin, India. Am Assoc Pet Geol Bull 85:309–323

Minnery GA (1990) Crustose coralline algae from the flower garden banks, northwestern Gulf of Mexico: controls on distribution and growth morphology. J Sedimentol Petrol 60:992–1007

Misra PK, Jauhri AK, Kishore S, Singh SK (2002) Calcareous algae from the Lakadong formation of the South Shillong Plateau, NE India. Rev Paléobiol Geneve 21:717–734

Misra PK, Jauhri AK, Tiwari RP, Kishore S, Singh AP, Singh SK (2011) Coralline algae from the prang formation (middle-late eocene) of the Lumshnong Area, Jaintia Hills, Meghalaya. J Geol Soc India 78:355–364

Murty KN (1983) Geology and hydrocarbon prospects of Assam shelf—recent advances and present status. Petroleum Asia Journal. In: Bhandari LL (ed) Petroliferous basins of India, vol 6. pp 1–14

Nebelsick JH, Bassi D (2000) Diversity, growth-forms and taphonomy: key factors controlling the fabric of coralline algal dominated shelf carbonates. In: Insalaco E, Skelton PW, Palmer TJ (eds) Carbonate platform systems: components and interactions, vol 178. Geological Society of London Special Publication, pp 89–107

Nebelsick JH, Rasser MW, Bassi D (2005) Facies dynamics in eocene to oligocene circumalpine carbonates. Facies 51:197–216

Nebelsick JH, Bassi D, Lempp J (2013) Tracking palaeoenvironmental changes in coralline algal-dominated carbonates of the lower oligocene calcareniti di castelgomberto formation (Monti Berici, Italy). Facies 59:133–148

Pahari S, Singh H, Prasad IVSV, Singh RR (2008) Petroleum systems of upper Assam Shelf, India. Geohorizons, pp 14–21

Perrin C, Bosence D, Rosen B (1995) Quantitative approaches to palaeozonation and palaeobathymetry of corals and coralline algae in Cenozoic reefs. In: Bosence DWJ, Allison PA (eds) Marine palaeoenvironmental analysis from fossils, vol 83. Geological Society of London Special Publication, pp 181–229

Pomar L, Brandano M, Westphal H (2004) Environmental factors influencing skeletal grain sediment associations: a critical review of miocene examples from the western Mediterranean. Sedimentology 51:627–651

Raju SV, Mathur N (1995) Petroleum geochemistry of a part of upper Assam Basin, India: a brief overview. Org Geochem 23:55–70

Rao VVK, Rajkumar J (1987) Exploration for hydrocarbon in North East India by O.N.G.C. In: proceedings volume of seminar on recent advances on the study of cenozoic geology in N.E.R. India, Dibrugarh University, pp. 1–37

Sarma A, Ghosh AK (2006) A new record of calcareous algae from shella Formation (Jaintia Group) of South Jaintia Hills, Meghalaya, India. Curr Sci 90:1276–1281

Sarma A, Ghosh AK (2007) Calcareous green algae from the umlatdoh limestone belonging to shella formation (Jaintia Group) of south Jaintia Hills, Meghalaya, India. Palaeobotanist 56:21–28

Scheibner C, Speijer RP (2008) Late Paleocene-early Eocene Tethyan carbonate evolution—a response to long- and short-term paleoclimatic change. Earth-Sci Rev 90:71–102

Tewari VC, Stenni B, Pugliese N, Drobne K, Riccamboni R, Dolenec T (2007) Peritidal sedimentary depositional facies and carbon isotope variation across K/T boundary carbonates from NW adriatic platform. Palaeogeogr Palaeoclimatol Palaeoecol 255:77–86

Tewari VC, Kumar K, Lokho K, Siddaiah NS (2010a) Lakadong limestone: paleocene-eocene boundary carbonates sedimentation in Meghalaya, Northeastern India. Curr Sci 98:88–95

Tewari VC, Lokho K, Kumar K, Siddaiah NS (2010b) Late cretaceous-paleogene basin architecture and evolution of the shillong shelf sedimentation, Meghalaya, Northeast India. J Indian Geol Congr 2:61–73

Urrutia FJ, Cruz LP (2008) Post impact carbonate deposition in the chicxulub impact crater region, Yucatan Platform, Mexico. Curr Sci 95:248–252

Wandrey CJ, Milici RC, Law BE (2000) Region 8, South Asia. In U.S. Geological Survey Assessment Team, 2000. U.S. geological survey world petroleum assessment 2000—description and results. U.S. geological survey digital data series DDS-60 Version 1.1: 4 CD-ROMs

Woelkerling WJ, Irvine LM, Harvey A (1993) Growth-forms in non-geniculate coralline red algae (Corallinales, Rhodophyta). Aust Syst Bot 6:277–293

Wray JL (1977) Calcareous algae. Elsevier Publishers, Amsterdam, p 190

Hydrocarbon Potential of the Paleogene Disang Group, Manipur Region, India-A Palynological Approach

Y. Raghumani Singh, B.P. Singh and Jianguo Li

Abstract In the present study, the rocks of the Disang Group of Manipur are evaluated for source rock potential for hydrocarbons. In these Paleogene rocks, amorphous organic matter is the most abundant component in association with other forms of organic matter. Other types of organic matters such as charcoal, partly biodegraded land plant fragments, black debris, spores and pollens are recorded as well. Rock-Eval and TOC analysis of the studied samples suggest that all the rocks have poor organic richness (TOC < 0.5 %) and poor hydrocarbon generation potential (S2 < 0.5 mgHC/g rock). The organic matter content is predominantly of Type III and Type IV. The T_{max} and Productive Index values support the results of visual kerogen analysis. Most of the kerogen is of low level of maturity inferred from light colour of amorphous organic matter in some samples. This conclusion is also supported by Low T_{max} values and low productive index obtained from these samples. TAI (Thermal Alteration Index) values above 3.5 suggest highly mature to overmature mixed palynofacies. The Disang Group of the Manipur appears poor to moderate gaseous hydrocarbons as far as hydrocarbon potential is concerned.

Y.R. Singh (✉)
Department of Earth Sciences, Manipur University, Imphal 795003, India
e-mail: yengmani@gmail.com

B.P. Singh
CAS in Geology, Banaras Hindu University, Varanasi 221 005, India

J. Li
Nanjing Institute of Geology and Palaeontology, Chinese Academy of Sciences, 39 East Beijing Road, Nanjing 210008, China

191

1 Introduction

Manipur belongs to the north-eastern region of India which shares international border with Myanmar on the eastern and southern sides. The remaining half of this state is neighboured to the states of Nagaland, Assam and Mizoram respectively on the northern, western and south-western sides (Fig. 1). The hill-ranges of Manipur and Nagaland states of India, which form an integral part of the Indo-Myanmar Range (IMR) have accretionary prism due to subduction of the Indian plate below the Myanmar plate during the Apline-Himalayan tectogenesis (Acharyya et al. 1986). Cretaceous and Tertiary sedimentary sequences dominantly occur in the Manipur state. They are associated with minor igneous and low- to medium-grade phyllitic schist, quartzites, marble, and gneiss. The northeast and eastern part of the state is occupied by the older group of Metamorphic Complex and Ophiolite Mélange Zone. These Ophiolites are associated with exotic sedimentary blocks of chert, limestone, red and black clay/shale, sandstone and conglomerate. The central part of the Manipur state is composed of the Paleogene flysch sediments including Disang and Barail groups and that of western part mainly consist of molasses succession of Surma and Tipam groups (Fig. 1). The Paleogene rocks are well exposed in the Imphal valley and eastern part of the Manipur state and are represented by the Disang and Barail groups (Fig. 2). The Disang Group is subdivided into two formations namely, Lower Disang and Upper Disang. The Lower Disang Formation is made up of mainly sandstone and shale, while the Upper Disang Formation is represented by a rhythmic series of sandstone, siltstone and shale containing mega and microfossils and trace fossils. The Barail Group is made up of thick bedded sandstone with alternation of shale and sandstone. The overlying molassic sequence of the Surma Group consists of alternation of sandstone and shale; with more argillaceous horizons in the middle associated with minor conglomerate. The generalised stratigraphic succession is given in the Table 1.

An account on the geology of the Manipur region is given by Theobald (1871), Pascoe (1914), Evans (1932), Nandy (1980) and Acharyya et al. (1989). Chungkham and Jafar (1998), Chungkham et al. (1992), Singh et al. (2010), Sijagurumayum et al. (2011, 2014) and Singh et al. (2013) have contributed considerably towards fossil findings including planktonic foraminifera and molluscs in this region. Recently, Singh and Meera (2013) have evaluated maturation of organic matter and type of organic matter from the Lower Tertiary rocks exposed at Sora, Changamdabi and Keirak areas of Imphal valley, Manipur. They further have suggested that the middle and upper parts of the Disang Group in these areas may have potential for exploration of hydrocarbons (gas). Recently, Singh et al. 2013 firstly reported dinoflagellate cysts namely *Hystrichokolpoma rigaudiae*, *Cordosphaeridium* sp. and microforaminiferal linings such as Planispiral type III, Planispiral type IV, Biserial type II, Trochospiral type I and Trochospiral type II from the Upper Disang Formation. Rock-Eval Pyrolysis is widely used for determining the amount and type of organic matter for source rock evaluation of hydrocarbon potential (Espitalié et al. 1977, 1984). In this study we have utilised
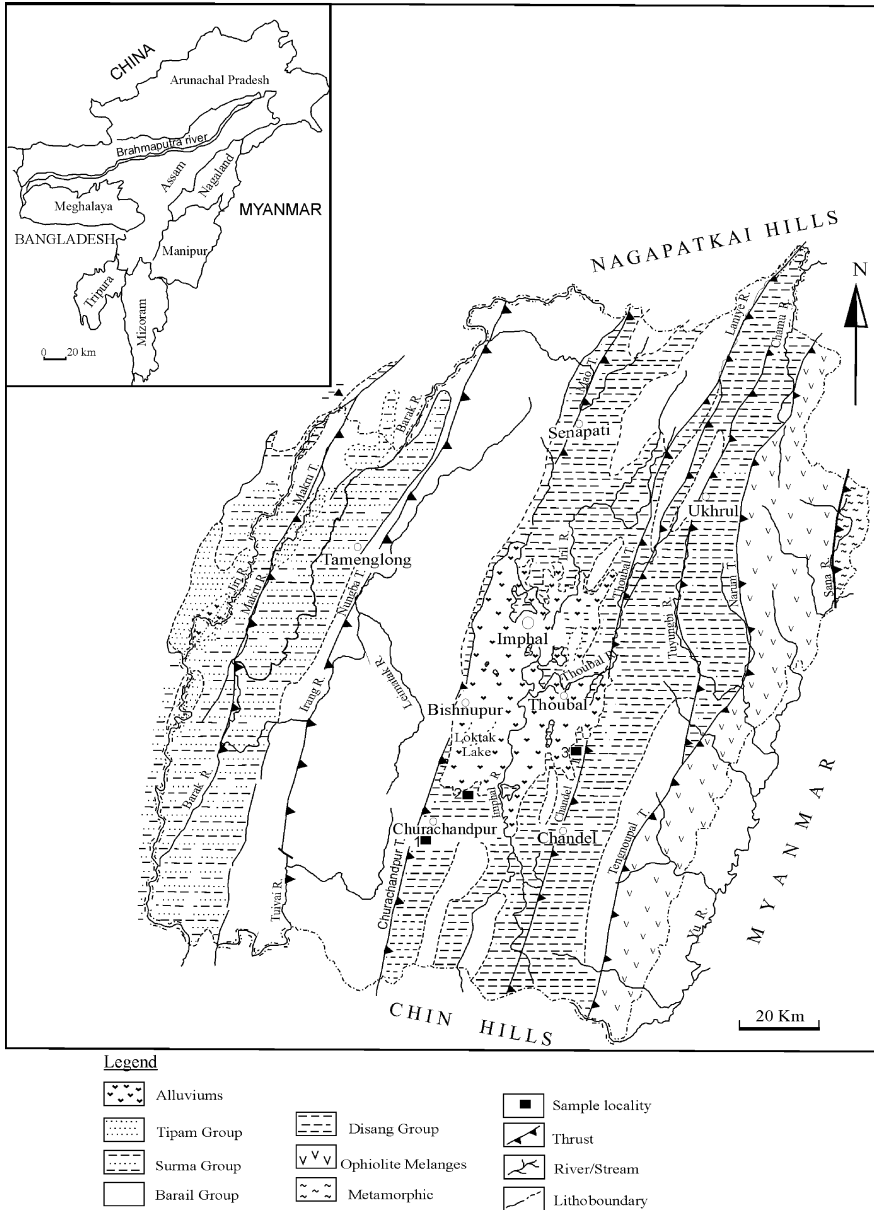
Fig. 1 Geological map of Manipur (after Singh et al. 2013) showing sample localities (*1* Gelmoul quarry, *2* Thanga Ngaram and *3* Khunutaba Ching, Kakching)

this technique for source rock evaluation for hydrocarbons from the outcrop samples of the Disang succession of Manipur region and the way of palynofacies as well. Total organic carbon (TOC) and other related parameters such as Si (free
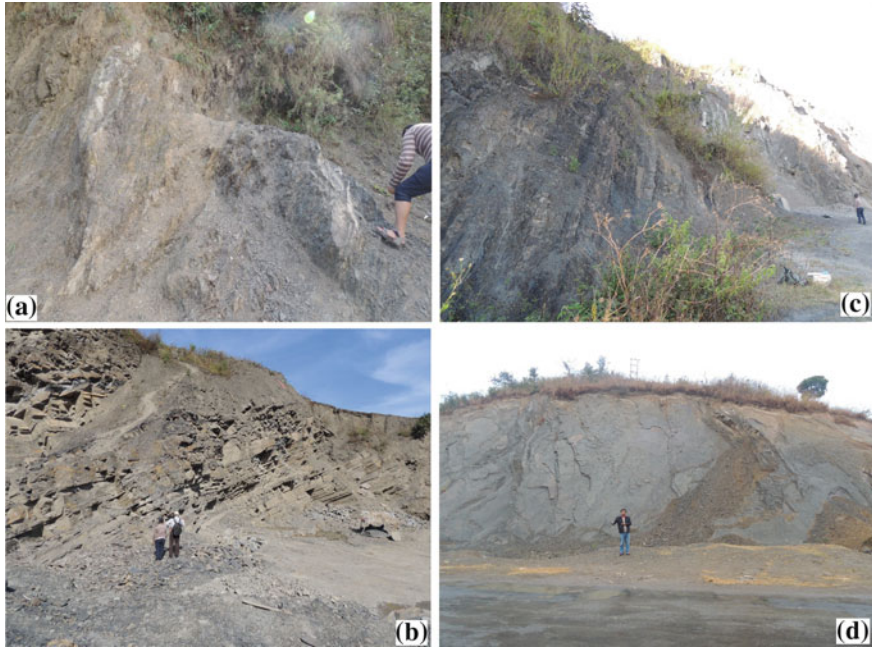
Fig. 2 **a** Splintery shale of Lower Disang at Thanga Ngaram, **b** alternation of sandstone and shale of the Upper Disang at lower part of Gelmoul quarry, Churachandpur, **c** alternation of sandstone and shale of Upper Disang at upper part of Gelmoul quarry (high of man is 1.5 m), **d** Upper Disang shale at Khunutaba Ching, Kakching

hydrocarbons present in the rock), S2 (remaining generation potential), S3 (oxidizable carbon), T_{max} (temperature maximum at peak of S2), HI (hydrogen index), OI (oxygen index), PI (production index) are being determined for the first time in this region.

2 Methodology

A total of 59 rock samples were collected from outcrops at four localities for this study. Most of them are shale and others are siltstone and sandstone (Fig. 2). Out of them, two samples, namely TNG-A and TNG-1 from the Lower Disang Formation at Thanga Ngaram (GPS: 24°31′12.1″N: 93°48′36.5″E), twelve shale samples from the Upper Disang Formation (one SO-2 from Khunutaba Ching, Kakching, GPS: 24°30′32.46″N: 94°00′50.07″E); (eleven samples from lower represented by G-1 to G-20) and (upper represented by GT-1 to GT-22) parts of Gelmoul quarry, (GPS: 24°20′40.4″N: 93°39′39.6″E).

Table 1 Generalised stratigraphic succession of Manipur (after Soibam 1998 and Anonymous of GSI 2011)

Age	Group	Formation	Description of rocks
(Quaternary-Pleistocene)	Alluvium		Dark grey to black clays, silt and sandy deposits of fluvio-lacustrine origin. Clay, sand, gravel, pebble, boulder deposits of the foothills and river terraces
Miocene	Tipam Group		Mottled clay, mottled sandy clay, sandy shale, clayey shale and sandstone Greenish to blue, moderate to coarse ferruginous sandstone with sandy shale, clay. Often brown to orange due to weathering. Molasse type of deposits
Miocene to Late Oligocene	Surma Group	Bokabil Formation	Shale, sandy shale, siltstone, ferruginous sandstone, massive to bedded ferruginous sandstone
		Bhuban Formation	Alternations of sandstone and shale with more argillaceous horizons in the middle and minor conglomerates. Transitional characters from Flysch to molasse sediments
Unconformity			
Oligocene to Late Eocene	Barail Group	Renji Formation Jenam Formation Laisong Formation	Massive to thickly bedded sandstone. Alternations of shale and sandstone with carbonaceous matters. Intercalation of bedded sandstone with shale
Middle to Late Eocene	Disang Group	Upper Disang Formation	Splintery shale and intercalation of shale, siltstone and sandstone showing occasionally rhythmite characters with fossils
Late Cretaceous to Early Eocene		Lower Disang Formation	Dark grey to black shale with minor sandstone bands
Unconformity			
Cretaceous to Early Eocene	Ophiolite Mélange Zone		Basic and ultrabasic intrusive and extrusive of peridotite, gabbro, serpentinite composition. Associated sediments are mainly pelagic, such as chert, limestone, shale etc.
Unconformity			
(Pre-Mesozoic or older)	Metamorphic complex		Low to medium grade metamorphic rocks of various composition-phyllitic schist, quartzite, micaceous quartzite, quartz-chlorite-mica-schist and marble
(?) *Unconformity*			
?Early Mesozoic rocks or Pre-Cambrian rocks	Basement complex		Unseen

TOC analysis and other parameters of the above samples have been performed by Rock Eval—VI in the Oil and Natural Gas Corporation (ONGC) at Dehra Dun, India. Palynological experiment was carried out at Department of Earth Sciences, Manipur University. Out of 59 samples, twenty six samples have been used for palynofacies analysis. Palynological preparation was made by using chemical treatment of Hydrochloric acid (35 %) and hydrofluoric acid (40 %) without any oxidation (Faegri and Iversen 1989). The organic matter residue after acid treatment was sieved using ASTM-400 before mounted on glass microscope slide in DPX. The slides were observed visually for Thermal Alteration Index (TAI) and organic content under a transmitted light microscope of Nikon E-200 (Staplin 1969). The source rock potential of the Disang Group has then discussed from the sights of TOC, the quantity and quality of organic matter, and maturation index (TAI). The visual estimation method follows that of Terry and Chilinger (1955) and a TAI value is adopted here (Staplin 1969). Classification and terminology of the dispersed organic matter follows that of Staplin (1969) and can be correlated with others, e.g. Masran and Pocock (1981), Venkatachala (1981), Tyson (1995), Batten (1981, 1996) and Ercegovac and Kostic (2006).

3 Source Rock Evaluation

Fourteen rock sample powders of the Disang Group were subjected for Rock-Eval Pyrolysis following Espitalié et al. (1977). The results are:

4 Kerogen Types and Maturity

Hydrogen and oxygen contents of the samples, measured as hydrocarbon-type compound and carbon dioxide yields, respectively, were normalized to organic carbon and displayed as hydrogen index (mgHC/g TOC) and oxygen index (mgCO$_2$/g TOC). They are plotted and compared to the van Krevelen-type diagram (Tissot and Welte 1984) to estimate the composition of kerogen types (Fig. 3). It can be seen from the figure that nearly all the samples fall in the area of Type IV with a few in the area of Type III, implying only a gas potential for these samples.

There are four types of kerogen such as type I-mainly algal produced, type-II-produced by spores and cuticles of plants and types III and IV-produced by the remains of the land plants. A plot of HI versus T$_{max}$ (Fig. 4) indicates that the samples from the Disang Group are thermally immature for hydrocarbon (HC) generation (sample nos. GT- 9, GT-12, GT-14, GT-17 and GT-20) and occupy gas prone area. Sample nos. GT- 7, GT-21, GT-22 are postmature (overmature) for HC in the maturity diagram. All the studied samples suggest the presence of kerogen types III and IV. Matrix effect is most noticeable at TOCs of less than around 1.5 %, which may generate and expel considerable quantities of gas and condensate
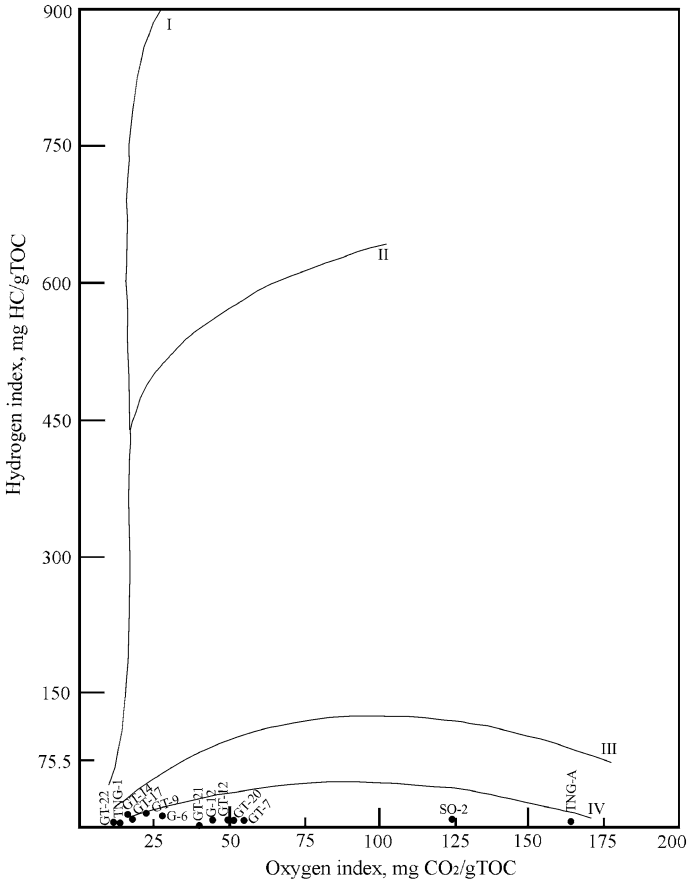
Fig. 3 Van Krevelen-type diagram for representation of type of kerogen

(Hunt 1996). The matrix effect appears likely in case of the Disang samples of the Manipur region as the TOC is <0.66 % and there is likely-hood of generation of gas.

5 Rock-Eval Pyrolysis and TOC

TOC and Rock-Eval Pyrolysis data and Rock-Eval parameters for the Disang Group are presented in Table 2. In immature sediments, organic matter dominated by marine components typically has hydrogen index values 200–400 mgHC/g TOC and the temperature at which pyrolysis yields the maximum of hydrocarbons (T_{max}) can be used as an indicator of the thermal maturity of the kerogen (Stein et al. 1989; Stein 1991). Immature organic matter has T_{max} values of less than 435 °C and
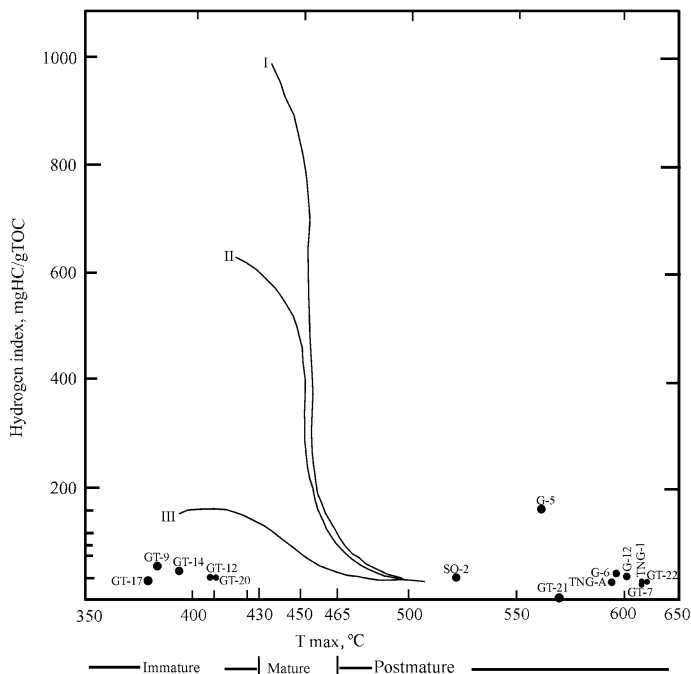
Fig. 4 A plot of HI versus T max for the Disang shale of the Gelmoul village (Upper Disang Formation; G-5, G-6, G-12, GT-7, GT-9, GT-12, GT-14, GT-17, GT-20, GT-21, GT-22); Sora (Upper Disang Formation, SO-2) and Thanga areas (Lower Disang Formation, TNG-A, TNG-1)

kerogen at the oil-generation stage generally has T_{max} values from 435 to 450 °C. High temperatures are indicative of the gas generating stage and temperature lower than 435 °C are indicative of thermal immaturity (Palmer and Zumberge 1981; Peters and Cassa 1994). In the studied samples T_{max} ranges from 381 °C (Sample GT-17) to 612 (sample GT-22). Thus GT-12 and GT-20 with T_{max} values of 409–412 °C reflect the occurrence of immature kerogen (Fig. 4). Very low T_{max} values may be indicative of some form of soluble organic matter as found in case of Upper.

Disang samples GT-9, GT-14 and GT-17 which has T_{max} values of 381–394 °C. This may represent the pyrolysis of soluble asphaltenes rather than kerogen (e.g. Clementz et al. 1979). Very high T_{max} values of 521–612 °C may be indicative of post mature/overmature stage or the occurrence of gas. Thus, samples G-6, G-12, GT-7, GT-21, GT-22, TNGA, TNG-1 and SO-2 are indicative of overmature or gas stage.

The potential source rocks are classified as Poor <0–2.5, Fair = 2.5–5, Good = 5–10, Very Good 10–20 and Excellent >20 on the basis of TOC percentage (Peters and Cassa 1994). All the studied samples are in the category of poor potential source rock (Table 2). The low values of the TOC (<0.66 %) imply a poor potential for these samples.

Table 2 Rock-eval data of sample powders from the Disang group of the Manipur region, Manipur

Formation	Sample name	TOC (%)	S1 (mgHC/ g rock)	S2 (mgHC/ g rock)	S3 (mgCO₂/ g rock)	T_{max} (°C)	HI (mgHC/ g TOC)	OI (mgCO₂/ g TOC)	PI	MINC (%)	PO = S1 + S2	Richness	Hydrocarbon type S2/S3
U.D	G-5	0.02	0.01	0.03	0.28	561	150	1400	0.2	0.03	0.04	Poor	0.107
U.D	G-6	0.33	0.01	0.04	0.09	597	12	27	0.14	0.08	0.05	Poor	0.44
U.D	G-12	0.4	0.01	0.04	0.17	602	10	42	0.21	0.54	0.05	Poor	0.23
U.D	GT-7	0.27	0.01	0.02	0.15	609	7	56	0.18	0.08	0.03	Poor	0.133
U.D	GT-9	0.36	0.01	0.05	0.08	386	14	22	0.15	0.1	0.06	Poor	0.625
U.D	GT-12	0.39	0.01	0.04	0.19	409	10	49	0.19	0.09	0.05	Poor	0.21
U.D	GT-14	0.31	0.01	0.04	0.06	394	13	19	0.18	0.13	0.05	Poor	0.666
U.D	GT-17	0.44	0.01	0.04	0.09	381	9	20	0.18	0.24	0.05	Poor	0.44
U.D	GT-20	0.21	0.01	0.02	0.11	412	10	52	0.21	0.32	0.03	Poor	0.18
U.D	GT-21	0.34	0.01	0.02	0.15	570	0	44	0.57	0.15	0.03	Poor	0.13
U.D	GT-22	0.66	0.01	0.05	0.08	612	8	12	0.23	0.3	0.06	Poor	0.63
L.D	TNG-A	0.13	0.01	0.01	0.22	594	8	169	0.46	0.07	0.02	Poor	0.045
L.D	TNG-1	0.39	0.01	0.03	0.06	609	8	15	0.17	0.96	0.04	Poor	0.5
U.D	SO-2	0.21	0.01	0.02	0.26	521	10	124	0.19	0.36	0.03	Poor	0.08

U.D Upper Disang formation and *L.D* Lower Disang formation

6 Characteristics of Organic Matter

The most often encountered dispersed organic matters in the samples include amorphous organic matter, charcoal, black debris, spore and pollen and structural terrestrial organic matter (biodegraded or partly biodegraded) (Table 3). Other matters, such as fungal remains and resin, are also encountered but always rare and thus not presented in the table.

Table 3 Distribution of organic matters to the upper Disang formation at Gelmoul quarry, Manipur

Sample name	Amorphous organic matter (AOM) %	Charcoal (%)	Black debris (%)	Structural terrestrial organic matter (%)	Spores and pollen
GT-1	94	4	2	–	–
GT-2	33	40	24	3	–
GT-4	100	–	–	–	–
GT-5	96	–	4	–	–
GT-6	83	3	14	–	–
GT-7	100	–	–	–	–
GT-9	90	–	10	–	–
GT-10	32	15	47	6	–
GT-12	96	2	2	–	–
GT-13	90	10	–	–	–
GT-14	70	17	8	5	–
GT-15	72	3	12	13	–
GT-17	72	2	9	17	–
GT-19	98	–	–	2	–
GT-20	93	7	–	–	–
GT-21	44	3	41	12	–
GT-22	12	31	36	21	–
G-1	10	72	11	7	–
G-2	5	80	6	9	–
G-4	13	57	15	15	–
G-5	55	14	12	12	7
G-6	75	9	8	5	3
G-12	9	22	14	54	1
G-14	77	6	11	6	–
G-19	100	–	–	–	–
G-20	93	7	–	–	–

(a) **Organic Matter Facies**

All seventeen samples of the Upper Disang Formation exposed at the upper locality of Gelmoul quarry, Churachandpur i.e. GT-1, GT-2, GT-4, GT-5, GT-6, GT-7, GT-9, GT-10, GT-12, GT-13, GT-14, GT-15, GT-17, GT-19, GT-20, GT-21, GT-22 contain grey to yellow coloured amorphous organic matter. The abundance of this organic matter ranges from 12 to 100 %. The structural terrestrial matter ranges from 2 to 21 % while the charcoal is 2–40 %. The black debris ranges from 2 to 47 %. However, some samples are absent of charcoal, black debris, structural terrestrial organic matter (Table 3) except amorphous organic matter. The dino-flagellates and microforaminiferal linings have been reported after treatment of nitric acid and potassium hydroxide (Singh et al. 2013). However, the maturity of OM indicates overmaturation of organic matter to some samples according to very high T_{max} value. The rock is assessed to have potential for sourcing gaseous hydrocarbon with respect to the TOC value that ranges from 0.32 to 0.72 % (Berry et al. 1998; Mukherjee et al. 1990). Most of the samples indicate their potential as a source rock of gaseous hydrocarbon. Of them, the samples GT-2, 10, 21, 22 are of gas potential in consisting mainly of terrestrial plant debris (charcoals, black debris, structural terrestrial organic matter and pollen and spores).

Nine samples of the Upper Disang Formation collected from the same locality of lower part of Gelmoul quarry are G-1, G-2, G-4, G-5, G-6, G-12, G-14, G-19 and G-20. The organic matter of these samples are represented by amorphous organic matter (5–100 %), black debris (6–15 %), structured terrestrial organic matter (5–54 %), charcoal (6–80 %) and spores and pollen (1–7 %). However, some samples do not show the presence of charcoal, structured terrestrial, black debris and spores and pollen except amorphous organic matter. A few spores, pollen, dinoflagellates are present here. The Thermal Alteration Index (TAI) values (Fig. 5 d, h, i) recorded are above 3.5, suggesting highly mature to overmature mixed palynofacies and source potential for the gas generation.

(b) **Spores Colouration**

The TAI (Thermal Alteration Index) scale 1–5 is widely used in hydrocarbon exploration. Among them, the one of Staplin (1969) is considered as the simplest and the most popular for evaluating the maturity of organic matters based on changes in spores colour. This technique is conducted in the present study, too, though it can only be taken on a few samples due to the absence of spores and pollen in all the samples. Of these samples namely G-5, G-6 and G-12, the TAI values of spores recorded are greater than 3.5, suggesting a high mature to over-mature nature of the organic matter and thus at a gas generation stage for Disang Group of Manipur. It also indicates that the maturity level of organic matter is at higher temperature (above 200 °C) under the metagenesis process.
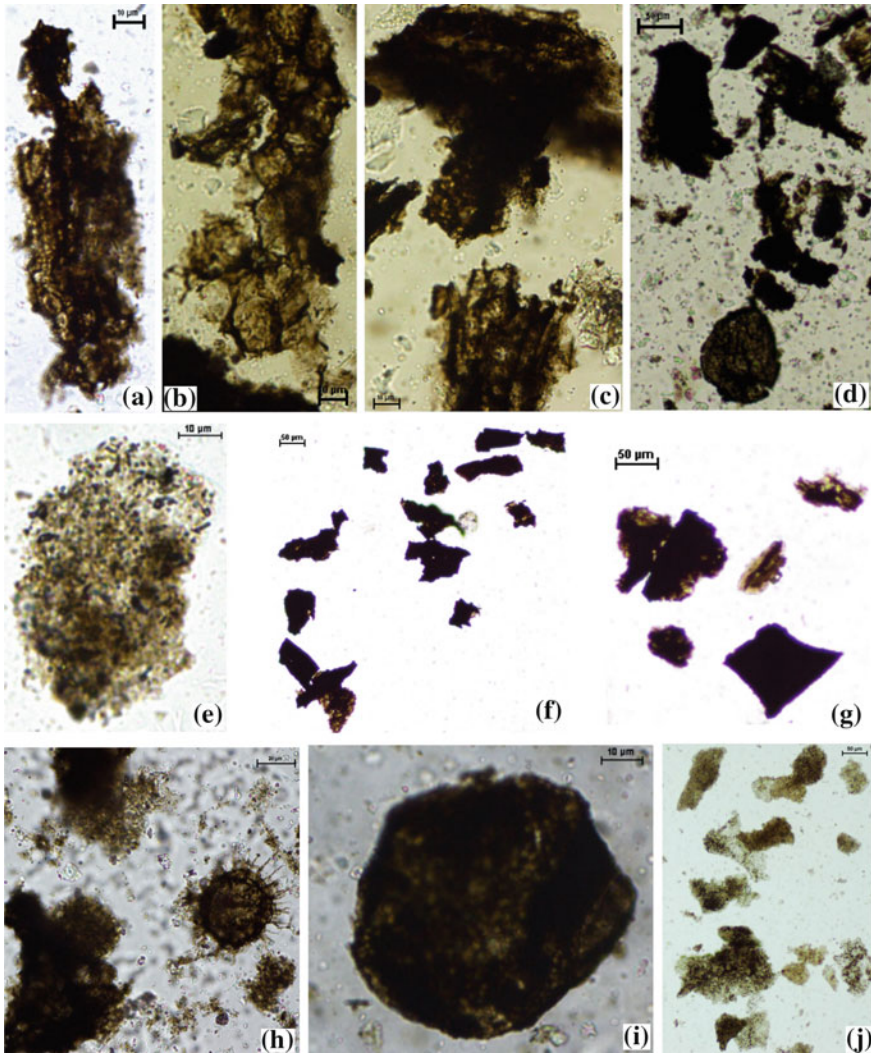
Fig. 5 **a–c** Partly biodegraded terrestrial organic matter, **d** spores with charcoal organic matter, **e** sapropelic amorphous organic matter with pyrite, **f, g** black debris, **h** dinocyst and associated amorphous organic matter, **i** spore showing high TAI value, **j** Sapropelic amorphous organic matter

7 Conclusions

Rock-Eval and TOC analysis of Disang rocks indicate that all the samples have poor organic richness (TOC < 0.5 %) and poor hydrocarbon generation potential (S2 < 0.5 mgHC/g rock). The organic matter content is predominantly of type III

and type IV. The T_{max} and Productive index values support the findings of visual kerogen analysis. Most of the kerogens are of low level of maturity because of light colour of amorphous kerogens. Low T_{max} values and low production index obtained for these samples also confirm their low maturity. The amorphous organic matter is more abundant than other types of organic matter. The source rock potential of Disang rocks recorded the different types of organic matter such as charcoal, partly biodegraded terrestrial, amorphous, black debris, spores and pollens. TAI values suggest highly mature to overmature mixed palynofacies. The source rock potential for the Disang Group of Manipur appears poor to moderate for gaseous hydrocarbons.

References

Acharyya SK, Roy DK, Mitra ND (1986) Stratigraphy and palaeontology of the Naga Hills ophiolite belt. Mem Geol Surv India 119:64–74

Acharyya SK, Ray KK, Roy DK (1989) Tectonostratigraphy and emplacement history of the ophiolite assemblage from Naga Hills and Andaman island-arc. India J Geol Soc India 33:4–18

Anonymous (2011) Geology and mineral resources of Manipur, Mizoram, Nagaland and Tripura. Geol Sur India Misc Publ 30 (4), 1(2):8–29

Batten DJ (1981) Palynofacies, organic maturation and source potential for petroleum. In: Brooks J (ed) Organic maturation studies and fossil fuel exploration. Academic Press, London, pp 201–224

Batten DJ (1996) Palynofacies and palaeoenvironment interpretation. In: Jansonius J, McGregor DC (eds.) Palynology: principles and application. American association of stratigraphic palynologists foundation, vol 3, pp 1011–1064

Berry CM, Pundeer BS, Mukherjee BK (1998) Hydrocarbon potential of Subathu sediments in Jammu-Kashmir, Himachal Pradesh and Uttar Pradesh areas-A palynological perspective. Bull ONGC 35:1–16

Chungkham P, Jafar SA (1998) Late Cretaceous (Santonian-Maastrichtian) integrated coccoliths, globotruncanid biostratigraphy of pelagic limestone from the accretionary prism of Manipur, Northeastern India. Micropalaeont 44:69–83

Chungkham P, Mishra PK, Jafar A (1992) Late and terminal cretaceous foraminifers assemblages from Ukhrul, Melange zone. Manipur Curr Sci 62:478–481

Clementz, DM, Demaison GJ, Daly AR (1979) 11th Annual offshore Technology Conference, Houston, Paper No. 3410, pp. 465–469

Ercegovac M, Kostic A (2006) Organic facies and palynofacies: nomenclature, classification and applicability for petroleum source rock evaluation. Int J Coal Geol 68:70–78

Espitalié J, Madec M, Tissot B (1977) 9th Annual Offshore Technology Conference, Houston, Paper No. 2935, pp. 439–444

Espitalié J, Marquis F, Barsony I (1984) Geochemical logging. In: Voorhees KJ (ed) Analytical pyrolysis: techniques and applications. Butterworth, London, pp 276–304

Evan P (1932) Explanatory notes to accompany a table showing the tertiary succession in Assam. Trans Min Geol Inst India 27:155–260

Faegri K, Iversen J (1989) Text book of pollen analysis. Wiley, New York, pp 1–328

Hunt JM (1996) Petroleum geochemistry and geology, 2nd edn. W.H. Freeman and Company, New York, p 743

Masran ThC, Pocock SAJ (1981) The classification of plant-derived particulate organic matter in sedimentary rocks. In: Brooks J (ed) Organic maturation studies and fossil fuel exploration. Academic Press, London, pp 145–175

Mukherjee BK, Tondon AN, Rawat CPS (1990) Geology and source rock evaluation of lower tertiary and sub-tertiary sequence in Himalayan Foothills: ONGC report-unpublished

Nany DR (1980) Tectonic pattern of Northeastern Indian and adjoining region. Indian Journ Earth Sci 7:103–107

Palmer SK, Zumberge JE (1981) Organic geochemistry of upper Miocene evaporate deposits in Sicilian basin, Sicily. In: Brooks J (ed) Organic maturation studies and fossil fuel exploration. Academic Press, London, pp 393–426

Pascoe EH (1914) The petroleum occurrences of Assam and Bengal. Mem Geol Surv India XL (2): 270–329

Peters KE, Cassa MR (1994) Applied source rock geochemistry. In: Magoon LB, Dow WG (Eds.) The petroleum system-from source to trap. AAPG Memoir 60, Tulsa: American association of petroleum geologists, pp 93–120

Sijagurumayum U, Singh YR, Kachhara RP (2011) Some mollusca from the upper Disang sediments exposed at Changamdabi, East Imphal district, Manipur. J Palaeontol Soc India 56 (2):165–169

Sijagurumayum U, Singh YR, Kachhara RP (2014) Eocene molluscan fossils from the upper Disang formation of Imphal valley, Manipur, India. J Palaeontol Soc India 59(1):59–68

Singh YR, Li J, Singh BP, Guruaribam V (2013) Microforaminiferal linings from the upper part of the upper Disang formation at Gelmoul quarry, Churachandpur, Imphal valley and their bearing on palaeoenvironment. Curr Sci 105:1223–1226

Singh YR, Meera N (2013) Source rock palynology of Disang sediments of Imphal valley. Manipur J Earth Sci pp 239–246 (Spl. volume)

Singh YR, Sijagurumayum U, Devi RKR (2010) Preliminary studies of fossils from the Palaeogene rocks exposed around Changamdabi area, Manipur. Mem Geol Soc India 75:143–148

Soibam I (1998) On the geology of Manipur. In: Souvenir, IX Manipur Science Congress, pp 12–19

Staplin FL (1969) Sedimentary organic matter, organic metamorphism and oil and gas occurrence. Bull Petrol Geol 17:47–66

Stein R (1991) Accumulation of organic carbon in Marine sediment. In: Bhattarcharji S (eds.) Lecture notes in Earth Sciences. Springer, Berlin 217 p

Stein R, ten Haven HL, Littke R, Rullkotter J, Welte DH (1989) Accumulation of marine and terrigenous organic carbon at upwelling Site 658 and nonupwelling sites 657 and 659: implications for the reconstruction of paleoenvironments in the eastern subtropical Atlantic through late Cenozoic times. In: Ruddiman WF (eds.), Proceedings of the ODP, science results, 108, college station, Tx (Ocean Drilling Program), pp 361–386

Terry RD, Chilingar GV (1955) Summary of "Concerning some additional aids in studying sedimentary formations". J Sediment Petrol 25:229–234

Tissot B, Welte DH (1984) Petroleum formation and occurrence, 2nd edn. Springer, Heidelberg

Theobald W (1871) The axis group in Western Prome, British Burma. Rec Geol Surv India 4:33–34

Tyson RV (1995) Sedimentation of organic matter: organic facies and palynofacies. Chapman and Hall, London 615p

Venkatachala BS (1981) Hydrocarbon source rock evaluation—a new palynological approach. J Petrol Asia 4:79–94

Identifying Relationship Amongst Vitrinite/Inertinite Ratio (V/I), Cleat Parameters, Vitrinite Reflectance, O/C Ratio and Permeability of Coal Seams and V/I Ratio as Exploration Tool: Study from Raniganj Coal Bed Methane Block, Essar Oil Limited, India

Souvik Sen and Satabdi Banerjee

Abstract Maceral data obtained from petrographic analyses was studied to determine the Vitrinite/Inertinite ratios (V/I) of different coal seams encountered in the core holes drilled at Raniganj Coal bed Methane block of Essar Oil Limited, India. Cleat density and spacing, vitrinite reflectance; O/C ratio and permeability data were studied and plotted against V/I ratio for different coal seams. Correlations between these parameters suggest that the V/I ratio is an effective tool to identify the coal seams with high cleat density, low cleat spacing and substantial permeability. These may facilitate to identify coal bed methane fairway. The V/I ratio is an effective tool for coal bed methane exploration.

Keywords V/I ratio · Cleat density · Cleat spacing · O/C ratio · Permeability

1 Introduction

Driven both by increasing energy shortages and environmental concerns, gas extraction from coal seams has attained global attention. In recent years, coal bed methane gas (CBM) has become an important source of energy in India to partially fulfill its growing energy demand. The Raniganj coal field in eastern India presently experienced a surge in CBM activities and more than 100 wells have been producing gas economically. The Raniganj CBM block of Essar locates at the easternmost part of Raniganj coal field (Fig. 1). Essar completed exploration phases and

S. Sen (✉) · S. Banerjee
Department of Geology and Geophysics, Essar Oil Limited (E&P), WEBEL IT Park,
Surya Sen Sarani, Near Gandhi More, Durgapur, West Bengal 713208, India
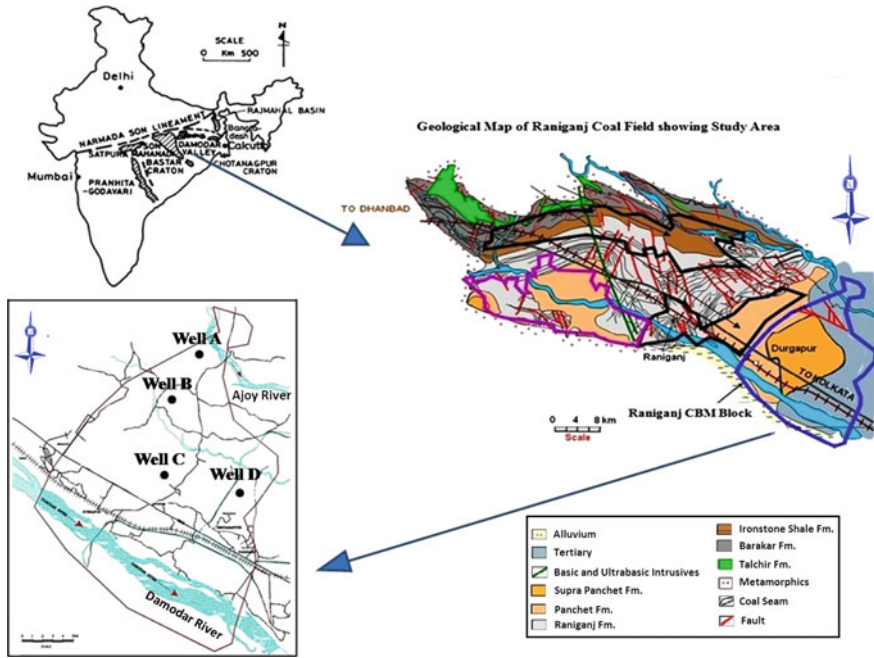e-mail: souvikseniitb@gmail.com

Fig. 1 Raniganj coal field and CBM block showing studied four core well locations

the block is presently in a development phase. Coal cores taken during exploratory phase were analyzed in the lab and the key CBM parameters were identified.

Petrographic analyses of coal yield information on a number of its physical components. Macerals determined are defined by the International Committee for Coal Petrology (ICCP 1963, 1971, 1975 and 1993). Maceral data is used to determine the V/I ratio seam-wise, which is the ratio of vitrinite over inertinite. This indicates the redox condition, i.e. the degree of oxidation and relative dryness/wetness of peat. This is the autochthonous peat forming conditions. V/I ratio can be used as inverse index of the degree of oxidation where the original peat was exposed (Harvey and Dillon 1985).

Cleats are natural opening-mode fractures formed in coal. Cleats usually occur in two sets that are, in most instances, mutually perpendicular and also perpendicular to bedding (Laubach et al. 1998). They account most of the permeability and much of the porosity of coal bed gas reservoirs and serve as permeability avenues for Darcy flow of fluids (gas and water) to the wellbore during production (Laubach et al. 1998). Cleats form by interdependent influences of desiccation, lithification, coalification and paleotectonic stress (Laubach et al. 1998). Cleat density and spacing are two important cleat parameters that directly affect coal permeability and hence production of coal bed methane. Cleat density is the number of cleats per unit length. Cleat density and cleat spacing are related inversely.

Vitrinite reflectance (VRo %) is defined as the percentage of vertically incident light reflected from a polished vitrinite surface within the coal. It is a measure of thermal maturity of organic matter and it ranks the maturity of coal (Cardott 2012; Mukhopadhyay and Dow 1994).

Permeability is a measure of ability of a porous material to allow fluids to flow. 'Darcy' is its unit of measurement. Coal cleat is important in enhancing CBM potential, as it is these interconnected fracture networks (permeability) that allow fluids (water and gas) to move through the coals and into a well bore for production (Laubach et al. 1998).

This study describes the relation between the V/I ratio and other coal parameters viz. cleat density, cleat spacing, vitrinite reflectance, O/C ratio and permeability and establishes V/I ratio as a CBM exploration tool.

2 Geology

The Raniganj Basin is semi-elliptical and covers ~ 3000 km^2 between the Damodar and Ajoy rivers, West Bengal, India (Fig. 1). The Raniganj CBM block of Essar Oil Limited lies in the easternmost part of the Raniganj Coal Field. Table 1 (Ghosh et al. 1996) presents the stratigraphy. Mainly soil and alluvium, and laterite capping at places cover the block. Below laterite or alluvium, in the northern part of the block, the Raniganj Formation is underlain by the Iron Stone Shale Formation. Towards E and S, the surface cover progressively overlies younger rocks i.e. Panchet Formation and the Tertiary sediments. In the eastern part of the block, the Rajmahal Volcanics (Trap rocks) are overlain by the Tertiary sediments (majorly sandstone and clay). This obscures the eastern limit of the coalfield.

We studied four cores from Wells A, -B, -C and -D. The wells encountered lithounits of Raniganj Formation containing fine- to coarse grained sandstones, shales, carbonaceous shales, siltstones and coal seams. These deposited in a fluvial depositional environment in Late Permian. Geophysical logs of the core holes from study area recorded six major group of coal seams regionally within 550–1450 m. Laboratory studies of coal core samples reveal them to be enrich in volatile and deficient in sulphur. These are coals of bituminous B–C in rank. Petrographic analyses revealed vitrinite and inertinite to be the major maceral constituents varying between 65.81–83.45 % and 8.49–22.28 %, respectively, on mineral matter free basis.

3 Analytical Approach

V/I ratio, cleat parameters, vitrinite reflectance, ash content, O/C ratio and permeability data were obtained from the analyses of core samples. Petrographic analyses quantify macerals. Vitrinite and inertinite contents were measured on mineral matter free basis and their ratio has been taken as V/I.

Table 1 Regional stratigraphic sequence in Raniganj Basin (modified after Ghosh et al. 1996)

Geological Age		Formation		Maximum Thickness (m)
Tertiary		Bengal basin clay, sand and limestone		300+
--*Unconformity*--				
Jurassic-Cretaceous		Rajmahal traps-intertrappeans		85+
--*Unconformity*--				
Triassic	Later	Supra-Panchet		200-300
	------------------------------------*Angular Unconformity*--			
	Early	Panchet		~600
------------------*Mostly gradational contact, Unconformity (local)/overlap at places*------------------				
Permian	Later	Raniganj	Damuda Group	1000
		Ironstone Shale		900
	Middle	Barakar		600
	Early	Talchir		300
--*Unconformity (erosional)*--				
Precambrian		Metamorphic rocks/Granite gneiss, schist with pegmatite and intrusives of metadolerite, dolerite and lamprophyre		

$$V/I = Vitrinite/Inertinite \qquad (1)$$

where Vitrnite represents [(mild aerobic ± molecular) oxidation + (biochemical + geochemical) gelification—rank changes to inertinite]. Inertinite represents [primary inertinite + severe or prolonged oxidation ± transportation + geological age + rank changes from vitrinite]. These are as per Harvey and Dillon (1985). They used Vitrinite/Inertinite ratio to indicate the degree of primarily aerobic oxidation related to the position of the water table relative to the peat surface.

Cleat parameters i.e. cleat density (number of cleats per cm) and cleat spacing (in millimeter) were measured directly from the coal cores. The methodology and procedure used for vitrinite reflectance measurements are standardized in the ISO 7404-5 (2009) and ASTM D2798-09a (ASTM 2010) norms for coals. Permeability of coal seams is mainly due to cleat network system. Permeability data came from Injection Fall-off test of the wells. In this test, first pressure is altered within the reservoir by injecting fluid into the formation followed by a shut in period to depressurize the well called pressure fall off period; pressure response of well is monitored as a function of time by sensitive pressure gauge suspended on a wire-

line close to the perforation (Earlougher 1977). A reservoir simulator is used to analyze and interpret the measured pressure drawdown response. It estimates reservoir permeability and skin factor (Ehlig-Economides et al. 1990). Normally low injection rate is maintained for low permeability coal reservoirs and the test does not exceed the formation fracture gradient.

We performed ultimate analysis as per ASTM D3176-09 (ASTM 2009). Carbon content was inherited from ultimate analysis. Oxygen content was determined by difference and O/C ratio has been calculated seam-wise.

4 Results

V/I data was plotted with cleat density, cleat spacing, vitrinite reflectance, O/C ratio and permeability. Tables 2, 3, 4, 5 and 6 present the dataset. Here the vertical arrangement of data is as per depth. Top–bottom in rows represent shallower to deeper coal seams. There is no systematic depthwise change of the studied parameters.
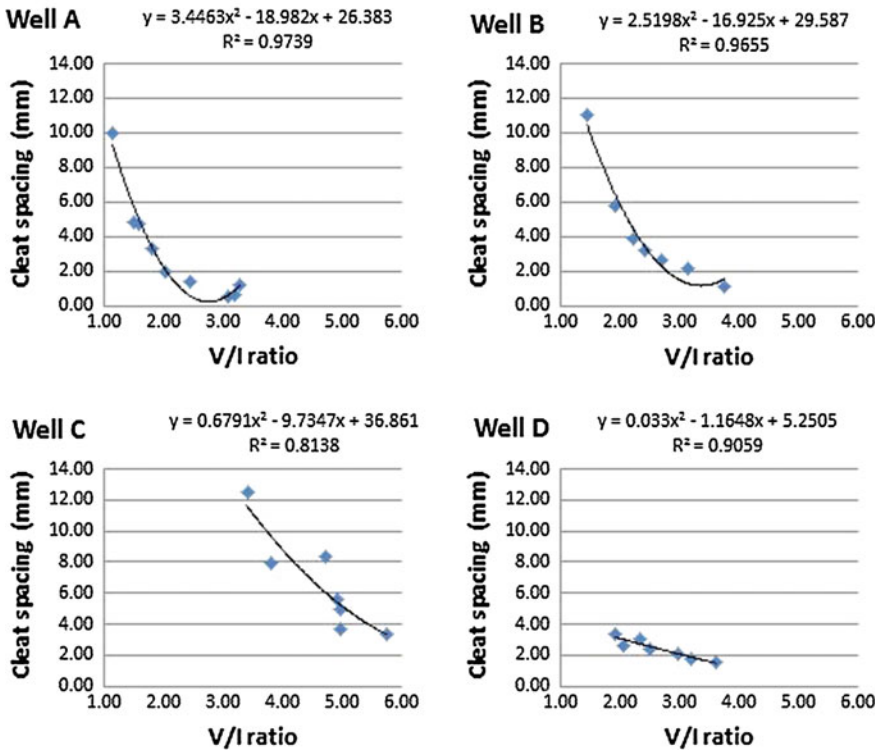
Fig. 2 Variation of cleat spacing (in millimeter) with V/I ratio in four wells of study area, Raniganj CBM block

4.1 Relation Between V/I and Cleat Parameters

The V/I ratio ranges 1.13–5.76 and cleat spacing 0.50–12.50 mm (Table 2). The cleat density ranges 0.86–20 per cm (Table 3). Cleat spacing versus V/I ratio was plotted for four core holes (Fig. 2). Result shows that cleat spacing decreases as V/I increases. On the other hand, V/I increases with cleat density (Fig. 3).
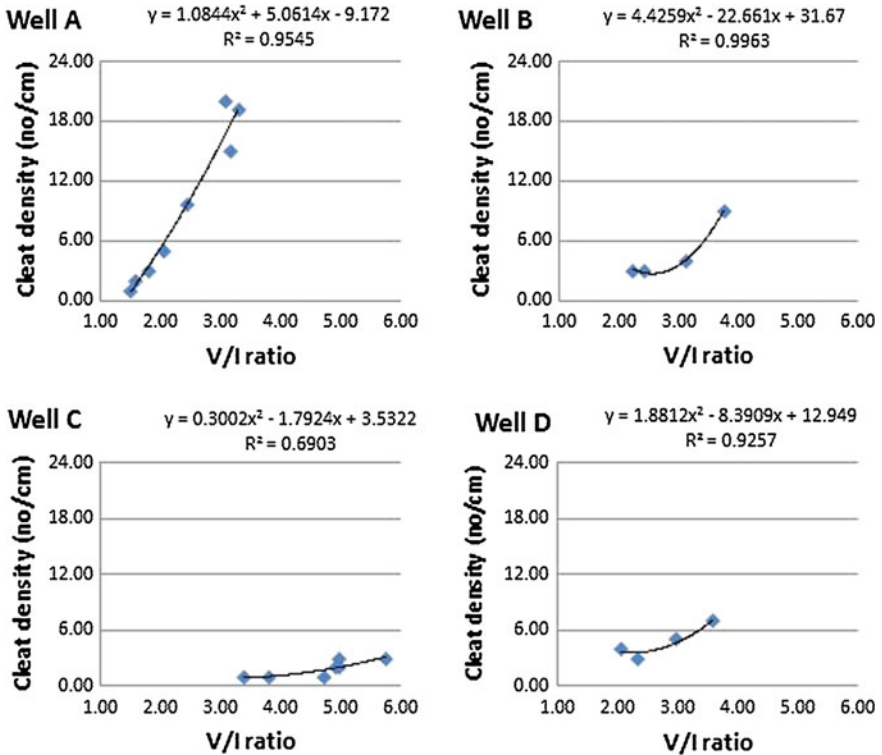

Fig. 3 Variation of cleat density (number of cleats per cm) with V/I ratio in four wells of study area, Raniganj CBM block

Table 2 V/I ratio and Cleat spacing (mm) of core holes Well A, B, C and D, Raniganj CBM Block, India

Well A		Well B		Well C		Well D	
V/I	Cleat spacing (mm)	V/I	Cleat spacing (mm)	V/I	Cleat spacing (mm)	V/I	Cleat spacing (mm)
1.57	4.77	2.41	3.24	5.76	3.33	2.33	3.01
2.04	2.01	2.22	3.93	4.99	3.67	2.06	2.66
3.29	1.23	3.75	1.08	3.39	12.50	2.97	2.10
3.08	0.50	3.13	2.22	4.72	8.41	3.60	1.50
3.18	0.67	1.44	11.02	3.81	7.91	2.5	2.42
1.79	3.34	1.91	5.77	4.99	5.00	1.9	3.31
1.5	4.91	2.7	2.61			3.2	1.83
2.44	1.45						
1.13	9.99						

Table 3 V/I ratio and cleat density (number of cleats per cm) of core holes Well A, B, C and D, Raniganj CBM Block, India

Well A		Well B		Well C		Well D	
V/I	Cleat density (no/cm)	V/I	Cleat density (no/cm)	V/I	Cleat density (no/cm)	V/I	Cleat density (no/cm)
1.57	2.00	2.41	3.00	4.93	2.00	2.33	3.00
2.04	5.00	2.22	3.00	5.76	3.00	2.06	4.00
3.29	19.20	3.75	9.00	4.99	3.00	2.97	5.00
3.08	20.00	3.13	4.00	3.39	1.00	3.60	7.00
3.18	15.00	1.44	8.29	4.72	1.00		
1.79	3.00	1.91	4.63	3.81	1.00		
1.5	0.86	2.7	2.89	4.99	2.00		
2.44	9.63						

4.2 Relation Between V/I Ratio and Vitrinite Reflectance

Vitrinite reflectance ranges 0.50–0.77 % (Table 4) suggesting sub-bituminous rank of coal. Vitrinite reflectance of the respective coal seams were plotted against V/I ratio. The data set shows V/I ratio increases with VRo % (Fig. 4).
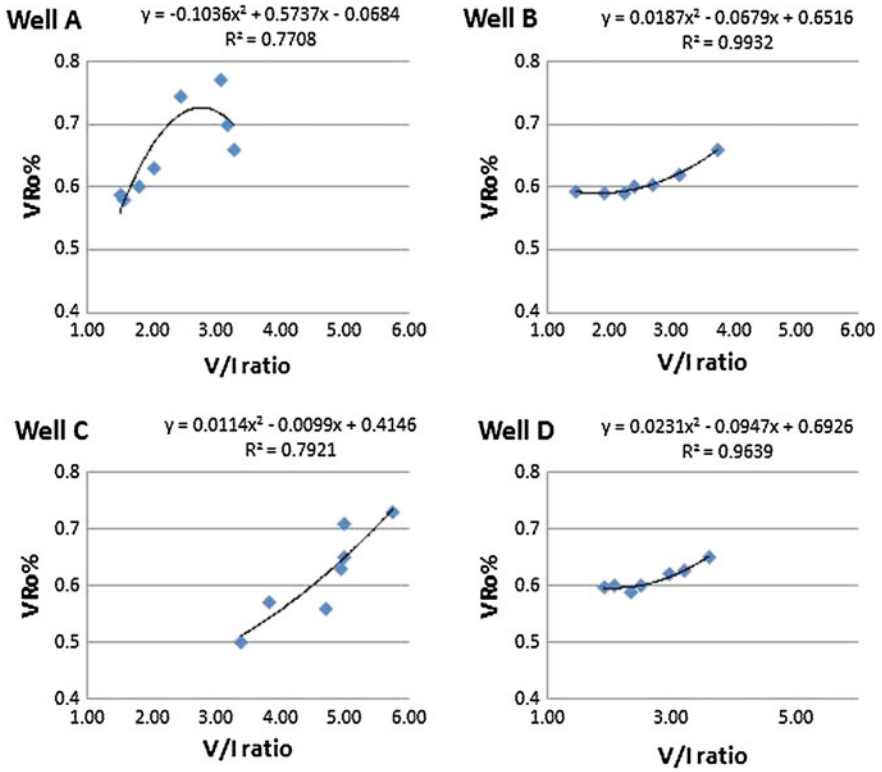
Fig. 4 Variation of vitrinite reflectance (VRo %) with V/I ratio in four wells of study area, Raniganj CBM block

Table 4 V/I ratio and VRo % of core holes Well A, B, C and D, Raniganj CBM Block, India

Well A		Well B		Well C		Well D	
V/I	VRo %	V/I	VRo %	V/I	VRo %	V/I	VRo %
1.57	0.58	2.41	0.6	4.93	0.63	2.33	0.59
2.04	0.63	2.22	0.59	5.76	0.73	2.06	0.6
3.29	0.66	3.75	0.66	4.99	0.71	2.97	0.62
3.08	0.77	3.13	0.62	3.39	0.5	3.60	0.65
3.18	0.7	1.44	0.59	4.72	0.56	2.5	0.60
1.79	0.6	1.91	0.59	3.81	0.57	1.9	0.60
1.5	0.59	2.7	0.60	4.99	0.65	3.2	0.63
2.44	0.74						

4.3 Relation Between V/I Ratio and O/C Ratio

The O/C ratio was calculated from the ultimate analysis data and plotted against V/I. The O/C ranges 0.35–0.90 (Table 5). When O/C was plotted against V/I ratio, their inverse relation was clear (Fig. 5).
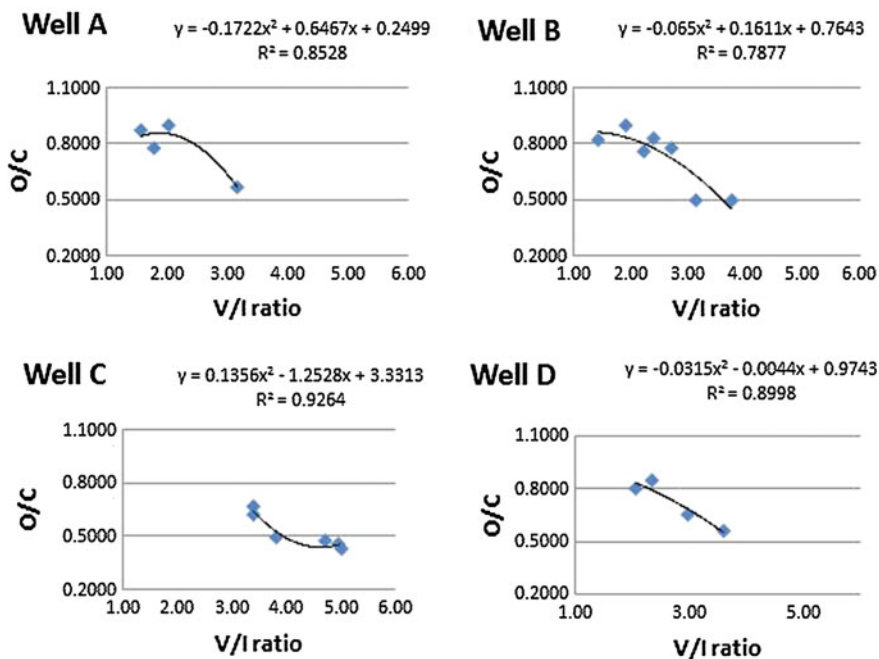
Fig. 5 Variation of O/C ratio with V/I ratio in four wells of study area, Raniganj CBM block

Table 5 V/I ratio and atomic O/C ratio of core holes Well A, B, C and D, Raniganj CBM Block, India

Well A		Well B		Well C		Well D	
V/I	O/C	V/I	O/C	V/I	O/C	V/I	O/C
1.57	0.8772	2.41	0.8301	4.93	0.4548	2.33	0.8480
2.04	0.9003	2.22	0.7582	3.39	0.6283	2.06	0.8001
3.18	0.5649	3.75	0.5022	3.39	0.6681	2.97	0.6497
1.79	0.7738	3.13	0.4999	4.72	0.4748	3.60	0.5611
		1.44	0.8205	3.81	0.4995		
		1.91	0.8993	4.99	0.4298		
		2.7	0.7734				

4.4 Relation Between V/I Ratio and Permeability

Table 6 presents permeability magnitudes for the coal seams. Permeability versus V/I plots reveal that permeability increases with V/I (Fig. 6). The permeability dataset does not show visually any relation with depth.
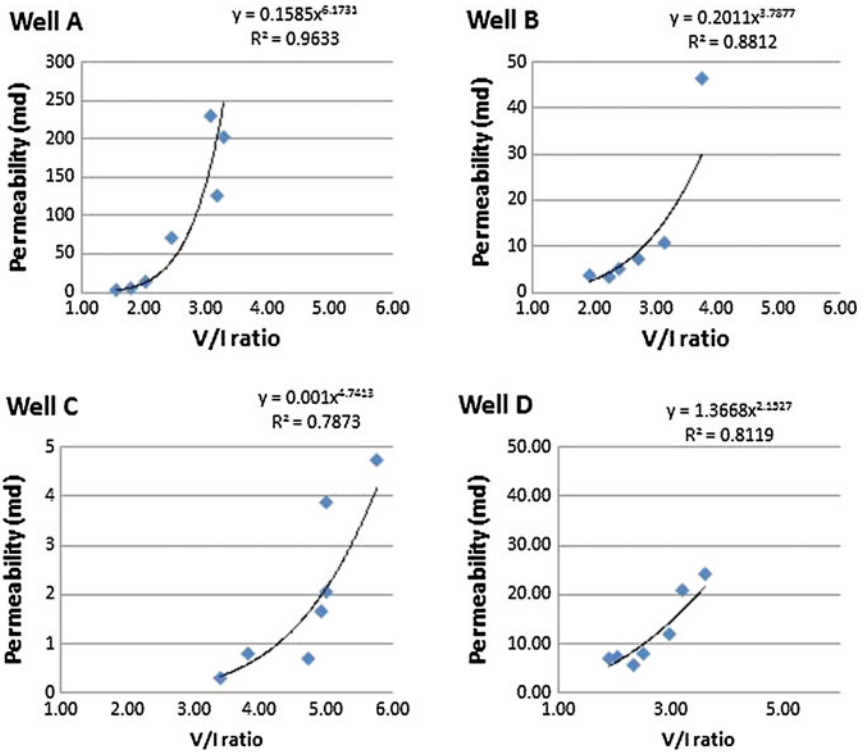

Fig. 6 Variation of permeability (mili darcy) with V/I ratio in four wells of study area, Raniganj CBM block

Table 6 V/I ratio and permeability (mili darcy) of core holes Well A, B, C and D, Raniganj CBM Block, India

Well A		Well B		Well C		Well D	
V/I	Permeability (mdarcy)	V/I	Permeability (mdarcy)	V/I	Permeability (mdarcy)	V/I	Permeability (mdarcy)
1.57	2.28	2.41	5.01	4.93	1.66	2.33	5.83
2.04	13.3	2.22	3.38	5.76	4.73	2.06	7.46
3.29	201.69	3.75	46.48	4.99	3.88	2.97	12.08
3.08	229.15	3.13	10.78	3.39	0.32	3.60	24.17
3.18	125.69	1.91	3.55	4.72	0.72	2.5	8.04
1.79	4.7	2.7	7.13	3.81	0.81	1.9	6.99
2.44	71.5			4.99	2.07	3.2	21.05

5 Discussions and Conclusions

High vitrinite and moderate to low inertinite content characterize the coal samples. High vitrinite content i.e. high V/I possibly indicate that the peat swamps promoted humification of bark and woody tissues (Suwarna and Hermanto 2007). However, vitrinite does not always relate to trees/woody plants (Scott and Glasspool 2007). Majority of the 'wood' in Late Carboniferous mires was actually lycopsid bark (DiMichele and Phillips 1994) and this had a chemical structure distinct from that of wood (Collinson et al. 1994). Additionally, tree ferns (which dominated Late Carboniferous coal-forming environments) were constructed largely of parenchymatous, non-woody tissues (DiMichele and Phillips 1994).

High vitrinite and low inertinite content indicate the absence of severe oxidation and dehydration during peat accumulation (Suwarna and Hermanto 2007). Vitrinite rich coals deposited presumably in wet and more anoxic environments. Relatively narrow range of V/I suggest that redox condition of peat remained unaltered when it accumulated. High V/I indicates aqueous to sub-aqueous condition in the swamp i.e. the peat accumulation was governed by a high groundwater level. This maintained the reducing environment in the peat land.

Abundant vitrinite with respect to intertinite (i.e. V/I > 1) indicates a telmatic environment; wet forest swamp (Teichmüller and Teichmüller 1982; Bustin et al. 1985), mainly from arborescent vegetation (Rimmer and Davis 1988) with highly reduced condition that prevailed during the coal-precursor deposition. Organic facies was interpreted from the petrographic indices, derived from maceral analysis. The facies indicates that the Raniganj coals deposited possibly in a wet limnic-telmatic zone with limited-clastic influx and little microbial attack activity. It could be a telmatic wet forest swamp under rapid burial condition. However, whether coal petrographic indices can interpret the peat forming environment and vegetation is questioned. Inappropriate use of the index has been discussed by others (Collinson and Scott 1987; Scott 1989b, 1991, 2002; DiMichele and Phillips 1994; Wüst et al. 2001; Moore and Shearer 2003; Scott and Glasspool 2007).

The study reveals that with the increase of V/I ratio value, cleat density, VRo % and permeability increase. As V/I increases, cleat spacing, ash content and O/C values decrease.

- Coal bed methane extraction and development requires knowledge of natural fractures i.e. cleats. Cleats influence recovery of methane, and the local and regional flow of fluids (hydrocarbon and water). Seams with higher V/I have higher cleat density and lower cleat spacing.
- Vitrinite Reflectance values increase with V/I. However, the relationship between vitrinite reflectance and V/I is only apparent. Vitrinite reflectance i.e. rank of the coal is not controlled by petrographic composition, but is due to subsidence (temperature) and exposure time to maximum temperature. The relationship between V/I and vitrinite reflectance in this study may suggest that for the set of studied coal seams the higher rank, i.e. higher vitrinite reflectance are characterized by higher vitrinite content.

- O/C ratio shows an inversely proportional relation with V/I. O/C indicates the degree of oxidation of organic materials in the forest mire. More the oxidation, higher will be the O/C and less will be the V/I.
- Most of the permeability in coal reservoir comes from cleat system. If all fractures in a coal bed were isolated, then flow rates observed (after draining those fractures directly intersected by the wellbore) would be limited by matrix permeability (i.e., no fracture enhancement of permeability) (Laubach et al. 1998). Inter-connected fractures enhance the permeability. For example, coal-bed permeability may be 3–10 times greater in the face cleat direction than in other directions (McCulloch et al. 1974). This reflects the preferred orientation and greater length of interconnection of fractures in that direction.

Seams with higher V/I have high cleat density as well as high permeability as supported by this study. V/I plays an important role in cleat formation, thus affect coal permeability to a greater extent.

Therefore this study suggests that V/I can be used as an exploration tool to identify coal seams with dense cleating and high permeability.

References

American Society for Testing and Materials (2009) ASTM D 3176-09, Standard practice for ultimate analysis of coal and coke

American Society for Testing and Materials (2010) ASTM D2798-09a, Standard test method for microscopical determination of the vitrinite reflectance of coal

Bustin RM, Cameron AR, Grieve DA, Kalkreuth WDm (1985) Coal Petrology, its principals, methods and applications, Victoria. British Columbia Canada, 2nd edn. pp 220–235

Cardott BJ (2012) Introduction to vitrinite reflectance as a thermal maturity indicator: AAPG search and discovery article No. 40928

Collinson ME, Scott AC (1987) Implications of vegetational change through the geological record on models for coal-forming environments. In: Scott AC (ed) Coal and coal-bearing strata: recent advances, vol 32. Geological Society of London Special Publication, London, pp 67–85

Collinson ME, Van Bergen P, Scott AC, de Leeuw J (1994) The oil-generating potential of plants from coal and coal-bearing strata through time: a review with new evidence from carboniferous plants. In: Scott AC, Fleet AJ (eds) Coal and coal-bearing strata as oil-prone source rocks, vol 77. Geological Society of London Special Publication, London, pp 31–70

DiMichele WA, Phillips TL (1994) Palaeobotanical and palaeoecological constraints on models of peat formation in the late carboniferous of Euramerica. Palaeogeogeogr Palaeoclimatol Palaeoecol 106:39–90

Earlougher RC Jr (1977) Advances in well test analysis, Monograph Series. Texas: SPE, 5

Ehlig-Economides CA, Joseph JA Ambrose RW Jr, Norwood C (1990) A modern approach to reservoir testing. *JPT* 42(12):1554–1563. SPE-19814-PA. DOI: 10.2118/ 19814-PA

Ghosh SC, Nandi A, Ahmed G, Roy DK (1996) Study of Permo–Triassic boundary in Gondwana sequence of Raniganj Basin. In: Proceedings IXth international Gondwana symposium. Oxford and IBH Publisher, New Delhi, pp. 195–206

Harvey RD, Dillon JW (1985) Maceral distributions in Illinois coals and their paleoenvironmental implications. Int J Coal Geol 5:141–165

ICCP, International Committee for Coal Petrology (1963) Handbook, 2nd edn. Centre, National de la Recherché Scientifique, Paris

ICCP International Committee for Coal Petrology (1971) International handbook of coal petrography, 1st supplement to 2nd edition. Centre National de la Recherché Scientifique, Paris

ICCP International Committee for Coal Petrology (1975) Analysis subcommission, fluorescence microscopy and fluorescence photometry and subcommission nomenclature. In: International handbook of coal petrography, 2nd supplement to 2nd edition. Centre National de la Recherché Scientifique, Paris

ICCP International Committee for Coal Petrology (1993) International handbook of coal petrography, 3rd Supplement to the 2nd edition. Centre National de la Recherché Scientifique, Paris

ISO 7404-5 (2009) Methods for the petrographic analysis of coal—Part 5: methods of determining microscopically the reflectance of vitrinite. International Organization for Standardization, Geneva, p 14

Laubach SE, Marrett RA, Olson JE, Scott AR (1998) Characteristics and origins of coal cleat: a review. Int J Coal Geol 35:175–207

McCulloch CM, Deul M, Jeran PW (1974) Cleats in bituminous coalbeds. U.S. Bur Mines, Rept. Invest. 7910, 23

Moore TC, Shearer JC (2003) Peat/coal type and depositional environment—are they related? Int J Coal Geol 56:233–252

Mukhopadhyay PK, Dow WG (eds) (1994) Vitrinite reflectance as a maturity parameter: applications and limitations. In: American chemical society symposium series, vol 570, p 294

Rimmer S, Davis A (1988) The influence of depositional environments on coal petrographic composition of the lower Kittanning seam, western Pennsylvania. Org Geochem 12:375–387

Scott AC (1989b) Deltaic coals: an ecological and palaeobotanical perspective. In: Whateley MKG, Pickering KT (eds) Deltas: sites and traps for fossil fuels, vol 41. Geological Society of London Special Publication, London, pp 309–316

Scott AC (1991) Applications of palaeobotany and palynology to coal geology. Bulletin de la Société Géologique de France 162:145–153

Scott AC (2002) Coal petrology and the origin of coal macerals: a way ahead? Int J Coal Geol 50:119–134

Scott AC, Glasspool IJ (2007) Observations and experiments on the origin and formation of inertinite group of macerals. Int J Coal Geol 70:53–66

Suwarna N, Hermant B (2007) Berau coal in East Kalimantan; its petrographics characteristics and depositional environment. J Geologi Indonesia 2(4):191–206

Teichmüller M, Teichmüller R (1982) Fundamental of coal petrology. In: Stach E, Mackowsky M-Th, Teichmüller M, Taylor GH, Chandra D, Teichmüller R (eds), Stach's textbook of coal petrology, 3rd ed. Gebrüder Borntraeger, Berlin, pp 535

Wüst RAJ, Hawke MI, Bustin RM (2001) Comparing maceral ratios from tropical peatlands with assumptions from coal studies: do classic petrographic interpretation methods have to be discarded? Int J Coal Geol 48:115–132

Plant-Microbe Association-Assisted Removal of Heavy Metals and Degradation of Polycyclic Aromatic Hydrocarbons

Hemen Sarma and M.N.V. Prasad

Abstract Contamination by polycyclic aromatic hydrocarbons and heavy metals is a rather serious problem across the world and poses a major threat to living organisms. These are considered to be carcinogens and are constituents of oil sludge. The magnitude of PAHs released into the environment has increased drastically in recent times. This is mostly due to petroleum waste or seepage during transportation of crude oil. There have been several instances of oil spills on the coasts of India and elsewhere. In northeast India, PAHs pollution is evident at the sites of drilling and refinery sites. The boiling points of high molecular weight PAHs are very high and they are almost difficult to decompose. Their hydrophobicity causes these compounds to accumulate and sequester in soil organic matter; thus, their desorption from soil limits the efficiency of biodegradation in situ. This chapter will focus on the various case studies where plant-microbe association has been used to assist bioremediation process of PAHs and heavy metals in oil-contaminated soil. Topics to be covered include how plants and microbes together effect the remediation process, bioavailability of PAHs, facilitating the movement of essential nutrients, air and water and production of biosurfactants in faster acceleration of the removal process.

Keywords Bioaugmentation · Biotransformation · Emulsified vegetable oil · Microbial consortia · Microbial degradation · Oil spills · Sludge and drilling fluids · Total petroleum hydrocarbons

H. Sarma
Department of Botany, N N Saikia College, Titabar, Assam 785 630, India

M.N.V. Prasad (✉)
Department of Plant Sciences, University of Hyderabad, Hyderabad, Telangana 500 046, India
e-mail: prasad_mnv@yahoo.com

1 Introduction

In today's world the environmental issue of the vast amount of petroleum waste in the form of oily sludge produced by petroleum industries and its storage, processing, transportation and disposal, has assumed enormous proportions. This amounts to a huge problem for petroleum producing countries. Processing and refining of crude oil generates a huge amount of sludge that is then stored in storage tanks. Oily sludge contains higher amount of heavy metals like nickel, chromium, zinc, manganese, copper, lead, etc. (Bhattacharyya and Shekdar 2003). This continues to gain global attention, mainly because of the toxicological risks posed by such metals to human health. Crude oil contains more than 17,000 organic compounds of which polycyclic aromatic hydrocarbons comprise up to 7 % in the total composition of Total Petroleum Hydrocarbons (TPH) (Mahler et al. 2005). They cause many serious health problems and diseases (such as cancer) around the world. TPH contamination is the result of extensive use of petroleum-based products and the potential sources of TPH infiltration into the environment include crude oil exploration and refining process, marine transportation, direct ocean dumping, coastal, municipal and industrial wastes, and runoff (Lucas et al. 2006).

Polycyclic aromatic hydrocarbons (PAHs) are recognized worldwide as priority pollutants because of their toxicity and carcinogenicity. PAHs along with other halogenated hydrocarbons present in crude oil create problems due their persistence in the environment. PAHs are almost difficult to decompose and are insoluble in water due to their high boiling points. Their hydrophobicity causes these compounds to accumulate and sequester in soil organic matter; thus, their desorption from soil limits the efficiency of biodegradation in situ (Maiti and Bhattacharyya 2012).

Crude oil is usually stored in storage tanks; these contain impurities present in the oil that are deposited at the bottom over a long period of time. During the cleaning process of these empty tanks, the tank bottom sludge is recovered and treated as waste. Sludge is generated from the waste water treatment plants too. In India, the average annual volume of oily sludge (a mixture of hazardous hydrocarbon waste) generated by oil refineries is approximately 28,000 tonnes (Bhattacharyya and Shekdar 2003). This is an alarming picture of environmental contamination that continues to expand rapidly across India. This waste residue is dumped into specially constructed sludge pits. These pits consist of a leachate collection system and polymer lining system to prevent the infiltration of heavy metals and PAHs into ground water (Bhattacharyya and Shekdar 2003). However, these pits face the drawback of being rather expensive to construct and maintain. Moreover, a large amount of land is required for this purpose and hence it is less popular because of the presence of unacceptably high levels of expenses entailed by it.

In northeastern India, crude oil was discovered in 1867 in Digboi in the state of Assam, where the first oil well in Asia was drilled. Since then, several oil wells have been drilled in various parts of upper Assam. Most oil drilling sites are located at the fringes of human settlements, paddy fields and tea gardens. A glimpse of some crude oil drilling sites and pipeline seepage is presented in Figs. 1 and 2
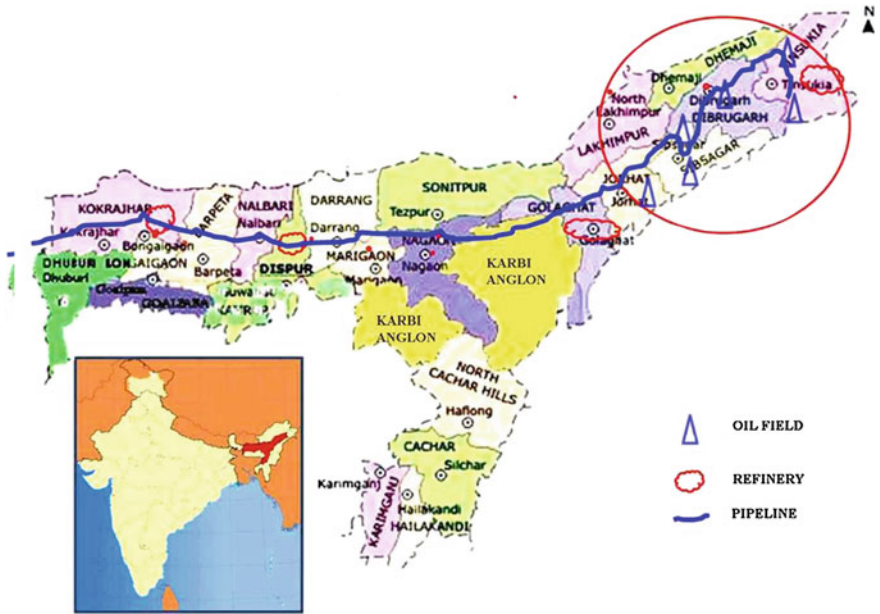
Fig. 1 Assam, one of the 7 North Eastern States of India is rich in oil fields and refineries with extensive networks of pipe line

Fig. 2 **a–d** Oil pipe lines, oil spills, sludge and drilling fluids

which show the extreme environmental impact of the contamination. During the transportation process of crude oil from drilling sites, high pressure generated in the pipeline causes leakage; this seepage into the adjacent soil and water ecosystems is detrimental to the surrounding flora and fauna. Furthermore, contamination might also take place due to seepage of crude oil from effluent pits and Group Gathering Stations/Oil Collecting Stations where crude oil is stored for refining purposes.

In general, oil enters into the ecosystem through various ways and some of the possible ways are:

1. Natural seeps from submarine deposits
2. Common tanker operations such as loading and unloading of oil and cleaning
3. Oil tanker accidents. For instance, 9 August 2010 was a black day in the shipping history of Mumbai when two ships collided, causing the MS Chitra to sink releasing up to 800 mt of fuel oil into the sea. The cargo also contained some toxic material though its release into the sea is still not known
4. Oil pipelines leakage. Due to the high viscosity of oil, it penetrates deep into the soil, reaching groundwater (Fig. 2)
5. Oil loss during drilling of oil wells in oil field or sea (Fig. 3)
6. Refining process of crude oil which produces waste.

Fig. 3 a–c Oil drenched mangroves in the western coast of India due to collision of two merchant ships releasing about 800 mt of oil into the sea

The biodegradation of PAHs is very difficult, particularly in case of high molecular weight PAHs compounds. Similarly, HMs are persistent in nature and not biodegradable. These pollutants accumulate in the soil system and enter into the food chain. The remediation of PAHs and HMs from soils is too expensive and time consuming. Several methods have been used to remediate contaminated soil that includes physical and chemical processes but these methods are found to be inefficient, and they also damage the natural structure and texture of the soil. Prospective new strategies to increase the bioavailability of PAHs and plant-microbe association (that accelerates removal of heavy metals and degradation of polycyclic aromatic hydrocarbons) are very important in the present context. The literature that addresses plant microbe consortia for the removal of heavy metals and PAHs in oil-contaminated sites is extensive. As we have observed in preparing this review, when assembled, it contributes to a clearer understanding of the pattern of accelerated removal of heavy metals and the degradation of polycyclic aromatic hydrocarbons by plant-microbe association. In this context, our goals in this review are

1. Evaluating the current research challenges in the acceleration of the removal process
2. Providing an insight into the role of plant microbes consortia in removal of PAHs and heavy metals
3. Highlighting the limitations and challenges associated with bioavailability of organic pollutants

2 Current Research Challenges in the Acceleration of the Removal Process

Polycyclic Aromatic Hydrocarbons (PAHs) and heavy metals (HM) are essential constituents of TPH which infiltrate into the environment (Pandey and Fulekar 2012); such infiltration poses a serious threat to environmental health. The molecular structure of PAHs reveals at least one cavity which is similar to many carcinogenic compounds that exist in the nature. They are persistent and nowadays create a real danger when they are accumulated in the biota in greater concentrations.

Heavy environmental metals which cannot be biologically degraded cause environmental problems. In fact, concentration of several HMs has now increased several folds. The estimated heavy metals load in recent decades has increased annually around 22,000 metric tonnes for cadmium, 939,000 metric tonnes for copper, 783,000 metric ton for lead and 1,350,000 metric ton for zinc (Singh et al. 2003); such high levels of enhancement of heavy metals in the environment is a consequence of industrialization and creates a grave concern for human health.

Oily waste penetrates and affects different ecosystems over a long period of time because of its persistent heavy metals (Table 1) and other non bio-degradable

Table 1 Heavy metals present in oily sludge (Bhattacharyya and Shekdar 2003)

Heavy metals	Concentration in oily sludge (mg/kg)
Nickel	17–25
Chromium	27–80
Zinc	7–80
Manganese	19–24
Cadmium	0.8–2
Copper	32–120
Lead	0.001–0.12

organics. Water containing even 1 ppm of oil becomes unfit for drinking and this is deleterious for diverse biota of any aquatic ecosystem. Besides, on the surface of open water, oily waste produces an emulsion layer that partially blocks gas exchange between water and air due to which the aquatic flora and fauna gradually suffocate and die.

The acceleration of the removal process of PAHs and heavy metals from contaminated sites has been an important challenge in recent research; such exercises have gained worldwide attention and researchers have conducted both ex situ and in situ experiments putting their best effort to the reclamation of oil polluting site. Moreover, fundamental aspects such as plant-microbe association, the screening of more hyperaccumulator plants (Sarma 2011), plant growth enhancing mechanisms, structural and functional changes in rhizosphere microbial communities in oily waste contaminated soil (Sarma and Sarma 2010; Wu et al. 2009; Chen et al. 2006), have gained attention in recent times.

TPH is lipophilic in nature and consists of alkanes, cycloalkanes, and PAHs. The main hydrocarbon categories are aliphatics, aromatics, asphaltenes and resins. Aliphatic hydrocarbons consist of alkanes, alkenes, alkynes and cycloalkanes, but aromatic hydrocarbons are monoaromatics and polycyclic aromatic hydrocarbons. The asphaltenes are phenols, fatty acids, ketones, esters and porphyrins, and the resins are pyridines, quinolines, carbazoles, sulfoxides and amides (Colwell and Walker 1977).

There are 16 PAHs that have been listed by the United States Environmental Protection Agency (US-EPA) as priority pollutants. PAHs do not degrade easily under natural conditions. Their persistence increases with increase in their molecular weight. They are present in all components of the environment; they are resistant to biodegradation and have a tendency for bioaccumulation which makes them key pollutants in crude oil (Haritash and Kaushik 2009). Some of these (with molecular weight of up to 202 g/mol), including pyrene and fluoranthene, have been degraded during aerobic reactions, but the remaining PAHs, such as benzo[a] pyrene, are only susceptible to co-metabolic removal. In the in situ experiment, it has been possible to identify that certain microorganisms co-metabolize these PAHs, but the same cannot not be ascertained in ex situ experiments. In addition to that, the production of sufficient microbial biomass is difficult in PAHs contaminated soil during in situ bioremediation process because hydrophobic PAHs are

bound tightly to the microbes in soil. Although there are developments in various bioremediation techniques for decontamination of total hydrocarbons including Polycyclic Aromatic Hydrocarbons, yet, in maximum cases, the success of these technologies is limited to low molecular weights PAHs only. It has already been reported that bacterial degradation of certain PAHs, such as naphthalene, phenanthrene and anthracene, has been possible; but such degradation of PAHs that contain more than five carbon rings such as benzo[a]pyrene and benz[a]anthracene, has still not been achieved (Peng et al. 2009). Biodegradation of polycyclic aromatic hydrocarbons (PAHs) is thus not so amendable to microbial degradation but has to be promoted further by rhizosphere effects of plants (Huang et al. 2004; Haritash and Kaushik 2009).

Usually, PAHs and long chain alkanes have low water solubility that reduces their bioavailability; this has been a critical limiting factor controlling growth and biodegradation rate for microorganisms (Koch 1990). This can be countered by using biosurfactants. Biosurfactants are metabolites that have been extensively tested for decontaminating areas polluted with heavy metals and PAHs. It is well established that biosurfactants have the capacity to solubilize and remove polycyclic aromatic hydrocarbons; many novel biosurfactants have in fact been characterized, including glycolipids, phospholipids, neutral lipids, fatty acids, peptidolipids, lipopolysaccharides (Banat 1995). Biosurfactants are generally nontoxic to microorganisms, especially hydrocarbon-degrading microorganisms (McCray et al. 2001). Biosurfactants with low critical micelle concentration (CMC) values and high degree of sorption to soil might have stronger abilities to remove oil from soil (Urum et al. 2004). Rhamnose lipids biosurfactants have been used for complexation of Pb^{2+}, Zn^{2+} and Cd^{2+} ions and maximum binding capacity on a molar basis of 0.2 Cd^{2+}/rhamnose lipid had been recorded. These potential applications emerge whenever the biological origin of biosurfactant promises better biocompatibility and good microbial degradability (Lang and Wullbrandt 1999). Besides, in bioremediation processes, the addition of composted or raw organic matter, and, sometimes, increasing the substrate levels for co-metabolism of the organic contaminants, accelerates the degradation of organic pollutants and the binding of metallic pollutants (Barker and Bryson 2002).

The microbial community structure changes periodically in soil contaminated with polycyclic aromatic hydrocarbons (PAHs) and the population count of both Gram-positive to Gram-negative bacterial depends on the extent of PAH losses in the soil (Antizar-Ladislao et al. 2008). The low molecular weight PAHs have been degraded in higher rates due to their increased solubility and bioavailability but the high molecular weight PAHs have a strong lipophilic character and are bound to the organic matrix of the soil in such a way that their bioavailability is less and hence their biodegradation is very slow.

Microbial consortium consisting of two strains of *Pseudomonas aeruginosa* and *Rhodococcal* species had earlier showed promising results where TPH degradation results were up to 90 % in liquid culture for the periods of six week (Cameotra and Singh 2008). Such degradation is also enhanced by rhamnolipid biosurfactant produced by the consortium.

Two bacterial strains *Bacillus subtilis* and *P. aeruginosa* have been isolated from petroleum contaminated soil samples from north-eastern India for the biodegradation of crude petroleum-oil hydrocarbons in soil and this has shown positive results for in situ bioremediation (Das and Mukherjee 2007). The microbes consortia (cyanobacteria, fungi and bacteria) credibly enhanced degradation of fuel oil where humidity, dissolved oxygen and nutrient availability were optimal (Gallego et al. 2006). Besides bacteria, many fungi are also capable of degrading PAHs, like *Trichoderma* sp for which there is a good deal of evidence. A maximum of 75 % removal for pyrene at 50 mg L^{-1} for axenic cultures of *Trichoderma* sp. has been recorded where pyrene served as the sole carbon source (Verma et al. 2007).

Petroleum sludge containing organics such as alkanes, aromatics, resins and asphaltenes can be degraded by the application of certain native strains like *Bacillus* sp, *Acinetobacter* and *Pseudomonas* sp. The ability of such bacteria to degrade the complex mixture of petroleum hydrocarbons from contaminated soil has in fact been actually carried out in Ankleshwar, India, (Verma et al. 2006) in which Bacillus sp. degraded TPH up to 59 % in total. The degradation effected by *Acinetobacter* sp. and *Pseudomonas* sp in particular were up to 37 and 35 % respectively.

The application of Plant Growth Promoting Rhizobacteria (PGPR) and specific microbes has been found to be effective and hence the use of plants-microbes with PGPR could become a model phytoremediation technique to treat TPHs (Zhuang et al. 2007). Phytoremediation is a green technology with the application of plants for in situ handling of polluted geo-surfaces, sediments, and water sources. This technique has been considered as one of the best remediation processes in recent times. This can be applied at sites with shallow contamination of organic, nutrient, or heavy metal pollutants that are open to one the following applications: Phytotransformation, Rhizodegradation, Phytostabilization, Phytoextraction, Phytovolatilization, Phytodegradation or Rhizofiltration. This also has certain advantages because of its cost effectiveness, and long-term practical applicability. Besides, it can be used as a polishing treatment in contaminated areas where low concentrations of pollutants exist for a longer period of time.

However, there are limitations to the use of phytoremediation. These include limited regulatory acceptance, extended time requirement, threat of contamination to grazing animals by entering into the food chain, and trouble in establishing and nurturing vegetation at some contaminated sites where pollution levels are extreme. Plants have a range of cellular mechanisms that demonstrate their capacity to resist high concentrations of organic pollutants without displaying toxic effects; such plants often accumulate and convert these organics into less toxic metabolites (Table 2). Furthermore, the release of root exudates, enzymes in rhizosphere and in the presence of organic carbon in the soil stimulates the degradation of organic contaminants in faster. On the other hand, in the remediation of metal contaminants, some plants have shown a potential role for phytoextraction (contaminants uptake and accumulate into aboveground biomass through xylem conducting system); rhizofiltration (metals filtering from water through root systems; phytostabilization (stabilizing the contaminants by erosion control).

Table 2 Techniques used in the phytoremediation of organic pollutants

Technique	Processes involved	Primary facilitators of the processes
Phytotransformation	Sorption, uptake, and transformation of contaminants	Trees and grasses
Rhizosphere biodegradation	Microbial biodegradation in the rhizosphere	Grasses, alfalfa, many other stimulated by plants
Phytostabilization stabilization of contaminants by	Stabilization of contaminants by binding, holding soils, and/or decreased leaching	Metals, organics various plants with deep or fibrous root systems

Recently it has been observed that different categories of plants are found to be the candidates for application in the phytoremediation process, for e.g. annuals (survives for a single growing season), biennials (survives no longer than two seasons), forbs (includes herbs, non-woody species), grass and grass-like species, perennials (survives longer than one season) and shrubs (woody plants less than 50 feet in height).

Phytotechnologies have been successfully applied for removal of many persistent organic pollutants from contaminated media (Gan et al. 2009). This technology focuses on the ability of plants to adsorb, accumulate and concentrate the organic xenobiotics into aboveground biomass. In addition to that, roots of plants release exudates that enhance compound biotransformation and microbial degradation (Fig. 4). Phytoremediation of TPH is also considered as plant-assisted bioremediation where actual degradation of PAHs, heavy metals and other organics can be done by certain bacteria and fungi in the rhizosphere. In general, the activity of microbes in plant root zones is high because exudates create a favourable environment for microbes. It is seen that root exudates positively alter or regulate the soil environment such as pH, moisture, oxygen etc. which enhance the acceleration of the removal process.

3 Plant-Microbes Association-Assisted Removal of PAHs and Heavy Metals

Contamination with petroleum hydrocarbons brings noticeable harm to both terrestrial and aquatic ecosystems. The Natural Resource Council Committee on Oil in the Sea of the US National Academy of Sciences, estimated that approximately 1.3 million tons of petroleum product (Oil) entered in marine ecosystems (world oceans) annually (http://oils.gpa.unep.org/facts/sources.htm).

Plant species like maize, rye and white clover have significantly enhanced the dissipation of phenanthrene and pyrene in the soil environment (Xu et al. 2006). *Brachiaria brizantha* a tropical grass has been seen to enhance the microflora viz.,
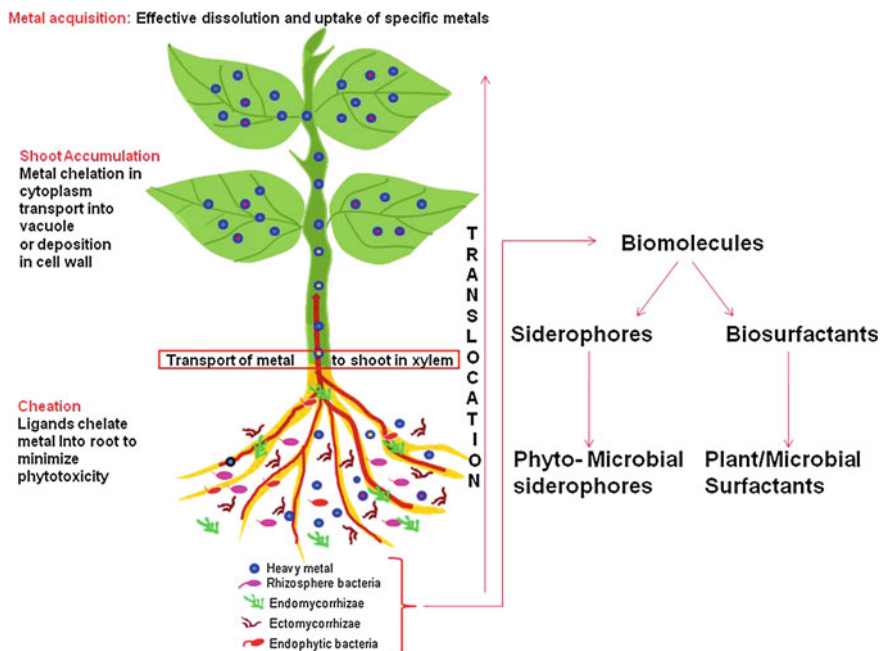
Metal acquisition: Effective dissolution and uptake of specific metals

Fig. 4 Mechanisms exhibited by plant roots that enhance biotransformation and microbial degradation of TPH

bacteria, fungi in their root zone; such activity of this grass has also been recorded when these are grown in sludge amended soil (Fig. 5). The grass thus effectively degrades alkanes, aromatics, cycloalkanes in petroleum hydrocarbon contaminated soil (Merkla et al. 2006).

The microorganisms sustained in contaminated soil require carbon sources to enhance their growth and activity, and this can be stimulated by adding nutrients, electron acceptors and oxygen and the process is known as biostimulation. To decontaminate polluted soil, plant rhizosphere has recently gained attention with regard to the remediation of organic pollutants such as PAHs and HMs. High levels of microbes associated with the root zone, the presence of some extracellular biotransformation enzymes including peroxidises, reductases, Cytochome P540, Laccases, Glutathione-S-transferease, are all positive factors that promote the bio-availability of these PAHs and their degradation (Ortega-Calvoa et al. 2013). It has also been experimentally proved that due to the influence of certain plant root exudates, biosurfactants are produced by certain rhizobacteria which facilitate the solubilization of oil pollutants from the soil. Since plants, through their exudation patterns, are able to influence the rhizosphere composition and increase soil microflora, it is essential to choose the appropriate plant to suit the particular rhizosphere (given the diversity of different rhizospheres) to quicken the remediation process.
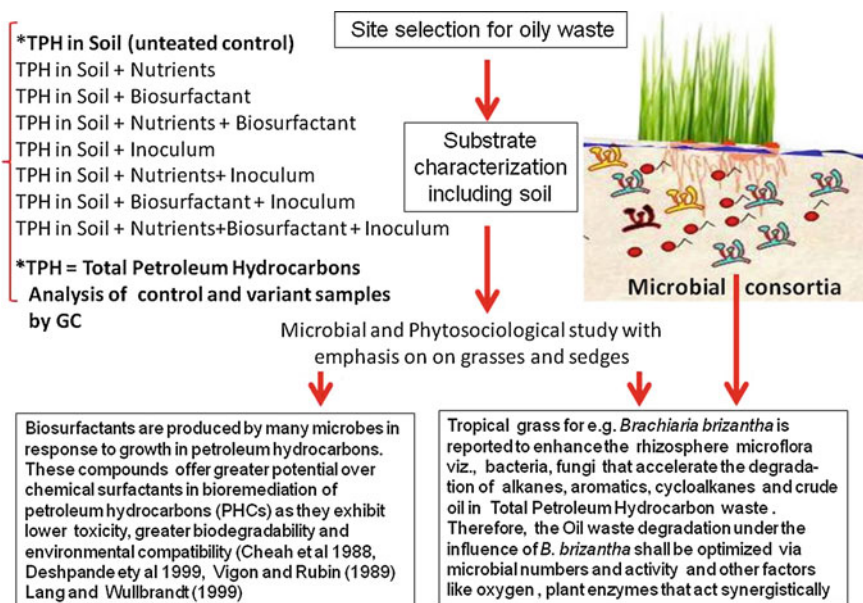
| Site selection for oily waste |

*TPH in Soil (unteated control)
TPH in Soil + Nutrients
TPH in Soil + Biosurfactant
TPH in Soil + Nutrients + Biosurfactant
TPH in Soil + Inoculum
TPH in Soil + Nutrients+ Inoculum
TPH in Soil + Biosurfactant + Inoculum
TPH in Soil + Nutrients+Biosurfactant + Inoculum

*TPH = Total Petroleum Hydrocarbons
Analysis of control and variant samples
by GC

Substrate characterization including soil

Microbial consortia

Microbial and Phytosociological study with emphasis on on grasses and sedges

Biosurfactants are produced by many microbes in response to growth in petroleum hydrocarbons. These compounds offer greater potential over chemical surfactants in bioremediation of petroleum hydrocarbons (PHCs) as they exhibit lower toxicity, greater biodegradability and environmental compatibility (Cheah et al 1988, Deshpande ety al 1999, Vigon and Rubin (1989) Lang and Wullbrandt (1999)

Tropical grass for e.g. *Brachiaria brizantha* is reported to enhance the rhizosphere microflora viz., bacteria, fungi that accelerate the degradation of alkanes, aromatics, cycloalkanes and crude oil in Total Petroleum Hydrocarbon waste. Therefore, the Oil waste degradation under the influence of *B. brizantha* shall be optimized via microbial numbers and activity and other factors like oxygen, plant enzymes that act synergistically

Fig. 5 Schematic representation enhancing the production of rhizospheric microbial consortia for oily sludge degradation mediated by *Brachiaria brizantha* and other grasses that would increase microbial numbers and activity, other favourable factors like oxygen availability, plant enzymes and synergistic degradation of TPH

A significant number of studies have been conducted on grasses, sedges and other plant species e.g., tall fescue (*Festuca arundinacea*), switchgrass (*Panicum virgatum*), ryegrass (*Lolium perenne*) and sunflower (*Helianthus annuus*). However, success of any bioremediation method depends upon the adaptation of the microbe and/or plant to the local environment. The phytoextraction capacity of three plant species, *Brassica campestris*, *Festuca arundinacea*, and *Helianthus annuus* has been successfully worked out for Pb, Cu, Cd, Ni and TPH and their remediation has been accelerated when supplemented with humic acid (Park et al. 2011). In the presence of humic acid (HA) the removal of TPH from the soil with *B. campestris*, *F. arundinacea* and *H. annuus* was enhanced to a degradation of 86, 64, and 85 % respectively. HA could act as an enhancing agent for phytodegradation of petroleum hydrocarbons in soil contaminated with diesel fuel and heavy metals by dynamically increasing dehydrogenase activity (Park et al. 2011).

The three microbial consortia (bacteria, fungi and bacteria–fungi complex) could degrade polycyclic aromatic hydrocarbons (PAHs), and the highest PAH removals had been recorded in soil and slurry inoculated with fungi (50.1 and 55.4 %, respectively) (Li et al. 2007). The application of a bacterial consortia in oily sludge contaminated soil with nutrients resulted in maximum biodegradation of total petroleum hydrocarbon (TPH) in which the alkane fraction of TPH was reduced by 94.2 %, the aromatic fraction of TPH was reduced by 91.9 %, and NSO (nitrogen-,

sulfur-, and oxygen-containing compound) and asphaltene fractions of TPH were reduced by 85.2 % in 1 year (Sanjeet et al. 2001).

Therefore, for an effective bioremediation process those plant-microbe consortia using indigenous organisms are always preferable, though their practical application in India is still very limited at present. The usefulness of surfactant applications in environmental remediation has been supported by many scientists (Bhandari et al. 2000; McCray et al. 2001). Mobilization and solubilization are the key mechanisms behind surfactant-enhanced removal of oil from soil (Deshpande et al. 1999).

Recently, Sun et al. (2012) have reported that both biostimulation as well as bioaugmentation (Fig. 6) through indigenous microbial strains might be used to enhance the degradation of PAH in soil. Many microbes with the ability to degrade PAHs have been isolated, and PAH degradation mechanisms, enzymatic action and genes characterization have been widely studied (Uyttebroek et al. 2007). However, only a few reports on the microbial metabolism of PAHs with four or more aromatic rings were published (Kanaly and Harayama 2000). Besides, PAH degradation by pure cultures may not represent the process under realistic environmental conditions, since the influence of indigenous strains is not considered (Ghazali et al. 2004). Microbial oxidation of four-ring PAHs, such as pyrene, naphthalene, phenanthrene and anthracene, by bacteria in soil (Sutherland et al. 1995) has been published; however, information is scanty about bacteria capable of utilizing
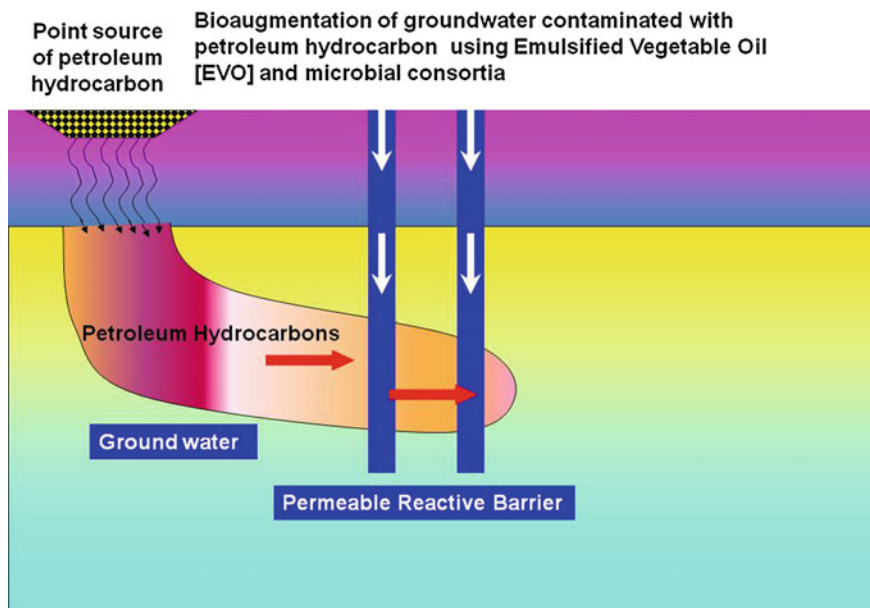

Fig. 6 Bioaugmentation of groundwater contaminated with petroleum hydrocarbon using emulsified vegetable oil (*EVO*) and microbial consortia

HMW-PAHs as a carbon source, such as benzo[a]pyrene and benz[a]anthracene. It has also been found that some basidiomycetes and deuteromycetes fungi removed naphthalene, phenanthrene, anthracene, pyrene, benzo[a]pyrene, fluorene, dibenzothiophene, catechol, benzo[a]anthracene, benzo[-ghi]-perylene, chrysene, benzo[b]fluoranthene and benzo[k]-fluoranthene more efficiently than bacteria did (Zheng and Obbard 2003).

The potential enzymatic processes involved during the degradation of contaminants include the cytochrome P-450 system (Yadav et al. 2006), lignin peroxidase, manganese peroxidase (Steffen et al. 2003) and laccase (Gianfreda et al. 1999). PAH-contaminated soil (375 mg PAHs/kg soil) had been successfully remediated in the Beijing Coking Plant using bioaugmentation with an indigenous bacterial strain which degrades PAH. LMW-PAHs including Naphthalene (40.0 %) and acenaphthene (33.3 %) were degraded to the greatest extent but no significant changes in the concentration of HMW-PAHs including pyrene, benz[a]anthracene, benzo[a] pyrene, indeno[1,2,3-cd]pyrene and dibenz[a, h]anthracene had been recorded. Most LMW-PAHs can be degraded by indigenous microbes; however, the course of action might be very slow (Sun et al. 2012). Till date, many more PAH degrades have been isolated, which has considerably added to the existing body of knowledge. However, until now, there has been no significant contribution regarding the development of plant-microbe consortia and their role in the accelerated removal of PAHs and heavy metals, which, therefore, presents a new dimension towards future research. However, the mechanisms driving specific plant-microbe interactions that result in successful phytoremediation of PAH-contaminated soils are still not fully understood. Nonetheless, there have been some successful experiments, as conducted by Meng et al. (2011), that showed the degradation of up to six ring PAHs due to combined treatment of plant and microbes.

The Energy Resources Institute (TERI), New Delhi has formulated new techniques using micro-organisms to clean up oil-contaminated sites at refineries in India and abroad. However, acclimatization of their chosen strains in a particular environmental condition is very important for successful ex situ bioremediation of PAHs and heavy metal contaminated soil. Nevertheless, microbial degradation of PAHs in soil is restricted by various factors that often results in lower bioremediation efficiency than the expected level (Arun and Eyini 2011). Plant species like *Cyperus odoratus*, *Cyperus laevigatus*, *Cyperus rotandus* and *Cyperus bravifolius* have been identified for the degradation of total petroleum hydrocarbons by adding inorganic supplements (Basumatary et al. 2012). Aquatic weeds *Typha* spp. and *Scirpus lacustris* have been proved to enhance removal rates during the remediation of the contaminated sites (Haritash and Kaushik 2009). The different factors associated with the biodegradability of the crude oil contaminated soil of Borhola oil fields of Assam, India, have already been evaluated (Gogoi et al. 2003). These factors include the availability of microorganisms that can metabolize the contaminant utilizing it as a carbon source through solubilization/desorption under favourable conditions of temperature, pH, sufficient metabolic nutrients and moisture. A number of bacterial strains (e.g., *P. aeruginosa*, *P. fluoresens*, *Mycobacterium* spp., *Haemophilus* spp., *Rhodococcus* spp., *Paenibacillus* spp) are

able to sustain themselves in TPH contaminated sites and are still known to degrade PAHs, a phenomenon that has been successfully isolated in the laboratory. The research findings in this field described in this paper have consolidated the body of work done on the collective role of plants and microbes to accelerate the remediation process of petroleum waste. However it may be emphasized here that there is an ample opportunity towards further research in new dimensions since the findings have not been able to address many issues like bioavailability of organic pollutants.

4 Bioavailability of Organic Pollutants: Major Limitations in Acceleration of Removal Process

Contaminated land is a worldwide legacy of industrialization requiring huge investments in order to restore it for further use (Riding 2013). The sites contaminated with petroleum hydrocarbons could be rehabilitated with the in situ remediation technique by injecting biosurfactants. This in situ application seems to be very practical and economical for cleaning up the environment. It has been established that microbes produce biosurfactants which increase PAHs bioavailability, mass flow of PAHs towards the rhizosphere, and adsorption of PAHs onto roots. Many microorganisms (*P. aeruginosa*, *Bacillus subtilis*, *Pichia pastoris*, etc.) can produce surface-active agents, which are known as biosurfactants and these naturally occurring substances are less harmful for natural ecosystems due to their low toxicity and biodegradable nature. Apart from micro-organisms, plants promote movement of microbes and increased soil aeration.

In some studies, surfactant micelles were used to increase the solubility of hydrophobic contaminants, but they tended to interact with the liposome of microorganisms and also break down upon contact with soil, thus limiting the efficiency of bioremediation. Engineered nanoparticles play an important role in microbial remediation. Amphiphilic polyurethane (APU) nanoparticles have shown a promising step in this direction; in an experiment, this APU had increased the solubilization rate of the model remediation compound Phenanthrene (PHEN) (Tungittiplakorn et al. 2005). These particles, made of polyurethane acrylate anionmer (UAA) or poly(ethylene) glycol (PMUA) precursor chains, have hydrophobic interiors that show high affinity for PHEN. As opposed to surfactants, the affinity of the nanoparticles to hydrophobic contaminants can be increased by modifying the hydrophobic segment of the precursor chain and their mobility can be increased by controlling the charge density of the modified nanoparticles. Another advantage offered by nanoparticles in bioremediation is in the form of magnetite nanoparticles. Magnetite nanoparticles are formed by the co-precipitation of ferrous and ferric salts under inert conditions. This technology possesses great industrial applicability in terms of easier separation, re-usability, and cost-effectiveness of organic contaminant removals. Li et al. (2009) have reported the use of

magnetite nanoparticles by coating them with dibenzothipohene-desulfurizing bacterial strains, *R. erthyropolis* LSSE8-1 and *P. delafiedelii*, for their biodesulfurization activity. The cells coated with ammonium oleate- modified magnetite nanoparticles showed repeated biodesulfurization activity and could be collected on the surface of the flask by using an external magnet. The use of magnetite nanoparticles also showed increased desulfurization activity.

5 Conclusions

The problem of contamination of the environment from crude oil seems to be insurmountable for the time being, since modern society cannot run without fuel and therefore persists in continued exploration of newer oil fields with every passing day. Since the last few decades many researchers from India and abroad have isolated many potential microbes which can be successfully used in the removal of HMs and degradation of PAHs in ex situ and in situ conditions. Similarly many hyperaccumulator plants have been identified. The research in this field is wide and most of the findings are quite satisfactory. However, in spite of this positive effort made by the scientists, the fact remains that the oily sludge and heavy metals contamination happens quite often in oil producing countries including India and cannot be mitigated properly. Therefore, it is time to formulate a common strategy and policy on a common platform in order to address this critical issue. The ecology of PAHs and heavy metals distribution in soil is subject to environmental contamination and can be successfully mitigated by application of plant-microbe consortia. Plant-microbe consortia accelerate the removal process more effectively and it is more effective than the mere application of either plants or microbes individually. In this case emphasis should be given on screening of more native microbes and plants during the development of the consortia because only native species are able to adapt to the contaminated site without much effort. This goal will be difficult to achieve unless the following critical limitations are resolved:

(1) Although many successful remediation cases with plant-microbes have been reported, we still know little about the process mechanism and how plant-microbes association accelerate the remediation process.

(2) Previous work in this field has enhanced our capacity building. Such research has mostly been carried out in labs or greenhouses, and so it is necessary to ascertain how remediation effects will change in field conditions. This requires the further support of more in situ experiments.

(3) The scope of application is currently limited in India because only a few plant-microbe consortia have been inventoried and it is here emphasized that only indigenous plants and microbes are able to accelerate the remediation process more effectively.

(4) Although some plant-microbe consortia can increase the degradation of PAHs, the consortia may not survive in unfavourable environmental conditions such

as low nutrient status and presence of heavy metals with high concentrations, and, therefore, discovering a more robust system for remediation definitely brings new challenges to us.

References

Antizar-Ladislao B, Katerina S, Angus JB, Nicholas JR (2008) Microbial community structure changes during bioremediation of PAHs in an aged coal-tar contaminated soil by in-vessel composting. Int Biodeter Biodegr 61:357–364

Arun A, Eyini M (2011) Comparative studies on lignin and polycyclic aromatic hydrocarbons degradation by basidiomycetes fungi. Bioresour Technol 102:8063–8070

Banat IM (1995) Biosurfactants production and possible uses in microbial enhanced oil recovery and oil pollution remediation: a review. Bioresour Technol 51:1–12

Barker AV, Bryson GM (2002) Bioremediation of heavy metals and organic toxicants by composting. The Sci World 2:407–420

Basumatary B, Bordoloi S, Sarma HP (2012) Crude oil-contaminated soil phytoremediation by using Cyperus brevifolius (Rottb.) Hassk. Water Air Soil Pollut 223:3373–3383

Bhandari A, Novak JT, Dove DC (2000) Effect of soil washing on petroleum hydrocarbon distribution on sand surfaces. J Hazard Sub Res 2:1–13

Bhattacharyya JK, Shekdar AV (2003) Treatment and disposal of refinery sludges: Indian scenario. Waste Manage Res 21:249–261

Cameotra SS, Singh P (2008) Bioremediation of oil sludge using crude biosurfactants. Int Biodeter Biodegr 62:274–280

Chen YX, Wang YP, Wu WX, Lin Q, Xue SG (2006) Impacts of chelate-assisted phytoremediation on microbial community composition in the rhizosphere of a copper accumulator and non-accumulator. Sci Total Environ 356:247–255

Colwell RR, Walker JD (1977) Ecological aspects of microbial degradation of petroleum in the marine environment. Crit Rev Microbiol 5:423–445

Das K, Mukherjee AK (2007) Crude petroleum-oil biodegradation efficiency of Bacillus subtilis and *Pseudomonas aeruginosa* strains isolated from a petroleum-oil contaminated soil from North-East India. Bioresour Technol 98:1339–1345

Deshpande S, Shiau BJ, Wade D, Sabatini DA, Harwell JH (1999) Surfactants selection for enhancing ex-situ soil washing. Water Res 33:351–360

Gallego JR, Gonzalez-Rojas E, Pelaez AI, Sanchez J, Garcia-Martinez MJ, Ortiz JE, Torres T, Llamas JF (2006) Natural attenuation and bioremediation of prestige fuel oil along the Atlantic coast of Galicia (Spain). In: Organic geochemistry 37, 12, Advances in Organic Geochemistry 2005—Proceedings of the 22nd international meeting on organic geochemistry, Seville, Spain, 12–16 Sept 2005, 1869–1884

Gan S, Lau EV, Ng HK (2009) Remediation of soils contaminated with polycyclic aromatic hydrocarbons (PAHs). J Hazard Mater 172:532–549

Ghazali MF, Zaliha NR, Salleh B, Basri M (2004) Biodegradation of hydrocarbons in soil by microbial consortium. Inter Biodeter Biodegrad 54:61–67

Gianfreda L, Xu F, Bollag JM (1999) Laccases: a useful group of oxidoreductases enzymes. Bioreme J 3:1–25

Gogoi BK, Dutta NN, Goswami P, Mohan TRK (2003) A case study of bioremediation of petroleumhydrocarbon contaminated soil at a crude oil spill site. Adv Environ Res 7:767–782

Haritash AK, Kaushik CP (2009) Biodegradation aspects of polycyclic aromatic hydrocarbons (PAHs): a review. J Hazard Mater 169:1–15

Huang XD, El-Alawi Y, Penrose DM, Glick BR, Greenberg BM (2004) A multiprocess phytoremediation system for removal of polycyclic aromatic hydrocarbons from contaminated soils. Environ Pollut 130:465–476

Kanaly RA, Harayama S (2000) Biodegradation of high-molecular weight polycyclic aromatic hydrocarbons by bacteria. J Bacteriol 182:2059–2067

Koch AL (1990) Diffusion the crucial process in many aspects of the biology of bacteria. Adv Microb Ecol 11:37–69

Lang S, Wullbrandt D (1999) Rhamnose lipids–biosynthesis, microbial production and application potential. Appl Microbiol Biotechnol 51:22–32

Li X et al (2007) Biodegradation of aged polycyclic aromatic hydrocarbons (PAHs) by microbial consortia in soil and slurry phases. J Hazard Mater. doi:10.1016/j.jhazmat.2007.04.040

Li YG, Gao HS, Li WL, Xing WL, Liu HZ (2009) In situ magnetic separation and immobilization of dibenzothiophene-desulfurizing bacteria. Bioresour Technol 100:5092–5096

Lucas AMR, Vazquez SC, Curtosi A, Mestre MC, Pelletier E, MacCormack WP (2006) Phenanthrene biodegradation in soils using an Antarctic bacterial consortium. Bioremediat J 10:191–201

Mahler BJ, Van Metre PC, Bashara TJ, Wilson JT, Johns DA (2005) Parking lot sealcoat: an unrecognized source of urban polycyclic aromatic hydrocarbons. Environ Sci Technol 39:5560–5566

Maiti A, Bhattacharyya N (2012) Biochemical characteristics of a polycyclic aromatic hydrocarbon degrading bacterium isolated from an oil refinery site of West Bengal, India. Adv Life Sci Appl 1:48–53

McCray JE, Bai G, Maier RM, Brusseau ML (2001) Biosurfactant-enhanced solubilization of NAPL mixtures. J Contam Hydrol 48:45–68

Meng L, Qiao M, Arp HPH (2011) Phytoremediation efficiency of a PAH-contaminated industrial soil using ryegrass, white clover, and celery as mono- and mixed cultures. J Soils Sediments 11:482–490

Merkla N, Schultze-Krafta R, Ariasb M (2006) Effect of the tropical grass Brachiaria brizantha (Hochst. ex A. Rich.) Stapf on microbial population and activity in petroleum-contaminated soil. Microbiol Res 161:80–91

Ortega-Calvoa JJ, Tejeda-Agredanoa MC, Jimenez-Sanchezaa C, Congiua E, Sungthonga R, Niqui-Arroyob JL, Cantosa M (2013) Is it possible to increase bioavailability but not environmental risk of PAHs in bioremediation? J Hazard Mater 261:733–745

Pandey B, Fulekar MH (2012) Nanotechnology: remediation technologies to clean up the environmental pollutants. Res J Chem Sci 2:90–96

Park S, Kim KS, Kim JT, Kang D, Sung K (2011) Effects of humic acid on phytodegradation of petroleum hydrocarbons in soil simultaneously contaminated with heavy metals. J Environ Sci 23(12):2034–2041

Peng SW, Zhou QX, Cai Z, Zhang ZN (2009) Phytoremediation of petroleum contaminated soils by *Mirabilis jalapa* L. in a greenhouse plot experiment. J Hazard Mater 168:1490–1496

Riding MJ (2013) Chemical measures of bioavailability/bioaccessibility of PAHs in soil: fundamentals to application. J Hazard Mater. http://dx.doi.org/10.1016/j.jhazmat.2013.03.033

Sanjeet M, Jeevan J, Ramesh CK (2001) Evaluation of inoculum addition to stimulate in situ bioremediation of oily-sludge-contaminated soil. Appl Environ Microbiol 67:1675–1681

Sarma H (2011) Metal hyperaccumulation in plants: a review focusing on phytoremediation technology. J Environ Sci Technol 4:118–138

Sarma A, Sarma H (2010) Enhanced biodegradation of oil products by some microbial isolate supplemented with heavy metals. Int J Bot 6:441–448

Singh OV, Labana S, Pandey G, Budhiraja R, Jain RK (2003) Phytoremediation: an overview of metallicion decontamination from soil. Appl Microbiol Biot 61:405–412

Steffen KT, Hatakka A, Hofrichter M (2003) Degradation of benzo[a]pyrene by the litter-decomposing basidiomycete Stropharia coronilla: role of manganese peroxidase. Appl Environ Microbiol 69:3957–3964

Sun GD, Xu Y, Jin JH, Zhong ZP, Liu Y, Luo M, Liu ZP (2012) Pilot scale ex-situ bioremediation of heavily PAHs-contaminated soil by indigenous microorganisms and bioaugmentation by a PAHs-degrading and bioemulsifier-producing. J Hazard Mater 233–234:72–78

Sutherland JB, Rafii F, Khan AA, Cerniglia CE (1995) Mechanisms of polycyclic aromatic hydrocarbon degradation. In: Young LY, Cerniglia CE (eds) Microbial transformation and degradation of toxic organic chemicals. Wiley-Liss Inc, New York, pp 269–306

Tungittiplakorn W, Cohen C, Lion LW (2005) Engineered polymeric nanoparticles for bioremediation of hydrophobic contaminants. Environ Sci Technol 39:1354–1358

Urum K, Pekdemir T, Copur M (2004) Surfactants treatment of crude oil contaminated soil. J Colloid Interface Sci 276:456–464

Uyttebroek M, Vermeir S, Wattiau P, Ryngaert A, Springael D (2007) Characterization of cultures enriched from acidic polycyclic aromatic hydrocarbon-contaminated soil for growth on pyrene at low pH. Appl Environ Microbiol 73:3159–3164

Verma P, George K, Singh H, Singh S, Juwarkar A, Singh R (2006) Modeling rhizofiltration: heavy metal uptake by plant roots. Environ Mod Assess 11:387–394

Verma M, Satinder KB, Tyagi RD, Surampalli RY, Valero JR (2007) Antagonistic fungi, Trichoderma spp.: panoply of biological control. Biochem Eng J 37:1–20

Wu H, Tang HS, Zhang X, Guo J, Song Z, Tian S, Smith DL (2009) Using elevated CO_2 to increase the biomass of a Sorghum vulgare × Sorghum vulgare var. sudanense hybrid and Trifolium pratense L. and to trigger hyperaccumulation of cesium. J Hazard Mater 170:861–870

Xu SY, Chen YX, Wu WX, Wang KX, Lin Q, Liang XQ (2006) Enhanced dissipation of phenanthrene and pyrene in spiked soils by combined plants cultivation. Sci Total Environ 363:206–215

Yadav JS, Doddapaneni H, Subramanian V (2006) P450ome of the white rot fungus Phanerochaete chrysosporium: structure, evolution and regulation of expression of genomic P450 clusters. Biochem Soc Trans 34:1165–1169

Zheng Z, Obbard JP (2003) Oxidation of polycyclic aromatic hydrocarbons by fungal isolates from an oil contaminated refinery soil. Environ Sci Pollut Res 10:173–176

Zhuang X, Chen Jian, Shim Hojae, Bai Zhihui (2007) New advances in plant growth-promoting rhizobacteria for bioremediation. Environ Int 33:406–413

Enhanced Oil Recovery Techniques for Indian Reservoirs

N. Sakthipriya, Mukesh Doble and Jitendra S. Sangwai

Abstract The overall oil production worldwide has declined due to the increase in maturity of the oil reservoirs. In developing countries like India, the oil production and demand plays a crucial role for the development of economy of the country. However, the domestic crude oil production is insufficient to meet the requirement for energy. Thus, there is a big challenge to minimize the gap between the demand and supply for crude oil. Several methods to enhance oil recovery have been developed to increase the production from matured reservoirs and are referred to as enhanced oil recovery (EOR) methods. This chapter discusses in detail about the various EOR methods, their applicability, and the screening criteria for various reservoir types. The EOR methods are further discussed in Indian contexts. This chapter also summarizes the details of various oilfields in India. The chapter will in general, help to understand the recent trends and the need of EOR for Indian oil reservoirs.

1 Introduction

Oil and natural gas have been an important source of energy for the mankind. The total energy requirement of the world has increased drastically in the past decade due to the increased demand from the developing countries like India, China and Brazil. According to British Petroleum (BP), statistical review of world energy (2013), India currently imports about 70 % of its total requirement of crude oil and natural gas, thus accounting for about 40 % of the import bills. Crude oil has the weakest global growth rate in terms of production among fossil fuels for the third successive year. The current crude oil production is insufficient to meet the

N. Sakthipriya · J.S. Sangwai (✉)
Petroleum Engineering Program, Department of Ocean Engineering,
Indian Institute of Technology Madras, Chennai 600 036, India
e-mail: jitendrasangwai@iitm.ac.in

M. Doble
Department of Biotechnology, Indian Institute of Technology Madras,
Chennai 600 036, India

requirement for the energy. Thus, there exists a big gap between the demand and supply of crude oil. The ultimate solution is to increase the recovery of oil from existing reservoirs in addition to the exploration of new reservoirs (Herron et al. 2004). Several methods have been developed to increase the production from mature reservoirs, which are referred to as enhanced oil recovery (EOR) methods. EOR is the process in which external agents in the form of fluids are injected into the reservoir for pressure maintenance and to alter the physiochemical properties of oil, gas, water and reservoir rock, which in turn increase the sweep efficiency (Donaldson et al. 1989). The recovery increases due to an impact of the injected fluids on the reservoir rock properties and fluid properties, like the interfacial tension (IFT), oil swelling, viscosity reduction, wettability modifications, favorable phase behavior, etc.

Oil and gas in the reservoir resides in the porous rock at high pressure and high temperature conditions. The primary recovery of these hydrocarbons is due to the initial reservoir pressure, which is sufficient for the fluid to flow. It is a well-known fact that, during the primary recovery, only 5–20 %, of the oil can be produced from the oilfield due to the existing pressure. To improve the recovery after primary phase, water is injected into the reservoir to displace the oil leading to ~30–50 % additional recovery from the reservoir. The challenge is to recover the residual oil in place, which is ~50 % from the original oil in place (OOIP). Figure 1 shows a schematic of average production resulting from various phases of crude oil recovery from the reservoir. On an average, one third of the OOIP in the reservoir can be recovered through primary and secondary recovery techniques (Blunt et al. 1993). This calls for further development of enhanced oil recovery (EOR) techniques to target the residual oil remaining in the reservoir at the end of secondary recovery.

Fig. 1 Various oil recovery techniques
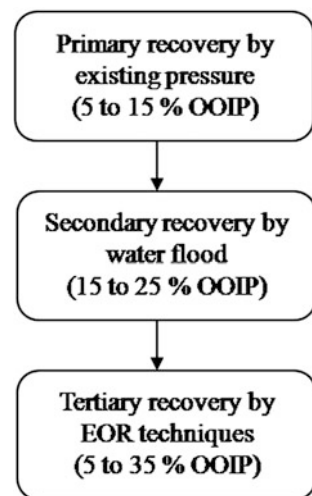
1.1 Need for Enhanced Oil Recovery

Table 1 shows the proved global crude oil reserves. Here, the proved reserves means reserves from which crude oil can be produced economically using available technology. According to BP statistical review of world energy (2010), worldwide oil production has decreased more rapidly by 2 million bpd, which is the largest drop since 1982. In 2008, oil production and exporting countries (OPEC) executed the production cut agreement to reduce the output of OPEC countries. This agreement is maintained throughout the year 2009, resulted in ~7.3 % decline of production out of which 75 % of the decline was from the Middle Eastern countries.

Ageing of oil wells is an everlasting and crucial alarm faced by the global oil and gas industry. In India, 75 % of oil and Natural Gas's (ONGC) production is coming just from 15 oilfields. In addition, oilfield in Ankleshwar, Rudrasagar and Bombay high wells started declining recent past. Most of the oil wells are either unproductive or produces insignificant oil. An oil well becomes less productive when ~30 % of oil in place has been recovered, which may be due to the reduced reservoir pressure, and developed compositional gradient. This produces lighter hydrocarbon component from the reservoirs in early phase leaving the higher end hydrocarbons (waxes) within the reservoir. These reserves tend to produce more waxy- and asphaltic crude oil, thus shows challenges in EOR. The production of the latter pose serious threat for the recovery of oil since waxes and asphaltene tends to deposit near the well bore, surface facilities and offshore and onshore production pipelines. Low permeability of the reservoir rock and the high viscosity makes crude oil immobile and hinder oil recovery in the existing wells (Bordoloi and Konwar 2008). In addition, high IFT between water and oil increases the capillary forces, which in turn retains the oil in reservoir rock (Banat 1995). The decreased gas trapping in the reservoir, responsible for pushing the oil upto the well, results in decreased production.

However, these reservoirs and the oil wells still show potential for increased production through reservoir management using improved recovery methods. Using typical EOR methods, an additional 5–35 % of OOIP can be extracted from an oil field. After the primary- and secondary recovery techniques, ~7000 BBL of crude oil is expected to stay back in the existing reservoirs. Hence, the target for

Table 1 Worldwide proved crude oil reserves (BP Energy Outlook 2030 2013)

S. No	Country	Thousand million barrels			
		1992	2002	2011	2012
1	North America	122.1	228.3	221.0	220.2
2	South and Central America	78.8	100.3	326.9	328.4
3	Europe and Eurasia	78.3	109.3	140.3	140.8
4	Middle East	661.6	741.3	797.9	807.7
5	Africa	61.1	101.6	126.6	130.3
6	Asia Pacific	37.6	40.6	41.4	41.5
7	World	1039.3	1321.5	1654.1	1668.9

EOR techniques is to recover the remaining oil effectively (Wu et al. 2012; Wang et al. 2013). According to the International Energy Agency, enhancing the oil recovery possibly will release ~300 BBL of trapped oil (Bassioni and Sanders 2013). As per the report by Senergy world magazine (2011), at the end of 2005 the global market for EOR was estimated to be 3.1 billion dollars (for barrels of crude oil), and rapidly increased to 62.5 billion dollars in 2009.

In most of the cases, the primary and secondary recovery methods produce very less crude oil than that estimated (one third of the OOIP), and this case is evidenced by X-ray tomographs (Lake et al. 1992; Iglauer et al. 2010; Al-dousari and Garrouch 2013). EOR can also be applied at the primary stage of an oilfield where available pressure in the reservoir is insufficient to induce the flow of oil through the producing wells. In the secondary stage, EOR is used to promote production rates by improving flow and suitable recovery conditions. Generally, EOR methods are engaged regularly during the tertiary stage where oilfields have high water cut and low productivity (Adasani and Bai 2011). EOR also involves major financial risks due to various suspicions. Pilot studies on EOR methods for the suitability for given reservoirs should be done before implementing at commercial scale. If the pilot study works technically and financially, the process can be expanded at oilfield scale.

2 Methods of EOR

There are several types of hydrocarbon reservoirs ranging from dry gas, wet gas, gas condensate, light oil, brown oil, heavy oil and extra heavy oil reservoirs. In addition, the in situ reservoir properties vary in different oilfields. EOR methods are classified broadly as, chemical injection; gas flooding; microbial and thermal injection (see Fig. 2). The EOR methods target the oil and rock reservoir properties by several mechanisms. In addition, cold heavy oil production (CHOP), cold heavy oil
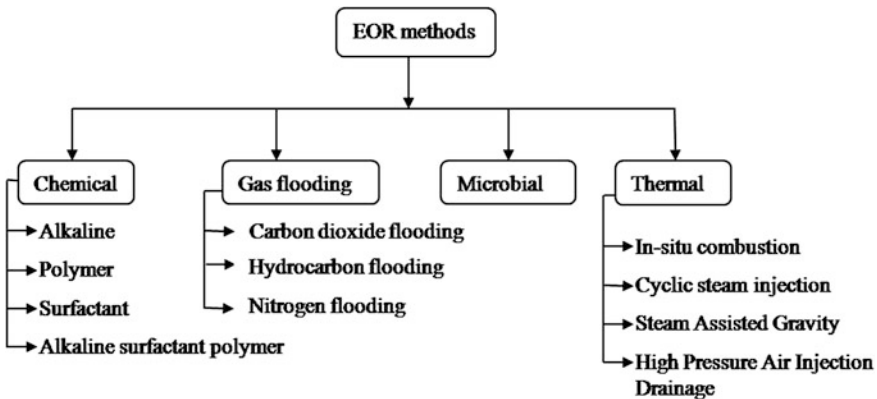

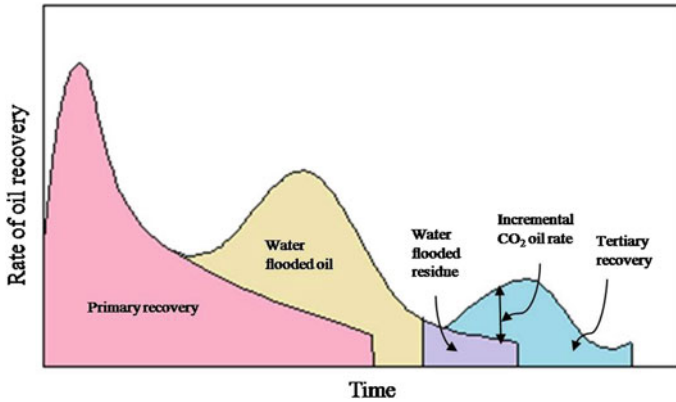**Fig. 2** Various techniques used for enhanced oil recovery

Fig. 3 Expected oil recovery through various EOR techniques (Taglia 2010)

production with sands (CHOPS), microwave technique, surface mining, solvent injection and ultrasound are other techniques employed to enhance the recovery of crude oil (Jiang et al. 2014). Surface mining is suitable for reservoirs with depth less than 70 m and recovers ~5 % of OOIP. On the other hand, CHOP/CHOPS recover ~5–10 % of OOIP (Ivory et al. 2010; Jiang et al. 2014). The largest percentage of OOIP is produced during primary recovery and over the period of time the decline starts when the reservoir is no longer productive, water flooding is done to augment the oil recovery and further enhancement is done through various enhancement methods (see Fig. 3).

2.1 Chemical EOR

Chemical methods are generally used to decrease the IFT between oil and used water, and after water flooding to increase the oil recovery (Yang et al. 2005). Chemical recovery methods include polymer flooding, surfactant flooding, alkaline flooding, and the composite, alkali-surfactant-polymer (ASP) flooding. These methods involve mixing of the above chemicals in carrier fluid (primarily water) prior to the injection. Figure 4 shows the process of chemical flooding schematically.

Polymer flooding, introduced in 1960, is a widespread chemical EOR practice (Wang et al. 2013). Water soluble polymers increases the viscosity of the injected water thereby making the viscous oils to move efficiently. This is suitable mainly for heterogeneous reservoirs. Polymer flooding is employed efficiently for the oil with high water saturation during the initial period of water flooding with high mobile oil saturation (Wang et al. 2013). The viscoelastic property of the polymer solution helps to displace the oil remaining in micro-pores that cannot be displaced by water flooding alone (Needham and Hoe 1987). When water displaces oil, the mobility ratio of oil and water is so high that the injected water enters the reservoirs,
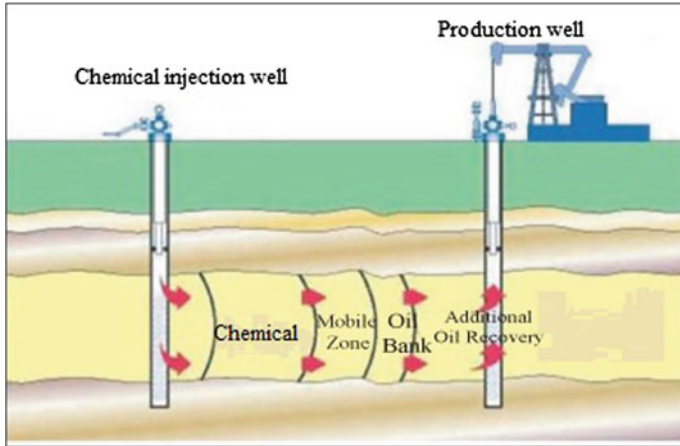
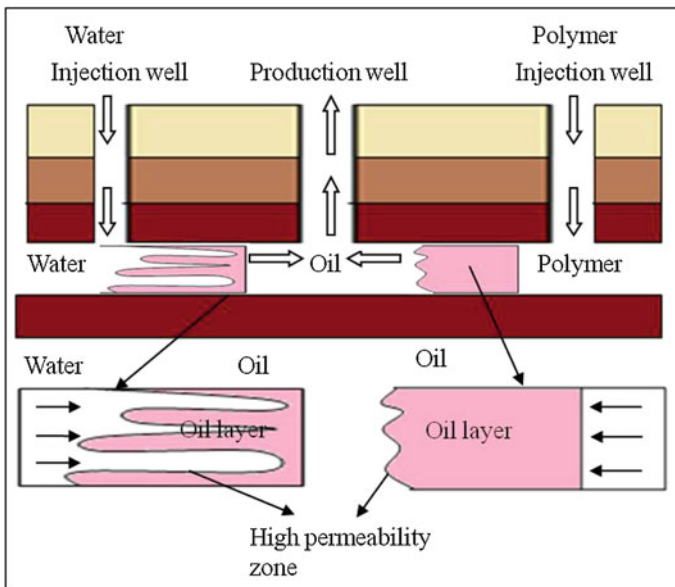**Fig. 4** Schematic of chemical EOR method

Fig. 5 Mobility control using polymer flood

which is termed as viscous fingering. Injection of polymer solution into the reservoir decreases the oil-water mobility ratio and displacement happens evenly to sweep a huge volume as shown in Fig. 5. Though the polymers control the mobility effectively, they are not suitable for reservoirs having temperature greater than 194 ° F (Sabhapondit et al. 2002). After polymer flooding process, more than half of the OOIP remains behind due to the entrapment of oil in the pores of the reservoir rock.

Fig. 6 Schematic of surfactant flood
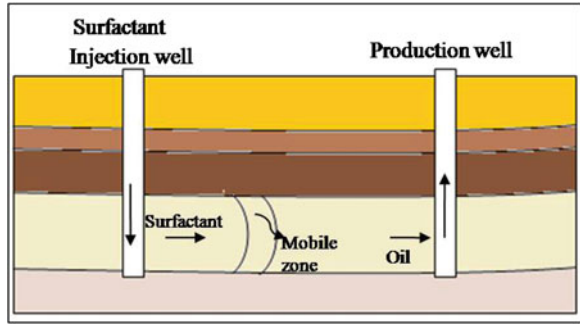
Figures 6 and 7 show the injection of surfactant into the reservoir and elongation of oil drop. The surfactant reduces the IFT between oil and water by getting adsorbed at the interface between the crude oil and water and makes spherical oil droplets to deform and elongate to overcome the capillary forces persuading a huge raise in the capillary number (Mokhatab and Towler 2009; Wu et al. 2012; Al-dousari and Garrouch 2013). These surfactants also helps to reverse the rock wettability by changing the oil-wet rock to water-wet, emulsify the oil and help the oil to come out of the rock and mobilize the entrapped oil in porous rock (Taylor and Nasr-El-din 1996; Li et al. 2000; Nedjhioui et al. 2005; Mandal and Ohja 2008). Explicitly, surfactants of specific structure and high purity are required (Yang et al. 2005). Due to versatility, currently Gemini surfactants have acquired more attention. Micelles formed by anionic geminis significantly lowers the surface tension than other anionic surfactants (Gao and Sharma 2013).However, there is still a scope in developing the surfactant systems, which help to reduce the IFT between oil and water at high salinity and high reservoir temperature conditions (Hezave et al. 2013).
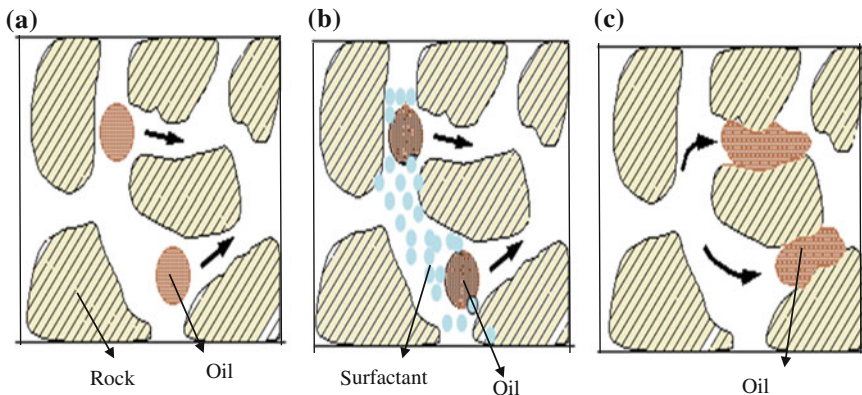

Fig. 7 Deformation of rock and elongation of oil; **a** oil between the reservoir rock; **b** addition of surfactant; **c** elongation of oil between the reservoir rocks

Alkali flooding is typically employed alone or along with surfactant and polymer flooding. It is applied in the areas with relatively poor physical properties, such as ST, rock wettability, etc., and low permeability reservoirs. It involves the addition of NaOH to the injection water to enhance the recovery. Generally, acidic compounds in the crude oil are drifted to the interface by the injected alkali and reacts with aqueous phase hydroxide to form surfactant in situ (Wang et al. 2009). Since this kind of flooding procedure is simple and inexpensive, it continues to receive much attention for EOR (Wanli et al. 2000). Alkali Surfactant Polymer (ASP) flooding gathers the benefits of all three types of chemicals and develop the volumetric sweep efficiency. The alkali component reacts with organic acids present in the crude oil forming petroleum emulsion, which in turn interacts with surfactant to create very low IFT and alters wettability (Gao et al. 1995). It is well suited for carbonate formations since the alkali added with the surfactant can significantly reduce the anionic surfactants adsorbed on calcite and dolomite rock (Hirasaki et al. 2008). This mixture can produce molecular interactions affecting the physico-chemical and rheological properties of the crude oil (Smitter et al. 2001). The molecular interactions exhibit some properties that depend on the electrical charge, hydrophobicity, non-polar tail, flexibility and additives of the polymer and the surfactant (Qi et al. 2013). Generally, the hydrophobic nature of polymer and surfactant induce molecular interactions in situ (Dubin et al. 1992; Iglesias et al. 2003).

2.2 Microbial EOR (MEOR)

This method is used to enhance the production from the mature brown and heavy oil reservoirs. Strains of microbes are injected into the crude oil reservoir. These microbes digest the long chain hydrocarbon molecules to shorter chains and generate bio-surfactants, acids and gases, raise the API gravity and decrease the cloud point (Etoumi 2007). Microbes can either be cultivated at the surface, injected into the reservoir downhole; or they can be directly cultivated in the reservoir by providing the nutrients at the wellbore. MEOR is effective for reservoirs of temperature range ∼158–248 °F. Crude oil from shallower and cooler reservoirs are more biodegradable than the oil in the deeper and hotter reservoirs (Wenger et al. 2001; Larter et al. 2012). Generally, microbes are non-carcinogenic, non-combustible, non-pathogenic and environment friendly (Mokhatab and Towler 2009). Use of microbes to enhance oil production appears to be a viable and cost effective when compared to other conventional methods because they occur naturally. MEOR intends to target the drainage of oil into the well and, at the same time, degrades the waxes and asphaltenes of waxy crude oil or heavy oil (Brown 2010). The bio-surfactants, fatty acids, alcohols and solvents produced in situ by the microbes solubilize the hydrocarbons and eliminates damage caused by paraffin from well bores
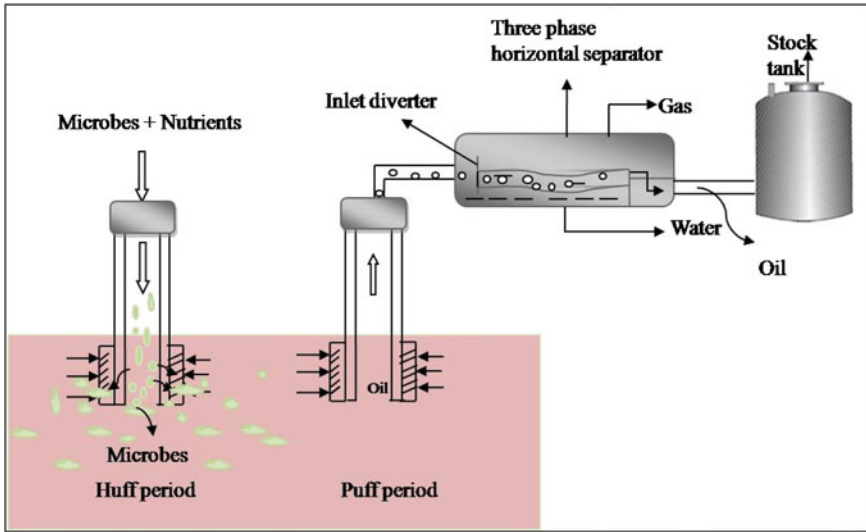
Fig. 8 Illustration of huff and puff microbial EOR

(Sadeghazad and Ghaemi 2003). The bio-surfactant that are surface-active agents are less toxic, highly biodegradable, effective at extreme temperature, salinity and pH conditions and increases the bioavailability of hydrophobic substrates (Pereira et al. 2013). Gas solubility of the hydrocarbons can be increased by creating hydrophobic cavities of micelles, which are due to bio-surfactants (Miller and Zhang 1997). In the matured oil reservoirs, the bio-surfactants come in contact with a small drop of the oil struck in the pores of the reservoir rock, reduce the IFT, and mobilize the trapped oil by reducing the viscous forces (Ramakrishna 2008). Figure 8 shows the schematic of huff and puff microbial enhanced oil recovery. In this method, the microbe and the nutrient enter into the well, and the well is kept shut in for some period. During this time span, microbes produce various metabolites to squeeze out the oil from the reservoir rock. Table 2 shows the various metabolites produced from the microbes and their role in enhancing the oil recovery.

**Table 2** Role of byproducts produced during microbial EOR method (Ramakrishna 2008)

S. No	Bioproducts	Role in EOR
1	Acids	Increase in permeability, emulsification
2	Biomass	Selective plugging, wettability alteration
3	Biosurfactant	Emulsification, de emulsification, IFT reduction
4	Gases	Increased pressure, IFT and viscosity reduction, oil swelling
5	Polymers	Selective plugging, viscosity reduction
6	Solvents	Rock dissolution, viscosity reduction

2.3 Gas Injection Methods

These methods are classified into immiscible and miscible gas injection method. In immiscible gas injection, the gas is injected at lower pressure region of the reservoir. The former is further classified into gas injection and dispersed gas injection according to the injection area. In crestal gas injection technique, gas is injected at the gas cap on the top of the oil bearing zone, and in the case of dispersed method, gas is injected at the oil bearing zone. Miscible gas injection techniques categorized as enriched gas miscible displacement method, high pressure dry gas miscible displacement method and miscible slug flooding (Bhatia et al. 2014). In high pressure dry miscible gas displacement, component of the light oil get evaporated and make a homogeneous mixture of gas and oil at interfaces, which helps to move the residual oil from the reservoir. Volatile hydrocarbons (propane and butane) are used in this method. In miscible slug flooding, intermediate hydrocarbon gases are injected before the dry gas injection start. This creates a slug at the front which get displaced by the gas reducing the total cost of the project and increases the oil recovery. Gas injection methods are most widely used for light oil, gas condensate and volatile oil reservoirs (Alvarado and Manrique 2010).

CO_2 flooding is more appropriate when the reservoir pressure is depleted through primary and secondary production. It is particularly effective in reservoirs having low-density crude oil and depth of >2000 ft. CO_2 injection reduces the greenhouse gas and ultimately terminates in CO_2 sequestration (Srivastava et al. 2012). When the injected CO_2 become miscible with the residual oil the physical forces, making the two phases away from each other vanishes, thereby enabling the CO_2 to move the crude oil from the rock pores and thrusting it into production tubing (Fig. 9). According to the US Energy Information Administration (USEIA) (2013), CO_2 floods involve the injection of CO_2 alternated with water (as in case, water-alternating-gas or WAG floods). This help to reduce the trend of low viscous CO_2 to escape through the displaced oil due to gravity segregation. If the injected CO_2 breaks through from the production well, any gas injected afterwards will follow the way, thereby reducing the overall efficiency (Fig. 10).

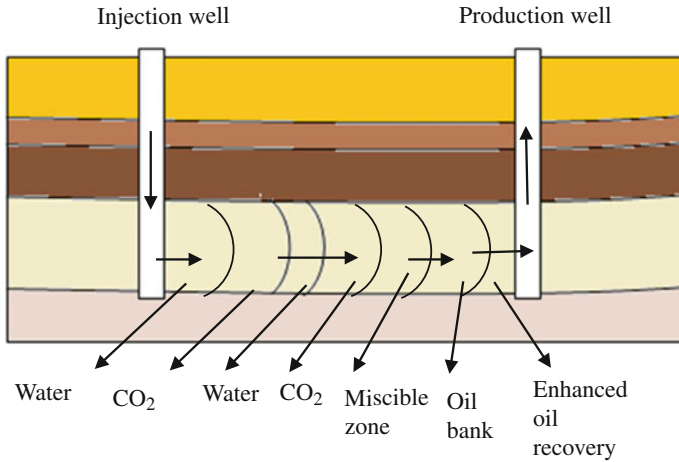**Fig. 9** Schematic of carbon dioxide flood (Shah et al. 2009)
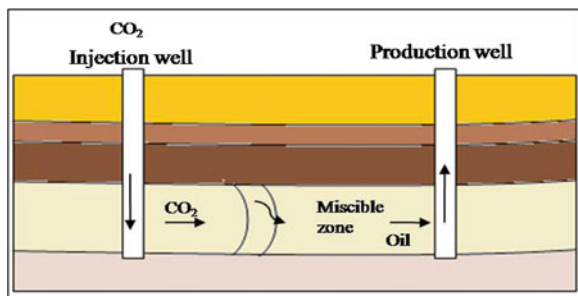
Fig. 10 WAG- carbon dioxide flood

Hydrocarbon flooding engages the injection of hydrocarbon gas into the reservoir. Inside the reservoir, the gas dissolves with the oil, raises the sweep efficiency, and decreases the viscosity in the presence of water (Bhatia et al. 2014). It can also be generated in situ from the impulsive ignition of oil when air is injected into the reservoir. However, this shows the poor mobility ratio compared to other conventional methods. Hydrocarbon gas injection is mostly implemented where the gas supply cannot be monetized.

Though the gas injection can recover the oil effectively, it has poor sweep efficiency. This poor sweep efficiency is due to the unstable viscosity, permeability variation and segregation of the injected gas under gravity. To overcome these problems, foam injection is introduced in 1980. This is a promising technique to increase the gas injection conformance at the well bore and to increase the sweep efficiency in miscible and immiscible gas EOR (Ocampo et al. 2013). Foam has the ability to reduce the gas mobility to overcome the permeability variations (Ashoori and Rossen 2010). There are several types of foam injection techniques such as CO_2 foam, steam foam, surfactant alternating gas (SAG) foam. Strong foam can be produced if there exist a high critical pressure gradient (Feng et al. 2008). Surfactant is added alternating to the gas injection and can be applied to the field, which contains the constraining injection pressure (Shan and Rossen 2004). However, if straight-line relative permeability occurs, this SAG process should not be applied to naturally fractured reservoirs though strong foams can be developed in the fractures (Ashoori and Rossen 2010). In high permeability areas, foam acts as a high viscous liquid and diverts the injected fluid to low permeability rocks, thus it can be a better alternative to polymer flooding in the case of high permeability rocks (Nguyen et al. 2000).

2.4 Thermal EOR

Thermal EOR methods use the form of thermal energy, which is injected into the reservoirs to decrease the viscosity of oil and degrade hydrocarbon in situ, thereby improving the oil recovery. Four common recovery methods involving thermal injection are: in situ combustion (ISC); cyclic steam stimulation (huff and puff/ CSS); steam-assisted gravity drainage (SAGD) and high pressure air injection (HPAI). Figure 11 shows schematically the ISC, which employs the injection of air to ignite the small fraction of oil, generates heat internally, and produces the combustion gases to enhance the oil recovery especially for heavy oil sandstone reservoirs (Yazdani and Maini 2005; Alvarado and Manrique 2010; Capper et al. 2011; Knorr and Imran, 2011). Figure 12 shows schematically the CSS. CSS and SAG Dare performed to recover bitumen and heavy oil from reservoirs (Jiang et al. 2014). SAGD is most popular in the oil sands and extra heavy crude reservoirs of Alberta, and tested in Venezuela with some degree of accomplishment. An interesting study could be the use of solar power to generate steam and drive enhanced oil recovery. The steam generated by solar energy can be used as an alternative to steam injection derived from natural gas. Recently, solar EOR projects are running in California. Solar EOR may be a real alternative to conventional thermal EOR in regions with plentiful sunshine as the economics start to become viable with higher oil prices (Naderi and Babadgli 2010). In the current decade, HPAI is receiving the popularity due to its economic feasibility. It is applicable for light crude oil reservoirs, particularly for in light oil and low permeability carbonate reservoirs (Alvarado and Manrique 2010). As per the report by SAOGL (2013), thermal methods minimize the physical damage and provide an option where other EOR techniques cannot be applied. However, these methods are lengthy, leaves residue in the reservoirs decreasing permeability, porosity, and alter wettability. Significant heat losses do happen in the case of reservoirs with thin formations and high water saturation present in the pay zone (Jiang et al. 2014).

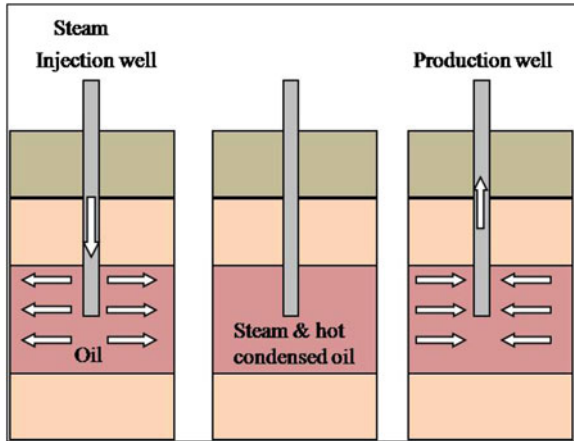Fig. 11 Schematic of In-situ combustion (Shah et al. 2009)
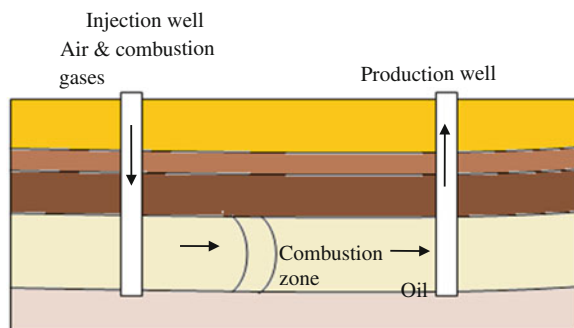
Fig. 12 Cyclic steam stimulation (Shah et al. 2009)

2.5 Ultrasonic and Microwave EOR

Ultrasound is swinging sound pressure wave with a frequency higher than the maximum value of the normal human hearing range. Power ultrasounds in the 20–100 kHz ranges enhance the reaction and at higher power values. Ultrasound changes the properties, such as solubility, mobility, etc. Transducers produce and sense ultrasonic waves in water and break the strong bonded molecules into several parts (Alhomadhi et al. 2013). Application of high frequency sound waves into the reservoir enhances the oil recovery unconventionally. Acoustic waves with high intensity is generated inside the well bore by sending an acoustic emitter and these waves then pass through the porous media and mechanically stimulate the fluids (Hamida 2006). This ultrasound is used to stimulate the water flooding and improves recovery by ~ 16 %. However, the influencing mechanisms are not fully researched (Mohammadian et al. 2011). The awareness about this field is rather less. Another method, such as microwave heating is the thermal stimulation method performed by microwave irradiation. This depends on various parameters, such as heating period, amount of matter, etc. (Datta and Anantheshwaran 2001). Oil and water has both positive and negative particles, which behaves as microscopic magnets. As the positive particles move towards the porous medium, the negative particles get repelled and, thus the heat transfers leading to improved oil recovery (Hascakir et al. 2008).

2.6 Nanotechnology in EOR

Nanotechnology is gaining attention in upstream oil and gas industries. Until now, nanoparticles have become an attractive means for EOR only at laboratory-scale, and ultimately many researchers at lab scale have observed oil recovery for various permeability sandstone rocks (Hendraningrat et al. 2013). Nano EOR is performed by injecting 1–100 nm nano-particles into the reservoir to reduce the viscosity and alter the mobility (Ayatollahi and Zerafat, 2012). These particles alter the chemical interactions responsible for IFT, phase behaviour and contact angle of fluids (Ogolo and Onyekonwu 2012). Recently, nano-emulsions have also gained attention to recover the residual oil. It contains the emulsion made of 5–500 nm particles (Sharma et al. 2014). The success of these nano-emulsions depends on the preparation of the emulsion. Figure 13 represents the schematic of nano-particles in contact with the oil. It illustrates that, a thin film forms at the oil droplet surface and it alters the contact angle of the trapped oil and the rock, which, in turn, reduces the IFT. Implementation of nano-EOR on the reservoir is based on several physical properties of the reservoir, e.g. porosity, permeability, depth of the reservoir, viscosity of the oil, API gravity of the oil, etc.

2.7 Screening Criterion for EOR Methods

The oilfield shows varying characteristics of rock- and fluid properties. It is therefore essential to know the applicability of EOR methods for specific reservoir conditions. Figures 14, 15 and 16 show the screening criteria of EOR based on permeability, oil viscosity and reservoir depth. Table 3 shows the applicability of EOR for various reservoir conditions.
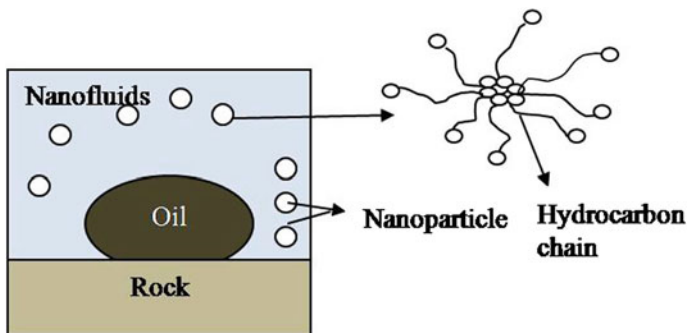

Fig. 13 Illustration of a nanoparticle assisted oil recovery (Das et al. 2008)
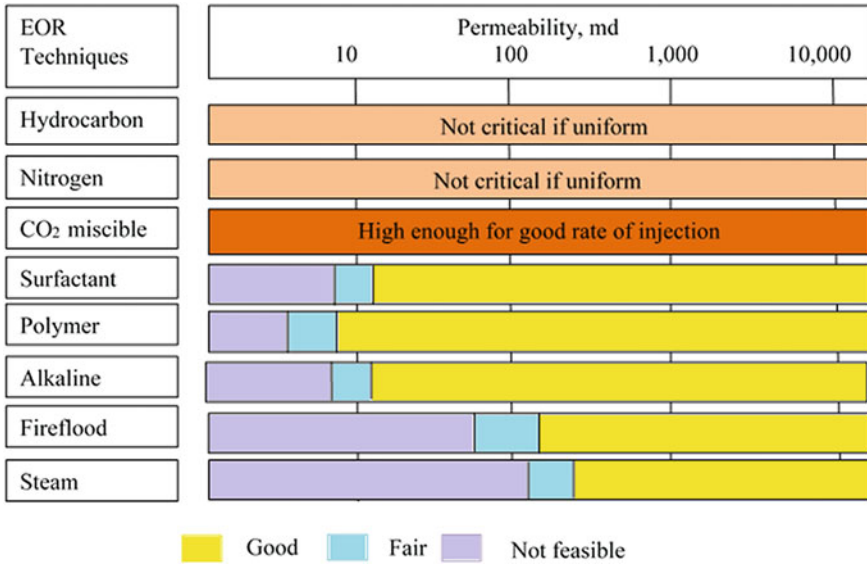
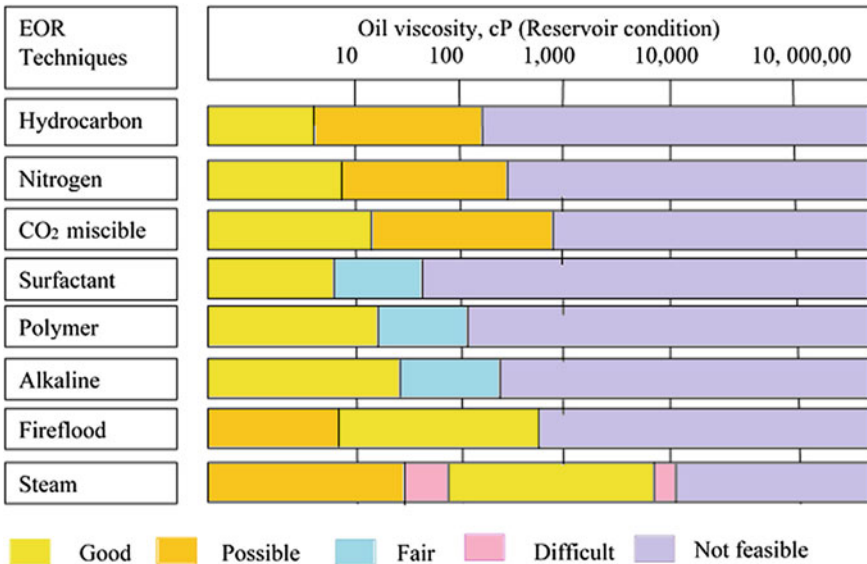**Fig. 14** Screening criteria for EOR methods by permeability (Taber and Martin 1983)

Fig. 15 Screening criteria for EOR methods by viscosity of oil (Taber and Martin 1983)
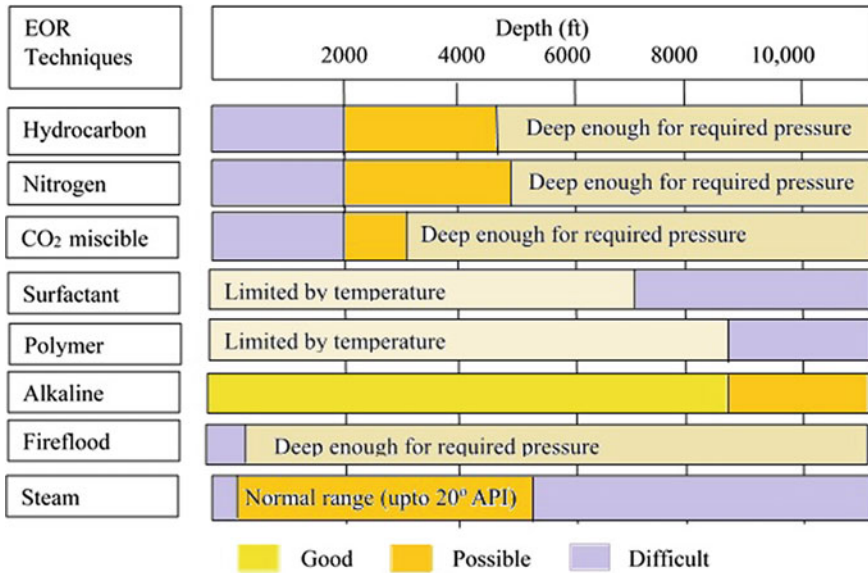
Fig. 16 Screening criteria for EOR methods by depth (Taber and Martin 1983)

3 EOR Techniques: Global Scale

Proved reserves of oil and gas estimates have increased slightly all over the world. Currently oil reserves are estimated to be 1.64 trillion bbl and gas reserves to be 7.02 quadrillion cf, which is 0.4 and 2 % higher compared to the last year. OPEC share has also declined for both the resources. Worldwide oil production is edged up ∼1 % in 2013 (Xu and Bell 2013). The total world oil production from EOR is ∼3 million bpd. It has remained relatively at a lower level over the years. Figure 17 shows the worldwide EOR production rate. Using thermal EOR techniques, ∼2 million bpd oil has been obtained in the recent past. Brazil, China, Canada, California, Indonesia, Oman, Trinidad, Tobago and Venezuela are the countries, which implemented the steam injection for heavy oil sand reservoirs (Kokal and Al-Kaabi 2010). CSS has been effectively executed in Issaran oil field (Egypt), one of the first heavy oil carbonate fields. Steam injection is also followed in Bahrain oil field.

When compared with the total worldwide production, China plays the major role in attempting the EOR technique to maximize the total oil production, which involves mostly the chemical EOR. Daqing oil field in China, which plays the largest role in EOR, employed polymer flooding in most of the wells to increase the sweep efficiency and oil displacement efficiency (Wang et al. 2013). In Saudi Arabia, chemical EOR is implemented in Safania reservoir resulting significant improvement in recovery (Almalik et al. 1997).

Table 3 Applicability of EOR for various oil reservoirs (Adapted from Taber and Martin 1983; Shah et al. 2009)

| S. No	EOR methods	API gravity	Reservoir fluid composition	Depth (ft)	Permeability (md)	Viscosity (cP)	Requirements	Limits
1	Alkaline	13–35	Organic acids	<8400	>20	<200	Naphthenic acids, asphaltenes	Salinity
2	CO₂ injection	25–48	C2-C12	>3000	Not critical	<15	Steep dip, anisotropic	Salinity, fissuring
3	Hydrocarbon flood	30–52	C2-C7	>5000	Not critical	<10	Hydrocarbon intermediate	Low reservoir pressure
4	ISC	8–38	C30+	>500	>100	<1000	Asphaltenes, paraffin	Fissuring
5	N₂ flood	37–55	High % of C1-C7	>5000	Not critical	<10	Steep dip, anisotropic	Fissuring
6	Polymer flood	15–39	Not critical	<8400	>10	<150	High permeability	Fissuring
7	Steam flood	8–32	C30+	300-5000	>600	>20	Low salinity, asphaltenes, paraffin	Hydrophobicity, water saturation
8	Surfactant flood	25–45	Light intermediates	<7800	>20	<30	Low water-cut sand content	Clay content fissuring
9	SAGD	>15	C30+	>3280	>100	<1000	Thick reservoir	Depth more than 1000 m
10	THAI	6–20	Not critical	>300	Not critical	>300	Thick reservoir	Fissuring
11	VAPEX	>15	Not critical-	>3280	Not critical	<500–	Thick reservoir	Depth more than 1000 m
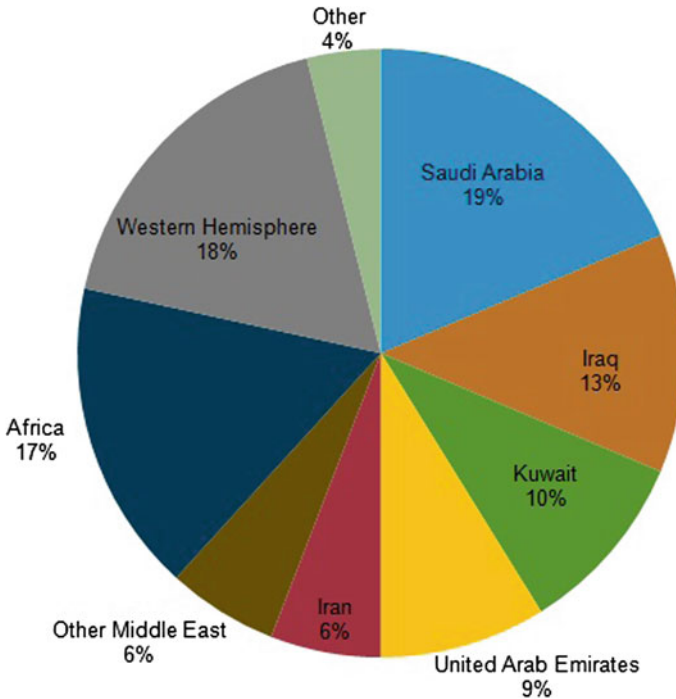
Fig. 17 Worldwide EOR production rate (Kokal and Al-Kaabi 2010)

Microbial EOR at the commercial scale are performed in many oilfields in China. Two different microbes are used to degrade wax and bitumen in the Sha-3 reservoir in Zhuangxi oilfield, China. This reservoir consists of low permeability and highly waxy oil, with temperature of 197.6–239 °F. The microbial degradation process has created 24.6 % of increase in oil recovery. In addition, the percentage of light oil is increased from 3.6 to 6.22 % due to wax degradation (Chen et al. 1999). In China, single strain F-2 and hybrid strain F-23 are used to reduce the viscosity of heavy oil at 113 °F in 6 days using nitrogen and phosphorous as nutrient resulting in 99.15 % reduction in the viscosity of the crude oil (Zhang et al. 2012). In an another case, *Brevibacillus brevis* and *Bacillus cereus* isolated from produced water are used to degrade the long-chain alkanes enhancing the oil recovery in Chaoyanggou Daqing low permeability oilfield in China. The viscosity of the waxy crude oil is reduced by 40 % and accumulative oil increment is observed to be 14,500 tons (Xiaolin et al. 2012). The light oil reservoirs of Gulf region (UAE), Masjed-I Soleyman field (Iran), The Prudhoe Bay oilfield (Alaska, US), Piedras Coloradas field, (Argentina), etc., are some the oilfields in world utilizing the microbes for EOR (Ferguson et al. 1996; Aimaghrabi et al. 1998; Maure et al. 1999).

CO_2 injection has received increased attention all over the world due to the intention to reduce the emission of greenhouse gases. As the US struggles to reduce

the exporting of energy sources and decreasing greenhouse gases emission, CO_2 injection is followed in the Permian Basin in the US and the Weyburn field in Canada. Hydrocarbon gas injection supplies one third of a million bpd from projects in Venezuela, Canada and Libya. In UAE, the Abu Dhabi Company for onshore oil operations started an EOR project in November 2009 to test the injection of CO_2 to increase the oil recovery. Saudi Aramco is currently assessing the use of CO_2 injection and planned a series of pilot studies in mature fields like Ghawar. Pilot scale studies are performed in Abudhabi oilfield containing carbonate cores with a porosity of 10–24 % and permeability 77–149 md and the ultimate recovery factor is increased up to 85 % (Haroun et al. 2012).

4 Indian Scenario for Enhanced Oil Recovery

India is undergoing an emerging trend of economy with other countries like China, Brazil, etc. India's oil and gas industry is intently undergoing exploration opportunities without any major discoveries. In India, crude oil is produced in both onshore and offshore oilfields. According to USEIA report (2012), onshore reserves provide 53 % of oil production and the rest comes from offshore oilfields. Major Indian crude oil reserves are in the western coast (Mumbai High) and in the northeastern parts (Assam, Tripura, etc.). Onshore fields are located in Assam, Andhra Pradesh, Arunachal Pradesh, Gujarat, Nagaland, Rajasthan and Tamil Nadu. Oil India Limited (OIL), Oil and Natural Gas Corporation (ONGC) have the onshore field for the production of crude oil whereas; the offshore production takes place at Bombay High, which is jointly ventured by ONGC and other private companies. Until date, private and foreign firms, such as British Gas, Cairn Energy, Nikko Resources and Reliance Industries control very few oilfields. The operators are struggling to improve the declining production through EOR technologies.

As per the report by USEIA 2012, at the end of 1995, India had 5500 million barrels of reserves. After a decade, it showed only 1 % increase in reserves and at the same time 10 % increase in consumption of crude oil. According to the report by USEIA (2013), the special purpose legal entity, Indian Strategic Petroleum Reserves Limited (ISPRL), possessed by the Oil Industry Development Board, would run the projected amenities. The Indian government planned to start cargo space of 37 million barrels of crude oil at Mangalore, Padur and Visakhapatnam in 2005. In 2006, oil demand in India was 100,000 bpd and during the same year, ONGC accounted for 75 % of country's oil production. The Indian Oil and Gas sector plays the major role in Indian economy and thus falls among the six core industries in India. According to report by the World Energy Council (2013), ONGC plays the foremost role in Indian upstream oil and gas sector. Indian oil sector is mainly conquered by nationalized venture, though the government had taken steps in the past to hold greater foreign connection. Earlier, the foreign

companies played a lead role in discovering various offshore openings. For example, in 2009, Cairn India discovered the largest oilfield, Mangala, of the RJ-ON-90/1 block having 130,000 bpd production capacity in Barmer basin. However, foreign venture in India has faded recently since Indian industries have heavy competition and the existence of strict exploration and production laws (Report by USEIA 2013).

According to MoPNG, India had 8803 million barrels of crude oil reserve and 1437 billion cubic meters of natural gas reserve as on 1st April 2010. In late 2011, the government proposed plans to increase the capacity of proved crude oil reserves to 132 million barrels before 2020 and after a year, India had 5.5 billion barrels. In 2011, according to the energy outlook 2030 report by BP, India was the fourth largest crude oil consumer following China, Japan and US. India had 5.5 billion barrels of proved reserves in 2012 with world's sixth largest refining capacity of 2.56 million bpd, representing approximately 3 % of the world capacity (Report by USEIA 2012). In 2013, the demand of crude oil is over 4 million bpd and in 2021, it is expected to be 14 million bpd. This gap can be reduced by the application of EOR on various mature reservoirs across India. It is reported in the India energy portal (2013) that the total crude oil production has been stagnated to around 32–33 MMT for the past 16 years. The government set goals to achieve 132 million barrels of the crude reserves by 2020. In addition, various government organizations have committed to set up an independent support of assets that might help in foreign energy acquirement (Sharma 2010). With the current rate of production, these proven reserves will meet the needs of Indian economy for the next 20 years. Over the past few decades, the gross domestic product (GDP) of India has increased from 36 billion USD to about 1.25 trillion USD. By 2035, India is expected to become the third largest economy next to US and China with the annual growth rate of 6.2 %.

The Rajasthan joint venture of Cairn India (70 %) and ONGC (30 %) is planning to drill 48 infill wells by 2014, which is further targeted to go for EOR application, which may include chemical intervention to sustain plateau production rates for a longer period. According to BP statistical review of energy (2013), India has only 0.4 % of proven oil resources and 0.6 % of world natural gas resources. Due to the increasing oil consumption, the unwavering production rate is not satisfying the demand, thereby making makes India dependent on importing more than 6 % of its crude oil requirement from other countries to overcome the needs (Patra 2013). Figure 18 shows the energy map of India, which depicts various oilfields, gas reservoirs, coalfields, thermal power plant and nuclear power plant present in the country. Figure 19 shows the total oil production in various states and the statistics of imports from other countries. Gujarat plays the key role in oil production followed by Rajasthan and Northeast regions. The oil producing regions in India are Assam, Gujarat, Mumbai and Rajasthan. In Assam, oilfields are located in Dibrugarh, Digboi, Makam, Naharkatia and Surma. In Gujarat the oilfields are located in Ankleshwar, Balol, Jhalora, Kalol, Mehsana, Sanand, Santhal and Viraj (Qazi and Qazi 2007).
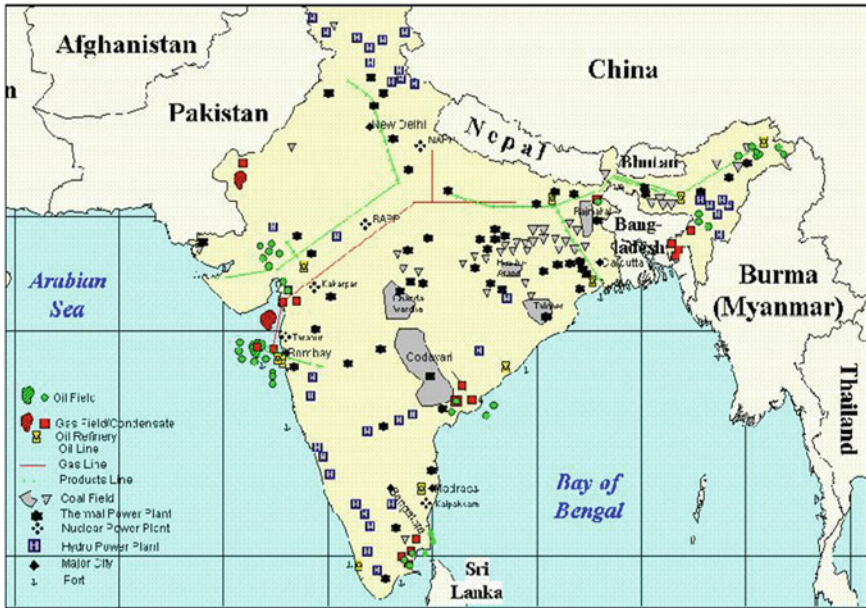
Fig. 18 Energy map of India (Report by USEIA 1997)
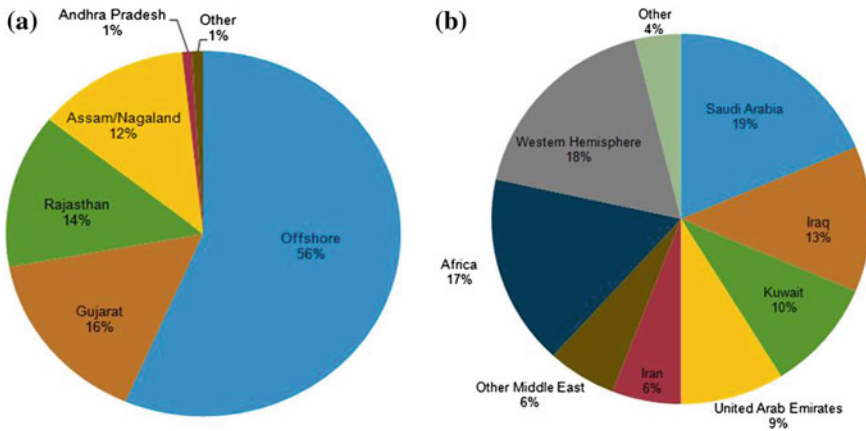
Fig. 19 Oil production and oil import in India; **a** production rate of oil in various states; **b** oil imports from various countries (Report by USEIA 2013)

4.1 Basins in India

Petroleum basins in India are showing immense guarantee for fresh findings with increasing thirst for the country's energy and fuel. Figure 20 shows the various basins in India. Assam-Arakan Basin, (Jorhat), Cauvery Basin (Chennai),
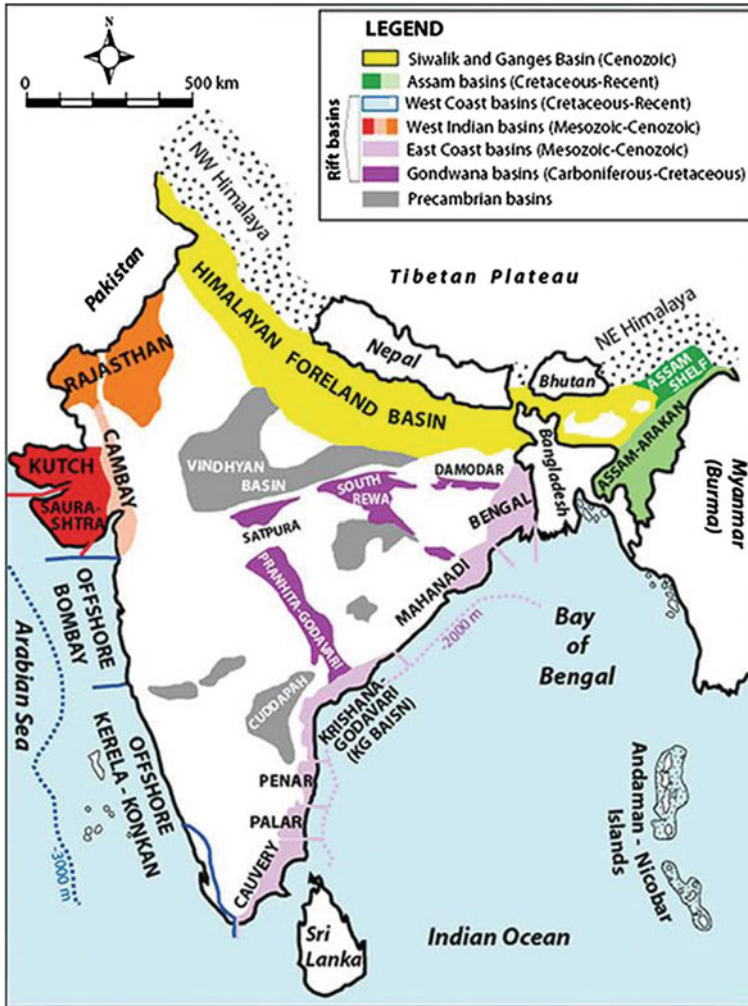
Fig. 20 Various basins in India (Rasoul 2008)

CBM-BPM Basin (Kolkata) and Frontier Basin (Dehradun), Krishna-Godavari Basin (Rajahmundry), Western Offshore Basin (Mumbai) and Western Onshore Basin (Vadodara) are in the control of ONGC. The Assam-Arakan basins in the northeast India hold more than 10 % of the country's crude oil reserves. Recently, Gujarat State Petroleum Corporation and Andhra Pradesh Gas Infrastructure Corporation discovered many new wells in Barmer basin in Rajasthan and the offshore Krishna-Godavari basin and expands the country's production to some extent (Report by USEIA 2013). The Cambay basin is a narrow elongated rift expanding from north to south on the western edge of India (Gupta et al. 2012). It

Fig. 21 Various fields in Barmer basin (Sullivan et al. 2007)

contains several small and big hydrocarbon fields in Tertiary sediments (Pratap et al. 2006). The Deccan Trap forms the technical basement of petroliferous Cambay basin. Padra, a small field situated on eastern border of Cambay basin is unique, as here, in addition to Tertiary sediments, the Deccan Trap basaltic rocks are commercial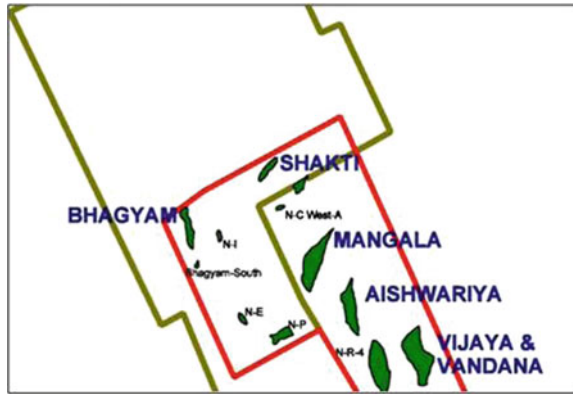 oil producers. The depth to the basement varies from about 400 m in the east to about 800 m in the west towards the basin axis (Kumar et al. 2002). In the matured Cambay basin, 5000 wells have been drilled and 1150 million tons of OOIP has been recovered (Sharma and Kulkarni 2010).

The Mangala Field was discovered in January 2004 in tertiary Barmer Basin (Yashwant et al. 2006). The Mangala oilfield contains sweet waxy crude oil with 20° API and low gas oil ratio (GOR) of about 180 scf/bbl with the viscosity of in situ oil ranging from 9–22 cP (Kumar et al. 2008; Mckenzie et al. 2011). Figure 21 shows the various oilfields in Barmer basin, Rajasthan. The Cauvery, Krishna-Godavari, Mahanadi and Palar are the four sedimentary basins along the east coast of India. Mahanadi Basin covering 18,000 km^2 onshore and 12,500 km^2 offshore is in the northern part along the east coast of India. The Krishna-Godavari Basin covers an area of 15,000 km^2 onshore and extends into the Bay of Bengal. Palar, a smallest basin falls between the Cauvery in the south and the Krishna-Godavari in the north (Talukdar 1982).

4.2 EOR Techniques in Indian Reservoirs

India is the world's fifth largest energy consumer, sixth largest oil consumer and imports more than half of the demand from the overseas. This prevailing scenario involves the need of sufficient and consistent energy to the Indian people in the midst of growing demand of energy and support by economic growth. Secondly, import of oil is the driving force for energy security and vital to meet the India's
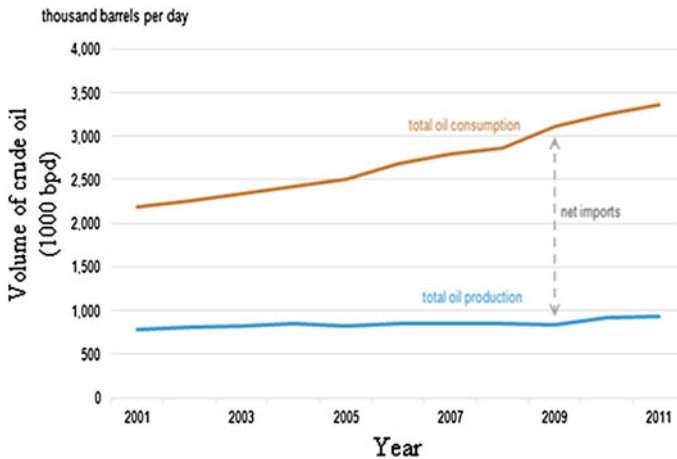
Fig. 22 Demand and supply of oil in India (Report by USEIA 2013)

vast energy requirement. Increase in import leads the nation to larger geopolitical difficulties and international price volatility (Ahn and Graczyk 2012; Patra 2013). Hence, this increasing demand not only affects the consumers, but also plays the key role in political and international level (Rasoul 2008). Figure 22 shows the demand and supply gap. In India, only about 27 % of the OOIP is being produced economically. Recovering the remaining oil and gas resources poses formidable technical and financial challenges. To recover the last drop of oil economically from the reservoir, lot of research work is going on. As the production from many onshore fields is in decline, companies are now looking to implement EOR technologies to boost and maximize domestic production. For instance, Cairn India is finalizing polymer flood on a pilot scale on the Mangala oilfield and with the initial encouraging results, it is now considering a full field wide application of the technique.

Thermal method comprises approximately 70 % of all EOR techniques followed in India, which includes 50 % of in situ combustion (Ramachandran et al. 2010). In many heavy oilfields in onshore assets operated by ONGC, in situ combustion has been used. Balol and Santhal oilfield were discovered in 1971 in the northern part of Gujarat. The production was started in 1971 on Santhal and in 1985 on Balol oilfield (Turta et al. 2007). This project is initiated at Balol field (Gujarat) on pilot scale and later, the project is expanded to commercial scale at Balol and Santhal field, Gujarat (Chattopadhyay et al. 2003; Chattopadhyay et al. 2004). ISC has been implemented in Balol oilfield in 1990 and it is commercialized in Santhal field since 1997 for enhancing the heavy oil recovery. Santhal field is a North-South sloping monocline surrounded by Mehsana Horst towards the west and falling towards the east. Production was started in Mehsana asset on 1968 with the rate of production of about 191 bpd. OOIP has decreased from an average 25, 15 and 9 % on successive three decade. In Santhal field about 15 MMT of trapped oil has been recovered with

the aid of in situ combustion process (Panchanan et al. 2006). ISC is implemented technically and commercially in this field and production has improved by 540 tons over the period of 5 years (Chattopadhyay et al. 2004). In addition, the research on ISC projects is being carried at the Institute of Reservoir Studies (IRS), ONGC, Ahmadabad, India (Taglia 2010). In light oil onshore asset of ONGC, air injection technique is followed to enhance the oil recovery. The reservoir temperature is typically 158 °F with a viscosity of around 2–3 cP. Air injection enhanced the oil recovery by about 62 % (Mitra et al. 2010). CO_2-WAG flooding is implemented in an Eocene sandstone reservoir in Cambay basin Gujarat, which is at a temperature of 172 °F and a pressure of 1508 psi. After the implementation, WAG is raised to 11,000 m^3/day from 200 m^3/day and water cut is reduced significantly (Srivastava et al. 2012). Immiscible hydrocarbon WAG is employed in Ankleshwar asset (Gujarat) containing a sandstone reservoir of depth 2800 m. The reservoir contains saturated light oil at 266 °F reservoir temperature with 47 °API and 0.2 cP viscosity. This reservoir is not suitable for miscible flooding due to the requirement of higher miscibility pressure compared to the reservoir pressure of 3500 psi. The enhancement of 30 % in the oil recovery is observed after the implementation of WAG EOR. WAG is also implemented in light oil reservoir with the temperature of 262 °F and pressure of 3271 psi in Gandhar oilfield (Gujarat) and 40 % of improvement in oil recovery has been observed (Srivastava and Mahli 2012).

Sanand oilfield located in Ahmedabad-Mehsana tectonic block of Cambay Basin, Gujarat, was discovered in 1962 and the production was started in 1969 (Pratap and Gauma 2004). Polymer flooding was introduced in the year 1985 through 5 spot injection techniques, thereby 23 % of proved the oil in place has been recovered (Tiwari et al. 2008). In the Ahmedabad asset (Gujarat), ONGC has carried out polymer flooding pilot studies on the Kalol field with some success and are conducting pilot studies in Ankleshwar using miscible gas flooding and CO_2 injection (Panchanan et al. 2006). Jhalora oilfield located in Ahmedabad-Mehsana tectonic block of Cambay Basin, Gujarat, was discovered in 1967 and the production was started in 1978 (Pratap and Gauma 2004). Overall, Jhalora field contains 29 wells and, until now, it has produced 3.41 MMT oil. ASP flooding is implemented in K-IV well in Jhalora field having sandstone rock and 23 % of an incremental displacement efficiency is observed (Jain et al. 2012). ASP flooding is also implemented in Viraj oilfield in Cambay basin and the enhancement of 18 % recovery of OOIP is observed (Pratap and Gauma 2004). Polymer flooding is also applied in Mangala Field of Barmer Basin in pilot scale and the water cut is reduced effectively (Pandey et al. 2012).

Microbial EOR is not implemented in India due to the lack of various studies on the reservoirs suitable for this operation. Mesophilic bacterial consortium (FIB-19) is injected into the surface flow lines of ten wells of Mehsana Asset (Gujarat, India) containing heavy oil and found 67 % wax degradation at 98.6 °F (Biswas et al. 2012). ONGC and TERI developed bacterial strains effective up to 194 °F from formation water samples. Based on encouraging results in ONGC's wells, OIL has implemented MEOR in its fields having wells with a temperature of 158–185 °F, in two phases of 3 and 5 wells in 2005 and 2008, respectively, in Mehsana asset,

Table 4 Oilfields in India

S. No	Oilfield	Operator	State	Year of discovery	Production rate (bpd)	Area (km²)
1	Aishwarya	Cairn, ONGC	Rajasthan	2013	10,000	–
2	Allora	Heramec, GSPCL	Gujarat	1967	70–80	6.85
3	Ankleshwar	ONGC	Gujarat	1958	21,000	–
4	Asjol	GSPCL, HOEC	Gujarat	1995	75,000	15
5	Balol	HOEC	Gujarat	1971	4400	27.3
6	Bhagyam	Cairn, ONGC	Rajasthan	–	25,000	–
7	Bhandut	GSPCL, NIKO	Gujarat	–	146,795	6
8	Bombay high	ONGC	Mumbai	1965	140	–
9	Dholasan	GNRL	Gujarat	1972	75,000	8.7
10	Dholka	Joshi Technologies	Gujarat	1995	720	–
11	Digboi	IOCL	Assam	–	–	13
12	Gandhar	ONGC	Gujarat	1983	30,000	–
13	Hazira	GSPCL, NIKO	Gujarat	1995	2000	50
14	Jhalora	ONGC	Gujarat	1967	1663	–
15	Jorajan	HOEC	Assam	–	–	–
16	Kalol	ONGC	Gujarat	–	–	–
17	Kusijan	HOEC	Assam			
18	Kosamba	ONGC	–	–	–	–
19	Lakshmi-Gauri	Cairn	Gujarat	2005	–	–
20	Lunej	ONGC	Gujarat	1958	30,122	11.2
21	Kanawara	GNRL	Gujarat	1971	–	6.3
22	Mangala	Cairn, ONGC	Rajasthan	2004	15,000	–
23	Moran Hugrijan	HOEC	Assam	1953	–	–
24	Narimanam	ONGC	Tamilnadu	–	4032	–
25	Naharkatia	OIL	Assam	1953	50,203	–
26	Navagam	ONGC	Gujarat	–	–	–
27	North kadi	ONGC	Gujarat	1969	174	
28	North Kathana	GNRL	Gujarat	1975	–	12.2
29	Panna-Mukta	RIL, BG, ONGC	Mumbai	2010	35,000	430
30	Pramoda	HOEC, ONGC	Gujarat	2005	–	–
31	Ravva	Cairn, ONGC, Ravva oil	AP	1987	–	331
32	Raageshwari	Cairn	Rajasthan	2012	500	–
33	Saraswathi	Cairn	Rajasthan	2011		–
34	Sabarmathi	GSPCL, NIKO	Gujarat		74,000	5.8
35	Santhal	ONGC	Gujarat	1985	3958	–
36	Sanand	ONGC	Gujarat	1962	–	–
37	Shanti-Tarajan	HOEC	Assam	–	–	–
38	Sobhasan	ONGC		1960	377	–
39	South kadi		Gujarat		–	–
40	Unawa	GSPCL	Gujarat	1984	111,000	5.7
41	Viraj	ONGC	Gujarat	1977	–	–
42	Wavel	Joshi Technologies	Gujarat	2004	75	–

Table 5 Name of the oilfields in India and their properties

S. No	Field	Reservoir conditions							Existing EOR process	Proposed EOR process	Criteria for applying proposed EOR
		P (Psi)	T (°F)	k (d)	η_{OIL} (cP)	ϕ (%)	D (ft)	°API			
1	Balol	1500	154	3–8	300	28	1049	45	ISC	–	–
2	Dholka	–	–	1.9–8.7		15–50	900–1200	40	Natural depletion	Steam flooding	Since the depth is low from the surface steam flooding can give better recovery
3	Gandhar	3271	262	5–40		18–25	2850	42	WAG	–	–
4	Hazira	–	–	–	–	–	1500		Water drive	–	For low depth water flooding is good
5	Jhalora	1962	–	1.9–8.7	30–50	25–35	1270	22.3	ASP	–	–
6	Kalol	–	180	1	18–20	20–30	1500	–	Polymer flooding and water injection	–	–
7	Kanawara	–	–	1.4	–	–	3500	–	Natural depletion	ISC	Because of low permeability and high depth
8	Mangala Bhagya Aishwarya	–	180	–	9–22	30	900–1200	27	Polymer flooding	–	–
9	Mangala	–	140	–	5	–	–	27	–	MEOR	Because of high waxy nature
10	Mehsana	1450	154	–	–	50–450	–	–	ISC	Microbial	Because of low temperature and high viscosity
11	Panna	2550	1800	–	–	–	1737	–	Water injection	–	Since it is near (50–60 m) to sea level, water injection is good
12	RAVVA	–	–	–	–	–	3400	–	Natural depletion	Polymer flooding	Since the temperature and pressure is high. It is preferred
13	Sabarmathi	–	–	–	–	–	659	–	–	–	–
14	Sanand	2059	185	1.5	20–30	20	1325	21.2	Polymer flooding	–	–
15	Santhal	1450	154	3–5	50–200	28	–	40	–	–	–
16	Sobhasan	426	–	15–5	13–24	–	–	–	–	–	–
17	Viraj	1977	178	4.5–9.9	50	30	1300	19	ASP flooding	Polymer flooding	Since the permeability is very low, polymer flooding is preferred

*P-pressure, T-temperature, D-depth, μ- permeability, η-viscosity, ϕ -porosity, °API- API gravity, GSPCL-Gujarat State Petroleum Corporation Limited, GNRL-Gujarat Natural resources Limited, RIL-Reliance Industries Limited, BG-British Gas, HOEC-Hindustan Oil Exploration Corporation Limited, IOCL-Indian Oil Corporation Limited

Gujarat. Recently ONGC and TERI has implemented MEOR jointly in 50 wells at ONGC, Ahmedabad and Gujarat asset and 5 oil wells in Assam asset. The Mangala field discovered in 2004 in Barmer basin (Rajasthan) consists of five reservoirs with 1.3 billion barrels of OOIP (Zalawadia and Pwade 2013). The crude oil in this field is highly waxy in nature with the wax appearance temperature (WAT) of 43 °F. Owing to this waxy nature and temperature of 140 °F, MEOR can be a better option for this field to increase the oil recovery. In general EOR techniques has been implemented in many fields but still more improvement is required to improve the economy and decrease the dependency of importing oil from the foreign countries. Table 4 shows the various oilfields located in India and its operators and Table 5 shows the reservoir conditions of various oilfields and the existing EOR process (Figs. 20, 21 and 22).

References

Adasani AA, Bai B (2011) Analysis of EOR projects and updated screening criteria. J Petrol Sci Eng 79:10–24

Ahn SJ, Graczyk D (2012) Understanding energy challenges in India policies, players and issues, pp 1–116. International Energy Agency. https://www.iea.org/publications/freepublications/publication/India_study_FINAL_WEB.pdf

Aimaghrabi I, Chaalal O, Islam MR, AI-Ain (1998) Thermophilic bacteria in UAE environment can enhance biodegradation and mitigate well bore problems. SPE 49545:778–788

Al-Dousari MA, Garrouch AA (2013) An artificial neural network model for predicting the recovery performance of surfactant polymer floods. J Petrol Sci Eng 109:51–62

Alhomadhi E, Amro M, Almobarky M (2013) Experimental application of ultrasound waves to improved oil recovery during water flooding. J King Saud Univ, pp 103–110

Almalik MS, Attia AM, Jang LK (1997) Effects of alkaline flooding on the recovery of Safaniya crude oil of Saudi Arabia. J Pet Sci Eng 17:367–372

Alvarado V, Manrique E (2010) Enhanced oil recovery: an update review. Energies 3:1–47

SAOGL (Sino Australia Oil and Gas Limited) An introduction to enhanced oil recovery techniques (2013) http://www.sinoaustoil.com/irm/content/pdf/Sino%20Australia%20Oil%20and%20Gas%20Technical%20Information.pdf. Accessed June 2013, pp 1–18

Annual energy outlook 2012 with projections to 2035 (2012) US Energy Information Administration. http://www.eia.gov/forecasts/aeo/pdf/0383%282012%29.pdf. Accessed June 2012, pp 1–252

Ashoori E, Rossen WR (2010) Can formation relative permeabilities rule out a foam EOR process. SPEJ 17:340–351

Ayatollahi S, Zerafat MM (2012) Nanotechnology assisted EOR techniques: new solutions to old challenges. SPE 157094:1–15

Banat IM (1995) Biosurfactants production and use in microbial enhanced oil recovery and pollution remediation: a review. Bioresour Technol 51:1–12

Bassion G, Sanders A (2013) Application of EOR/IOR techniques. Flow assurance: tackling tomorrow's challenges Oslo, Norway, 13–14 November 2013

Bhatia J, Srivastava JP, Sharma A, Sangwai JS (2014) Production performance of water alternate gas injection techniques for enhanced oil recovery: effect of WAG ratio, number of WAG cycles and the type of injection gas. Int J Oil Gas Coal Tech 7:132–151

Biswas SK, Kukreti V, Rana DP, Sarbhai MP, Bateja S, Misra TR (2012) Application of microbial treatment for mitigating the paraffin deposition in downhole tubular and surface flow lines of wells-A success story. SPE 154662:1–7

Blunt M, Fayers FJ, Franklin M (1993) Carbon dioxide in enhanced oil recovery. Energy Convers Manage 34:1197–1204

Bordoloi NK, Konwar BK (2008) Microbial surfactant-enhanced mineral oil recovery under laboratory conditions. Colloids Surf B 63:73–82

BP Statistical Review of World Energy June (2010) http://www.bp.com/liveassets/bp_internet/globalbp/globalbp_uk_english/reports_and_publications/statistical_energy_review_2008/STAGING/local_assets/2010_downloads/statistical_review_of_world_energy_full_report_2010.pdf. British Petroleum, London, United Kingdom. Accessed June 2010, pp 1–50

BP Statistical Review of World Energy June (2013) http://www.bp.com/content/dam/bp/pdf/statistical-review/statistical_review_of_world_energy_2013.pdf. British Petroleum, London, United Kingdom. Accessed June 2013, pp 1–48

BP Energy Outlook 2030 (2013) http://www.bp.com/liveassets/bp_internet/globalbp/globalbp_uk_english/reports_and_publications/statistical_energy_review_2011/STAGING/local_assets/pdf/BP_World_Energy_Outlook_booklet_2013.pdf. British Petroleum, London, United Kingdom. Accessed Jan 2013, pp 1–86

Brown LR (2010) Microbial enhanced oil recovery. Curr Opin Microbiol 13:316–320

Capper L, Kuhlman MI, Vassilellis GD, Marvin Schindler M, Fitzpatrick N (2011) Advancing thermal and carbon dioxide recovery methods beyond their conventional limits: downhole innovation. SPE 150515:1–24

Chattopadhyay SK, Ram B, Bhattacharya RN, Das TK (2003) Enhanced oil recovery by in-situ combustion process in Balol field of Cambay basin—A case study. A paper presented at Indian oil and gas review symposium, Mumbai, India 8–9 Sep 2003

Chattopadhyay SK, Ram B, Bhattacharya SK, Das TK (2004) Enhanced oil recovery by in-situ combustion process in Santhal field of Cambay basin, Mehsana, Gujarat, India-A case study. SPE-89451: 1–6

Chen W, Miao M, Chen L, Wan D (1999) Enhance oil production in high waxy oil reservoir by single well cyclic microbial injection-production. SPE 57303:1–3

Das SK, Choi SUS, Yu W, Pradeep T (2008) Nanofluids science and technology. Wiley-Interscience, Hoboken

Datta AK, Anantheshwaran RC (2001) Handbook of microwave technology for food application. Newyork, Basel. ISBN 0-8247-0490-8

Donaldson EC, Chilingarian GV, Yen TF (1989) Enhanced oil recovery, II, Processes and Operations, Elsevier publications, ISBN 978-0-444-42933-9

Dubin PL, Gruber JH, Xia J, Zhang H (1992) The effect of cations on the interaction between dodecylsulfate micelles and poly (ethyleneoxide). J Colloid Interf Sci 148:35–41

Etoumi A (2007) Microbial treatment of waxy crude oils for mitigation of wax precipitation. J Pet Sci Eng 55:111–121

Feng LR, Yan W, Liu S, Hirasaki GJ, Miller CA (2008) Foam mobility control for surfactant EOR. SPE 113910:1–16

Ferguson KR, Lloyd CT, Spencer D, Hoeltgen J (1996) Microbial pilot test for the control of paraffin and asphaltenes at Prudhoe Bay. SPE 36630:1–8

Gao B, Sharma MM (2013) A family of alkyl sulfate gemini surfactants. 2. Water–oil interfacial tension reduction. J Colloid Interf Sci 407:375–381

Gao S, Li H, Li H (1995) Laboratory investigation of combination of alkaline-surfactant-polymer for Daqing EOR. SPEJ 10:194–197

Gupta SD, Chatterjee R, Farooqui MY (2012) Formation evaluation of fractured basement, Cambay basin. J Geophys Eng, India, p 9

Hamida T (2006) The influence of ultrasonic energy on capillary fluid displacement. SPE 106521:1–30

Haroun M, Hassan SA, Ansari A, Kindy NA, Sayed NA, Ali B, Sarma H (2012) Smart nano-EOR process for Abu Dhabi carbonate reservoirs. SPE 162386:1–13

Herron EH, King SD (2004) Heavy Oil as the Key to U.S. Energy Security. http://www.petroleumequities.com/cgi-bin/site.cgi?p=energysecurity.html&t=5. Accessed Dec 2004

Hezave AZ, Dorostkar S, Ayatollahi S, Nabipour M, Hemmateenejad B (2013) Effect of different families (imidazolium and pyridinium) of ionicliquids-based surfactants on interfacial tension of water/crudeoil system. Fluid Phase Equilibr 360:139–145

Hirasaki GJ, Miller CA, Puerto,M (2008) Recent advances in surfactant EOR, meeting the energy needs of a growing world economy. Paper presented at the international petroleum technology conference, Kualalumpur, Malaysia 3–5 Dec 2008

Hascakir B, Acar C, Demiral B, Akin S (2008) Microwave assisted gravity drainage of heavy oils. IPTC 12536:1–9

Hendraningrat L, Li S, Torsaeter O (2013) A core flood investigation of nanofluid enhanced oil recovery. J Petrol Sci Eng 111:128–138

Iglauer S, Wu Y, Shuler P, Tang Y, Goddard WA (2010) New surfactant classes for enhanced oil recovery and their tertiary oil recovery potential. J Petrol Sci Eng 71:23–29

Iglesias BR, Lorenzo AC, Concheiro A (2003) Poly (acrylic acid) micro gels (carbopol 934) / surfactant interactions in aqueous media. Part 1: nonionic surfactants. Int J Pharm 258:165–177

India analysis (2013) U.S. Energy Information Administration. http://www.eia.gov/countries/cab.cfm?fips=in. Accessed 18 March 2013

India—An energy sector overview (1997) US energy information administration. http://www.lib.utexas.edu/maps/middle_east_and_asia/india_energy_1997.gif

Ivory J, Chang J, Coates R, Forshner K (2010) Investigation of cyclic solvent injection process for heavy oil recovery. J Can Petrol Technol 49:22–33

Jain AK, Dhawan AK, Misra TR (2012) ASP flood pilot in Jhalora K-IV—A case study. SPE 153667:1–7

Jiang T, Zeng F, Jia X, Gu Y (2014) A new solvent-based enhanced heavy oil recovery method: cyclic production with continuous solvent injection. Fuel 115: 426–433

Knorr KD, Imran M (2011) Solvent chamber development in 3-D physical model experiments of solvent vapour extraction processes (SVX) with various permeabilites and solvent vapour qualities. SPE 149190:1–18

Kokal S, Al-Kaabi A (2010) Enhanced oil recovery: challenges and opportunities. World petroleum council official publication. Global energy solution. http://www.world-petroleum.org/docs/docs/publications/2010yearbook/P64-69_Kokal-Al_Kaabi.pdf. pp 64–69

Kumar A, Pendkar N, Sangeeta (2002) Delineation and evaluation of basaltic Deccan basement reservoir of padra field, cambay basin, India field study. SPWLA 43rd annual logging symposium, 2–5 June 2002

Kumar S, Kumar P, Tandon R, Beliveau D (2008) Hot water injection pilot: a key to the waterflood design for the waxy crude of the Mangala field. IPTC 12622:1–11

Lake LW, Schmidt RL, Venuto PB (1992) A niche for enhanced oil recovery in the 1990s. Oilfield Rev 4:55–61

Larter SR, Huang H, Adams J, Bennett B, Snowdon LR (2012) A practical biodegradation scale for use in reservoir geochemical studies of biodegraded oils. Org Geochem 45:66–76

Li GZ, Mu JH, Li Y, Yuan SL (2000) An experimental study on alkaline/surfactant/polymer flooding systems using nature mixed carboxylate. Colloid Surf A 173:219–229

Mandal A, Ojha K (2008) Optimum formulation of alkaline-surfactant-polymer systems for enhanced oil recovery. SPE-114877:1–12

Maure MA, Dietrich FL, Diaz VA, Arganaraz H (1999) Microbial enhanced oil recovery pilot test in Piedras Coloradas field Argentina. SPE 53715:1–28

Mckenzie TJ, Wenk ADJ, Khan P, Gavioli P, Andrew CP (2011) World's first hybrid inflow control completion in India's largest onshore. SPE 141540:1–18

Miller RM, Zhang Y (1997) Measurement of biosurfactant-enhanced solubilization and biodegradation of hydrocarbons. Methods Biotechnol 2:59–66

Mitra U, Bhushan BV, Raju PV, Kumar S, Sur S, Mehta SA, Moore RG (2010) Feasibility of air injection in a light oilfield of western India. SPE 126234:1–8

Mohammadian E, Shirazi MA, Idris AK (2011) Enhancing Oil Recovery through Application of Ultrasonic Assisted Water flooding. SPE 145014:1–10

Mokhtab S, Towler B (2009) Wax prevention and remediation in subsea pipelines and flowlines. Deepwater technology. World oil defining technology for exploration drilling and production 2009, p 230

Naderi K, Babadagli T (2010) Influence of intensity and frequency of ultrasonic waves on capillary interaction and oil recovery from different rock types. Ultrason Sonochem 17:500–508

Nedjhioui M, Moulai MN, Morsli A, Bensmaili A (2005) Combined effects of polymer/surfactant/oil/alkali on physical chemical properties. Desalination 185:543–550

Needham BR, Hoe PH (1987) Polymer flooding review. J Pet Technol 39:1503–1507

Nguyen QP, Alexandrov AV, Zitha PL, Currie PK (2000) Experimental and modeling studies on foam in porous media: a review. SPE 58799:1–22

Ocampo A, Restrepo A, Cifuentes H, Hester J, Orozco N, Gil C, Castro E, Lopera S, Gonzalez C (2013) successful foam EOR pilot in a mature volatile oil reservoir under miscible gas injection. IPTC 16984:1–9

Ogolo NA, Onyekonwu MO (2012) Enhanced oil recovery using nanoparticles. SPE 160847:1–9

Panchanan GK, Kumar V, Mukherjee TK, Bhattacherya RN (2006) An overview of santhal field, an EOR implemented field of cambay basin, inferred from 3D seismic. Paper presented at Geohorizons 2006, p 48–52

Pandey A, Kumar SM, Jha MK, Tandon R, Punnapully SB, Kalugin MA, Khare A, Beliveau D (2012) Chemical EOR pilot in mangala field: results of initial polymer flood phase. SPE 154159:1–8

Patra DC (2013) India's energy scenario in 2013—challenges and prospects. Hydrocarbon Asia, Jan–Mar 2013:6–9

Pereira JFB, Gudiña EJ, Costa R, Vitorino R, Teixeira JA, Coutinho JAP, Rodrigues LR (2013) Optimization and characterization of biosurfactant production by *Bacillus subtilis* isolates towards microbial enhanced oil recovery applications. Fuel 111:259–268

Pratap V, Sood RK, Ram B (2006) IOR strategies in brown fields of Mehsana asset of north Cambay basin, India. SPE 102298:1–11

Pratap M, Gauma MS (2004) Field implementation of alkaline surfactant flooding-A maiden effort in India. SPE 88455:1–5

Qazi SA, Qazi NS (2007) Geography of the world. APH Publishing Corporation, New Delhi, pp 1–391

Qi WK, Yu ZC, Liu YY, Li YY (2013) Removal of emulsion oil from oilfield ASP wastewater by internal circulation flotation and kinetic models. Chem Eng Sci 91:122–129

Ramachandran KP, Gyan ON, Sur S (2010) Immiscible hydrocarbon WAG: laboratory to field. SPE 128848:1–11

Ramakrishna S (2008) Biotechnology in petroleum recovery: the microbial EOR. Prog Energ Combust 34:714–724

Rasoul S (2008) Putting India on the World's petroleum map, http://www.geotimes.org/feb08/article.html?id=feature_oil.html. Geotimes, Earth, Energy and Environment news, Accessed Feb 2008

Sabhapondit A, Borthakur A, Haque I (2002) Characterization of acrylamide polymers for enhanced oil recovery. J Appl Polym Sci 87:1869–1878

Sadeghazad A, Ghaemi N (2003) Microbial prevention of wax precipitation in crude oil by biodegradation mechanism. SPE 80529:1–11

Shah A, Fishwick R, Wood J, Leeke G, Rigby S, Greaves M (2009) A review of novel techniques for heavy oil and bitumen extraction and upgrading. Energy Environ Sci 700:700–714

Shan D, Rossen WR (2004) Optimal injection strategies for foam IOR. SPEJ 9:132–150

Sharma T (2010) Introduction to Indian upstream oil and gas sector, Innovation Norway. http://ullriggcentre.no/internet/UllriggCentre.nsf/8843a10c4f5bf977c1256eb60067a105/54a9252f807dafeec125776200418a96/$FILE/Indian%20Oil%20and%20Gas%20Scenario.pdf. Accessed Sep 2010

Sharma SS, Kulkarni PK (2010) Gas strike in shale reservoir in Dholka field in Cambay basin. SPE 129082:1–6

Sharma T, Suresh Kumar G, Chon BH, Sangwai JS (2014) Thermal stability of oil-in-water Pickering emulsion in the presence of nanoparticle, surfactant, and polymer. doi: 10.1016/j.jiec.2014.07.026

Smitter LM, Guedez J, Muller AJ, Saez AE (2001) Interactions between poly (ethylene oxide) and sodium dodecyl sulfate in elongational flows. J Colloid Interf Sci 236:343–353

Srivastava JP, Mahli L (2012) Water alternating gas (WAG) injection a novel EOR technique for mature light oil fields a laboratory investigation for GS -5C sand of gandhar field. A paper presented in biennial international conference and exposition in petroleum geophysics, Hyderabad

Srivastava RP, Vedanti N, Akervol I, Bergmo P, Biram RS, Dimri VP (2012) CO_2-EOR: a feasibility study of an Indian oilfield, SEG Los Vegas 2012 annual meeting. 1052:1–5

Sullivan TO, Zittel RJ, Beliveau D, Wheaton S, Warner H, Woodhouse R, Ananthkrishnan B (2007) Evidence and verification of very low water saturations within the fatehgarh sandstone, barmer basin, India, SPWLA 48th Annual Logging Symposium,3–6 June 2007

Taber JJ, Martin FD (1983) Technical screening guides for the enhanced recovery of oil. SPE 12069:1–20

Taglia PPG (2010) A report on enhanced oil recovery (EOR)—petroleum resources and low carbon fuel policy in the midwest. Accessed July 2010, pp 1–35

Talukdar SN (1982) Geology and hydrocarbon prospects of east coast basins of India and their relationship to evolution of the Bay of Bengal. SPE 10443:9–12

Taylor KC, Nasr-El-Din HA (1996) The effect of synthetic surfactants on the interfacial behavior of crude oil/alkali/polymer systems. Colloids Surf A 108:49–72

The Challenges and Opportunities for Enhanced Oil Recovery (2011) Senergy. http://www.senergyworld.com/media-centre/newsletter/update-in-brief/the-challenges-and-opportunities-for-enhanced-oil-recovery-%28eor%29. Accessed 24 Mar 2011

Tiwari D, Marathey RV, Patel NK, Ramachandran KP, Maurya CR, Tewari PK (2008) Performance of polymer flood in Sanand field, India-A case study. SPE 114878:1–8

Turta AT, Chattopadhyay SK, Bhattacharya RN, Condrachi A, Hanson W (2007) Current status of commercial in situ combustion projects worldwide. J Can Petrol Technol 46:8–14

Wang D, Zhang Y, Liu Y, Hao C, Guo M (2009) The application of surfactin biosurfactant as surfactant coupler in ASP flooding in Daqing oil field. SPE 119666:1–8

Wang Z, LeX Feng Y, Zhang C (2013) The role of matching relationship between polymer injection Parameters and reservoirs in enhanced oil recovery. J Petrol Sci Eng 111:139–143

Wanli K, Yi L, Qi B, Guangzhi L, Zhenyu Y, Jichun H (2000) Interactions between alkali/surfactant/ polymer and their effects on emulsion stability. Colloids Surf A 175:243–247

Wenger LM, Davis CD, Isaksen GH (2001) Multiple controls on petroleum biodegradation and impact on oil quality. SPE 71450:1–14

World Energy Council (2013) http://www.worldenergy.org/wpcontent/uploads/2013/09/WER_2013_2_Oil.pdf

Wu YF, Mahmoudkhani A, Watson P, Fenderson T, Nair M (2012) Development of new polymers with better performance under conditions of high temperature and high salinity. SPE 155653:1–11

Xiaolin W, Zhaowei H, Xumou D, Wei L, Rui W, Xiaolei W (2012) The application of microbial enhanced oil recovery in Chaoyanggou Daqing low-permeability oilfield. Open Petrol Eng J 5:118–123

Xu C, Bell L (2013) Worldwide reserves, oil production post modest rise. Oil Gas J 111:1–6

Yang J, Qiao W, Li Z, Cheng L (2005) Effects of branching in hexadecyl benzene sulfonate isomers on interfacial tension behavior in oil/alkali systems. Fuel 84:1607–1611

Yashwant SR, Flynn M, Ananthakrishnan B, Compton PM (2006) The Mangal field, Rajasthan India—a story of rapidly advancing subsurface understanding in readiness for development. AAPG annual convention 2006, Houston

Yazdani A, Maini BB (2005) Effect of drainage height and grain size on production rates in the vapex process: experimental study. SPEJ 8: 205–213

Zalawadia HA, Pawde C (2013) Case study on handling paraffinic and viscous crude of mangala oil field of Rajasthan-India. SPE 164670:1–18

Zhang Y, Fu B, Ma D, Lin Q (2012) Studies on the application of chemical and biological viscosity reduction technology. Proc Int Conf Pipelines Trenchless Technol 2012:269–278

India: Petroleum Policies and Geopolitics

Kesava Chandra Varigonda

1 Introduction

India has, since the 1980s, been inordinately dependent on imported petroleum, since the quantity of indigenously extracted petroleum has been insufficient to cater to the growing demand for petroleum-derived fuels. The exponentially increasing import dependency not only ran contrary to India's ultimate aim of energy independence but also represented a considerable drain on the national budget. Since the late 1990s the Indian government made a concerted effort in improving India's indigenous petroleum production by opening up its upstream sector to privatisation. India's state-owned oil and gas companies also acquired equity stakes in oil fields globally with the intent of supplementing direct oil import with import from 'Indian-owned' oil fields. India's intention to increase its utilisation of natural gas—seen as a 'clean' energy source—led to the government's efforts, since the late 1990s, to increase gas imports as well as increase indigenous production from conventional oil and gas fields and unconventional sources such as coal bed methane and shale gas.

This paper studies the implications of India's policies for reducing its petroleum imports through greater privatisation of its indigenous upstream sector and through equity oil acquisitions, and increasing its natural gas supply as a clean energy source. It attempts to understand some of reasons for the lack of success in stemming the growth of fuel import dependency. Based on this, the paper also puts forth some future trajectories and policy options.

K.C. Varigonda (✉)
Lee Kuan Yew School of Public Policy, Singapore, Singapore
e-mail: sppkcv@nus.edu.sg

2 Growing Demand for Petroleum and Natural Gas

Crude oil is perhaps India's most important energy source. India has always been heavily dependent on petroleum-derived fuels for much of its energy-based needs. India's industrial, energy and agricultural sectors rely considerably on petroleum-derived fuels. The dependency of the burgeoning transportation sector on petroleum-derived products comes to around 98.5 % (TERI 2013a, b). India's electricity sector is also considerably reliant on diesel-powered generators while kerosene lamps remain a primary source of power for many below poverty-level households. As of 2011, nearly 39 % of petroleum-derived fuels are utilised in the transportation sector and 17 % in the industrial sector (International Energy Agency (IEA) 2014). With increasing economic growth, greater industrialisation and the steady rise in the transportation sector, the demand for petroleum-derived fuels also continues to rise exponentially.

Unlike petroleum-derived products, which power the demand-intensive transportation and industrial sector, indigenous natural gas was sufficient to cater to the indigenous demand in the 1990s, which mainly stemmed from the fertiliser industry. Towards the turn of the century several policymakers including India's former President A.P.J. Abdul Kalam spoke often of the need for aiming towards energy independence, and the possibility of achieving it through a concerted shift to clean energy fuels, or fuels that did not detrimentally impact climate change (*The Hindu* 15 August 2005). Natural gas, though not entirely 'clean', is far more benign than either coal or crude oil-derived fuels. There is therefore a concerted effort towards incorporating a greater percentage of gas in the country's energy and power generation mix (Fig. 1).
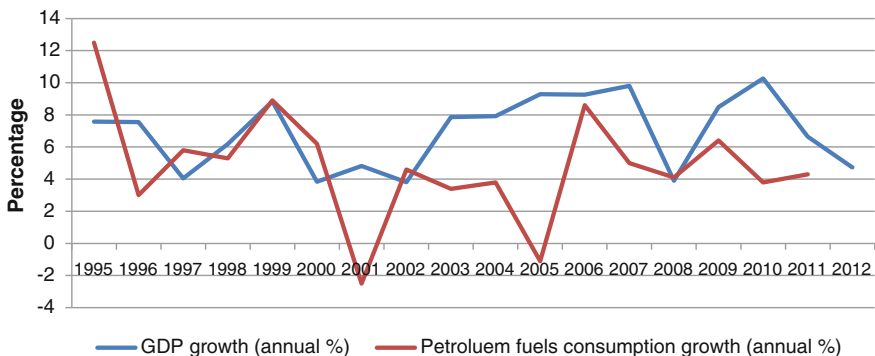

Fig. 1 Empirical correlation between petroleum derived fuel consumption and GDP growth [*Source* The World Bank, "Databank"; Ministry of Petroleum and Natural Gas (2012a)]

3 Impact of Rising Petroleum Import Dependency

India's indigenous petroleum and gas sector had traditionally been under the purview of its state-owned oil and gas companies—particularly Oil and Natural Gas Corp. (ONGC), which held a near-monopoly of the sector from the late 1950s to the early 1990s, and to a lesser extent by Oil India Limited (OIL) (Rai 2011). Due primarily to several key discoveries of lucrative oil and gas fields by ONGC—in basins such as Cambay, Assam-Arakan, Cauvery and primarily Bombay High, India's recoverable crude oil reserves increased steadily from 127.8 million tonnes (Mt) in 1970 to 738.8 Mt by 1990 (Ministry of Petroleum 2008), as did the annual crude oil production, from just 6.8 Mt in 1970 to 32.7 Mt by 1990.

During this period the demand for petroleum-derived fuels has also exponentially increased. To cater to this demand, India's indigenous petroleum refining industry underwent substantial growth and increase in capacity. However, India's indigenously produced crude oil was not adequate to meet the extent of that consumed in refineries (as measured by refinery throughput), falling short by 11.7 Mt in 1970 and 19 Mt by 1990 (Ministry of Petroleum 2012a, b). The Indian government therefore resorted to greater imports of crude oil to offset this shortfall; from 11.7 Mt in 1970, imports steadily increased to 20.8 Mt by 1990. Nearly 40 % of the overall crude oil consumed in refineries was being imported by 1990.

In 1990 India was spending some 59.2 billion rupees (US$970 million in today's currency) on crude oil imports (Ministry of Petroleum 2008), up from US$16 million in 1970. India's primary source of crude oil remained the Middle East, with around 45 % from Iraq, UAE and Saudi Arabia and 23 % from Iran. This lack of geographical diversification of petroleum supply sources meant that the Indian economy bore the brunt of international oil price rises in the aftermath of the Arab oil embargo in the early 1970s and the Iranian Revolution in the late 1970s and early 1980s. The exponential increase in crude import costs drove domestic fuel prices up and resulted in spiralling inflation. The strain of crude oil import expenditure on India's budget contributed directly to India's balance of payments crisis of 1991 (Mudiam 1994).

The steady growth in India's indigenous oil and gas sector, particularly during the 1970s and 80s under ONGC's aegis, stalled somewhat in the early 1990s. This was primarily due to the decline in oil production from ONGC-operated fields in Bombay High, as well as ONGC's inability to make further lucrative discoveries or to capitalise effectively on existing reserves. ONGC officials themselves admitted to severe lack of funding for the development of crude oil fields (Rai 2011). Srinivasan (1997) blames internal corruption and prioritisation of short term gains over longer term planning for the ONGC's lack of productivity in crude oil production. The resuscitation of India's indigenous petroleum sector was deemed imperative by the Indian government; the alternative was further increase in India's oil import dependency.

In a bid to stem the stalling of indigenous production and halt further import dependency, the Indian government slowly opened its indigenous oil and gas

upstream sector to privatisation. In 1992 the Indian government decided to open its upstream sector to limited privatisation. Indigenous and foreign private companies were able to form joint ventures with India's state-owned companies in the development of oil fields—usually the ones already discovered, although they were not allowed 100 % ownership in operations of oil fields. Further decrease in crude recoverable reserves was seen throughout the 1990s, with reserves dropping to 660 Mt by 1999—the lowest in a decade. The reserve to production (R/P) ratio stood at 20.3, indicating the number of years the present proven reserves would be expected to last at current production rates. Meanwhile, India's crude oil import dependency leapt to 70 % in 2000, with US$1.1 billion spent that year on imports.

4 Impact of Privatisation on Petroleum Production

By the late 1990s, the Indian government decided to fully open the oil and gas sector to privatisation. India's Hydrocarbon Vision 2025, written in 1997, envisaged attracting "major oil and gas companies" as central to the development of the indigenous oil and gas sector (Ministry of Petroleum 1997a, b). The 9th Five Year Plan (Planning Commission 1997) stated, "The Government of India has thrown open the major segments in exploration and production…for private investment." The government hoped to increase private participation through issuance of competitive bidding rounds for exploration of oil and gas fields among the state-owned and private (both indigenous and foreign-based) companies on an even plane. Private companies would be able to develop oil and gas fields both solely or through joint venture with state-owned companies.

Through this policy emerged the New Exploration Licensing Policy (NELP). The first round of NELP was launched in 1999. Based on geological data of India's sedimentary basins provided by the Directorate General of Hydrocarbons (DGH) through its surveys and appraisal, the Indian government would offer several blocks at a certain time of the year and private and state-owned oil and gas companies would be able to bid for these blocks. The Indian government would then enter into Production Sharing Contracts (PSCs) with the operating companies which also involves profit-sharing from the sale of oil and gas between the government and participating companies at contractually determined proportions. The government provided several other incentives to encourage private participation including a reduction in royalty if companies chose to explore in deep water areas as a means of encouraging "exploration in deep water and frontier area" (Ministry of Petroleum 1999). Exemption from import duty and allowance of recovery of the exploration, development and production cost of the operating companies were among several incentives. According to India's DGH, "the terms and conditions of this open and attractive policy rank among the most attractive in the world" (Directorate General of Hydrocarbons (DGH) 2012).

The privatisation of the NELP and pre-NELP era has, to quote Rai (2011), "weakened ONGC's monopoly status in the upstream sector." In 1995, prior to

NELP and in the initial years of pre-NELP privatisation era, out of India's total estimated sedimentary area of 3.14 million km^2, around 15 % of India's sedimentary basins had been explored to at least a moderate extent, most of it by ONGC and OIL. Around 50 % was completely unexplored. As of 2013, nine rounds of NELP have taken place, the first completed in 2000 and the last in 2012. Around 254 onshore, shallow and deep water offshore blocks have been awarded through competitive bidding, to state-owned, private and joint venture companies.

As of 2013, around 0.846 million km^2 of sedimentary basin area, present in 19 of India's 28 basins is being explored. Around 78.3 % is offshore, in both shallow and deep water. Of this, nearly 45 % is under private/JV operations as compared to 52 % under ONGC. However with nearly 78 % of India's basins still underexplored, including those in deep water and frontier areas, privatisation of India's upstream oil and gas sector has not yet achieved a primary aim of the policy (Fig. 2).

In 2011 India's recoverable crude oil reserves stood at 757.4 Mt, an increase of nearly 100 Mt from 1999. Of this, ONGC still operated 73 % while private/JV companies operated 16.3 % (DGH 2012). This increase in recoverable reserves has also largely been due to the discoveries initiated by private or joint venture operators along with ONGC in Rajasthan and eastern offshore basins. Between 1999 and 2012 the increase in annual crude oil production from indigenous reserves has not been substantial. However the proportion of crude oil produced through private and JV operators is over 30 % of the total. Perhaps the most important achievement of privatisation in the NELP and pre-NELP rounds is that the oil production and accretion of reserves with the help of privatisation and joint ventures has largely augmented the decrease in oil production from ONGC that has continued through the years.

In 1999 when privatisation was still nascent, annual crude oil production stood at 32.6 Mt of which 77.4 % came from ONGC and 12.5 % from private/JV operations and the rest from OIL. Bombay High contributed 52 % of crude oil produced while
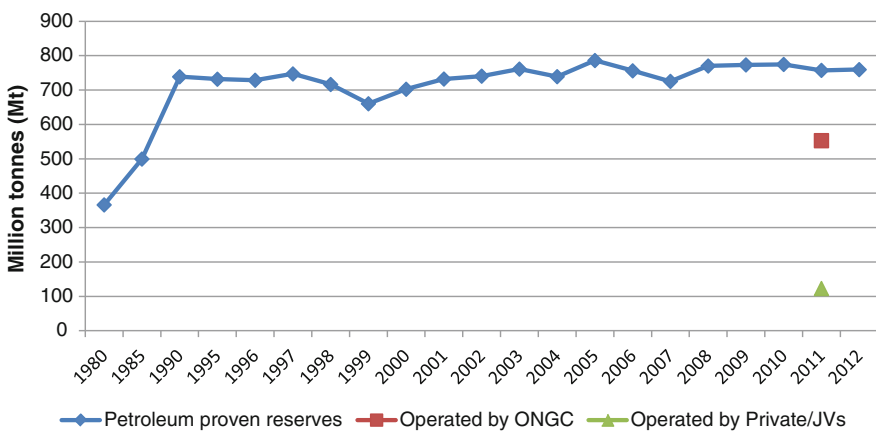

Fig. 2 Petroleum—indigenous proven reserves, 1980–2012 [*Source* Ministry of Petroleum and Natural Gas (2012a); Directorate General of Hydrocarbons (2012)]

another 38 % was divided among Cambay, Cauvery, KG basin and Assam. Annual crude oil production in 2012 increased slightly to 38.3 Mt of which 30.4 % came from private/JV operations and 59 % from ONGC. This was due mainly to petroleum production from crude oil reserves in the Mangla, Bhagyam and Aishwarya oil fields in Rajasthan. These fields were discovered by Cairn and ONGC in the mid-2000s from blocks procured during the pre-NELP years. In 2012, Bombay High contributed to 44.1 % of crude oil produced while the Rajasthan basin contributed 22.7 %. Here again, the decline in production from the largely ONGC-operated Bombay High has been augmented by production from other basins, particularly the Rajasthan basin (Figs. 3 and 4).
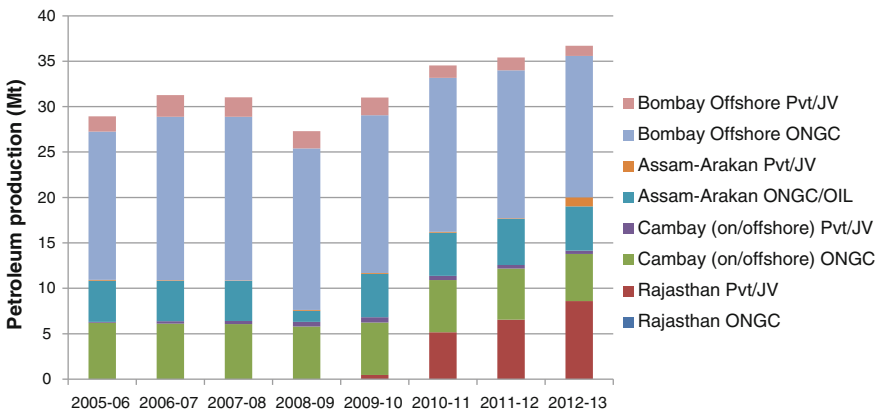

Fig. 3 Petroleum production by state-owned and private/JV companies from major basins (*Source* Directorate general of hydrocarbons (DGH) Annual Reports)
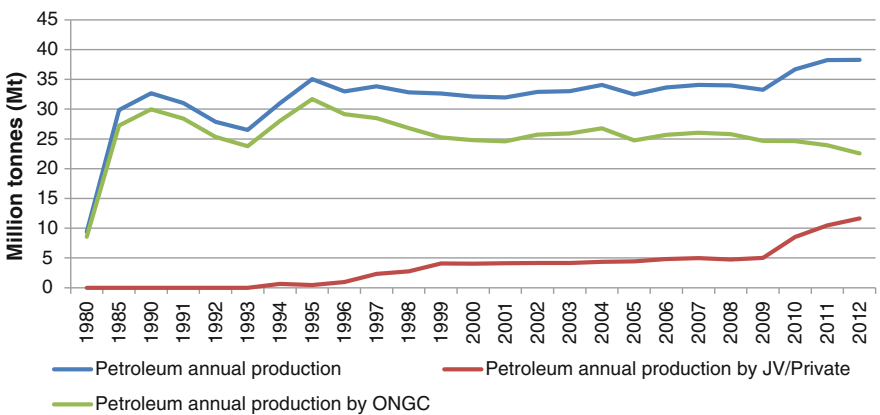

Fig. 4 Petroleum annual production by ONGC and JV/private operators, 1980–2012 [*Source* Ministry of Petroleum and Natural Gas (2012a)]

4.1 Some Reasons for the Failure of Privatisation

In spite of a total investment of US$21.3 billion made during the NELP rounds by private and public companies (*Press Information Bureau* 12 January 2014), privatisation has not resulted in the much-hoped-for dramatic increase in annual crude production that was witnessed in the 1970s and 80s, for instance. The primary reason perhaps has been the lack of such discoveries as the fields in Bombay High or Cambay in the 1980s and 1970s. Successfully developed oil and gas fields such as those in Rajasthan, Kutch and KG basin were still a minority amidst the 108 total oil field discoveries, the overwhelming number of which have yet to be developed.

While nearly 58 private Indian companies and 48 foreign oil and gas companies have entered into the Indian upstream sector, "top private foreign players such as Exxon, Shell, Chevron, Statoil and Conoco Phillips have not participated in a single NELP round" (Azhar 2011). Some analysts have blamed inadequate commercial incentives by the Indian government to international oil and gas companies—for instance, lack of adequate tax breaks for commercial oil and gas production. BHP Billiton and Santos held India's bureaucratic hurdles responsible for their decision to exit India's upstream sector, due to "delays in getting approvals to start work" (*The Hindu* 9 December 2013).

The lack of major private oil and gas investors may also be due to the lack of confidence in the propensity and commercial viability of India's indigenous oil and gas reserves. Of the 360 oil and gas blocks offered in several NELP rounds, 254 have been awarded to private and state-owned companies, out of which 74 blocks have been relinquished by their operators due mainly to commercial non-viability. This is exacerbated by the lack of a complete geological and geo-scientific data of all the sedimentary basins, the availability of which would assist companies in making more informed bids. The DGH has, as of 2013, completed 48 % appraisal of India's total sedimentary basins; of this, 65 % of the onshore basins and 49 % of the deep water basins are yet to be appraised. This is somewhat below the objectives propounded in India's hydrocarbon vision 2025, which envisioned a 75 % appraisal by 2015 and 100 % by 2025 (Ministry of Petroleum 1997a, b).

4.1.1 A Comparison with the Brazilian Experience in Privatisation

The Brazilian indigenous petroleum sector has had a similar trajectory to that of India's in the 1990s. Like ONGC, the national oil company Petrobras has traditionally held a monopoly on the country's oil sector. In the early 1990s annual crude production in Brazil equalled that of India's, as did its total petroleum reserves. Yet its privatisation programme, initiated in the late 1990s, has transformed the country from being traditionally oil import-dependent to self-sufficiency to a net exporter of crude oil, since the late 2000s. Crude oil production in 2011 stood at 107 Mt, nearly double that at 1999.

The success of privatisation has been imperative to this development. By 2019 only 25 % of Brazil's sedimentary area under concessions contracts was operated by Petrobras. The overwhelming majority was under private or JV companies, including major players such as Shell, ExxonMobil, Statoil, TOTAL and BG among others (Rodriguez and Suslick 2009). A comparative study between the Brazilian and Indian models reveal stark differences in policy and implementation, which may have led to the success of privatisation in Brazil as compared to India.

The Brazilian government began its annual auctions of blocks in its sedimentary area, beginning 1999. It however followed a concessions-based contract rather than a PSC-based one as in India. In the former, the oil extracted still belongs to the production company, unlike in the PSC model where the production company's control of the oil is restricted to profit-sharing with the government. The National Petroleum Agency (ANP), the regulatory body equivalent of DGH, has managed to collate and categorise most of the geo-scientific data into a comprehensive repository, which has been available to all the indigenous and multinational oil companies involved in bidding since 2000. These policies have bestowed a greater control to the oil companies potentially investing in the Brazilian sector as compared to the Indian sector. According to De Oliveira (2011), these policies allowed private oil companies "to take advantage of their ability to manage the geological, technological, financial and marketing risks…".

Perhaps the most important aspect rendering privatisation more lucrative in Brazil however is the confidence in the Brazilian oil sector. The ready availability of geo-scientific data allowed for greater transparency and control for private oil companies, while the familiarity of Petrobras towards Brazil's sedimentary areas prompted several multinational companies to forming joint ventures with it (De Oliveira 2011). Furthermore the Petrobras-operated oil fields, including the lucrative Campos Basin, discovered in the 1980s, have also consistently produced substantial petroleum even during the pre-privatisation years, generating a confidence that it would continue to do so. On the other hand the ONGC-operated Bombay High fields steadily declined in production from the early 1990s onwards. As Table 1 shows, two aspects have determined the variation in the results of Brazilian and Indian privatisation: accordance greater control and say to private companies and confidence in the local upstream sector (Fig. 5).

4.1.2 Future Amendments to Policy

India's 12th Five Year Plan, commissioned in 2012, has in some sense admitted to the failure of NELP, stating that reforms were required in India's indigenous upstream sector. Policy recommendations are tilted towards greater privatisation through attracting major international oil and gas companies—in which the government has till date not been as successful. Recommendations include faster "decision-making for awarding and development of NELP blocks (Planning Commission 2012)," which would also signal minimal bureaucracy, delay and red-tape on the part of

Table 1 Distinction between the Brazil and Indian privatisation of upstream sector

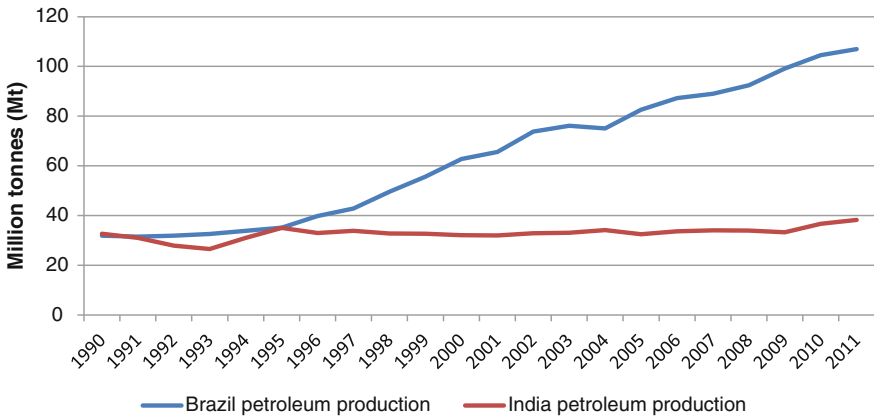|	Brazil	India
Start of privatisation	1999	1999
Mode of privatisation	Concessions—companies have ownership of extracted oil. Royalties paid to the state	Production sharing contracts (PSC)—state owns extracted oil. Companies share profit with government
Availability of geo-scientific data	Since 2000	Estimated from 2015
State-owned upstream oil and gas firm	Petrobras—46 % privatised	ONGC and OIL
State of oil production pre-privatisation	Steady growth in oil production	Decline and stagnation in oil production

Fig. 5 A comparison of petroleum production in Brazil and India pre and post privatisation [*Source* International Energy Agency (2014)]

government functionaries, as well as providing greater transparency and technical data on sedimentary basins to the participating companies.

Perhaps the most important policy recommendation is the eventual introduction of the Open Acreage Licensing Policy (OALP) which would, unlike NELP, allow private and state-owned companies to pick and choose the blocks they would like to operate on at any time throughout the year. In NELP, data on the blocks up for bidding—often deemed incomplete—are provided by DGH only at the time of bidding. The key aspect of OALP would be the presence of a National Data Repository (NDR) that would store and make publicly available all the collected geo-scientific data of India's sedimentary basins. The greater transparency that OALP accords as compared to NELP is expected to be more investor-friendly and hence should encourage greater privatisation. OALP would also accord greater control of the bidding process to the bidding companies instead of the government;

companies would be able to bid all year round on blocks of their choosing, and would be able to base their decisions based on the readily available geo-scientific data. The Indian government has planned the consolidation of the NDR since at least the mid-2000s. The government hopes to replace the existing NELP system with OALP by 2015, effectively making the 10th round of NELP in 2014 the last one.

Indian companies have meanwhile embarked on exploration into several other sectors including unconventional reserves. Extensive deposits of oil shale—estimated at around 400 Mt are believed to be present along with coal in the Assam-Arakan basin and in the Arunachal Pradesh state (DGH 2013). The DGH is currently evaluating the prospects of petroleum production from shale oil reserves in these regions. However the development of these reserves has historically been deemed logistically and technically very challenging if nearly impossible, with the potential of debilitating impact on the environment. In addition the Arunachal Pradesh state is also claimed by China as part of 'South Tibet'. This contested region had been the setting of a China-India border war in 1962 and continues to be highly sensitive in regards to regional security. The question therefore remains of whether India would be allowed free access to energy resources in this region by China. Some analysts have suggested that the proven presence of large-scale shale deposits might provoke another Chinese invasion "to grab the oil" (*The Times of India* 25 September 2011).

5 Increasing Natural Gas Supply

India's Hydrocarbon Vision 2025, written in 1999, envisaged a greater role for natural gas, particularly as a 'clean energy' fuel in India's power sector, which traditionally has relied inordinately on coal as fuel—which, with its high carbon content was deemed particularly adverse to climate change. The vision envisaged domestic production from coal bed methane (CBM)—or methane trapped within coal reserves, gas hydrates and other unconventional sources, as well as gas imports, in addition to conventional gas production, as catering to the increased demand in the near-future.

5.1 Challenges in Gas Production Through Conventional Means

Privatisation in the NELP era has contributed substantially to growth in annual gas production. While privatisation contributed towards gas production in Bombay Offshore, the discovery of the D6 block in the Krishna Godavari (KG) basin in the mid-2000s, by India's private oil and gas behemoth, Reliance Industries Ltd. (RIL),
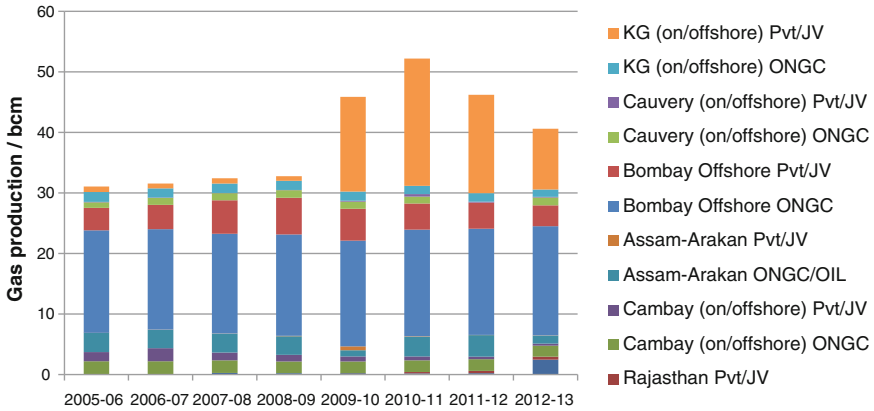
Fig. 6 Gas production by state-owned and private/JV companies from major basins (*Source* DGH annual reports)

proved particularly lucrative. It was billed the world's largest gas discovery of its time. Gas production in the basin began in 2009, causing the overall indigenous gas production to increase from 32.9 bcm in 2008–09 to 52.2 bcm in 2010–11, as seen in Figs. 6 and 7. Over 51 % came from private/JV operations, most of it from the RIL-operated field.

However this was followed by an equally sudden decline, to 40.6 bcm by 2012–13. This was primarily due to the steep decline in gas produced from the KG basin. While some reports have suggesting a deliberate tactic on the part of RIL to curb gas output by stalling the digging of new wells because gas prices at which RIL would be allowed to sell were deemed too low added further fuel to the controversy linking the price of gas to production (*The Hindu* 7 September 2013), RIL has
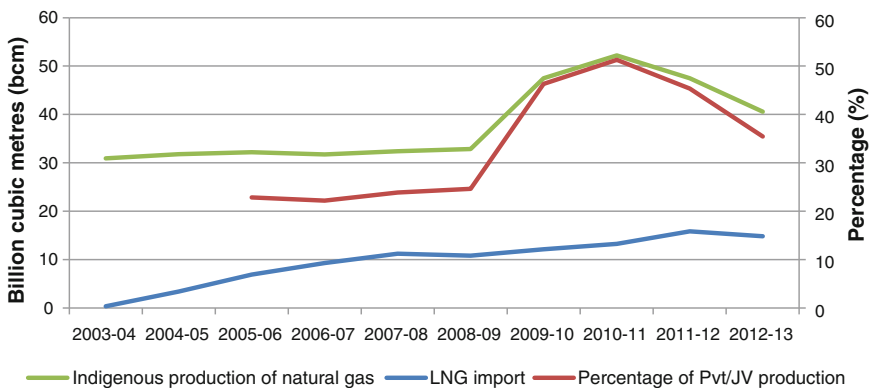

Fig. 7 Natural gas indigenous production, percentage of Pvt/JV production, and import [*Source* Ministry of Petroleum and Natural Gas (2012a); Petroleum Planning and Analysis Cell (PPAC), "Natural Gas"]

however blamed "geological complexities" and the attendant rise in production costs for the delay in the digging of new wells and the attendant decline in gas production.

The sudden increase and equally sudden decline in gas produced from the KG basin and the consequent decline in indigenous gas production has had a considerable impact on India's policy of pursuing clean energy. The annual gas produced indigenously in 2012–13 was around 12 bcm lesser than the projected estimate according to the 12th Five Year Plan (Planning Commission 2012). It seems hardly probable that the projected increase to 84.5 bcm annual production in 2016–17 would be met. The original PSC agreement used in NELP states that the sale price of any gas indigenously extracted would be determined based on a predetermined pricing formula (Ministry of Petroleum 2010). In the aftermath of allegations that linked low gas production and developmental delays to disagreements between RIL and the Indian government as regards gas pricing, the Indian government, through the implementation of a new pricing formula, approved a highly controversial increase to the sale price of gas. The price was nearly doubled to US$8.4 per million British Thermal Units (BTU) from its previous figure of US$4.2.

This was once again accompanied by allegations of the Indian government's decision to raise gas prices for the sake of a potential increase in the quantity of gas produced from the RIL operated fields as well as an enticement for greater private investments. While some analysts opine that gas prices must be market-determined, others are of the opinion that an increase in gas production from the RIL fields be a precondition for any potential hike in gas sale prices (*The Hindu* 19 February 2014). Other major private firms as British Petroleum (BP), which in mid-2013 was forced to surrender its block in the KG basin due to clashes with India's Ministry of Defence (*The Hindu* 19 June 2013), has also supported RIL's stance—signalling perhaps the solidarity among private companies on the issue of gas pricing and gas production.

The new pricing, originally due to be implemented from April 2014, was further postponed till post the national elections in April. Thus the decision regarding the implementation of the new pricing would be determined by the victors of the elections. The politicisation of gas pricing policies essentially threatens to overshadow economic and technological considerations, while further filibustering also forestalls development in gas production. The 12th Five Year Plan recommended the implementation of more transparent pricing mechanisms for gas produced. While higher gas prices may be more investor-friendly, it is imperative that the prices are formulated such that they are also made affordable to the indigenous consumers.

5.2 Attempts to Import Natural Gas

The Indian government's attempts to augment its indigenous gas production through imports met with partial success due mainly to a combination of

geopolitical and financial reasons. India's attempts to import gas through pipelines from Iran, Central Asia and Myanmar did not materialise. The proposed Iran-Pakistan-India (IPI) pipeline project which involved transportation of gas produced from fields in Iran to India, was delayed for a considerable period before being shelved in 2011, due primarily to the US-led and international sanctions against Iran. The sanctions placed political pressure on Indian government to withdraw from the partnership, while the lack of loans from banks or guarantee from insurers placed a financial strain on the pipeline project which the Indian government was unable to afford. Another proposed gas pipeline project, the Turkmenistan-Afghanistan-Pakistan-India (TAPI) has also been indefinitely delayed due to security concerns for India; concerns include the physical security of gas pipelines from militants in Afghanistan and Pakistan, as well the prospect of Pakistan cutting off gas supply to India in the event of severe deterioration of bilateral relations (Nathan et al. 2013).

The Myanmar-Bangladesh-India (MBI) pipeline, proposed in 2004, which involved transporting gas from the fields in Myanmar to India could not materialise; mutual disagreements on the terms of the pipeline deal between India and Bangladesh and a deterioration in bilateral relations led to Bangladesh, the primary transit state, backing out in mid-2005. In addition, India did not have the financial resources for the construction of a direct Myanmar-India gas pipeline (Varigonda 2012). By 2009, India's primary competitor for Myanmar's gas, China, had secured a gas pipeline deal with Myanmar instead. The Myanmar-China gas pipeline commenced operations in mid-2013. India has however been far more successful in LNG import.

In 2004 India's first LNG terminal commenced operations. India has since then been able to import gas in the form of LNG, primarily from Qatar, with which the Indian government secured a long-term import contract in 2005. Gas imports from Qatar make up around 85 % of India's total imports. From 0.34 bcm in 2003–04, India's LNG imports shot up to 14.8 bcm in 2012–13. With indigenous natural gas productions having stalled in recent years, India's LNG import is set to increase considerably. India has constructed three more LNG terminals to cater to projected increase in gas imports.

5.3 Gas Production from Unconventional Sources

The Indian government also put forth the policy of sourcing for unconventional natural gas sources indigenously, primarily through CBM and shale gas. While the exploitation of CBM was initiated in the early 2000s through a NELP-style privatisation, its lack of success has prompted the government to allow the state-owned Coal India into the fray recently. This development may further increase state involvement in the CBM sector. Shale exploration is still very nascent, and is at present only open to state-owned oil and gas companies. The future trajectory of shale gas in India may however be determined by India's relations with the US and the extent of involvement of US companies in the sector.

5.3.1 Coal Bed Methane (CBM)

India's prognosticated CBM reserves are estimated at around 2.61 tcm (trillion cubic metres). The 9th Five Year Plan viewed gas production from CBM reserves as one of the primary 'thrust areas' in the upstream sector the near future. Accordingly the Indian government approved the CBM policy in 1997, which like NELP, involved issuance of blocks by the government to both private and state-owned companies in an open competitive bidding system, with the option for private companies to possess sole participating interest in the development of the blocks (Ministry of Petroleum 1997b). The CBM policy was launched in 2001 and till date four bidding rounds of CBM have been held.

By 2013 CBM reserves made up a 26,000 km^2 area, of which 59 % is currently under operation. Apart from state-owned ONGC, RIL, Essar and Great Eastern Energy Corp. Ltd. (GEECL) are the main private companies involved in CBM operations. Conspicuously absent however are international oil and gas companies. Gas production commenced in 2007 and by 2011–12, 0.084 bcm of CBM-derived natural gas was produced. In 2012–13, this value increased to 0.11 bcm, with 82 % coming from the CBM reserves of the Raniganj coalfields in West Bengal, operated by GEECL. Gas in place reserves in the blocks under operation is estimated at 280.2 bcm. Nevertheless natural gas from CBM reserves has contributed to only 0.18 % of the total gas produced that year.

India's implementation of its CBM policy—also through privatisation—had not been as successful, even over a decade since its launch. This primarily has been reflected in the near non-existence of international private oil and gas companies within the CBM sector. The government policy differentiated blocks allocated for CBM exploration and extraction and blocks allocated for coal extraction, due to "the fact that both coal and oil and gas sectors are governed by different administrative ministries" (Planning Commission 2012). This rendered simultaneous exploration and extraction of coal and CBM impossible despite the fact that CBM was present in coal beds. As such companies involved in coal extraction, including the state-owned behemoth, Coal India (CIL), were essentially kept out of the CBM exploration and extraction sector.

Perhaps in the hope that the participation of traditional coal producing companies would boost CBM exploitation, the Indian government put forth the option of simultaneous operations of CBM and coal in the 12th Five Year Plan. The Ministry of Petroleum and Natural Gas held consultations with the Ministry of Coal in 2012 and 2013 on a roadmap "for carving out areas for simultaneous operations" (Ministry of Petroleum 2011). By December 2013 the Indian government gave its approval for Coal India (CIL) to simultaneously explore and extract coal and gas from CBM, whether solely or through joint venture partnership with private companies, in hopes that the involvement of CIL would increase CBM-derived gas production.

5.3.2 Shale Gas

The Indian government has also noted the potential impact of shale gas, or gas trapped in shale formations, particularly in light of the impetus it has received in countries such as the United States (USA) and Canada and its stunningly successful incorporation into the American energy production mix. The production of shale gas in the USA since the mid-2000s has propelled its overall annual gas production from about 511 bcm in 2005 to 681 bcm in 2012 (U.S. Energy Information Authority (EIA), "International Energy Statistics"). Owing to the successful development of its shale gas reserves, the USA was able to not only stem the steady decline in indigenous gas production seen in the early 2000s but is also expected to become a gas exporter in the near future.

The Indian government signed a Memorandum of Understanding (MoU) with the US Department of State in 2010 detailing mutual cooperation in the development of India's indigenous shale gas resources, concentrated primarily on resource assessment, technical studies and local training (*Press Information Bureau* 8 November 2010). India's prognosticated shale gas reserves were estimated by the EIA to be much as 1.8 tcm situated chiefly in the Cambay, Gondwana, Krishna-Godavari and Cauvery onshore basins. In 2011 ONGC began exploration for shale gas in India's sedimentary basins, in the process discovering Asia's first shale gas reserve in Durgapur, as well as in the Cambay region.

A major impediment to indigenous shale development is the complex technical expertise necessary—particularly in the implementation of hydraulic fracturing, which Indian companies do not wholly possess. In 2012 ONGC entered into an agreement with US' ConocoPhillips for joint exploration and development of India's shale gas reserves. ONGC's collaboration with ConocoPhillips could involve technology transfer and implementation.

The draft policy on development of India's shale oil and gas reserves, prepared by the Indian government in 2012 envisaged a privatisation strategy on the lines of NELP, by which international and indigenous private companies would be able to bid for blocks assigned by the Indian government on an equal plane (Ministry of Petroleum 2012b). In September 2013 the Indian government approved shale gas exploration, yet only by state-owned oil and gas companies including ONGC and OIL, mostly in blocks that were already granted to the companies in the NELP, pre-NELP or the Nomination era. India's Petroleum Ministry clarified that indigenous and foreign private oil and gas companies would be allowed to explore for shale within their allocated lease areas after two years (*The Economic Times* 2 December 2013). This was despite considerable interest expressed by Indian oil and gas companies such as RIL and Essar. This apparent bias towards state-owned enterprises in favour of privatisation has been heavily criticised as being discouraging towards private investment in India's already beleaguered upstream sector.

While US cooperation with India first began (and still continues) in the indigenous shale development sector with the ONGC-ConocoPhillips tie-up, it has soon shifted towards the option of US export of its excess shale-derived natural gas to India. US law currently does not allow export of shale gas to any country, with

which the US does not possess a Free Trade Agreement (FTA), and India does not, but the US has made yet another exception in 2013, allowing for shale gas export to non-FTA countries, including India (*The Hindu* 18 May 2013).

The Indo-US collaboration within the shale gas sector seems entwined with India's support for US-led bilateral sanctions against Iran. The US has often pitched shale gas import to India as a compensation for the latter's compliance with the US-led sanctions. Shale gas imports were meant to serve as both a viable alternative to any potential gas import from Iran, as well as a recompense for India's declining oil imports from Iran (*The Economic Times* 15 June 2013). The shelving of the IPI pipeline, as well as the decision of Indian crude oil refineries to reduce petroleum imports from Iran in 2010 and 2011 may well have influenced the US' decision. India's state-owned Gas Authority of India (GAIL) has already signed a deal with a US firm to import shale-derived gas from at least 2017.

The implementation of shale oil and gas development however is also predicated upon the considerable utilisation of the country's finite water resources. As of 2011 nearly 90 % of freshwater is withdrawn for use in the water-intensive agricultural sector. Several analysts predict an impending water shortage in the event of large-scale diversion of water towards shale development (The Energy and Resources Institute (TERI) 2013a, b), which could have a debilitating impact on agricultural output and the availability of drinking water. The dependence of the shale industry upon the availability of water may in future impede its overall growth.

6 Equity Oil Field Acquisitions

The Indian government had also put forth "the possibility of acquisition of acreage in other countries for equity oil…" by India's state-owned oil and gas companies for perhaps the first time in the 9th Five Year Plan (Planning Commission 1997). India's state-owned oil and gas companies—particularly ONGC—was directed to explore and purchase operating shares in potentially lucrative oil and gas fields. Ideally it was envisioned that the crude oil or gas extracted from these fields could directly be imported back to the home country. This was seen as a hedging strategy that would potentially provide some leverage, independence and control of oil imports to India, through the state-owned companies, in the highly price-volatile international oil market. The emphasis of India's equity strategy was therefore primarily on providing an alternative to crude oil imports.

The 10th Five Year Plan (Planning Commission 2002) had also called the acquisition of equity oil and gas fields as one alternative to the "stagnating domestic production of crude and the widening gap between demand and supply of oil and gas." From the mid-1990s onwards, ONGC's international wing, ONGC Videsh Ltd. (OVL), "re-oriented its focus on acquiring quality overseas oil and gas assets (OVL, "Assets")," and to engage in exploration, development and production of oil and gas from these assets.

6.1 Challenges in Equity Oil Fields Acquisition

India's foray into equity oil and gas acquisitions closely followed that of China's, and may have derived its inspiration from the latter. While global oil and gas field exploration and production had traditionally resided in the hands of multinational oil and gas companies, the increasing presence of state-owned global exploration and production companies beginning in the 2000s would be led by Chinese and Indian firms. The Chinese government initiated their 'going out' strategy through their national oil companies, particularly China National Petroleum Corp. (CNPC) and Sinopec in the early 1990s—like India, largely in response to supplementing increasing oil imports (IEA 2007).

The primary determinant of the relative success of India's equity acquisitions has perhaps been the relative monetary and other incentives offered by the Indian government and state oil companies to the host country that possesses equity fields. In this regard the engagement between Indian and Chinese state oil companies, whether through competition or cooperation, has often played a crucial rule. In the case of the Greater Nile Oil Project (GNOP) fields in Sudan for instance, political support and intense diplomatic efforts by the Indian government was credited to have influenced the Sudanese government to enable OVL to buy the minority stake, despite efforts by CNPC, which already owned a 40 % stake in the fields, to block OVL's efforts (Patey 2011). CNPC and ONGC would, ironically, continue to work together as joint operators of the GNOP fields despite their initial adversity.

However India's relative lack of influence in the host country with respect to China's has resulted in several initial failures in acquiring equity oil fields. For instance OVL lost the bid to acquire an offshore oil block in Angola in 2004 to a joint-venture bid from the Chinese and Angolan state owned companies, the Sinopec Sonangol International (SSI). Analysts opine that the Angolan government favoured China over India since "India's offer of US$310 million for infrastructure development could not compete with $725 million from China," while misunderstandings in operational strategies between Sonangol and OVL also did not endear the latter to the host government (Vines et al. 2009). Also the Chinese government had till then provided nearly US$2 billion in loans to the Angolan government, far greater than the approximately US$30 million in credit provided by India.

The 'China factor' in India's difficulty in acquiring equity oil fields was emphasised by Indian Prime Minister Dr. Manmohan Singh, who in January 2005 stated, "I urge our oil and gas PSUs to think big…they have to be more fleet-footed in making use of global opportunities…I find China ahead of us" (Sinha and Dadwal 2005). In August 2005 India's ONGC was again outbid by CNPC in the acquisition of PetroKazakhstan, Kazakhstan's third-largest producer of crude oil. CNPC had to increase its bid of about US$3.1 billion to a final US$4.18 billion in the face of ONGC's competitive bid of US$3.6 billion (*Asia Times* 24 August 2005). Some analysts have also alleged favouritism on the part of PetroKazakhstan, based on the Kazakhstan government's strong relationship with China, for allegedly disallowing India in making any further bids, thereby granting full stakes to CNPC.
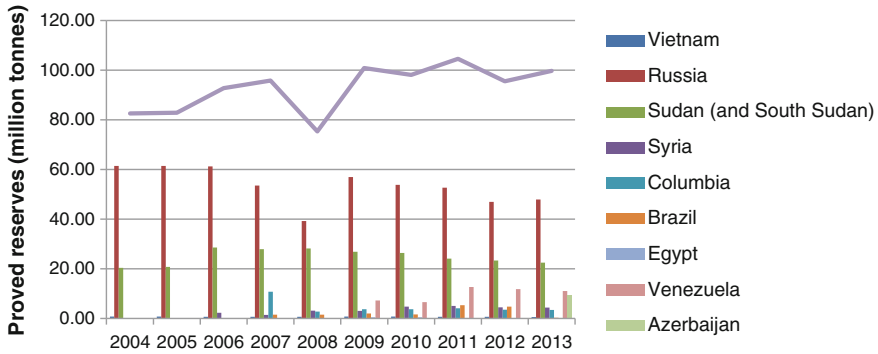
Fig. 8 Proven reserves in OVL's global equity oil acquisitions (*Source* ONGC Annual Reports)

In the case of Syria however, ONGC and CNPC would partner to form a partnership to create the Himalaya Energy Syria joint venture company, and had acquired equal stakes in the Al Furat oil fields worth a total of US$573 million. Likewise in 2006 ONGC and CNPC would again join hands to acquire the Columbian oil company Omimex de Columbia and thereby gain access to its then proven crude reserves of over 300 million barrels in Columbia. By mid-2000s, the Indian government shifted its stance from a mode of competing with its Chinese counterparts to cooperation. In January 2006, the Indian and Chinese governments signed a MoU that directed cooperation in, among other things, acquisition of overseas equity assets. India's Petroleum Minister Mani Shankar Aiyer stated, "We look upon China not as a strategic competitor but as a strategic partner" (*China Daily* 13 January 2006). This cooperation was however rather temporary. In 2013 OVL successfully blocked China's Sinochem from acquiring assets in the BC-10 offshore block in Brazil, opting instead to increase its own shares from 12 to 27 % (Fig. 8).

6.2 Challenges in Petroleum Production

As of 2013, OVL is currently involved in 32 oil and gas exploration, production, development and pipeline projects in 16 countries, 11 of them being oil and gas producing equity assets. By 2013, OVL's total proven oil reserves increased to 99.69 Mt, spread among fields in eleven countries. Around 48 % of the reserves were present in Russia, 22.5 % in fields located in Sudan and South Sudan and about 11 % in Venezuela. While the overall petroleum production doubled to 6.84 in 2009, by 2013 production declined to 4.34 Mt due to decline in production from several fields. Russia's fields produced the majority of crude oil, about 44.5 %, while Sudan and South Sudan together produced 13.8 % and Columbia 12.7 %.

Indeed the steady decline in annual crude production in some of the initially lucrative fields in countries such as Sudan (and South Sudan), where production

declined from 3.32 Mt in 2004 to 0.6 Mt by 2013; and Syria, from 1.1 Mt in 2007 to 0.13 Mt in 2013 has essentially diminished the prudence of overseas investments as a viable source of crude oil. OVL purchased equity shares in fields that were primarily in high-risk, politically volatile, potentially lower-profit regions that were either avoided or not actively pursued by Western-based oil majors. In 2003 ONGC's Chairman Subir Raha stated, in regards to OVL's investments in Sudan, "All this talk about investment in a country with poor human rights record is a sham" (*The Hindu* 9 January 2003). India was unfazed over global criticism of its partnership with a regime that was alleged to have perpetrated the Darfur crisis in the late 2000s.

However the ensuing civil war and the eventual bifurcation of the country into Sudan and South Sudan essentially rendered continued operations highly unsafe and impeded optimal petroleum production to a large extent. Production from oil blocks in South Sudan were halted for security reasons from January 2012 to mid-2013, and oil production from the fields straddling the two countries is prognosticated to only decline further, rendering ONGC's once-lucrative supply of oil a liability (Patey 2014). Likewise the Syrian civil war that began in 2011 has largely been responsible for the steep decline in crude production from the Al Furat fields.

OVL's continued attempts at oil exploration in offshore blocks in South China Sea regions that belongs to Vietnam, but are under territorial dispute with China, despite being carried out under considerable diplomatic objection from China and considerable expenditure, have also not been very successful in striking oil (*The Hindu* 21 November 2013). On the other hand, while OVL's exploratory ventures in Iran led to the discovery of the oil-rich Farsi block in 2009, India declined to acquire equity shares, citing commercial unviability in their development (*The Times of India* 27 March 2013). However the US-led sanctions on Iran, which has increasingly taken aim at investments by Indian oil firms in the country and which also extends to global banks refusing to provide credit and insurance refusing to insure crude oil-based investments in the country, has perhaps rendered the acquisition of Iranian oil fields both commercially unviable to OVL, and owing to constant pressure from the US government to cut down on such investments, diplomatically unviable to the Indian government (*The Hindu* 20 September 2013) (Fig. 9).

6.3 Utility of Equity Oil as Source of Oil Supply

While OVL's crude production from its equity possessions came to 10 % of India's total indigenous production in 2003, this increased to 18 % by 2011 when equity oil production was at its peak. This rather substantial amount could, if imported back to India, offset (though to a small extent) the quantity of directly imported crude. However the overwhelming proportion of crude oil extracted from equity oil fields has, it is estimated, been sold in the international oil market rather than being imported or transported back to the India (IEA 2007).

While the relative monetary incentive of opting to sell the oil in the international market rather than importing back to India is considerably higher, contractual
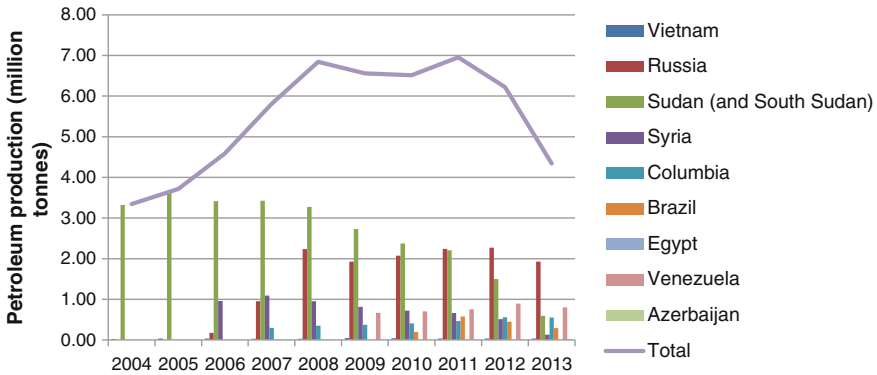
Fig. 9 Annual petroleum production from OVL's global equity oil acquisitions (*Source* ONGC Annual Reports)

obligations, decisions of the host country and other partners and stakeholders of specific fields all determine the final destination of the crude oil produced. This is particularly pertinent since OVL owns minority stakes several of its key equity oil acquisitions, especially those in Sudan, Syria and Russia. Therefore while equity acquisitions allow ONGC to acquire a more global footprint and increase its profits, it has not resulted in any short-term benefits towards increasing India's petroleum supply.

India's equity oil acquisitions, designed to act as a substitute to direct crude oil imports, have been unable to fulfil their usefulness. However despite the steady decline in annual production in its major equity oil fields, and the lack of any short-term improvement to indigenous energy security through its equity-produced crude oil, India's Petroleum Minister Veerappan Moily stated in March 2013 that "the government is encouraging national oil companies to aggressively pursue equity oil and gas opportunities overseas" (*Press Information Bureau* 24 March 2013). The disenchantment with equity oil acquisition has been expressed in the India's Integrated Energy Policy (Planning Commission 2006) which stated, "obtaining equity oil abroad does not particularly increase oil security beyond diversification…obtaining equity oil should be mainly looked upon as a commercial investment decision."

However, equity oil is still envisaged as playing a particularly central role in future crude oil supply scenario by several analysts, particularly within OVL. India's Minister of State for Petroleum Ratanjit Singh announced in 2011 that OVL aims to increase its annual crude oil production to 20 Mt by 2020 (*The Economic Times* 18 Aug 2011).

7 Future Trajectories: Falling Production, Rising Imports

In 1990 consumption of crude oil-derived products such as petroleum, diesel, kerosene and LPG among others, came to nearly 60 Mt. In 2005 this nearly doubled to 110 Mt. By 2012 consumption stood at 155 Mt. India also aspires to be a

regional hub for export of petroleum products. The privatisation of the indigenous petroleum refining sector, led by Reliance Industries Ltd. (RIL) in particular, gave rise to an export-based refining industry in the early 2000s. In 2000 6.5 Mt of petroleum-derived fuels was exported out, amounting to 9 % of the fuels produced from refining petroleum. By 2012 61.5 Mt of petroleum-derived fuels were exported out, amounting to 28.8 % of the fuels refined.

Indigenously produced crude oil was able to cater to around half of the total crude oil consumption within refineries in 1990. In 2012, indigenous crude oil production contributed to just over 18 % of the total crude oil consumed in refineries. Increasing demand for crude oil and crude oil derived fuels has clearly outstripped indigenous supply—regardless of all the attendant increments during the NELP era. The direct result of the failure of indigenous petroleum production as well as equity oil acquisition is the increase in the proportion of petroleum imported. In 1995 India imported 26.9 Mt of petroleum. This quantity amounted to about 46.4 % of the total crude oil consumed by refineries. By 2000 this number increased to 70 Mt or 68.8 % of the total crude oil consumed. By 2012 India imported 184.2 Mt of petroleum or 85 % of the total crude oil consumed, spending some US$12.9 billion. India's import dependency has nearly doubled in the years of India's trial with privatisation of its indigenous upstream sector.

The 12th Five Year Plan (Planning Commission 2012) predicts little improvement to indigenous petroleum production till 2017, while predicting a 4.7 % corresponding annual increase in demand for petroleum products. On the other hand, the plan also predicts a 19.2 % annual increase in demand for natural gas, an increasing proportion of which would have to be catered through LNG import in the face of declining indigenous gas production (Fig. 10).
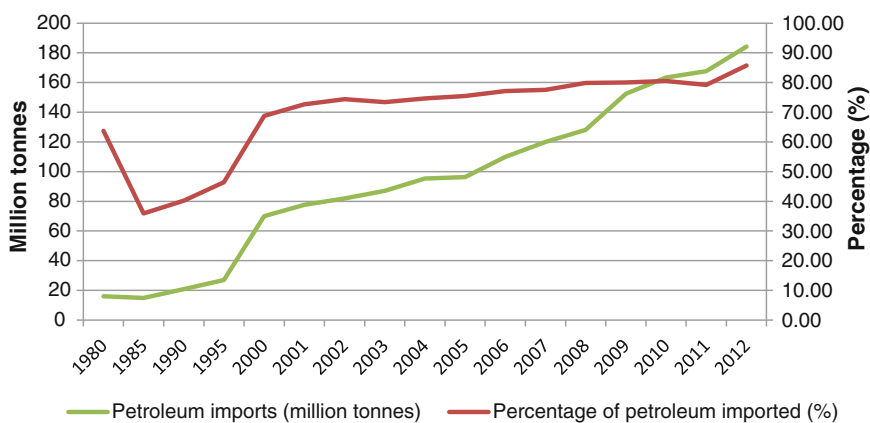

Fig. 10 Petroleum import, 1980–2012 [*Source* Ministry of Petroleum and Natural Gas (2012a); PPAC, "Petroleum"]

7.1 Options for Future Petroleum Supply

In a lecture presented at the Lee Kuan Yew School of Public Policy on 25 March 2014, Montek Singh Ahluwalia, India's Deputy Director of Planning Commission, has stated that among India's pressing economic issues is its large current account deficit. India's petroleum imports contribute substantially to this deficit. His proposes a shift in the supply side through a concerted transition to alternative energy sources, as well as greater energy efficiency in the demand side. The former however could only be envisaged as a longer-term strategy, particularly since solar and wind powers have not attained commercial viability for mass utilisation.

A 2009 study conducted by Parikh et al. (2009) in preparation for the 12th Five year plan considers a variety of policy choices and their implications for India's energy sector as a whole, based for instance on a coal-based, full-potential hydro based, natural gas induction based, and so on. The common denominator in all of their policies is the high percentage of crude oil in the fuel mix (around 28–30 %). In essence, whichever policy scenario is followed, petroleum (along with coal) is fated to continue to be India's primary fuel sources in the near future.

Based on evidence of the performances of ONGC and private/JV companies, greater privatisation is an imperative for improving (or even maintaining) indigenous petroleum production output. While the implementation of OALP is an important towards greater privatisation, India may consider following the Brazil example: making a short-term shift to a concession-based system instead of the current PSC-based system. This might in the long run serve to kick-start India's upstream sector. Adequate protections for current state-owned and operated oil and gas fields could be provided along with greater privatisation.

The relative success of indigenous upstream sector would however still warrant considerably import dependence to cater to the corresponding increase in demand. India's future reliance on petroleum imports could therefore be taken as inevitability—at least in the medium-term. Similarly India's LNG imports could also be expected to rise. As a result, the country's current account deficit is bound to increase further, particularly in the medium-term where indigenous supply is expected to be considerably lower than demand. One way of managing the resultant deficit is to restructure the country's economy towards an export-oriented trajectory. A partially export-oriented economy would offset the deficit stemming from rising imports—of which energy imports form a considerable part. This would require greater privatisation in several sectors of the economy and greater foreign investments. While the country aims to become a regional petroleum-products export hub, India would also have to partially export-orient its several of its manufacturing and heavy industries.

In 2011–12, the Middle East (comprising of Saudi Arabia, UAE, Kuwait, Iraq and Qatar) contributed to 56.3 % of total petroleum imports to India and Iran another 10 %. The continued lack of diversification of India's import sources mean that India's oil supply security would be highly affected by any price volatility and

socio-political instability in that region. In order to increase its fuel supply security in an era of increasing import dependency, India would have to explore new markets—particularly those in Latin America and Central Asia, among others.

References

Azhar M (2011) New exploration licensing policy (NELP) in India. OPEC Energy Rev 35(2):174–188

De Oliveira A (2011) Brazil's Petrobras: strategy and performance. In: Victor DG, Hults DR (eds) Thurber MC, oil and governance: state-owned enterprises and the world energy supply. University Press, Cambridge, pp 515–556

Directorate General of Hydrocarbons (2012) Hydrocarbon exploration and production activities: India 2011–12. http://www.dghindia.org/pdf/1DGH%20Annual%20Report%202011-12.pdf. Accessed 28 Feb 2014

Directorate General of Hydrocarbons (2013) Hydrocarbon exploration and production activities: India 2012–13. http://www.dghindia.org/pdf/2012_13.pdf. Accessed 28 Feb 2014

International Energy Agency (2007) World energy outlook 2007: China and India insights. http://www.worldenergyoutlook.org/media/weowebsite/2008-1994/weo_2007.pdf. Accessed 28 Feb 2014

International Energy Agency (2014) Statistics. http://www.iea.org/statistics/. Accessed 30 March 2014

Ministry of Petroleum and Natural Gas (1997a) India Hydrocarbon vision—2025. www.petroleum.nic.in/vision.doc. Accessed 28 Feb 2014

Ministry of Petroleum and Natural Gas (1997b) CBM policy approved by the government on the 19th July, 1997. http://petroleum.nic.in/newgazette/cbmpolicy.pdf. Accessed 28 Feb 2014

Ministry of Petroleum and Natural Gas (1999) Notification on formulation of New Exploration Licensing Policy. http://petroleum.nic.in/newgazette/goi1.pdf. Accessed 28 Feb 2014

Ministry of Petroleum and Natural Gas (2008) Indian petroleum and natural gas statistics 2006–07. http://www.infraline.com/ong/stat/2006-07/MoPNGIndPetNatGasStats-0607.pdf. Accessed 28 Feb 2014

Ministry of Petroleum and Natural Gas (2010) NELP IX model production sharing contract. http://petroleum.nic.in/nelp93.pdf. Accessed 28 Feb 2014

Ministry of Petroleum and Natural Gas (2011) Results-framework document 2011–12. http://petroleum.nic.in/rfd/rfd11-12.pdf. Accessed 28 Feb 2014

Ministry of Petroleum and Natural Gas (2012a) Indian petroleum and natural gas statistics 2011–12. http://petroleum.nic.in/pngstat.pdf. Accessed 28 Feb 2014

Ministry of Petroleum and Natural Gas (2012b) Draft policy for exploration and exploitation of shale oil and gas. http://www.eisourcebook.org/cms/Nov%202012/India%20(draft)%20Shale%20E%20&%20P%20Petroleum%20Policy.pdf. Accessed 28 Feb 2014

Mudiam PR (1994) India and the Middle East. British Academic Press, London

Nathan HSK, Kulkarni SS, Ahuja DR (2013) Pipeline politics—a study of India's proposed cross border gas projects. Energy Policy 62:145–156

Oil and Natural Gas Corporation Limited (ONGC) Annual reports. http://www.ongcindia.com/wps/wcm/connect/ongcindia/Home/Performance/Annual_Reports/. Accessed 28 Feb 2014

ONGC Videsh, Assets. http://www.ongcvidesh.com/Assets.aspx?AspxAutoDetectCookieSupport=1. Accessed 28 Feb 2014

Parikh KS, Karandikar V, Rana A, Dani P (2009) Projecting India's energy requirements for policy formulation. Energy 34:928–941

Patey L (2011) India in Sudan: troubles in an African oil 'Paradise'. In: Patey L, Large D (eds) Sudan looks east: China, India and the politics of Asian alternatives. James Currey, Suffolk

Patey L (2014) South Sudan: fighting could cripple oil industry for decades, African Arguments. http://africanarguments.org/2014/01/10/south-sudan-fighting-could-cripple-oil-industry-for-decades-by-luke-patey/. Accessed 28 Feb 2014

Petroleum Planning and Analysis Cell, Natural Gas http://ppac.org.in/content/4_1_NaturalGas.aspx. Accessed 28 Feb 2014

Petroleum Planning and Analysis Cell, Petroleum. http://ppac.org.in/content/3_1_Petroleum.aspx. Accessed 28 Feb 2014

Planning Commission (1997) 9th Five Year Plan. http://planningcommission.nic.in/plans/planrel/fiveyr/welcome.html. Accessed 28 Feb 2014

Planning Commission (2002) 10th Five Year Plan 2002–07. http://planningcommission.nic.in/plans/planrel/fiveyr/welcome.html. Accessed 28 Feb 2014

Planning Commission (2006) Integrated energy policy. http://planningcommission.nic.in/reports/genrep/rep_intengy.pdf. Accessed 28 Feb 2014

Planning Commission (2012) Twelfth Five Year Plan 2012–17. http://planningcommission.nic.in/plans/planrel/fiveyr/welcome.html. Accessed 28 Feb 2014

Rai V (2011) Fading star: explaining the evolution of India's ONGC. In: Victor DG, Hults DR (eds) Thurber MC, oil and governance: state-owned enterprises and the world energy supply. University Press, Cambridge, pp 753–808

Rodriguez MR, Suslick SB (2009) An overview of Brazilian petroleum exploration lease actions. Terrae 6(1):6–20

Srinivasan K (1997) ONGC's decline and what should be done. Economic and Political Weekly 32(8)

Sinha UK, Dadwal SR (2005) Equity oil and India's energy security. Institute for Defence Studies and Analyses 29(3). http://www.idsa.in/strategicanalysis/EquityOilandIndiasEnergySecurity_srdadwal%2C%20uksinha_0705. Accessed 28 Feb 2014

TERI (2013a) TERI energy data directory and yearbook 2012/13. TERI Press, Delhi

TERI (2013b) Shale gas in India: Look before you leap. http://www.teriin.org/policybrief/docs/Shale_gas.pdf. Accessed 28 Feb 2014

U.S. Energy Information Administration, International Energy Statistics. http://www.eia.gov/cfapps/ipdbproject/IEDIndex3.cfm. Accessed 28 Feb 2014

Varigonda KC (2012) The pipeline that wasn't: Myanmar-Bangladesh-India natural gas pipeline. J Energy Secur. http://www.ensec.org/index.php?option=com_content&view=article&id=348:india-bangladesh-and-the-myanmar-bangladesh-india-natural-gas-pipeline-how-not-to-acheve-energy-s&catid=123:content&Itemid=389. Accessed 28 Feb 2014

Vines A, Wong L, Weimer M, Campos I (2009) Thirst for African oil: Asian national oil companies in Nigeria and Angola, Chatham House. http://www.chathamhouse.org/sites/default/files/r0809_africanoil.pdf. Accessed 28 Feb 2014

The World Bank, DataBank. http://databank.worldbank.org/data/home.aspx. Accessed 28 Feb 2014